INVESTIGATION OF BIOELECTROCHEMICAL TREATMENT EFFICIENCY FOR REMOVAL OF BORON FROM GEOTHERMAL WATERS

A Thesis Submitted to
the Graduate School of
İzmir Institute of Technology
in Partial Fulfillment of the Requirements for the Degree of

DOCTOR OF PHILOSOPHY

in Environmental Science and Engineering

by
Ayşegül Yağmur GÖREN KARA

July 2022
İZMİR

ACKNOWLEDGMENTS

Firstly, I would like to express my deepest and sincere gratitude to my advisor Assoc. Prof. Dr. Hatice Eser ÖKTEN for her endless support, encouragement, guidance, and patience throughout my thesis. I would like to also thank my co-advisor Prof. Dr. Alper BABA for his guidance and support to enhance the scientific value of my thesis.

I would like to thank my sincere gratitude to my PhD Thesis Committee and Jury Members, Prof. Dr. Sait Cemil SOFUOĞLU and Prof. Dr. Nalan KABAY for sharing their valuable knowledge to improve the quality of my thesis.

I would like to thank the valuable specialists working in Biotechnology and Bioengineering Application and Research Center, Center for Materials Research, and Environmental Development Application and Research Center at İzmir Institute of Technology for their kind help and technical support.

Lastly, I would like to thank my mother Sibel GÖREN, my father Yakup GÖREN, my sister Başak BALTACI and her husband Ege BALTACI for their endless support, understanding, and love, and my special thanks go to my husband Eren KARA who helped me handle the difficulties and gave me moral support during my Ph.D. adventure since he entered my life. I am so blessed to have you.

ABSTRACT

INVESTIGATION OF BIOELECTROCHEMICAL TREATMENT EFFICIENCY FOR REMOVAL OF BORON FROM GEOTHERMAL WATERS

Microbial desalination cell (MDC) is a promising technology due to its simultaneous features of electricity production, wastewater treatment, and desalination. In this thesis, boron (B) removal from geothermal water and organic matter removal from yeast wastewater with energy production was studied using a three chamber (anode/desalination/cathode) lab-scale MDC system. Among operational conditions, electrode surface area was proven to be significant on B removal efficiency. Then, anode chamber of the conventional MDC was modified to include three-dimensional (3D) cubic electrodes as a novel design. B and organic matter removal efficiencies and the produced power density results were promising for 3D-electrodes. Further studies in order to increase the efficiency of MDC system was conducted by synthesizing 3D hybrid sponge electrodes with activated carbon-chitosan (AC-CS). MDC with 3D AC-CS anode provided a higher power density of 970 mW/m^2, B removal efficiency of 75.9%, and COD removal efficiency of >90% under optimized conditions. Furthermore, phytoremediation performance of *Lemna minor* L. on B removal was found to be 96.7 %. Also, removal of B and heavy metals from reverse osmosis (RO) permeate and concentrate streams using RO-MDC hybrid process was studied. The performance of RO-MDC system was proven to be significant on B and heavy metals removal efficiency. Lastly, feasibility of B removal from geothermal water using MDC-Donnan dialysis hybrid process was evaluated. The most important output of this study was decreased frequency for pH adjustment. Overall, MDC, being in its early levels of technology readiness, produced promising desalination and energy production results in removal of boron from geothermal brine.

ÖZET

JEOTERMAL SULARDAN BOR GİDERİMİNDE BİYOELEKTROKİMYASAL ARITMA VERİMİNİN İNCELENMESİ

Mikrobiyal tuzdan arındırma hücresi (MTH), elektrik üretimi, atık su arıtımı ve tuzdan arındırma gibi eş zamanlı özellikleri nedeniyle önemli ölçüde gelecek vaat eden bir teknolojidir. Bu tezde, jeotermal sulardan bor (B) arıtımı ve maya atık suyundan organik madde giderimi ile eş zamanlı enerji üretimi, üç hazneli (anot/tuzsuzlaştırma/katot) laboratuvar ölçekli MTH sistemi kullanılarak kapsamlı bir şekilde çalışılmıştır. Öncelikle, değişen işletme koşulları ile optimizasyon çalışmaları yapılmıştır. Özellikle, elektrot yüzey alanının etkisinin B giderim verimliliği üzerinde önemli bir değişken olduğu kanıtlanmıştır. Sonrasında, geleneksel MTH'nin anot hücresi, üç boyutlu kübik elektrotları içerecek şekilde tasarlanmıştır. Klasik MTH sistemi ile kıyaslandığında, B ve organik madde giderme verimleri ve üretilen güç yoğunluğu sonuçları artış göstermiştir. MTH sisteminin verimliliğini artırmak amacıyla aktif karbon-kitosan içeren üç boyutlu sünger elektrot sentezlenmiş ve optimize edilmiş koşullar altında 970 mW/m^2'lik güç yoğunluğu, %75,9'luk B giderim verimi ve >%90'lık KOİ giderim verimi gözlenmiştir. Çalışmanın ilerleyen safhalarında, bir ön arıtma seçeneği olarak *Lemna minor* L. bitkisi kullanılarak borun sulardan uzaklaştırılması değerlendirilmiştir. 5 mg/L başlangıç B derişimi, pH 8 ve 1.5 cm su derinliği ile yapılan deneysel çalışmada maksimum giderim verimi %96,7 olarak elde edilmiştir. Ters osmoz (TO)-MTH hibrit sistemi kullanılarak TO süzüntüsünden ve konsantresinden B ve ağır metallerin uzaklaştırılması çalışılmıştır ve sistemin etkili olduğu kanıtlanmıştır. Son olarak ise, MTH-Donnan diyalizi (DD) hibrit işleminin jeotermal sulardan B giderme performansı değerlendirilmiştir. Bu çalışmanın en önemli çıktısı, pH'ın DD sistemi tarafından ayarlanıyor olması sayesinde sistemin pH değerinin ayarlanmasındaki sıklığın azalmasıdır. Genel olarak, MTH teknolojisi gelişme seviyesinde olmasına rağmen, jeotermal tuzlu sudan borun giderilmesi, tuzsuzlaştırma ve enerji üretimi açılarından umut verici sonuçlar ortaya koymuştur.

TABLE OF CONTENTS

LIST OF FIGURES

Figure **Page**

Figure **Page**

Figure **Page**

Figure **Page**

LIST OF TABLES

Table **Page**

CHAPTER 1

INTRODUCTION

Water scarcity, which results in greater costs for clean water production and wastewater treatment from an economic viewpoint, becomes a major issue for both developing and developed countries. According to the World Health Organization (WHO), 748 million people lack access to safe and sustainable water, while at least 2 billion people consume contaminated water. While around 50% of the world's population has water shortage, one-third of same population has limited excess to energy services (Malley et al., 2009; Supply and Programme, 2014). Furthermore, exposure to microbially contaminated waters may cause serious health problems such as cholera, dysentery, diarrhea, hepatitis, polio, and typhoid. The WHO estimates that half a million people die each year from diarrhea due to lack of clean drinking water (World Health Organization, 2015). Therefore, access to safe and secure water resources is one of the most critical scientific and technological challenges encountered by the human race in the 21st century.

Agriculture, followed by public water supply, is the leading sector of water consumption in Mediterranean nations, according to the AQUAREC project (2003-2006) (Wintgens et al., 2002). The Turkish Statistics Institute reported that approximately 74% of the total abstracted water in Türkiye was consumed by the agriculture sector, mostly for irrigation purposes (TSI, 2022). Future projections regarding Türkiye, which evaluate the regional available water budget, point to high stress levels by the year 2040 (WRI, 2022). It becomes obvious that meeting water demand by solely exploiting conventional water resources such as surface water bodies and groundwater aquifers will be impossible in the near future. Given the limitations of an increasingly unpredictable climate in the era of climate change, utilization of unconventional water resources through recycling and reuse not only diversifies sources of supply but also provides water of abundant quantity and required quality. Utilization of unconventional water resources combined with water-efficient irrigation techniques, enhanced farming techniques, and switches to high-value-added crops (Plusquellec, 2009), provide the framework for sustainable agriculture that translates into food security.

As a result of a much needed paradigm shift worldwide, treated saline water is being considered as a viable option for replacing freshwater resources in agricultural irrigation. Spent geothermal fluid emerges as an important alternative water source to supply the demand for agricultural purposes. 73% of Türkiye's geothermal resources is located in Western Anatolia (MENS, 2022), which also has vast agricultural fields with crops such as cotton, olive, oat, wheat, barley, sugar beet, fruits and vegetables etc. However, vastly produced geothermal brine may pose a significant environmental risk due to its high ionic strength, specifically due to its sodium, chloride, sulfate, silicate and boron content. Particularly boron species, which are generally found in the uncharged boric acid form in natural waters, are costly to remove using high-throughput membrane technologies such as reverse osmosis. Alternative conventional treatment methods such as adsorption, coagulation, ion exchange, biological processes, electrocoagulation, and membrane filtration consume high energy and chemicals, produce toxic sludge and by-products, require pre-treatment as well as complex operation and maintenance procedures.

Recent advances in bioelectrochemical systems (BES) has facilitated development of energetically self-sufficient wastewater treatment and desalination. Microbial desalination cell (MDC) is considered to be an energy efficient, environmentally friendly, and sustainable solution. Being a fairly novel technology, MDC needed to be further studied for improvements in several critical areas such as energy production and desalination efficiency, membrane fouling and scaling, pH fluctuation, cost of electrode and membrane materials, and investigation of operational parameters (Borràs et al., 2021; Ragab et al., 2019a; Zahid et al., 2022). Therefore, recent studies have concentrated on enhancement of MDC performance. Being the first MDC study on geothermal water, the key objective of this thesis was to enhance the MDC system for boron removal from geothermal water with optimization of operational parameters, design and development of a novel MDC system, and synthesis of effective electrode materials. The significant potential of specifically designed MDC system for organic matter removal and energy production from yeast wastewater was considered as an important output. In addition, the performance of the MDC system as a post-treatment and pre-treatment process with regard to a Reverse Osmosis system was also considered.

1.1. Microbial Desalination Cells (MDCs)

Bioelectrochemical systems (BESs) as novel water and wastewater treatment methods have drawn attention due to their lower cost and less environmental impacts. Briefly, BESs can utilize microorganisms in wastewater to generate clean electricity, treated water and useful products (e.g. metals, hydrogen gas, hydrogen peroxide, methane) (Gujjala et al., 2022). The most investigated BESs are microbial fuel cells (MFCs), which are electrochemical devices converting chemical energy from organic substrates to electrical energy via microbial-catalyzed reactions (Hoang et al., 2022; Ramya and Kumar, 2022). MDCs have been substantially studied and enhanced in order to accommodate innovative multifunctional solutions relating to environmental and energetic considerations (Jatoi et al., 2022; Zahid et al., 2022). The types, configurations, and forms of membranes, as well as membrane-based processes, were used to classify the development of numerous MDC designs in the literature (Imoro et al., 2021). A classic MDC can be manufactured with the placement of ion exchange membranes (IEMs), namely anion exchange membranes (AEMs) and cationic exchange membranes (CEMs) (Salehmin et al., 2021).

MDC is a BES technology that is derived from the MFC technology, which typically consists of three chambers; the anode chamber, the cathode chamber, and the desalination chamber. The latter is placed in between the anode chamber and the cathode chamber, separated from them by an anion exchange membrane (AEM) and a cation exchange membrane, respectively (Zuo et al., 2022). Electrodes, which are placed at the anode and cathode chambers, are connected using conductive wiring. MDCs are known to perform wastewater treatment, desalination, and other redox activities simultaneously. Wastewater with high organic content is fed to the anode chamber while saline water is fed to the desalination chamber. Cathode chamber's function is generally to enhance electron transfer. A typical MDC configuration's working principle is depicted in Figure 1.1 (Goren and Okten, 2021a). In the anode chamber, microorganisms anaerobically convert the organic substrate into inorganic carbon, H^+ and electrons. Then, electrons flow towards cathode through an external electrical circuit and a current across the cell is formed. Oxygen as an external electron acceptor, which is provided at cathode cell, use these electrons to sustain reduction and produce water. Therefore, a potential electrochemical gradient is formed across the oxidative anodic and reductive cathodic

chambers, which drives the desalination process. Anions migrate from salty water in desalination cell across AEM into the anode, while cations move across CEM into the cathode chamber. Migration of ions in desalination cell across the membrane based on concentration gradient through diffusion is the driving force for desalination process.

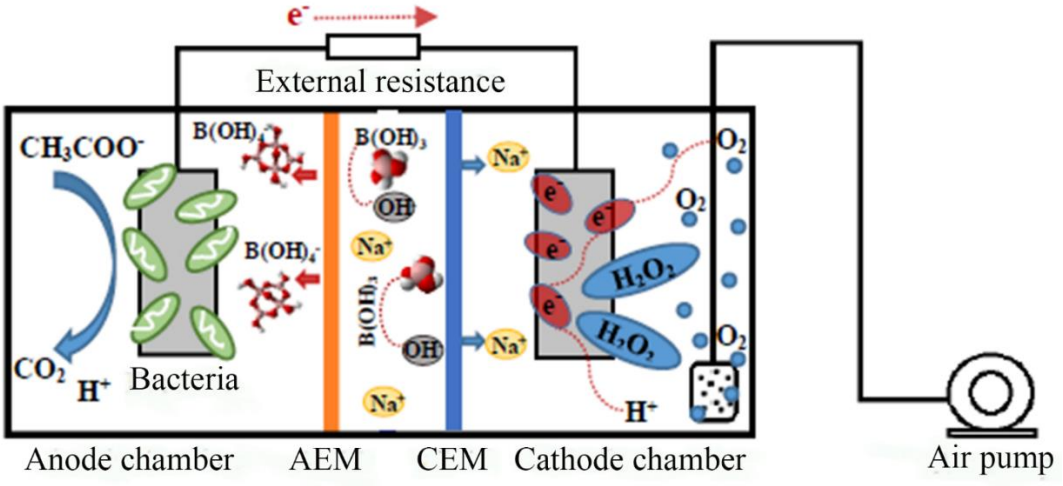

Figure 1.1. Possible reactions in MDC bioreactor.

Literature studies proved the MDC to be a developing technology with simultaneous electricity generation, wastewater treatment, and water desalination in a single reactor. Sevda et al. (2017) investigated the use of MDC for simultaneous seawater desalination and bioelectricity generation from petroleum refinery wastewater. They found that the maximum desalination efficiency and the highest total energy production as 19.9% and 9.5 Wh/m^3, respectively. The highest COD removal was obtained with 20 g/L NaCl concentration in the desalination chamber. Ebrahimi et al. (2018b) studied the effect of different catholyte solutions on salt removal and energy generation. Among the examined catholytes, the bio-catholyte achieved the highest power density value of 32.6 W/m^3. Also they achieved 80% COD removal and 0.38 g NaCl/L.h desalination rate. In order to enhance the performance of MDC, Gholizadeh et al. (2017) designed the ozone-cathode MDC. The maximum power density values and salt removal efficiencies for O3-MDC and O2-MDC were 4.06 W/m^2-74% and 0.369 W/m^2-55.58%, respectively. However, there is limited research in the literature about boron removal from waters using MDC technology specifically. A recent study employed an MDC-Donnan dialysis (DD) system for boron removal from aqueous solution using 2D electrodes. They observed 60 or 52% of boron removal for MDC system with DD pretreatment configuration (Ping et

al., 2015). The same authors also investigated mathematical modeling based evaluation and simulation of boron removal in BESs (Ping et al., 2016). These studies revealed that MDC holds considerable potential in desalination and energy production.

In addition to the lack of adequate research on boron removal by MDCs, there are important challenges to overcome for practical applications. A problem with conventional MDC is the salinity of the anolyte being increased during operation, which may affect the microbial activity and consequently impact the MDC performance. Thus, organic loading in anode chamber, salinity of anolyte solution and response of microbial community to changing environment become important aspects. Moreover, presence of divalent ions in the desalination chamber may have negative effects on MDC in terms of power generation and desalination. Membrane scaling, fouling, and inter-membrane distance are known to hinder MDC performance. Membrane scaling would reduce the desalination performance by inhibiting the mass transport of ions and consequently inducing pH imbalance. High inter-membrane distance would increase internal resistance, decreasing power generation in turn. On the other hand, low inter-membrane distance means a desalination chamber of small volume, which may decrease salt removal through a decrease in hydraulic retention time. Mode of operation is another significant factor affecting the MDC performance. MDCs operated in batch mode suffer pH fluctuations in cathode and anode chambers, leading to decrease in power density and desalination efficiency of the system. Consequently, tackling abovementioned challenges would considerably contribute to knowledge and application aspects of the MDC technology, bringing it a few steps closer to full-scale applications.

1.2. Motivation

In this thesis, I had several motivations of varying scales. My motivation in the large scale was to integrate two significant regional issues in order to produce an effective solution. Those issues were: (i) the water demand for agricultural irrigation dominates the total water consumption in Türkiye and (ii) discharge of untreated geothermal brine severely harms the agricultural crops and the soil. Since direct discharge of geothermal water was not only harmful to the environment but also was unlawful, I proposed treatment of geothermal brine to produce irrigation quality water. Treatment of geothermal brine, primarily entailed desalination processes, due to its high

ionic strength. Although current Turkish standards for evaluating the suitability of water for irrigation listed parameters such as electrical conductivity, total dissolved solids, and sodium adsorption ratio, the only mentioned ions were sodium, chloride and boron. Since, geothermal fluids in Türkiye were rich in boron, its removal for irrigation purposes was a requirement. Therefore, in a smaller scale, my motivation was to remove boron from geothermal brine preferably using an energy-wise self-sufficient treatment system. MDC was a continually advancing and promising process that combined water desalination, energy production and wastewater treatment in single system with potential for value-added chemical production. However, as MDC was just a decade old and at improvement stage, research on its application was limited when compared to conventional processes and some critical points needed to be addressed. The most important critical points to enhance performance of MDC process were electrode cost, pH fluctuation, anolyte type, limited knowledge on organic substance loading, membrane fouling, and inadequate application in real wastewater. The last motivation in this thesis was to enhance the performance of MDC process by studying several operational parameters. To make the MDC system flexible and self-sustainable for real scale practices, effects of operational parameters, real wastewater utilization, cost effective material production, MDC system modification, and usage as a post-treatment process were considered.

1.3. Thesis Overview

The main objective of this PhD thesis was to remove boron from geothermal brine to produce irrigation water using self-sufficient MDC system. The details of each chapter were described below:

i. In Chapter 2, a specifically designed MDC system was utilized for simultaneous boron removal from geothermal brine, organic matter removal from yeast wastewater, and energy production. To optimize MDC system performance, effects of operating parameters such as initial boron concentration, air flow rate, electrode surface area, catholyte solution, and operating mode were investigated in detail.

ii. In Chapter 3, anode chamber of conventional MDC was modified to include three-dimensional (3D) cubic electrodes as a novel design. Simultaneous boron removal from aqueous solution, organic matter removal from industrial wastewater, and energy production were studied. Effects of operating parameters (electrode type: 3D-electrode vs. 2D-electrode, anolyte temperature, and activated sludge to wastewater volumetric ratio) on MDC performance were studied.

iii. In Chapter 4, phytoremediation performance of *Lemna minor* L. on boron removal from synthetic and real geothermal water was evaluated as a pre-treatment process before MDC system. Effects of initial boron concentration, initial pH, water height in cell, and initial humic acid concentration were investigated.

iv. In Chapter 5, a 3D activated carbon-chitosan coated sponge electrode was synthesized in order to enhance the MDC system efficiency. Operating parameters such as boron concentration, electrode surface area, catholyte solution, and activated sludge volume were investigated in detail.

v. In Chapter 6, boron and heavy metals removal from reverse osmosis (RO) permeate and concentrate streams using MDC was evaluated. In RO-MDC hybrid system, geothermal water was first treated in the RO system and then water samples from concentrate and permeate streams were treated in the MDC. Moreover, organic matter removal and energy production efficiency were investigated.

vi. In Chapter 7, feasibility of boron removal from aqueous solutions using MDC-DD hybrid process was studied. Moreover, boron and heavy metals removal from RO permeate and concentrate streams were performed using MDC-DD hybrid process. Organic matter removal and energy production efficiency of process from yeast wastewater were also considered.

1.4. Contributions to the Literature

The contributions of this Ph.D. thesis to the literature are listed below:

i. Chapter 2: MDC processes generally investigated the effects of anolyte and catholyte solution, contaminant concentration, electrode material type, and operational time to enhance desalination and energy production performance (Jatoi et al., 2022; Saeed et al., 2015). However, studies investigating air flow rate in cathode cell, electrode surface area, and operation mode on performance of the MDC system were missing. The electrode surface area and operation mode were two of the most important parameters as they directly affected the cost and removal performance. Optimization of electrode surface area and operational mode might reduce the operational costs and increase the removal performance of the MDC. Aeration in cathode chamber might also increase the energy production owing to improved electron transfer from anode to cathode cell. Moreover, boron removal using MDC system has been only performed for synthetic aqueous solutions (Ping et al., 2016, 2015). In Chapter 2, for the first time in literature, boron removal from real geothermal brine with MDC system was studied. In addition, impacts of air flow rate, electrode surface area, and operational mode were investigated comprehensively to enhance applicability of MDC system.

ii. Chapter 3: Various MDC configurations were developed considering process sustainability, efficiency, and operational cost for environmentally safe water treatment and energy production (Gujjala et al., 2022). In Chapter 3, a specifically designed electrode cell in anode chamber was developed instead of direct use of commercial electrode material. This novel design showed high energy transfer and production with greater microbial attachment on electrode surfaces, presented ease of operation for electrode maintenance, and had a potential to be scaled up for real treatment plant applications.

iii. Chapter 4: The MDC system with various modifications was performed for boron removal from waters (Goren and Okten, 2022, 2021b). On the other hand, several inorganic and organic contaminants were not effectively removed by MDC without a pre-treatment process to achieve a regulated

reuse standard for irrigation and/or drinking purposes. In Chapter 5, the potential of *Lemna minor* L. plant as a pre-treatment option to MDC was considered for the first time in the literature.

iv. Chapter 5: Recently, carbon-based materials such as activated carbon, biochar, and graphene have been utilized to enhance porosity and electrical conductivity of electrode materials in MFC system (Yuan et al., 2019; Zhu et al., 2022), which in turn improved the energy production and desalination efficiency of the system. However, modification of electrode material in MDC has been only investigated in one study previously. Moreover, the high cost and complex synthesis procedures were important drawbacks of widely used carbon-based materials. In Chapter 5, novel 3D activated carbon-chitosan (AC-CS) composite sponge anode electrode was produced to enhance performance of MDC system as a cost effective electrode material. This new electrode material offered high electron transfer with its enhanced electrical conductivity.

v. Chapter 6: The MDC system's potential as an energetically self-sufficient post-treatment process was investigated. The MDC system was used at treating samples from reverse osmosis (RO) permeate and concentrate streams. This approach had the potential to decrease the energy consumption in conventional treatment methods while also treating wastewater and producing energy. Overall, the treatment performance of RO-MDC hybrid method was studied comprehensively for the first time in this PhD thesis.

vi. Chapter 7: The need for pH adjustment and prevention of pH imbalances in MDC system were the most crucial problems encountered during operation. In Chapter 7, the performance of MDC-Donnan dialysis (DD) hybrid processes for boron removal from geothermal brine and RO concentrate were studied first time.

CHAPTER 2

ENERGY PRODUCTION FROM TREATMENT OF INDUSTRIAL WASTEWATER AND BORON REMOVAL IN AQUEOUS SOLUTIONS USING MICROBIAL DESALINATION CELL

2.1. Introduction

Geothermal waters can be characterized by diverse physicochemical parameters depending on the depth at which resources reside, the geological characteristics of the rocks involved, and the source of water supply. Geothermal waters contain significant amounts of cations and anions along with neutral species. Specifically, boron content is critical in geothermal waters with such high concentrations, even exceeding its levels in sea water and brackish water. The main sources of boron can be either natural such as leaching from rocks, soils containing borates and borosilicates, and volcanic activities, or industrial such as manufacturing of detergents, cleaning products, semiconductor, borosilicate glass, cosmetics, fertilizers, flame retardants and dyestuff (Kartikaningsih et al., 2016). The most common boron species in geothermal waters and boron rich thermal springs are undissociated boric acid (H_3BO_3) and tetrahydroxoborate ions ($B(OH)_4^-$) (Yilmaz et al., 2008). H_3BO_3 is the dominant species at low pH values, while $B(OH)_4^-$ is dominant at high pH values (>8–9) (Barth, 2000; Kabay et al., 2015). Therefore, the pH adjustment must be applied based on the pKa value of boric acid to ionize it before treating boron containing water streams. The dissociation of boric acid as a weak acid was reported using following equations:

$$H_3BO_3 \leftrightarrow H^+ + H_2BO_3^- \ (pKa_1 = 9.14) \qquad (2.1)$$

This chapter has been published as:
A.Y. Goren, H.E. Okten, Energy production from treatment of industrial wastewater and boron removal in aqueous solutions using microbial desalination cell, Chemosphere 285 (2021) 131370.

$$H_2BO_3^- \leftrightarrow H^+ + HBO_3^{2-} \ (pKa_2 = 12.74) \quad (2.2)$$

$$HBO_3^{2-} \leftrightarrow H^+ + BO_3^{3-} \ (pKa_3 = 13.8) \quad (2.3)$$

In terms of environmental impacts of geothermal sources, uncontrolled discharge to environment following well tests or during regular operation pose a serious problem due to high boron content. Boron accumulates in the soil upon discharge and change the chemical, physical and biological properties of soils. Also, these waters mix with ground- water by percolating through the soil and may form complexes with heavy metals (i.e. Pb, Cu, Cd, Ni, Co), which may be more toxic than heavy metals forming them (Wuana and Okieimen, 2011). Consequently, boron has a significant impact on water resources and corresponding ecosystems (Gude, 2016).

Depending on concentration, boron may either support or hinder plant growth where geothermal water is used for irrigation. Deficiency of boron may result in loss of yield, reduced growth and even death (Yilmaz et al., 2008). Boron is an essential nutrient for plant growth and depending on plant type, there is a wide range of tolerance (blackberry, lemon: 0.5 mg/L; walnut, plum, pear, apple: 1 mg/L; sunflower, potato, cotton, tomato: 2 mg/L; asparagus, palm, bean, onion: 4 mg/L) (Hilal et al., 2011; Yilmaz et al., 2008). However, exposure to excess boron causes toxicity for nearly all plants. Additionally, long term ingestion of high boron concentrations through water or vegetables may lead to nausea, lethargy, diarrhea, vomiting, dermatitis, intellectual and physical problems at children and risk of miscarriage in pregnancies (Bryjak et al., 2008; Nielsen, 2002).

In order to tackle high concentrations of boron, treatment methods such as coagulation, sedimentation, filtration, adsorption, membrane filtration, ion-exchange, electrocoagulation, electrodialysis, and hybrid processes have been studied (Al-Bsoul et al., 2020; Al-Qodah et al., 2020; Banasiak and Schäfer, 2009a; Dominguez-Tagle et al., 2011; Yilmaz et al., 2008, 2007). However, challenges such as high operation costs, production of chemical sludge, excessive use of chemicals, membrane fouling, either individually or as a combination, hampers efficient use of these methods (Arar et al., 2013; Ozbey-Unal et al., 2018; Recepoğlu et al., 2018).

Bioelectrochemical systems (BESs) as novel water and wastewater treatment methods have drawn attention due to their lower costs and less environmental impacts. The most investigated BESs are microbial fuel cells (MFCs), which are electrochemical

devices that convert chemical energy from organic substrates to electrical energy via microbially-catalyzed reactions (Logan et al., 2007; Ren et al., 2014). Microbial desalination cell (MDC) is a BES technology that is derived from MFCs by inserting an anion exchange membrane (AEM) and cation exchange membrane (CEM) bordered desalination chamber between anode and cathode chambers, respectively (Kim and Logan, 2011; Tawalbeh et al., 2020). Electrodes at anode and cathode compartments are connected through a circuit, which transfers electrons that are produced by oxidation of organic substrates in anolyte under anaerobic conditions. Oxygen as an external electron acceptor, which is provided at cathode cell, uses transferred electrons to sustain reduction and produce water. Therefore, a potential electrochemical gradient is formed across the oxidative anodic and reductive cathodic chambers, which drives the desalination process. Anions migrate from salty water in desalination cell across AEM into the anode chamber, while cations move across CEM into the cathode chamber. Migration of ions in desalination cell across the membrane based on concentration gradient through diffusion is the driving force for desalination process. In the borate form (pH > pKa), the core boron species is fully hydrated in the solution that results in a larger radius and a charge enhancement of the ions [$B(OH)_4^-$]. Therefore, the ionized borate species readily diffuse through the AEM owing to their negative charge.

Even though having a promising potential in terms of energy self- sufficiency, MDCs may suffer from several setbacks such as salinity in- crease in anolyte having adverse effects on microbial activity, presence of divalent ions in the desalination chamber causing membrane scaling, and membrane fouling. Tackling these challenges will significantly contribute to bringing MDC technology a few steps closer to full-scale applications. Several studies reported the effects of operating parameters on energy production and desalination performance of MDC (Ebrahimi et al., 2018b; Malakootian et al., 2018; Sevda et al., 2017). However, most of these studies focused on effect of initial salt concentration, catholyte solution, electrode type, temperature of anolyte solution, and operating time, and there is no study about effect of electrode surface area, air flow rate in cathode chamber, and operating mode on MDC performance. So far, boron removal with MDC has only been studied using synthetic solutions (Ping et al., 2016, 2015). Furthermore, a very recent study by (Rahman et al., 2021b) has listed several possible modifications to MDC configurations in order to increase system's performance such as flow direction in desalination chamber, membrane spacing, volume, membrane material, electrode material/size, and mode of operation.

In this study, we investigated the performance of MDC in removing boron from synthetic solutions and real geothermal water and in removing COD from yeast industry wastewater, all the while producing energy. Objectives of this study were investigating (i) the effect of electrode surface area, air flow rate, and operating mode on MDC desalination performance, (ii) effect of operational parameters on energy production of MDC and (iii) performance of the optimized system in removal of boron from real geothermal water. It should be noted that this is the first study investigating the effect of electrode area and presenting performance of MDC on boron removal from real geothermal water. Consequently, this study is the most comprehensive study on applicability of a lab-scale MDC for simultaneous wastewater treatment, boron removal and energy production at optimum operating conditions.

2.2. Materials and Methods

2.2.1. MDC Set up and Operation

A specifically designed MDC bioreactor consisted of rectangular prism plexiglass chambers: anode, desalination, and cathode chambers (Figure 2.1). The dimensions of each identical chamber was 15 cm x 6 cm x 6 cm. Anode/desalination chambers and desalination/cathode chambers were separated using an anion exchange membrane (AEM, AMI- 7001, Membrane International Inc., USA) and a cation exchange membrane (CEM, CMI-7000, Membrane International Inc., USA), respectively. Chambers were clamped together with gaskets and O-rings using stainless steel bolts. Carbon graphite sheets of varying areas (18-72 cm^2) were used as electrodes, which were connected by a copper wire completing the electrical circuit.

Anaerobic activated sludge from the wastewater treatment plant of a food-grade yeast production facility was used as seed in the anode chamber. Also, wastewater taken from primary clarification tank of the same treatment plant was used as the source of organic substrate. Chemical Oxygen Demand (COD) and Total Kjeldahl Nitrogen (TKN) values for the yeast wastewater (pH 7.91) were 9280 mg/Land 413.75 mg/L, respectively. Anode chamber was filled with a mixture of activated sludge (270 mL) and yeast wastewater (270 mL) for all experiments. Synthetic boron solutions (5, 10 and 20 mg/L) and real geothermal water were fed to desalination chamber at different runs. During

operation, anode chamber and desalination cell were put on a magnetic stirrer with temperature control. Continuous stirring was applied in anode chamber in order to prevent sludge settling. Also temperature was adjusted to maintain 40 °C in desalination chamber, simulating field conditions for a future scale-up. The B solutions were prepared using boric acid (H_3BO_3, Sigma-Aldrich), and solution pH was adjusted to 9.5 using 0.1 M sodium hydroxide (NaOH, Merck-Millipore). The real geothermal water was obtained from Balçova Geothermal Power Plant in Izmir, Turkey. The pH and electrical conductivity of geothermal water were 8.04 and 1770 μS/cm, respectively. Physicochemical properties of yeast wastewater and real geothermal water were listed in Table B1. Phosphate buffer (0.1 M, pH 6.5), acidified water (pH 2.5) and regular tap water (pH 7.1) were used as catholytes. Various aeration rates (0, 1 and 2 L/min) were also investigated at the cathode chamber. Samples for analyses were collected from each chamber at specified time intervals. All experiments were conducted in batch mode at 40 °C and operating time of 12 d. Experimental runs were summarized in Table 2.1.

Table 2.1. Experimental runs with different operating parameters. SS: synthetic solution, RGW: real geothermal water.

<table>
<tr><th>Run (R)</th><th>Operation Mode</th><th>Desalination Chamber</th><th>Initial B Concentration (mg/L)</th><th>Electrode Surface Area (cm^2)</th><th>Catholyte Aeration (L/min)</th><th>Catholyte Type</th></tr>
<tr><td>1</td><td rowspan="10">Batch</td><td rowspan="9">SS</td><td>5</td><td rowspan="5">36</td><td rowspan="2">0</td><td rowspan="6">PBS</td></tr>
<tr><td>2</td><td>10</td></tr>
<tr><td>3</td><td>20</td></tr>
<tr><td>4</td><td rowspan="5">5</td><td>1</td></tr>
<tr><td>5</td><td rowspan="6">2</td></tr>
<tr><td>6</td><td>18</td></tr>
<tr><td>7</td><td>24</td></tr>
<tr><td>8</td><td>72</td></tr>
<tr><td>9</td><td rowspan="3">36</td><td>Acidified Water</td></tr>
<tr><td>10</td><td>Tap Water</td></tr>
<tr><td>11</td><td>RGW</td><td>10.5</td><td>PBS</td></tr>
<tr><td>12</td><td rowspan="3">Fed-Batch</td><td rowspan="3">SS</td><td>5</td></tr>
<tr><td>13</td><td>10</td></tr>
<tr><td>14</td><td>20</td></tr>
</table>

Most of the experimental runs were conducted in the batch mode (R1-R11). We started the experimental run once by filling the anode, cathode and desalination chambers with their respective solutions and operating the MDC until approximately 90% of the

organic substrate in anolyte – measured by COD – was depleted, which corresponded to 12 d of operation. In the fed-batch mode, at the end of 12 d, we drew treated wastewater from the anode chamber and fed fresh wastewater in the same volume we drew.

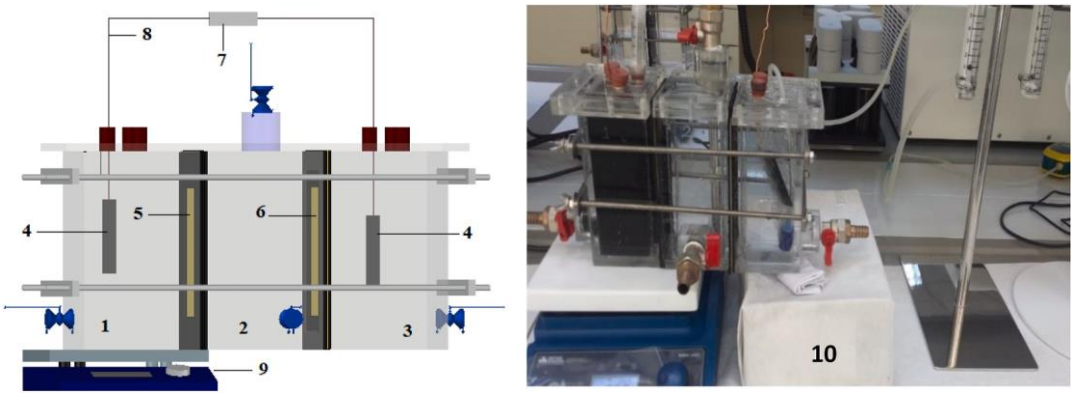

Figure 2.1. Schematic diagram of MDC bioreactor: (1) Anode chamber, (2) Desalination chamber, (3) Cathode chamber, (4) Carbon graphite electrode, (5) AEM, (6) CEM, (7) External resistor, (8) Copper wire, (9) Mechanic stirrer, and (10) Lab-scale MDC.

2.2.2. Analytical Methods and Calculations

Voltage (V) in the open circuit of MDC was continuously recorded every 15 min using a data logger (UNI-T, UT71C Digital Multimeter, China) by connecting to the computer. During operation, pH was measured daily by a pH meter (Mettler Toledo, SevenCompactTM, Switzerland). COD was measured through the closed reflux titrimetric method (Association, 1926). Power density was calculated based on water desalination. An inductively coupled plasma atomic emission spectrometer (ICP-AES, AGILENT 5110, USA) was used to determine the boron concentration at specified operating times. AEM surfaces (facing both the anode and desalination chamber), CEM surfaces (facing both the cathode and desalination chamber), and carbon graphite electrodes were investigated using scanning electron microscopy (SEM, Quanta 250FEG, USA). Energy dispersive X-ray spectrometry (EDX) was also performed for analyzing main elements present on the AEM and CEM surfaces. All analyses were conducted with triplicate measurements and average data were reported. Standard deviation values were calculated to be between 0.01 and 0.015 mg/L.

The current (I) through the electrical circuit was determined from the measured voltage under 100 Ω external resistance (R_{ex}) according to the following equation:

$$V = I \times R_{ex} \tag{2.4}$$

Power density (P, mW/m^3) was calculated per volume (v, m^3) of anode chamber using the following equation:

$$P = \frac{(V \times I)}{v} \tag{2.5}$$

Furthermore, the coulombic efficiency (CE, %) for decomposition of organic matter was calculated by following equation (6):

$$CE(\%) = \frac{MW_{O2} \int_0^t Idt}{nFV_a\left(C_{COD,i} - C_{COD,e}\right)} * 100 \tag{2.6}$$

where MWO_2 is the molecular weight of oxygen (32 g/mol), n is number of the e^- transferred from organic matter degradation (n: 4 mole/mol), F is the Faraday's constant (96485 C/mol), $C_{COD,i}$ is the total input COD concentration in anode chamber (9.228 g/L), $C_{COD,e}$ is the effluent COD concentration in anode chamber, and Va is the volume of anode chamber (0.54 L).

2.3. Results and Discussion

2.3.1. Synthetic Solution Experiments: Energy Production, Removal of Boron and COD

MDC performance may be affected by various operating parameters such as catholyte and anolyte solutions, electrode and membrane materials, size and number of chambers, organic and salt content of wastewater, temperature, and concentration of saline water (Al-Mamun et al., 2018). These operating parameters determine wastewater treatment efficiency, desalination efficiency, COD removal, and energy production. In this study, effects of initial boron concentration, air flow rate, electrode surface area, and operating mode of the system were investigated to enhance the energy production, and removal efficiencies for boron and COD (Table 2.1).

A negative control experiment was performed under the optimum operating conditions (initial boron concentration of 5 mg/L, electrode surface area of 36 cm^2, catholyte solution of PBS buffer, and air flow rate of 2 L/min) without bacteria to determine the difference, if any, in boron removal efficiency during the same period of time as the biotic experiments. It was clearly seen that in the absence of microbial population only a small fraction of boron content (1.31 mg/L) was removed from the desalination chamber, most probably being accumulated on the AEM, and rate of diffusion was significantly impaired due to lack of electrochemical gradient.

2.3.1.1. Effect of Initial Boron Concentration

Initially, MDC was operated using different initial boron concentrations of 5 mg/L (R1), 10 mg/L (R2) and 20 mg/L (R3) at specified operating parameters (Table 2.1). The maximum boron removal efficiencies were 39.7% ($C_{f,B}$: 12.07 mg/L), 39.4% ($C_{f,B}$: 6.06 mg/L) and 45.2% ($C_{f,B}$: 2.74 mg/L) for R3, R2, and R1, respectively (Figure 2.2a, 2.2c, 2.2e). Residual boron concentrations for all runs not only exceeded the WHO limit value for agricultural irrigation (1 mg/L), but they also exceeded 2.4 mg/L, which was the limit value for safe drinking water according to WHO guidelines (Edition, 2011).

Energy production and ion concentration gradient were reported as the two main driving forces for salt removal in MDC systems which accelerate desalination at higher salt concentrations (Yang et al., 2015). On the other hand, (Ping et al., 2015) studied B removal from aqueous solutions using MDC-Donnan dialysis hybrid system and they reported increased efficiency with decreasing salt loading rate. Similar to the results obtained in the literature, we found that the B removal efficiency seemed to increase with decreasing initial concentration. It should also be noted that the removed portion of the boron concentration in R1 and R3 were 2.26 mg/L and 7.93 mg/L, respectively. When the ion concentration difference between the desalination chamber and anode chamber was high, as it was the case in R3, even though more boron was removed from the desalination chamber comparative to R1, the removal efficiency was calculated to be 39.7%, which was lower than the efficiency calculated for R1, 45.2%. Consequently, in our opinion, using absolute measures instead of relative ones was more straightforward in the reporting of initial boron concentration related experimental data. High ion transfer to the electrochemical cells could contribute to charge accumulation and extended desalination times at higher salt concentrations. Therefore, B removal efficiency could be

improved with increasing operating time with fed-batch mode.

In addition, B concentrations in anode chamber were measured to investigate a possible boron toxicity on anaerobic microorganisms. At the end of 12 d, boron concentrations in anolyte were 1.42 mg/L, 1.77 mg/L, and 5.92 mg/L for R1, R2, and R3, respectively. The remaining boron in the desalination solution dropped from 20 to 12.07 mg/L, and the boron content in anolyte solution increased from 0 to 5.92 mg/L and the remaining boron was detected on the membrane surface. Similar results were observed for the initial boron concentrations of 5 and 10 mg/L. None of the B concentrations observed in anolyte had a significant adverse effect on COD removal (Figure 2.2b, 2.2d, 2. 2f). Therefore, based on the COD removal efficiencies it could be concluded that boron had no toxic effect on microorganisms. The COD concentration decreased from 9200 to 415 mg/L at R3 at the end of the 12 d operation, resulting in a 95.5% removal efficiency. For R1 and R2, removal efficiencies were 89.4% (C_{COD}: 978.9 mg/L) and 90.0% (C_{COD}: 918.2 mg/L), respectively. Initial boron concentrations did not seem to have a significant effect on COD removal efficiency.

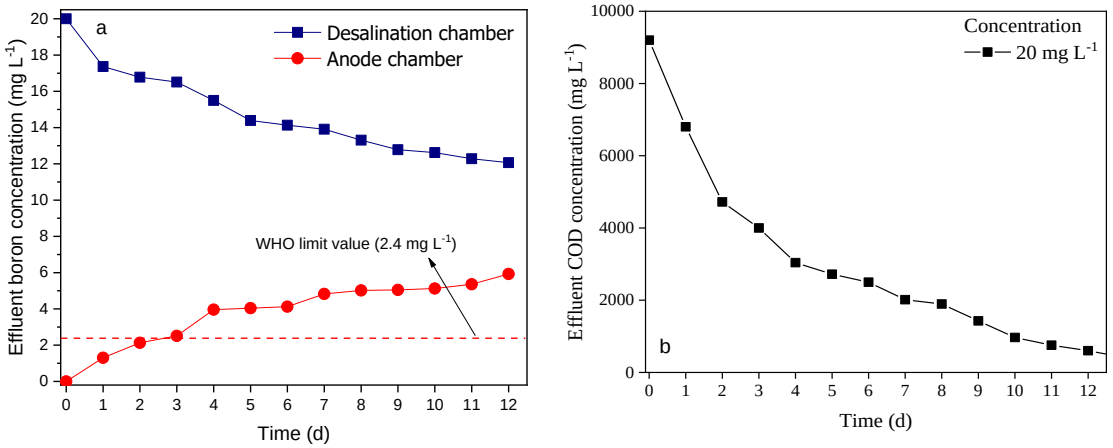

a) b)

Figure 2. 2.Effluent boron concentration in the anode and desalination chamber and COD concentration in the anode chamber a-b) 20 mg/L boron, c-d) 10 mg/L boron, e-f) 5 mg/L boron, and g) electrical potential, power density, and CE at optimum initial boron concentration. (electrode surface area: 36 cm^2, catholyte solution: PBS buffer, and air flow rate: 2 L/min).

(cont. on next page)

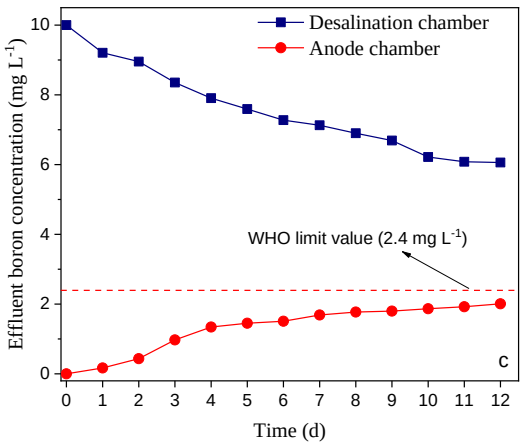

c)

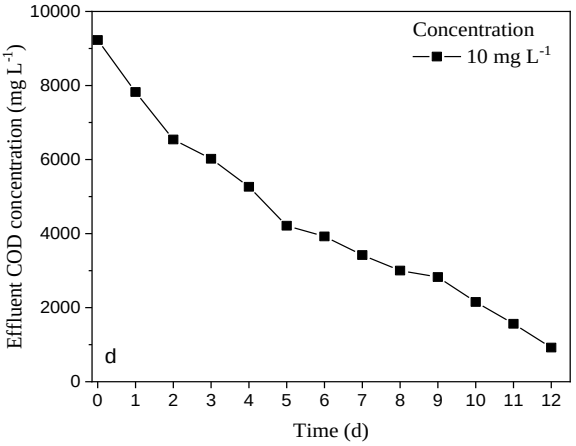

d)

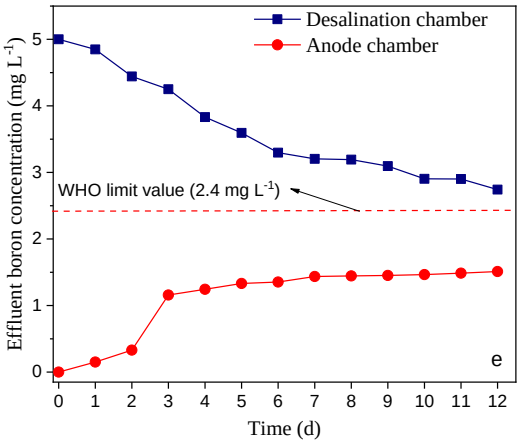

e)

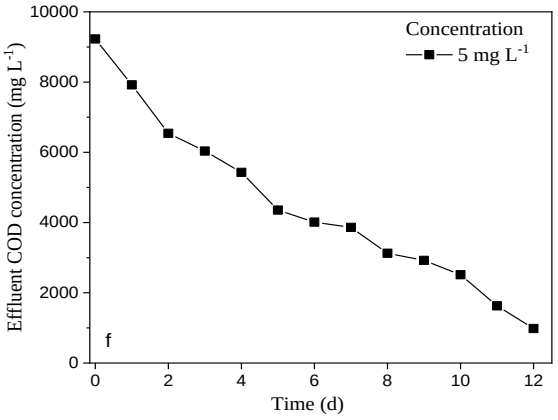

f)

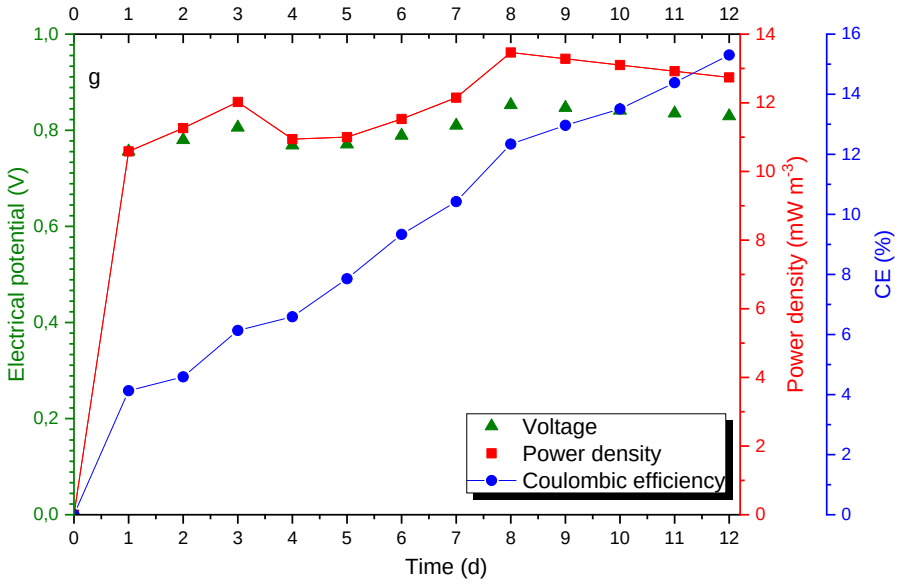

g)

Figure 2.2. (cont.)

Daily pH measurements in chambers showed decrease from 9.5 to 8.38 after 1 d of operation at desalination chamber using PBS buffer as a catholyte solution (Figure B.1a). Adjustments to pH 9.5 using NaOH solution (0.1 N) were done daily. Boron transforms to borate ions with larger hydrated radius and negative charge at pH values above 9.14 (Kabay et al., 2015). Thus, raising pH above the pKa value of 9.14 in desalination chamber was critical in order to sustain removal of boron at MDC. On the other hand, no significant changes in pH at anode and cathode chambers were observed.

The maximum open circuit voltage (OCV) values were measured to be 852 mV (20 mg/L B), 783 mV (10 mg/L B) and 669 mV (5 mg/L B) (Figure B.2a). The voltage was almost stable at maximum voltage for 2 d which indicated that the microorganisms were successfully grow and produced enough electron for the energy production at the anode chamber. Furthermore, to understand the power density, the anode and cathode chambers connected with external resistance of 100 Ω. The results showed that the power density increased with time and attained maximum power density of 13.44 mW/m^3 in 10 d for initial boron concentration of 20 mg/L. We observed that OCV increased with increasing initial boron concentration. When increasing initial boron concentration, because of a stronger driving force owing to increasing ionic strength of the water, the OCV was improved to a higher level. The maximum power density values were calculated to be 13.44 mW/m^3 (20 mg/L B), 11.35 mW/m^3 (10 mg/L B), and 8.29 mW/m^3 (5 mg/L B) (Figure B.2b). A sudden surge in cell voltage was measured at day 1 due to the fresh source of electron donors (anaerobically acclimatized yeast wastewater), producing values of 760, 620, and 610 mV at 20, 10, and 5 mg/L B, respectively. After the cell voltages increased to reach previously mentioned maximum values, they entered a slightly decreasing trend most probably due to increase in internal resistance, which was the result of conductivity reduction and substrate depletion in anode chamber.

The overall CE was a function of COD concentration in anode chamber. CE values were determined by integrating the measured current relative to the theoretical current based on the consumed organic matter in anode chamber. The CE values were 12.6-15.3% across a range of initial boron concentration from 5 to 20 mg/L. The highest CE value was 15.3% at initial boron concentration of 20 mg/L. The higher CE value obtained at initial boron concentration of 20 mg/L could be attributed to higher concentration gradient lowering over potential caused by mass transport limitation on the anode electrode surface and anion exchange membrane surface. The CE values observed in this study were comparable with the other studies using synthetic wastewater as

substrate. (Anusha et al., 2018) studied on application of silver-tin dioxide composite cathode catalyst for enhancing performance of microbial desalination cell and the highest coulombic efficiency was found to be 14.4±0.2% in a five-chambered MDC. In a separate study, the methylene blue removal using polypyrrole modified cathode in bio-electro fenton coupled with MDC was studied and the average CE was found as 28.8% (Huang et al., 2018).

2.3.1.2. Effect of Airflow Rate

Effect of varying aeration rates on the removal of boron were investigated at specified air flow rates of 0 L/min (R1), 1 L/min (R4) and 2 L/min (R5) (Figure 2.3). Initial boron concentration was 5 mg/L and other operating parameters were kept constant (Catholyte solution: PBS buffer, $S_{electrode}$: 36 cm^2).

Microorganisms metabolizing the organic substrate at anode chamber produced electrons (e^-) which were transferred via the electrical circuit to the terminal electron acceptor of oxygen at the cathode chamber (Malakootian et al., 2018; Mirzaienia et al., 2017). With increasing dissolved oxygen concentration, boron removal efficiency increased. In the absence of supplied oxygen (no aeration), boron concentration decreased from 5 mg/L to 2.74 mg/L. With aeration in the cathode chamber, initial boron concentration of 5 mg/L was reduced below 2.4 mg/L meeting the boron limits set by WHO in drinking water. Maximum boron removal efficiencies were 45.2% ($C_{f,B}$: 2.74 mg/L), 51.5% ($C_{f,B}$: 2.425 mg/L), and 61.3% ($C_{f,B}$: 1.935 mg/L) at R1, R4, and R5, respectively. Increasing concentration of dissolved oxygen facilitated the e- transfer from anode chamber to cathode chamber, thereby consecutively improving electrical potential gradient and boron removal efficiency (Bergel et al., 2005). This was also observed in the measured OCV values of the system, which were measured to be 660 mV (R1), 668 mV (R4), and 676 mV (R5) (Figure B.3a-b). Similarly, the power density of the system increased from 7.71 mW/m^3 (R1) to 8.46 mW/m^3 (R4). Results showed that the OCV and power density increased with increasing air flow rate in cathode chamber due to the increased e^- acceptor (O_2) concentration in chamber, which caused improved e^- transfer from anode chamber to cathode chamber, resulting in low internal resistance due to increased electrical potential gradient. Consequently, these results demonstrated that air supply was beneficial in terms of enhanced power generation. Rest of the experimental

runs were conducted with 2 L/min aeration.

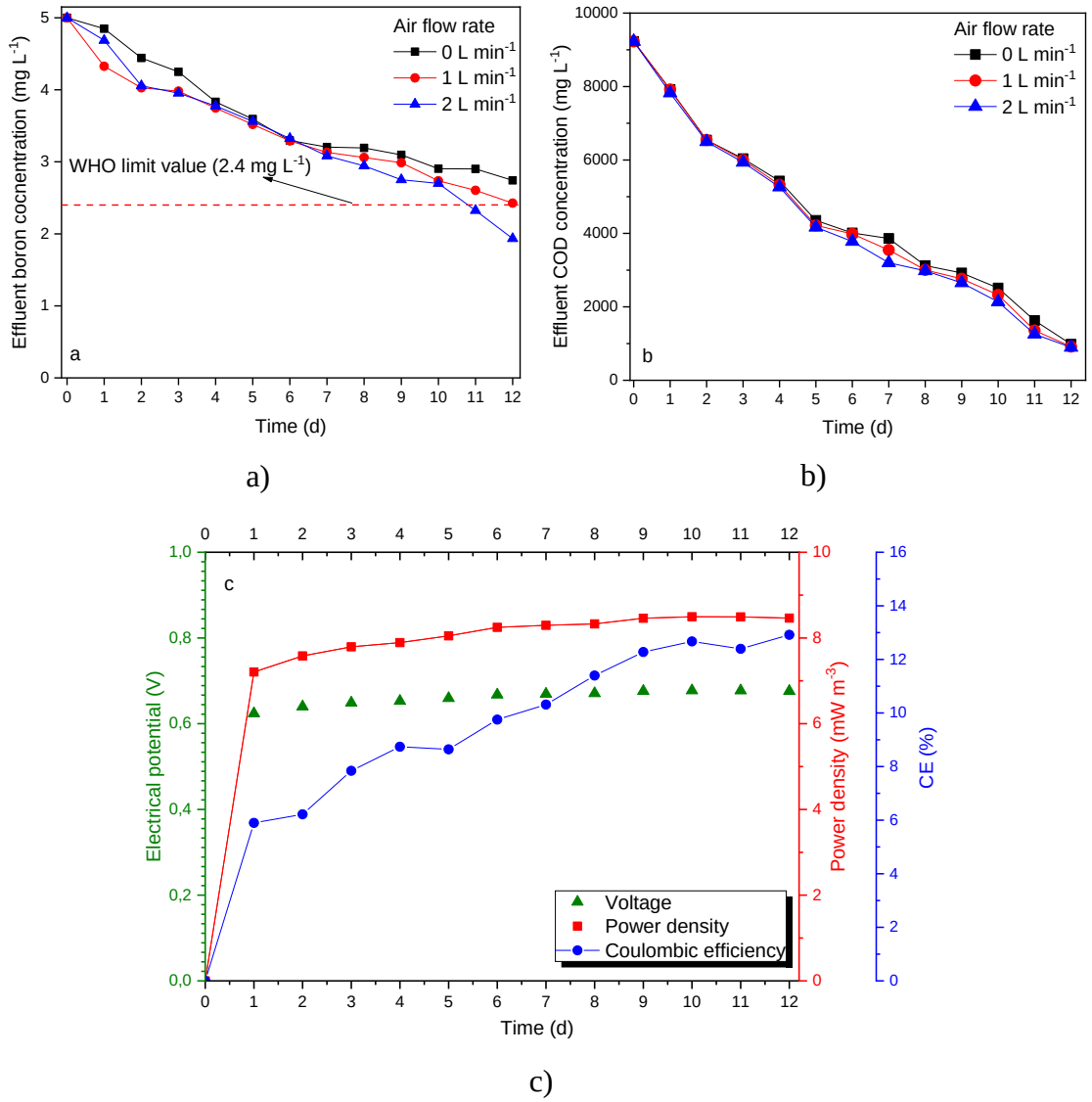

Figure 2.3. Effect of air flow rate on effluent boron concentration a), COD concentration b), and electrical potential, power density, and CE at optimum air flow rate c). (C_{Boron}: 5 mg/L, electrode surface area: 36 cm^2, catholyte solution: PBS buffer).

The CE values were also found to be 12.7, 12.8, and 12.9% for air flow rate of 0, 1, and 2 L/min, respectively. The cathode chamber was aerated with the O_2 which dramatically facilitated the electron transfer, it could be reasonable to expect a decrease in the MDC internal resistance. The decreased in internal resistance most probably reduce the MDC energy loss during electron transfer and thus enhance the CE. These results are good agreement with the literature. The removal of ammonium and phosphate ions using MDC with carbon cloth as air cathode and the CE values of the system were in the range

of the 7-15% (Chen et al., 2015). In a separate research, electricity production and desalination in a separator coupled stacked microbial desalination cell with buffer free electrolyte circulation was studied. The CE values were determined for three types of reactors and the CE values were reported in the range of 11-64% (Chen et al., 2012). Overall, our results demonstrated that air supply is beneficial in terms of high cell potential, power production, CE.

(Malakootian et al., 2018) studied arsenic removal from aqueous solutions using MDC and they found that the arsenic removal efficiency increased with increasing dissolved oxygen concentration. The maximum arsenic removal efficiency was found to be 75.0% at dissolved oxygen concentration of 6 mg/L within the operating time of 120 min. In a separate study, (Clauwaert et al., 2007) studied electricity production using an MFC without air supply and they found that the oxygen in cathode chamber was one of the most important operating parameters.

Results showed that aeration of cathode chamber did not have a significant effect on the COD removal efficiency of MDC. COD removal efficiencies were 89.4% ($C_{f,COD}$: 982 mg/L), 90.1% ($C_{f,COD}$: 916 mg/L), and 90.3% ($C_{f,COD}$: 897 mg/L) for air flow rates of 0, 1, and 2 L/min at operating time of 12 d, respectively. Previous studies on COD removal using MDC set-ups showed satisfactory COD removal efficiencies. For instance, the maximum COD removal from petroleum refinery wastewater using MDC was 70.5% at initial salt concentration of 20 g/L and using an acidified catholyte solution (Sevda et al., 2017). In a separate study, the highest COD removal rates from industrial wastewater by microbial fuel cell were in the range of 80-90% (Firdous et al., 2018).

2.3.1.3. Effect of Electrode Surface Area

Electrode material and electrode surface area are important parameters which affect the MDC performance in terms of desalination efficiency, energy production, and wastewater treatment (Wang et al., 2013). Carbon felt, carbon brush, activated carbon cloth, carbon cloth, graphite brush embedded in graphite granules, and graphite paper are commonly used electrode materials in MDC set-ups due to their high stability, conductivity, and low cost (Cao et al., 2009; Pant et al., 2010; Ragab et al., 2019b). However, none of the published studies investigated the effect of electrode surface area on MDC performance. In this study, we investigated the effect of different electrode

surface areas of 18 cm^2 (R6), 24 cm^2 (R7), 36 cm^2 (R1), and 72 cm^2 (R8) on boron and COD removal efficiencies (Figure 2.4). Initial boron concentration of 5 mg/L was used at optimized conditions.

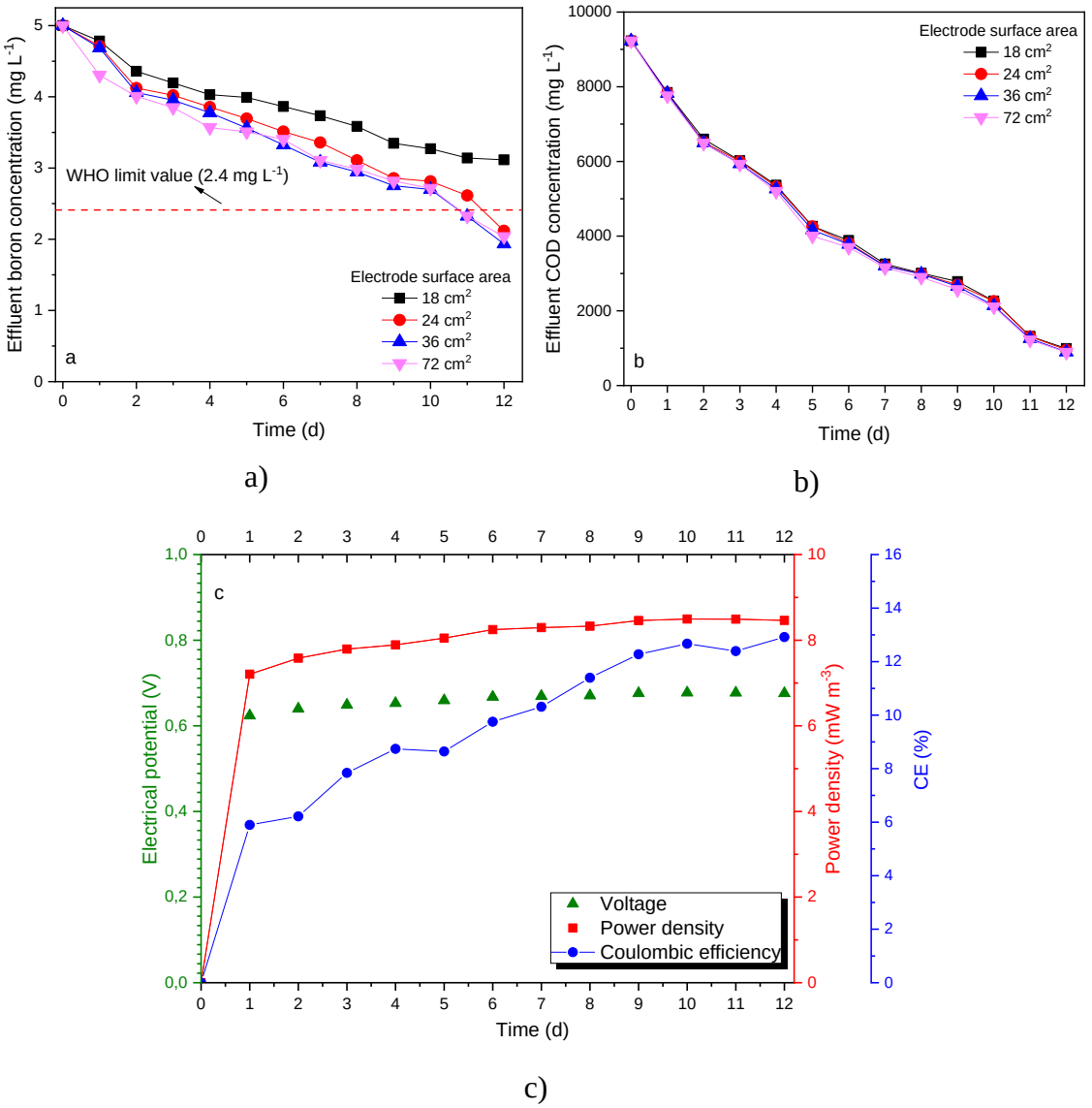

Figure 2.4. Effect of electrode surface area on effluent boron concentration a), COD concentration b), and electrical potential, power density, and CE at optimum electrode surface area c). (Catholyte solution: PBS buffer, C_{Boron}: 5 mg/L, air flow rate: 2 L/min).

Electrode surface area has a great impact on colonization of microorganisms, transportation of organic substrate, and formation of biofilm layer by microorganism. The colonization of microorganisms, transportation of organic substrate, and formation of biofilm layer by microorganisms can probably increase with the increment of the electrode surface area. Above mentioned probabilities were verified with experimental

results. As expected, the boron removal efficiencies increased with the increasing electrode surface area. Boron removal efficiencies were measured to be 37.7% ($C_{f,B}$: 3.115 mg/L), 57.6% ($C_{f,B}$: 2.118 mg/L), 61.3% ($C_{f,B}$: 1.934 mg/L), 61.4% ($C_{f,B}$: 1.932 mg/L) for R6, R7, R1, and R8, respectively. A significant increase in boron removal efficiencies were observed when results from R6 were compared with the other runs. Nevertheless, the removal efficiencies for R1 and R8, giving the maximum removal efficiencies, were practically the same. The bacteria that growth on the anode electrode surface oxidize the organic compounds, whereby generated e- move towards the cathode electrode. Borate ions moved from the desalination chamber to anode chamber, when electricity is generated concurrently. On the other hand, even if the electrode surface area increases, the amount of microorganisms in the anolyte solution and the amount of e^- they can produce is constant. Therefore, by increasing the surface area to a certain point, it is possible to increase the biofilm in the electrode surface area and thus increase the boron removal. However, the increasing electrode surface area could not show significant effect on removal efficiency due to the limited microorganism amount in anolyte solution. An initial approach of using 36 cm^2 electrodes was proven to be sufficient, since doubling the electrode area has not improved the boron removal efficiency. Rest of the experimental runs were conducted using 36 cm^2 electrodes.

Effluent COD concentrations were found to be 991, 954, 897, and 892 mg/L for electrode surface areas of 18, 24, 36, and 72 cm^2, respectively. As expected, there was no significant change at COD concentration as there was no change at the activated sludge volume and/or industrial wastewater volume in anode chamber. As a conclusion, changing activated sludge volume or wastewater type to improve microbial activity could be an effective method to improve the performance of MDC. However, there is no study about the effect of anaerobic activated sludge volume in anode chamber on MDC removal and energy production efficiency. Moreover, effect of electrode surface areas on OCV and power production were investigated (Figure B.4a-b). The highest OCV and power densities were found to be 607 mV and 6. 83 mW/m^3 (R6), 612 mV and 6.94 mW/m^3 (R7), 676 mV and 8.46 mW/m^3 (R1), 678 mV and 8.52 mW/m^3 (R8), respectively. The higher electrode surface area favored OCV and power density of the system owing to the higher e^- accumulation with the higher microorganism colonization on electrode surface area. These results confirmed that the electrode surface area can be significant operating parameter of MDC system.

As expected, the CE values increased with increasing electrode surface area from 18 to 72 cm^2. However, there was no significant difference in terms of CE values between 18-24 cm^2 and 36-72 cm^2 electrode surface experiments. The CE values were found to be 11.7, 11.8, 12.9, and 13.0% for electrode surface areas of 18, 24, 36, and 72 cm^2, respectively. Highest CE values were achieved at both electrode surface areas of the 36 and 72 cm^2 owing to decrease in internal resistance with the increasing biofilm formation resulted with high electron production and organic matter degradation.

2.3.1.4. Effect of Catholyte Solution

Phosphate buffer, ferricyanide, sodium acetate, and sodium chloride solutions, sodium phosphate buffer brackish water, mineral solution with microalgae as biocatalyst, and acidified water were commonly used as the catholyte solution in MDCs (Cao et al., 2009; Davis et al., 2013; Ge et al., 2014; Jacobson et al., 2011a, 2011b; Kim and Logan, 2011; Morel et al., 2012; Qu et al., 2012; Wen et al., 2014). There is a requirement for a cost effective, environmentally safe, and efficient catholyte solution for possible commercialization and scale-up of MDCs. Therefore, it is important to find the most suitable catholyte solution in order to develop cost effective and commercially feasible MDCs for boron removal from aqueous solutions. In this study, phosphate buffer (R1), acidified water (R9) and regular tap water (R10) were investigated as catholyte solutions (Figure 2.5).

Results showed that boron removal efficiency decreased when acidified water and tap water were used as catholyte solution. At the end of the operating time of 12 d, boron removal efficiencies were found to be 61.32% ($C_{f,B}$: 1.934 mg/L) , 44.1% ($C_{f,B}$: 2.795 mg/L), and 40.3% ($C_{f,B}$: 2.986 mg/L) for R1, R9 and R10, respectively. It should be considered that the concentration gradient of catholytes in MDC system might increase water flux from cathode chamber to desalination chamber. In MDC using PBS solution, the borate ion transfer was more efficient than that obtained through acidified water and tap water solution which led to a high performance of non-buffer saline catholyte in spite of pH imbalance. Furthermore, the boric acid was most probably remaining uncharged form due to the significant pH imbalance in desalination solution using acidified and tap water, which inhibit the formation of negatively charged borate ions and so effective removal of boron. When low concentration of phosphate buffer was used, the ions

concentration in desalination chamber could become higher than that of the cathode chamber. Therefore, water would move from cathode chamber to desalination chamber because of salt gradient, which might lead to higher desalination rate in MDC. However, (Kim and Logan, 2013) stated that these effects were negligible.

High concentrations of oxygen present in cathode chamber improved OH^- release, facilitating greater migration of positively charged ions from desalination chamber to cathode chamber. The close boron removal rate achieved in this study could be explained by the ionic charge of boron. As boron was negatively charged in desalination chamber, no significant effect of catholyte solution on boron removal was observed.

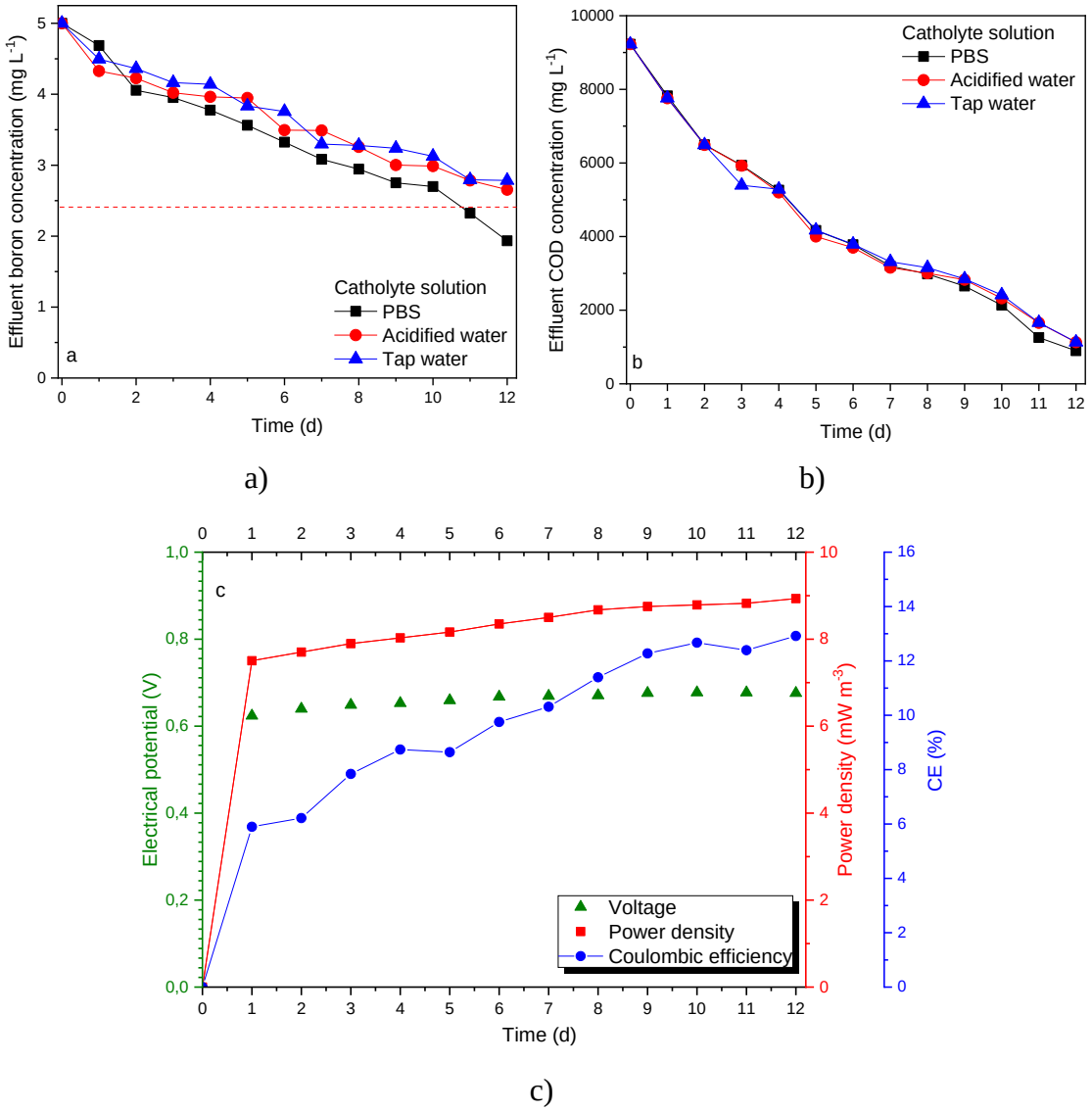

a) b)

c)

Figure 2.5. Effect of catholyte solution on effluent boron concentration a), COD concentration b), and electrical potential, power density, and CE at optimum catholyte solution c). (C_{Boron}: 5 mg/L, electrode surface area: 36 cm^2, and air flow rate: 2 L/min).

pH changes in desalination and cathode chamber were observed during operation (Figure B.1b). Acidified water solution resulted in the highest pH variation in desalination chamber, decreasing from 10.5 to 6.54 during the first 24 h of operation. The main reason that acid solution reduced boron removal efficiency could be explained by desalination solution becoming acidic, resulting in boron remaining in the form of uncharged boric acid. Cathode chamber's pH exhibited the quite opposite trend with an increase from 2.5 to 5.78 in the first 24 h. The anolyte solution showed the lowest pH variation when acidified water used as catholyte solution. On the other hand, MDC using phosphate buffer and tap water showed relatively lowest pH variation at desalination solution. The pH in desalination chamber decreased from 10.5 to 8.97 and 10.5 to 8.53 during the first 24 h of the operation for PBS buffer and tap water, respectively. No significant pH change was observed in anolyte for phosphate buffer and tap water solutions. Furthermore, effluent COD concentrations were found to be 897, 1128, and 1132 mg/L for R1, R9, and R10, respectively. As expected, there was no significant change at COD concentration.

The maximum OCV and power density values at R10, R1, and R9 were 642 mV and 7.61 mW/m^3, 676 mV and 8.93 mW/m^3, 714 mV and 9.43 mW/m^3, respectively (Figure B.5a-b). The lowest power density and OCV was achieved using tap water due to the low cell potential related to neutral pH of the solution. In contrast with tap water and PBS buffer, obtained results indicated that the acidified water increased OCV and power density of MDC due to the higher cell potential owing to lower pH of the solution. Furthermore, the acidified water caused significant pH variations in MDC system, which is resulted with excess chemical consumption due to the need of pH adjustment. Since the best results were obtained with PBS as catholyte, it was used for the rest of the experiments.

Furthermore, the effects of different catholyte solutions on CE values were determined and the maximum CE values were found to be 12.6, 12.9, and 14.0% for tap water, PBS buffer, and acidified water, respectively. These results obviously showed that the highest CE values were achieved at acidified water showing that the combination of oxygen and wastewater as the electron acceptor had the considerable benefit in CE. Since it is a strong oxidant and quickly depletes all the electrons in the cathode chamber and exerts a strong pull on electrons from the anode, as well as having good buffer capacity (Pandit et al., 2011).

2.3.1.5. Fed-batch Operating Mode

The effect of fed-batch operating mode on boron and COD removal was also investigated for varying initial boron concentrations (5 mg/L – R12, 10 mg/L – R13 and 20 mg/L – R14) at three cycles under determined optimum operating conditions (Figure B.6). Treated industrial wastewater in anode chamber was removed from the cell at the end of the operating time of 12 d (1st cycle), then fresh industrial wastewater was fed in anode chamber and it was repeated twice. Results showed continued decrease in boron concentrations under fed-batch operating mode. Effluent boron concentrations were 1.93, 1.46, and 1.05 mg/L for initial boron concentration of 5 mg/L at the end of cycles 1, 2, and 3, respectively. The highest boron removal efficiency was found to be 79% at the end of the third cycle. At the end of 12 d operations, boron migration from desalination chamber to anode chamber was quite slow as the system reached saturation. However, migration of B from desalination chamber to anode chamber was facilitated with the feed of fresh wastewater in anode chamber due to the increasing concentration gradient. The highest boron removal efficiencies were also found to be 78.8 and 74.5% for initial boron concentrations of 10 and 20 mg/L at the end of the third cycle, respectively. Furthermore, COD removal efficiencies were 89.7, 90.2, and 95.6% for R14, R13 and R12 at the end of each cycle. Results showed that there was no significant change in COD removal efficiency values at all cycles for different boron concentrations.

Results concluded that the boron removal efficiency of the MDC system was enhanced with fed-batch operation mode. (Luo et al., 2012b) studied desalination, wastewater treatment, and energy production using MDC in fed-batch mode. They reported that the maximum salt removal efficiency, COD removal efficiency and power production were 66.0%, 53.8% and 8 W/m^3 at optimum operating conditions in fed-batch mode. In a separate study, the highest power production and salt removal efficiency were found to be 1.1 W/m^3 and 64.2% using micro-algae and synthetic wastewater as a catholyte and anolyte solution, respectively (Kokabian and Gude, 2015). These studies showed that results were good agreement with the literature. Moreover, the COD and desalination efficiency of proposed MDC system were significantly high compared to the literature.

2.3.2. Membrane Fouling and Biofilm Formation in MDC

SEM images of AEM and CEM before (Figure 2.6a, 2.6d) and after (Figure 2.6b, 2.6c, 2.6e, 2.6f) the experimental runs were investigated. AEM images implied that the anode side of the AEM was colonized by microbes, forming a biofilm layer on membrane surface (Figure 2.6b). On the other hand, the desalination chamber side of the AEM did not show any signs for agglomeration of microbial origin but that of coarser grains (Figure 2.6c). In addition, the CEM surfaces facing desalination chamber and catholyte solution were covered with coarser crystal shape aggregations (Figure 2.6e and 2.6f). Biofilm formation on membrane surface might cause a decrease in membrane resistance, deterioration of membrane structure, and decrease of ion transfer and flux through membranes.

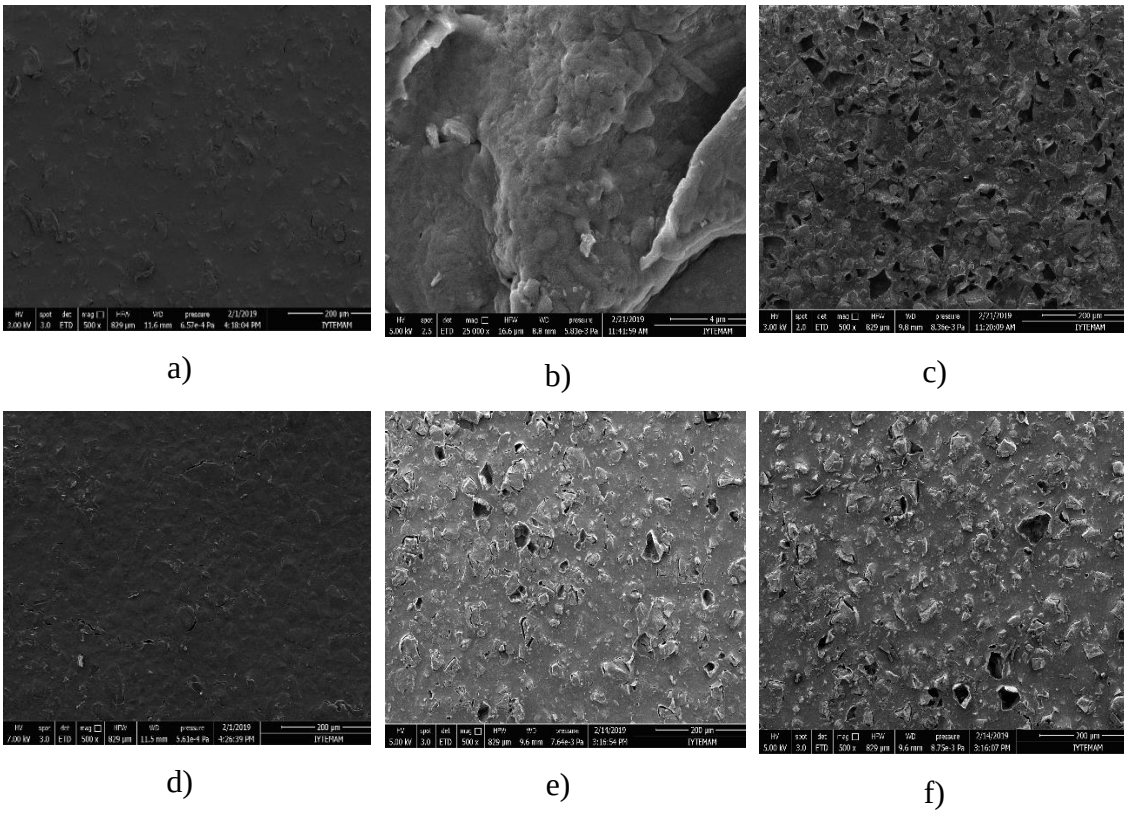

a) b) c)

d) e) f)

Figure 2.6. SEM images of membranes before and after operation. AEM surface before operation a), AEM surface facing with anode solution b), AEM surface facing with desalination solution c), CEM surface before operation d), CEM surface facing with cathode solution e), and CEM surface facing with desalination solution f).

The EDX results also showed a change of ion content on the membrane surfaces (Table B2). Carbon content of the AEM surface facing with anode solution decreased considerably from the initial 59.84% to 49.38%. The decreasing carbon content and increasing oxygen content was predicted to be on account of the deposition of organic matters on the AEM surface facing anode solution. Elements such as B and Cl were present on AEM surface after the operation. The B content of AEM was found to be 30.25 and 28.21% for surfaces facing anode solution and desalination solution, respectively. The presence of B and Cl elements were due to the transfer of anions from the desalination chamber and the composition of the wastewater (Angelov et al., 2013). As expected no significant change in carbon content was observed on the CEM surfaces. Oxygen content has increased significantly on CEM surface facing the catholyte due to active aeration that has been done.

Consequently, it could be concluded that there was more to be done in developing means to find an efficient way for in-situ membrane cleaning and to produce novel membrane materials which were more resistant to biofouling and ion agglomeration in MDC set-ups.

2.3.3. Boron Removal from Real Geothermal Water

An experimental was (R11) performed using real geothermal water at optimized conditions. Effluent boron and COD concentrations of treated geothermal water using MDC were presented in Figure B.7a and Figure B.7b, respectively. Boron concentration decreased from 10.5 mg/L to 5.8 mg/L at the end of the 12 d in geothermal water. Observed boron removal efficiency for real geothermal water (44.3%) was higher than that for 10 mg/L B synthetic solution (39.4%) for the same experimental conditions. This was probably due to the high ionic strength of the geothermal water. Concentration gradient of the system increased with the increasing ionic strength of the aqueous solution. As expected, boron removal efficiency of MDC for geothermal water improved owing to increased concentration gradient. Moreover, the COD removal efficiency was 90.6% at real geothermal water, while the COD removal efficiency was found to be 90.0% at 10 mg/L boron containing synthetic solution removal experiment. These results showed that there was no significant change at COD removal efficiencies for both synthetic and real geothermal water removal experiments.

2.3.4. Cost Assessment of MDC

This study demonstrated that the MDC could desalinate water with high ionic content, such as boron containing aqueous solution, and more complex waters, such as geothermal brine, and reduce energy consumption. The high energy consumption and treated water price are key factors in the operating cost of the desalination processes. Using the MDC, similar boron removal efficiencies were achieved with the single pass reverse osmosis system. While the MDC is an energetically self-sufficient system, reverse osmosis systems consume almost 2.2 kWh of electricity for treatment of 1 m^3 saline water. Furthermore, the MDC has almost 100% water recovery, while reverse osmosis processes maintain about 50% of the feed water as concentrate. In a scenario that conducts the MDC as pre-treatment before conventional desalination processes, the energy required by other desalination processes can be reduced owing to bioenergy production ability of MDC. The energy benefits of MDC processes should be further investigated with pilot scale studies.

A basic cost assessment was carried out to calculate the material cost of the MDC system including, AEM, CEM, carbon electrode, copper wire, Plexiglas, and other apparatus. The total material cost of the system for 540 mL MDC reactor set-up was found to be 30.2 $, and the AEM and CEM accounted for 23.5% of the total material cost. Therefore, the production of cost effective AEM and CEM could significantly reduce the material cost of MDC reactors. Besides, the high capital cost and low water production rates of bio-electrochemical systems are a major problem which hinder the its application in real scale. For instance, to accomplish a similar amount of water production, the MDC needs longer operating time than reverse osmosis processes, which may be balanced using a larger reactor volume, but that in turn increases capital costs. On the other hand, the benefits from wastewater treatment must be considered as MDC processes are an integrated technology of both desalination and wastewater treatment, when evaluating MDCs performance. The MDC systems can be constructed in a location that may access both saline and wastewater streams. Consequently, the capital cost of the MDC system can be similar to that of small scale wastewater treatment plants, with a possibility for further decrease, profiting from the development of low cost ion exchange membrane materials.

2.3.5. Resource Recovery Potential of MDC

The studied configuration of MDC allowed for the removed boron from the geothermal brine and synthetic solutions to accumulate at the anode chamber. Since the solution matrix of the anode chamber was quite complex due to activated sludge and yeast industry wastewater, boron recovery was not feasible. However, the primary objective of this study was to desalinate water streams such as geothermal brine that had high ionic content and for this particular study, high boron content. Following desalination, we aimed to produce irrigation quality water since agriculture sector claimed more than 70% of freshwater resources in Aegean region of Turkey, which was also rich in geothermal energy resources. Apart from that, supporting the desalination mechanism with selective adsorbents equipped MDC with the potential for resource recovery from geothermal brine regarding elements such as As, Li and B. Currently, a scaled up hybrid reactor configuration that employs adsorption, electrodialysis and membrane desalination is being studied in our lab.

2.4. Conclusion

This study revealed MDC as an environmental friendly and alternative solution for simultaneous boron removal from geothermal water and COD removal/energy production from industrial wastewater. Among the investigated operating parameters, electrode surface area had the most significant effect on boron removal efficiency, followed by air flow rate and catholyte solution. Furthermore, the removal efficiencies for selected electrode surface areas except for the electrode surface area of 18 cm^2, giving the promising removal efficiencies, were practically the same. The highest boron and COD removal efficiencies were achieved at air flow rate of 2 L/min, electrode surface area of 36 cm^2, initial boron concentration of 5 mg/L, using PBS buffer as the catholyte solution in the fed-batch mode. Even though the WHO's limit for boron concentrations in drinking waters was met the optimized experimental conditions, none of the experiments produced water at irrigation quality. In that aspect, MDC could be used as a polishing step applied to the effluents of other membrane treatment technologies such as nanofiltration and reverse osmosis. Results revealed that MDCs were promising systems for COD removal from industrial wastewaters with removal efficiencies exceeding 90%.

The simultaneous power generation helps with the desalination efficiencies through generation of chemical and electrical potential gradients. The highest electrical potential and power generation were found to be 852 mV and 13.4 mW/m^3 for 20 mg/L boron concentration. The results from fed-batch experiments showed that the MDC set-up continued desalination, yet more pronounced decreases in removal rate were observed in the subsequent cycles. It was obvious that the factors contributing to the internal resistance such as organic and inorganic membrane fouling and inter-membrane distance had to be tackled in further studies.

CHAPTER 3

SIMULTANEOUS ENERGY PRODUCTION, BORON AND COD REMOVAL USING A NOVEL MICROBIAL DESALINATION CELL

3.1. Introduction

In the era of climate change, water scarcity drives the inevitable paradigm shift regarding water resources and as a result, unconventional water resources are also being used to compensate for the decrease in the quantity of conventional ones. Geothermal water emerges as an important alternative water source to supply the demand for drinking, domestic, agricultural and industrial purposes. However, geothermal water sources may contain components of unfavorable nature or of unacceptable levels due to hydrogeology of aquifers and anthropogenic sources, hindering the exploitation of geothermal water resources (Aksoy et al., 2009; Baba and Ármannsson, 2006). Geothermal waters can be characterized by diverse physicochemical parameters depending on their hydrogeological properties, characteristics of the rocks involved, the depth at which resources occur and the source of water supply. Geothermal waters may contain significant amounts of neutral species, cations and anions (Haklıdır and Şengün, 2020; Villalba et al., 2020). These parameters largely determine the technology to be used in geothermal water treatment in regard with the relevant limits that are dictated by the final use. Amongst the ions that are present, boron content is critical in geothermal waters, which contain higher concentrations than sea water and brackish water.

Boron in geothermal waters has been found due to natural sources including soils containing borosilicate and borate, mineral dissolution from rocks, and volcanic activities or anthropogenic sources like cleaning products, detergents, borosilicate glass, semiconductors, fertilizers, and flame retardants production (Kartikaningsih et al., 2016).

This chapter has been published as:
A.Y. Goren, H.E. Okten, Simultaneous energy production, boron and COD removal using a novel microbial desalination cell, Desalination 518 (2021) 115267.

At low pH values in geothermal water sources, H_3BO_3 is the dominant species (the uncharged form of boron), while above pH 9.2, negatively charged $B(OH)_4^-$ is the dominant species (Barth, 2000; Kabay et al., 2015). Long term exposure to boron through drinking water and/or vegetables may cause several symptoms such as diarrhea, dermatitis, nausea, lethargy, and also more severe issues such as physical and intellectual setbacks at children, nonfunctional cardiovascular, nervous, and reproductive systems (Bryjak et al., 2008; Hou et al., 2010; Melnyk et al., 2005; Nielsen, 2002). The limit values recommended for boron in drinking water from WHO and European Union (EU) are 2.4 mg/L and 1 mg/L, respectively (Directive, 1998; Organization, 1998). In Turkey, the maximum permissible level of boron in drinking water is set at 1 mg/L by Directive of Water Intended for Human Consumption (Official Journal, 2013). Furthermore, boron is an important micronutrient for plants, its required levels for growth depend on the plant type. Reported tolerable boron concentrations in irrigation water for plant growth vary, for instance as asparagus, palm, bean, and onion may be able to tolerate 4 mg/L B, blackberry and lemon orchards may tolerate only 0.5 mg/L B. (Hilal et al., 2011; Yilmaz et al., 2008). Exposure to boron above tolerance levels may be detrimental for plants (García-Sánchez et al., 2020). Therefore, in the case of using geothermal brine as irrigation water, removal of boron becomes a critical and challenging topic.

Several techniques have been developed for treatment of boron in water and wastewater, including coagulation, sedimentation, filtration, adsorption, membrane processes such as reverse osmosis (RO), biological process, ion-exchange, electrocoagulation, electrodialysis, and hybrid processes (Ban et al., 2019; Chen et al., 2020; Hussain et al., 2019; Kayaci et al., 2020; Skoczko, 2020). However, most of these technologies have numerous disadvantages such as high operating and maintenance costs, high amount of sludge formation and chemical consumption, need for additional pretreatment, and high energy consumption. Bioelectrochemical systems (BESs) are promising, emerging, and environmentally friendly technologies compared to conventional treatment processes (Jafary et al., 2020; Ma and Hou, 2019). The most studied BESs are microbial fuel cells (MFCs) and microbial desalination cells (MDCs), which convert chemical energy from organic matter to electrical energy using microorganisms (Kim and Logan, 2013; Ping et al., 2016, 2015). While MFCs and MDCs are able to couple biological wastewater treatment with energy production, MDCs are also able to perform desalination. Microbial desalination cell (MDC) is practically derived from MFCs by inserting (i) an anion exchange membrane (AEM) between anode

chamber and desalination chamber and (ii) a cation exchange membrane (CEM) between desalination and cathode chambers (Kim and Logan, 2013). Electrons that are produced due to oxidation of organic substrates at anode chamber, which is kept strictly anaerobic, are given to the circuit connecting anode and cathode electrodes. The objective is to form an electrochemical gradient across the oxidative anodic and reductive cathodic chambers, facilitating the desalination process. Migration of ions in desalination cell across the membranes based on concentration and electrochemical gradients through diffusion is the driving force for desalination process.

However, MDCs present several drawbacks such as low removal efficiency, membrane fouling, low energy production due to the electrode type and material, and decrease in microbial activity related to salinity increase (Wang et al., 2013; Zuo et al., 2018). Moreover, the commonly used carbon felt, carbon paper, and graphite felt electrode materials in MDC have significant drawbacks, such as low electrode surface area for microbial colonization and organic substrate transport, unsuitable surface to form biofilm layer by microorganisms, difficulties of maintenance, and low flexibility (Ma and Hou, 2019; Pant et al., 2010; Zhang et al., 2019). Recently, research on investigation of three dimensional (3D) carbonaceous electrodes have attracted interest owing to their significant benefits on BES performance such as, high surface area and easy multiple direction transport of pathways with macro-porous structure, and high electron storage capacity (Do et al., 2018; Li et al., 2017; You and Kamarudin, 2017). The MFCs were enhanced with modifying the electrodes with 3D nano-sized and porous materials including, N-doped carbon cloth, biochar, carbon nanotube-chitosan modified carbon paper, graphene/polyaniline nanocomplex modified carbon cloth, and graphene/polyaniline modified carbon paper (Sun et al., 2017; Wang et al., 2017; Yuan et al., 2019). However, there is only one research article investigating the potential of MDC with 3D sponge electrode coated using carbon nanotube-chitosan (Ma and Hou, 2019). The MDC using 3D sponge electrode showed a high power density of 1776.6 mW/m^2 and desalination rate of 16.5 mg/h, which were considerably higher than those of two dimensional (2D) carbon felt electrodes under same operating conditions. It should be noted that these materials were also prone to some drawbacks such as, high cost, difficult synthesis, and requirement of advanced facilities (Ahirrao et al., 2019; Do et al., 2018). Therefore, studies related to electrode material and type have attained significant attention. Moreover, several studies investigated the performance of MDCs on wastewater treatment, desalination, and energy production under different operating

conditions (Liaquat et al., 2021; Rahman et al., 2021a; Ramírez-Moreno et al., 2021). Catholyte solution, anolyte solution, temperature, initial salt concentration, intermembrane distance, retention time, and mode of operation were widely investigated operating parameters for optimization of MDC process (Al-Mamun et al., 2018; Ge et al., 2014; Hemalatha et al., 2017; Kim and Logan, 2011). (Ebrahimi et al., 2018b) investigated the performance of MDC for energy production and salt removal using different catholythes such as phosphate buffer solution (PBS), non-buffer saline solution, and bio-catholyte. The MDC using bio-catholyte solution showed the highest power density (32.6 W/m^3) and desalination rate (0.38 g NaCl/Lh), while the power density and desalination rate of MDC with saline buffer solution were 29.4 W/m^3 and 0.34 g NaCl/Lh, respectively. Effects of retention time (30-120 min), temperature (mesophilic, thermophilic, and psychrophilic), and dissolved oxygen concentration (2-6 mg/L) on MDC process for optimization of arsenic removal from aqueous solution were investigated in a separate study (Malakootian et al., 2018). The maximum arsenic removal efficiency of 56 % was achieved at temperature range of 25-30 °C, retention time of 120 min, and dissolved oxygen concentration of 6 mg/L.

In this study, we designed a novel MDC reactor with 3D cubic electrodes contained in a cell, which was placed in the anode chamber. We investigated and compared the performance of MDC with 2D and 3D cubic electrodes in removing boron from synthetic solutions and real geothermal water and in removing COD from yeast industry wastewater, all the while producing energy. Objectives of this study were investigating (i) the effects of activated sludge volume, anolyte temperature, and electrode type on 3D-MDC performance in batch mode operation, (ii) effect of operational parameters on energy production of 3D-MDC, and (iii) performance of the optimized system in removal of boron from real geothermal water using 3D cubic electrodes and 2D carbon graphite electrode. It should be noted that this is the first study investigating the effect of activated sludge volume and presenting performance of MDC on boron removal from real geothermal water. Consequently, this study is the first and most comprehensive research paper on applicability of conventional 2D-MDC and novel 3D-MDC for simultaneous boron removal, wastewater treatment, and energy production at optimum operating conditions.

3.2. Materials and Methods

3.2.1. Characterization and Preparation of Water Samples

Geothermal water was collected from geothermal power plant deep wells located in İzmir, Turkey and was kept in polyethylene containers throughout experiments. All species present in geothermal water were analyzed using American Public Health Association (APHA) standard methods (Federation and Association, 2005). Characterization of geothermal water yielded the following results, EC: 1770 µS/cm, pH: 8.04, K: 30.1 mg/L, Na: 452 mg/L, Ca: 24.8 mg/L, Mg: 7.44 mg/L, SO_4^{2-}: 178 mg/L, Mn: 0.027 mg/L, Cl^-: 205 mg/L, F^-: 8.21 mg/L, SiO_4^{4-}: 24 mg/L, As: 0.17 mg/L, B: 10.48 mg/L, Fe: 0.055 mg/L, and Li: 1.41 mg/L. Industrial wastewater was collected from a yeast production facility's wastewater treatment plant in İzmir. Industrial wastewater was also characterized, pH: 7.72, COD: 9228 mg/L, K: 868 mg/L, NH_4^+: 452 mg/L, NO_3^-: 25.6 mg/L, Na: 1608 mg/L, Ca: 299 mg/L, Mg: 77.5 mg/L, SO_4^{2-}: 1117 mg/L, PO_4^{3-}: 7.68 mg/L, Mn: 0.183 mg/L, Cl^-: 1573 mg/L, F^-: 0.2 mg/L, SiO_4^{4-}: 66 mg/L, As: 0.007 mg/L, B: 0.142 mg/L, and Fe: 0.571 mg/L. Synthetic boron (B) solutions were prepared daily by dissolving boric acid salt (H_3BO_3, Sigma-Aldrich). Solution B concentrations simulated geothermal water composition of Turkey (Baba and Sözbilir, 2012; Ozbey-Unal et al., 2018). Solution pH was adjusted to pH 9.5 using 0.1 M sodium hydroxide (NaOH, Sigma-Aldrich). Catholyte solution was prepared using 10 mM potassium phosphate buffer (K-PB).

3.2.2. MDC Set up and Operation

MDC bioreactor consisted three identical plexiglass chambers: anode, desalination, and cathode chambers, with dimensions of 15 cm × 6 cm × 6 cm (Figure 3.1a). Chambers were clamped together using gaskets and O-rings with stainless steel bolts in order to prevent leakage. Anode and desalination chambers were separated by an anion exchange membrane (AEM, AMI-7001, Membrane International Inc., USA) while cathode and desalination chambers were separated by a cation exchange membrane (CEM, CMI-7000, Membrane International Inc., USA). Carbon graphite material was used for 2D electrodes (GoodFellow, England). Our previous studies have shown 36 cm^2

to be the optimum electrode area for 2D electrodes in our MDC system (Goren and Okten, 2021a). The novel MDC design accommodated a plexiglass electrode cell in the anode chamber, with dimensions of 6 cm × 4.5 cm × 4.5 cm, bearing 9 mm^2 holes on its surfaces (Figure 3.1b). The electrode cell held 1 cm^3 3D cubic electrodes (Walfront, Canada) each having a surface area of 6 cm^2. In both cases, 2D and 3D electrodes, electrical connection between electrodes was done via copper wiring.

Anode chamber was filled with anaerobic activated sludge and yeast wastewater mixtures of varying volumetric ratios (S:WW = 1:1, 1:2, and 1:5) and the mixtures were continuously stirred (185 rpm) to prevent settling. Cathode chamber was filled with phosphate buffer and it was aerated at a rate of 2 L/min with air. Desalination chamber was filled with boron containing solutions or geothermal wastewater. The initial boron concentration was selected as 5 mg/L as an optimum concentration for MDC with 2D electrodes based on our previous study (Goren and Okten, 2021a). Anolyte solution temperatures (20 ºC, 40 ºC, and 60 ºC) and electrode geometry at optimum conditions were investigated. Based on the preliminary studies, the reactor was operated for 12 days, the day marking 90% substrate degradation based on COD measurements. During experiments, voltage values were recorded to calculate the power density of the system.

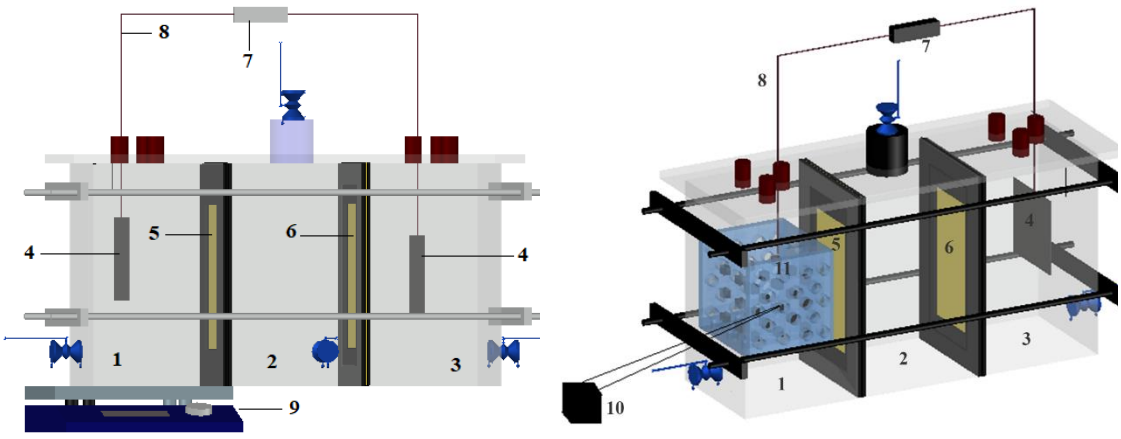

a) b)

Figure 3.1. The schematic diagram of MDC bioreactors a) and b): (1) Anode chamber, (2) Desalination chamber, (3) Cathode chamber, (4) Carbon graphite electrode, (5) AEM, (6) CEM, (7) External resistor, (8) Copper wire, (9) Mechanic stirrer, (10) 3D cubic electrode, and (11) anode electrode cell.

3.2.3. Analytical Methods

Voltage (V) in the open circuit of MDC was recorded every 15 min using a data logging system (UNI-T, UT71C Digital Multimeter). Daily pH changes were measured by a pH meter and adjustments were done (Mettler Toledo, SevenCompactTM). Samples from experimental runs were collected daily, acidified using 0.1N HCl, and then stored at 4 °C until analysis. Boron concentrations were measured using an inductively coupled plasma optical emission spectrometer (ICP-OES, AGILENT 5110). Anions and cations in water samples were measured using ion chromatography (IC, Dionex ICS-5000). All analyses were conducted in triplicate measurements. COD was measured using a closed reflux titrimetric method according to standard methods. AEM and CEM surface morphologies were examined by scanning electron microscopy (SEM, Quanta-250FEG). Furthermore, elemental mapping of membrane surfaces was done using Energy Dispersive X-ray spectrometry (EDX, Quanta-250FEG).

Boron and COD removal efficiencies were calculated following the equations (3.1) and (3.2), respectively:

$$R_B(\%) = \frac{\left(C_{B,i} - C_{B,e}\right)}{C_{B,i}} \times 100 \quad (3.1)$$

$$R_{COD}(\%) = \frac{\left(C_{COD,i} - C_{COD,e}\right)}{C_{COD,i}} \times 100 \quad (3.2)$$

where $C_{B,i}$ and $C_{B,e}$ were the initial and effluent boron concentrations in desalination chamber, respectively. $C_{COD,i}$ and $C_{COD,e}$ were the initial and effluent COD concentrations in anode chamber, respectively.

Current (I) under 100 Ω external resistance (R_{ex}) was determined by $V = I \times R_{ex}$. Power density (P, mW/m^3) was determined through $P = (V \times I) / v$, where v (m^3) was the volume of the anode chamber. Furthermore, the ratio of transferred electric charge (1) to its maximum value obtainable (coulombic efficiency - CE, %), and (2) to total e^- available in the anode chamber (coulombic recovery - CR, %) were calculated by equations 3.3 and 3.4, respectively:

$$CE(\%) = \frac{MW_{O2} \int_0^t Idt}{nFV_a(C_{COD,i} - C_{COD,e})} \times 100 \quad (3.3)$$

$$CR(\%) = \frac{MW_{O2} \int_0^t Idt}{nFV_a(C_{COD,i})} \times 100 \quad (3.4)$$

where MWO_2 was the molecular weight of oxygen (32 g/mol), n was number of the e^- transferred from organic matter degradation (n: 4 mol e^-/mol), F was the Faraday's constant (96485 C/mol), and V_a was the volume of anode chamber (0.54 L).

3.3. Results and Discussion

3.3.1. Effect of Activated Sludge Volume

The major energy production mechanism of bioelectrochemical systems depended on the biodegradation of organic matter from various types of sludge or wastewater by microbial activity (Al-Mamun et al., 2018; Noori and Najafpour Darzi, 2016). Microbial growth in the absence of an electron acceptor was one of the main factors that determined the performance of MDCs. Hence, understanding microbial growth mechanisms, medium composition, organic matter concentration, the activated sludge or wastewater types and microorganism physiology would help to improve the MDC efficiency (Gholizadeh et al., 2017; Hemalatha et al., 2017; Meng et al., 2019; Salman and Ismail, 2020; Tamta et al., 2020; Tawalbeh et al., 2021, 2020; Utami et al., 2015). Anaerobic activated sludge volume's effect on MDC performance has not been studied before.

In this study, we varied the S:WW parameter (1:1, 1:2, and 1:5) and investigated its effect on B removal (Figure 3.2a) and COD removal (Fig. 3.2b). While varying S:WW did not have a significant effect on B removal efficiency (62%), increasing activated sludge's volume from 90 mL (1:5) to 270 mL (1:1) improved COD removal efficiency from 60.1% to 90.3%. Charge-selective diffusion of ionic species through the membrane is the main driving mechanism in desalination with MDC. That mechanism can be further enhanced by concentration and electrochemical gradients. Since the boron concentration used in this part of the study was low (5 mg/L), the concentration gradient's improving effect on the rate of diffusion was not present. Although increasing S:WW values were

expected to form an electrochemical gradient, which in turn would enhance the diffusion rate and thus removal efficiency, it was not possible to discern the data points for each experimental run due to the low initial concentration of boron. In order to elucidate the effect of concentration gradient, the removal rate of 0.256 mg B/Ld, which was acquired for S:WW of 1:1, was compared with results from (Goren and Okten, 2021a)] for 10 mg/L and 20 mg/L initial boron concentrations. Results showed considerable improvements in removal rate, 0.343 mg B/Ld for 10 mg B/L and 0.7 mg B/Ld for 20 mg B/L.

The considerably low COD removal efficiencies at S:WW of 1:5 and 1:2 were probably due to the low microbial concentration and hence activity in anolyte. These results also showed that decreased activated sludge volumes implied longer operating periods in order to meet required COD removal efficiencies. Throughout the study, calculated standard deviation values for the replicates were too low (below 0.1 mg/L) to be discerned on the plots.

The open circuit voltage (OCV) of the system was recorded to be 452, 646, and 676 mV for S:WW of 1:5, 1:2, and 1:1, respectively (Figure C.1a). The power density of the system increased from 3.78 to 8.46 mW/m^3 with the increase in volumetric ratio from 1:5 to 1:1 (Figure 3.2c). The higher OCV and power density produced at higher activated sludge volumes were likely due to higher energy production with increasing microbial activity (Figure 3.2c). Similarly, the CE and CR values of the system increased with the increasing S:WW. The maximum CE values were 14.26%, 13% and 12.9% for ratios of 1:1, 1:2, and 1:5, respectively. Also the CR values followed a decreasing trend of 11.66%, 11.14%, and 7.79% for decreasing activated sludge volumes of 270 mL, 180 mL and 90 mL, respectively. As can be seen in Eq. 3.3 and 3.4, the CE and CR values were expected to decrease with increase in the initial COD concentration in anode chamber. Therefore, the simultaneous increase in OCV, power density, CE, and CR being observed at 1:1 ratio was due to increasing COD removal efficiency in anode chamber with the increasing microbial activity for organic matter degradation. Our results were also in good agreement with the literature. For instance, in an MFC study CE values of 10% and 25% were reported when the organic loading was increased from 500 mg/L to 4500 mg/L, respectively (Rodrigo et al., 2007).

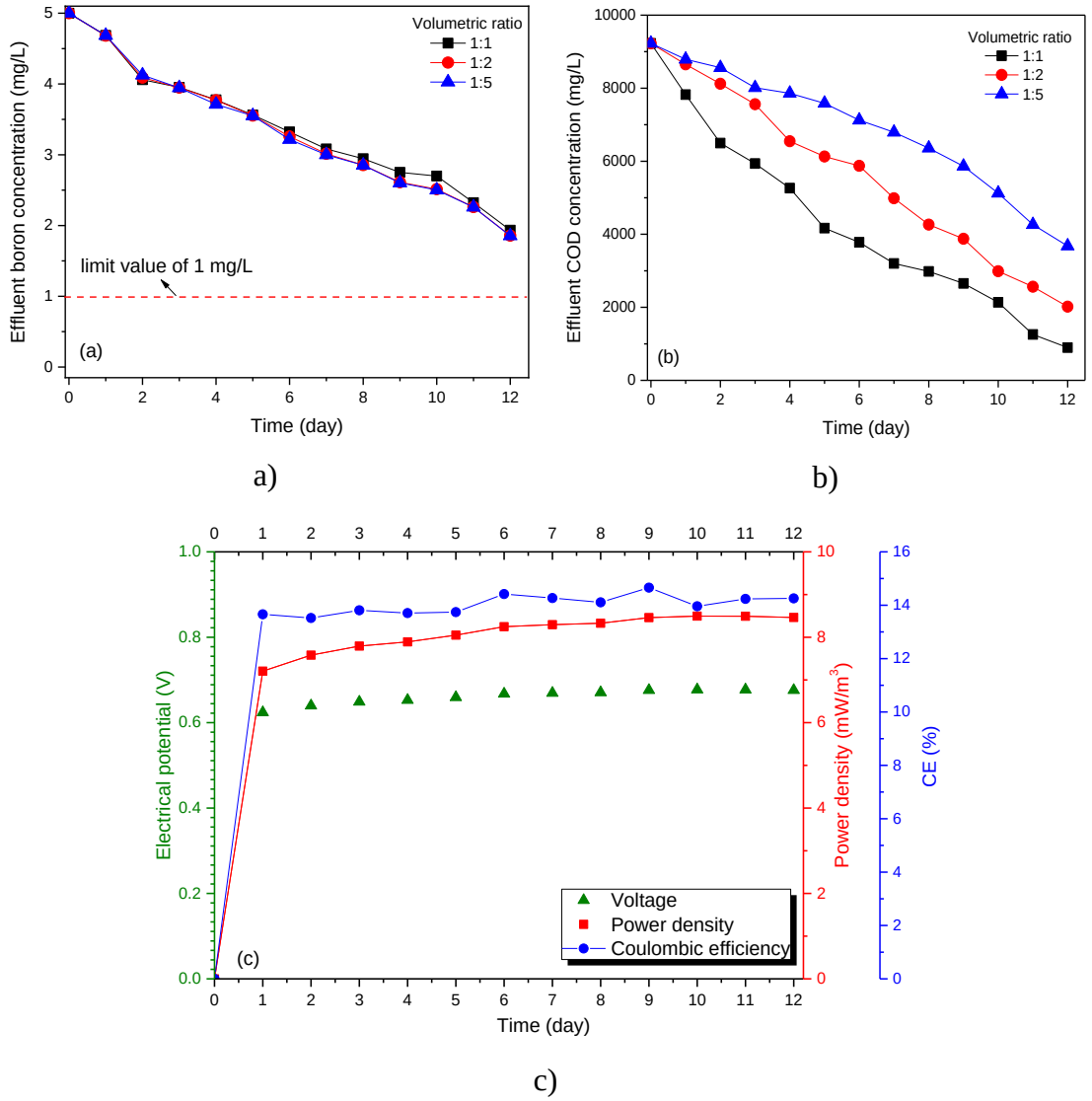

Figure 3.2. Effect of varying volumetric ratios on boron removal a) and COD removal b); electrical potential, power density, and Coulombic efficiency at optimum volumetric ratio of 1:1 c).

3.3.2. Effect of Anolyte Solution Temperature

Temperature is another important operating parameter that may significantly impact the performance of bioelectrochemical systems. Factors such as internal resistance, solution conductivity, electrode potential, and microbial growth that may affect the MDC performance are all temperature dependent (Larrosa-Guerrero et al., 2010; Tkach et al., 2017). Low operating temperatures, i.e. room temperature, at MDC system can be cost effective, which reduce the requirement for external power for heating. Although MFC performances under different temperatures have been investigated before

(Jadhav and Ghangrekar, 2009; Song et al., 2017; Wei et al., 2013), there are limited studies for MDCs (Malakootian et al., 2018, 2019; Ragab et al., 2019a).

In this study, three different anolyte solution temperatures (20 ºC, 40 ºC, and 60 ºC) were investigated for previously determined optimum operating conditions ($pH_{catholyte}$: 6.5, Q_{air}: 2 L/min, V_{sludge}: 270 mL, $V_{wastewater}$: 270 ml, C_{Boron}: 5 mg/L, $S_{electrode}$: 36 cm^2). As presented in Figure 3.3a, the highest boron removal efficiency of 61.3% ($C_{f,B}$: 1.93 mg/L) was observed at anolyte temperature of 40 ºC. Boron removal efficiencies were also found to be 47.7% ($C_{f,B}$: 2.62 mg/L) and 44.7% ($C_{f,B}$: 2.76 mg/L) for anolyte temperature of 20 and 60 ºC, respectively. Anaerobic processes are commonly maintained at 30 ºC - 40 ºC (mesophilic) and 50 ºC - 60 ºC (thermophilic) temperature ranges (Levén et al., 2007). At mesophilic temperatures, the metabolic rate of microorganisms increases resulting in better substrate degradation rates (Sanchez et al., 2000; Zábranská et al., 2000), accelerated electron generation by microorganisms, increasing current production and hence improving desalination efficiency (Jacobson et al., 2011a). Therefore, the mesophilic anolyte solution temperature of 40 ºC yielded the best B removal efficiency. On the other hand, temperatures of 20 ºC and 60 ºC resulted in similar removal efficiencies. The metabolic activity of microorganisms decreases at temperatures below 20 ºC (psychrophilic). In thermophilic temperatures, the microbial growth and decay are faster with enhanced metabolic activity, which reduces the removal of ions (Malakootian et al., 2018). (Mirzaienia et al., 2017) investigated the nickel and lead removal from industrial wastewater using MDC and reported that the highest removal efficiency was achieved at mesophilic temperature. In another study of (Malakootian et al., 2018) the maximum arsenic removal efficiency was 68 % at optimum operating conditions (dissolved oxygen concentration of 6 mg/L, mesophilic temperature, operating time of 120 min) for the studied MDC setup.

COD removal efficiencies were 76.9 % ($C_{f,COD}$: 2128 mg/L), 90.3% ($C_{f,COD}$: 897 mg/L), and 78.3% ($C_{f,COD}$: 1998 mg/L) for anolyte temperatures of 20 ºC, 40 ºC, and 60 ºC, respectively (Figure 3.3b). As expected, the highest removal efficiency was obtained at 40 ºC owing to faster substrate degradation. Expectedly, the COD removal efficiency decreased significantly at 20 ºC with the decrease in microbial activity rate. Furthermore, the effluent COD concentration remained constant at 60 ºC after the 10th day most probably due to faster growth and decay rates of microorganisms.

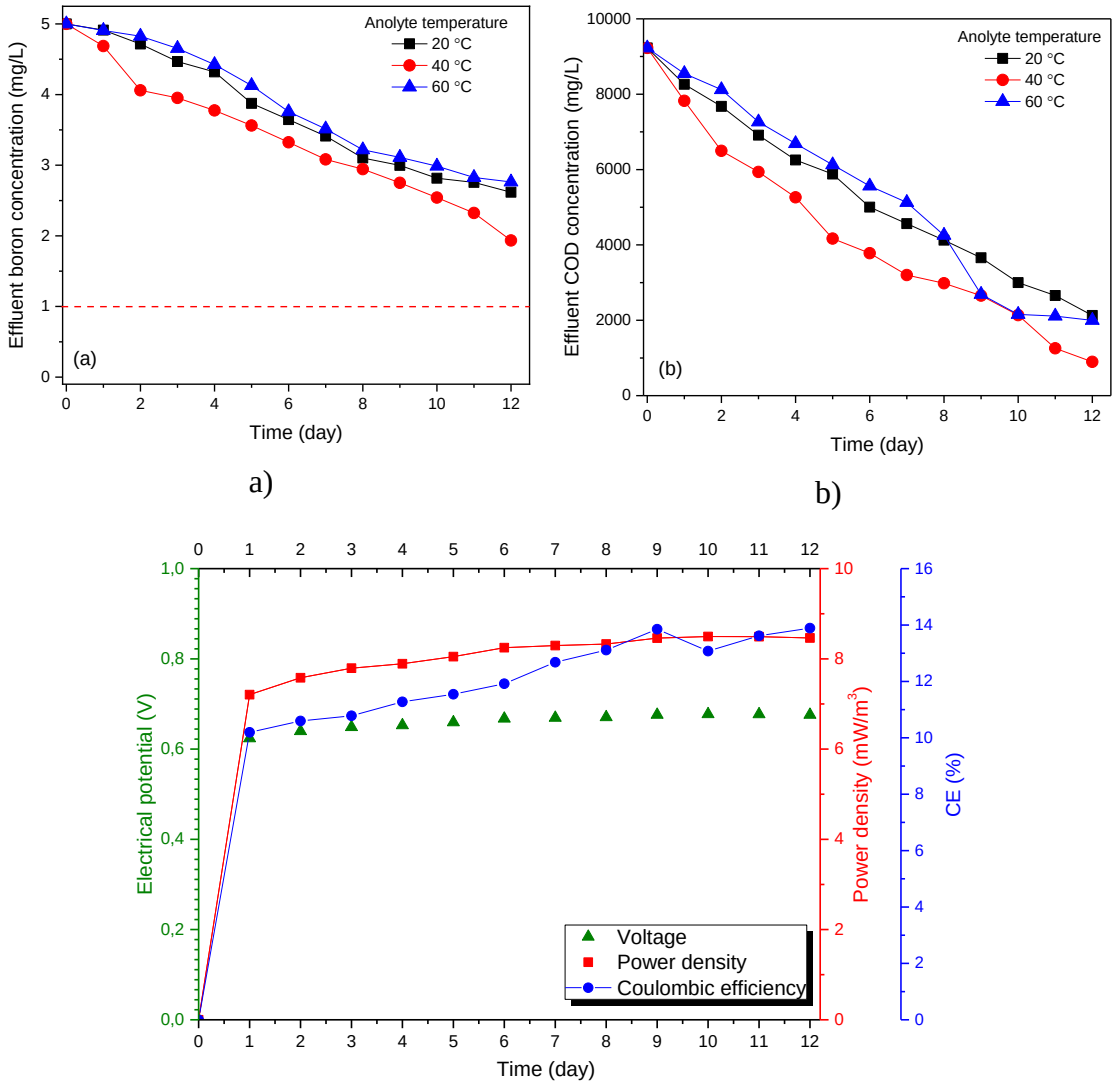

Figure 3.3. Effect of anolyte temperature on boron removal a), COD removal b); electrical potential, power density, and Coulombic efficiency at optimum temperature of 40 °C c).

The results on OCV and power density showed that the energy production performance of the system was also affected by anolyte solution temperature (Figure 3.3c). We observed that at the operating time of 12 days, OCV was 676 mV at anolyte solution temperature of 60 ºC, which was almost 1.2 times higher than 20 ºC (571 mV) and 60 ºC (556 mV) results (Figure C.2a). The highest power density values were found to be 6.04 mW/m^3, 8.46 mW/m^3, and 5.73 mW/m^3 for anolyte solution temperatures of 20 ºC, 40 ºC, and 60 ºC, respectively (Figure C.2b). These results most probably explained with that the microbial activity rates for microorganism growth and organic matter degradation were increased with increasing temperature up to a certain temperature that

microorganisms can live (Grady Jr and Lim, 1999). Besides, increasing microbial growth may also enhance biofilm formation at an electrode surface. The conductivity of the anolyte solution is increased with increase in temperature as reported Arhenius Laws and thus the electron transfers increases (Larminie et al., 2003). Furthermore, according to the Bulter-Volmer equation (Bard and Faulkner, 2001), the reactions on the electrode surfaces are increases at high temperatures. On the other hand, as mentioned before, in thermophilic temperatures (> 60 ºC), the energy production efficiency of the system decreases due to the faster decay of microorganisms.

Similar trends were observed for the CE and CR values of the MDC system. The CE and CR values were 12.9% and 9.9%, 13.9% and 11.7%, and 12.8 % and 9.6% for temperatures of 20 ºC, 40 ºC, and 60 ºC, respectively. As expected, the highest CE and CR values were obtained at 40 ºC. Consequently, our results suggested that the MDC at moderate anolyte solution temperature (40 ºC) was possible for real application for geothermal brine treatment with higher energy production.

3.3.3. Effect of Electrode Type

The electrode material affects the MDC's performance in terms of desalination efficiency, energy production, and wastewater treatment. Recently, researchers focused on the development of three-dimensional electrode materials due to their high effective surface area which is favorable for biofilm growth, and high conductivity which can provide efficient electron transfer between the microorganisms, high charge storage capability and electrolyte penetration (Hou et al., 2014; Yuan et al., 2018). Therefore, we designed a novel MDC system with 3D cubic carbon electrodes to improve the effective use of electrode materials.

The effect of novel electrode cell with 3D cubic carbon electrodes on boron and COD removal efficiencies was compared with the carbon plate electrode material (Figure 3.4a and 3.4b). The electrode surface areas of both electrodes was selected as 36 cm^2 (V_{sludge}: 270 mL, Q_{air}: 2 L/min, $V_{wastewater}$: 270 ml, $pH_{catholyte}$: 6.5, $T_{anolyte}$: 40 ºC, and operating time: 12 days). The boron and COD removal efficiencies increased with 3D cubic electrodes. Boron removal efficiencies were measured as 61.3% ($C_{f,B}$: 1.934 mg/L) and 64.9% ($C_{f,B}$: 1.756 mg/L) for 2D and 3D electrodes, respectively. The increase in boron removal efficiency with 3D cubic electrodes was most probably due to the

increasing ion transfer with the increase in microbial activity owing to enhanced available electrode surfaces for microbial growth. Furthermore, when plate electrodes were used in the anode cell, it was not possible to operate the system using high electrode surface areas due to the anode chamber size, but thanks to the novel electrode cell, it was possible to work in higher surface areas taking up less space. The COD removal efficiencies using plate and 3D cubic electrodes were quite similar. The highest COD removal efficiencies were 90.3% ($C_{f,COD}$: 897 mg/L), and 90.7% ($C_{f,COD}$: 856 mg/L) for 2D and 3D electrodes, respectively.

There are limited number of studies on boron removal using MDC from synthetic solutions and real water resources (Goren and Okten, 2021a; Ping et al., 2015). (Ping et al., 2015) studied boron removal from synthetic solutions using MDC process with Donnan dialysis pretreatment system and they reported that the highest boron removal efficiencies were found to be 60 and 52% at initial boron concentration of 5 and 20 mg/L, respectively. In our previous study, the highest boron removal efficiency using MDC was found to be 45.2% under optimized conditions (electrode surface area of 36 cm^2, catholyte solution of phosphate buffer, operating time of 12 days, initial boron concentration of 5 mg/L, and air flow rate of 2 L/min), while the highest removal efficiency was 39.4% for initial boron concentration of 10 mg/L at same operating conditions (Goren and Okten, 2021a). Moreover, the maximum boron removal from real geothermal water was found as 44.3% at optimized conditions.

The MDC energy production performance was investigated with respect to two different electrode type under optimum operating conditions (Figure 3.4c). On the tenth day, MDC achieved the maximum voltage of almost 680 mV for 2D plate type electrode (Figure C.3a). Voltage was almost stable at maximum voltage for 2 days which indicated steady microbial growth, producing electrons for the energy production at the anode chamber. Furthermore, to understand the power density, anode and cathode chambers were connected with an external resistance of 100 Ω. Results showed that the power density increased with time and attained the maximum power density of 8.50 mW/m^3 in 10 days for 2D plate electrode (Figure C.3b). After that, the power density decreased with operating time which might be attributed to the depletion of organic matter at the anode chamber (Mohan et al., 2014). The highest OCV and power density values were achieved using 3D cubic electrodes due to the increasing metabolic activity of microorganisms owing to high electrode surface areas for biofilm formation. The maximum OCV and power density values of 718 mV and 9.55 mW/m^3 were recorded at the end of the

operating time of 8 days, respectively. However, the power density decreased from 9.55 mW/m^3 to 8.82 mW/m^3 at the end of 12 days. As mentioned above, a decrease in power generation might be attributed to the effect of decreased electron formation due to the depletion of organic matter resulting in a decrease of microbial activity.

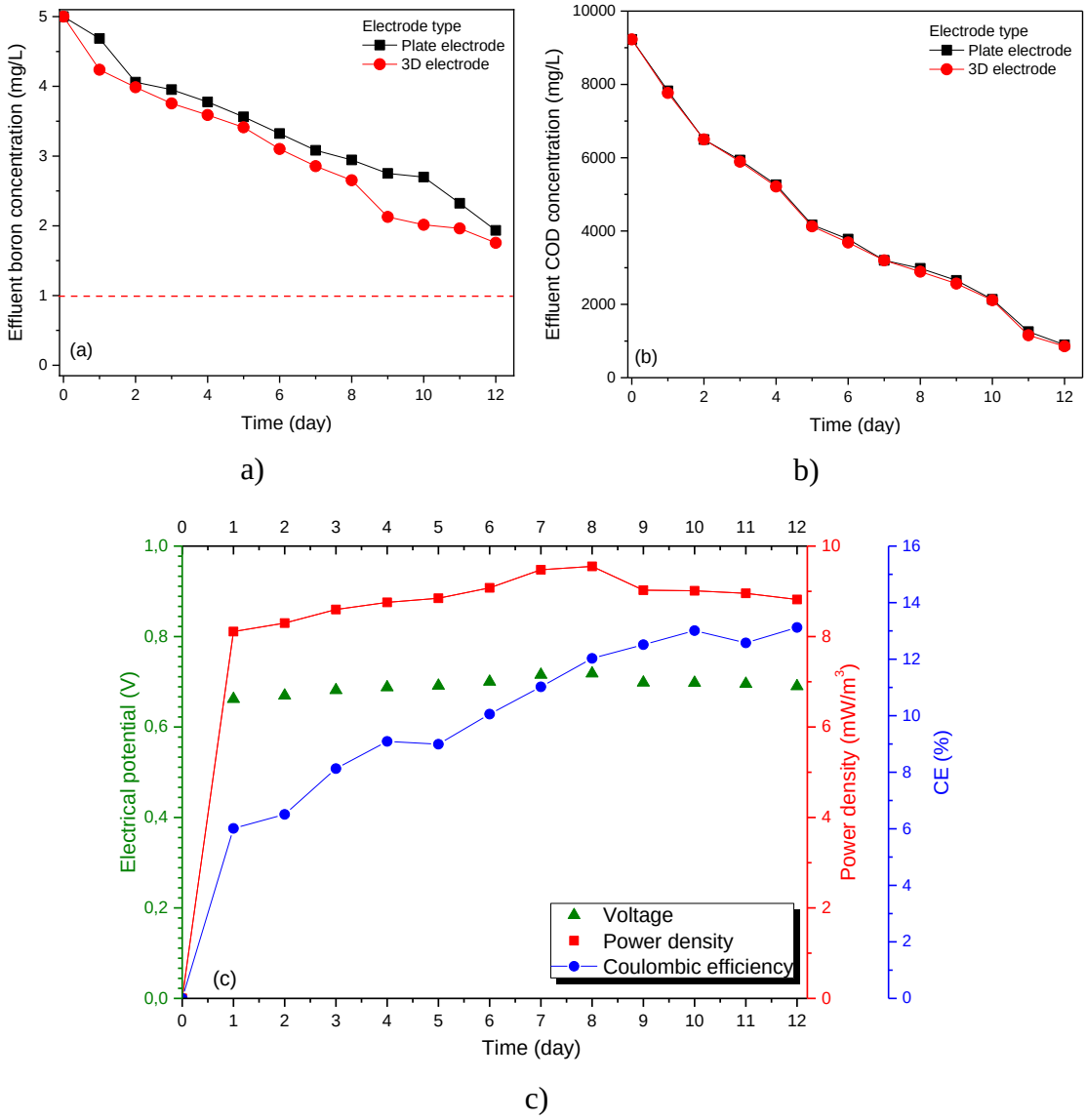

Figure 3.4. Effect of electrode type on boron removal a), COD removal b); electrical potential, power density, and Coulombic efficiency at optimum for 3D electrode c).

Moreover, similar trends were observed for the CE and CR values using electrode types of plate and 3D cubic. The CE and CR values were 12.9% and 11.7% for plate type electrode and 13.1% and 11.9% for 3D cubic electrodes, respectively. The increase in CE and CR values using 3D cubic electrodes could be explained that as the considerable amount of anode chamber was filled with the 3D cubic electrodes, electron transfer was

significantly accelerated due to a decrease in the internal resistance. Consequently, in addition to the advantages mentioned above, this novel MDC could also facilitate MDC's real-scale operations considering the ease of operation of electrode materials, high energy production, in addition to comparable desalination and wastewater treatment efficiencies.

3.3.4. Geothermal Water Treatment

MDC was operated with plate and 3D cubic electrodes, treating real geothermal water at optimized conditions. Measured power density, OCV, effluent boron, and COD concentrations were presented in Figure 3.5. As expected, the boron removal efficiency increased with 3D cubic electrodes. The highest boron removal efficiencies were found to be 44.3% ($C_{f,B}$: 5.836 mg/L) and 55.5% ($C_{f,B}$: 4.658 mg/L) for plate and 3D cubic electrodes, respectively. The initial EC value for the geothermal water was measured as 1770 μS/cm. Although the treated geothermal water's final EC value was not measured for 3D-MDC setup, it was recorded as 53.82 μS/cm for the 2D-MDC setup. Given that the boron removal efficiency has been enhanced with the 3D-MDC setup, the final EC value measured at the desalination chamber would be expected to be lower than the value acquired with the 2D-MDC setup. Observed boron removal efficiency for real geothermal water (55.5%) was lower than that for 5 mg/L boron synthetic solution (64.9%) for the 3D electrodes under same experimental conditions. This was most probably due to the high boron content of the real geothermal water. Besides, real geothermal water contains other molecules such as anions, cations, and heavy metals. Competition between boron and other species in water might decrease the mass transfer ratio of boron from desalination chamber to anode chamber. Furthermore, the maximum COD removal efficiency was 91.5% ($C_{f,COD}$: 786 mg/L) for 3D cubic electrodes, while it was 90.6% ($C_{f,COD}$: 856 mg/L) for 2D electrodes. The maximum OCV of 699 mV and power density of 9.04 mW/m^3 were recorded at the end of the operating time of 12 days for 3D electrodes. The highest CE and CR values of 13.2 % and 12.1 % were achieved using 3D cubic electrodes. These results confirmed that the novel MDC with 3D cubic electrodes showed comparable boron removal, industrial wastewater efficiency, and energy production for treating real geothermal water.

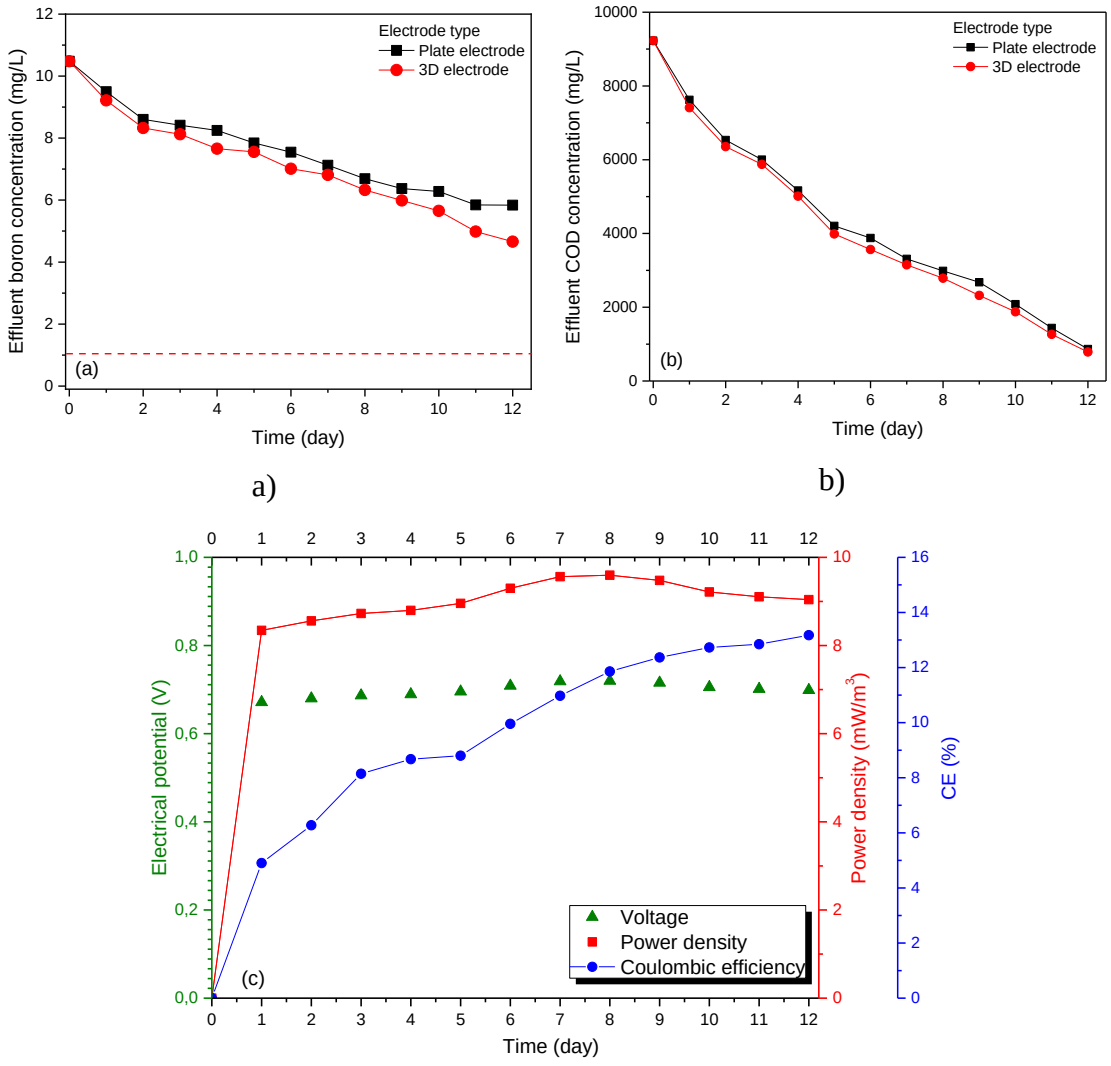

Figure 3.5. Effect of electrode type on geothermal water treatment: boron removal a), COD removal b), voltage, power density, and coulombic efficiency c).

3.3.5. Membrane Fouling and Biofilm Formation

Biofilm formation occurs on the surface of AEM-anode side due to microbial colonization (Luo et al., 2012b; Zhu et al., 2014). Biofilm formation on the surface of AEM, which is called as biofouling, widely occurs when the MDC system has been operated for a long time. AEM's structural integrity, stability, and functional groups on the surface is compromised due to the growth of biofilm, resulting in deposition of organic matter on AEM surface. This phenomenon causes the increase in internal resistance of the system, which adversely affects the performance of MDC process (Luo et al., 2012a).

Figure 3.6 demonstrated the SEM images of AEM and CEM surfaces. At the end

12 days, visible deformations and color change on AEM- anode side were observed. The color of the AEM was changed from light brown to black at the high activated sludge volumes, while this change was observed less for the low activated sludge volume. Furthermore, as presented in Figure 3.6a, the AEM surface facing the anode chamber showed formation of biofilm at the surface of the membrane due to direct contact of the AEM to mixture of industrial wastewater and anaerobic activated sludge. On the other hand, AEM-desalination side demonstrated considerable crystalline salt accumulation (Figure 3.6b). Similarly, the CEM on both sides showed crystalline salt aggregates (Figure 3.6c and 3.6d). On the other hand, there was no biofilm formation on both CEM surfaces as they were isolated from microorganisms.

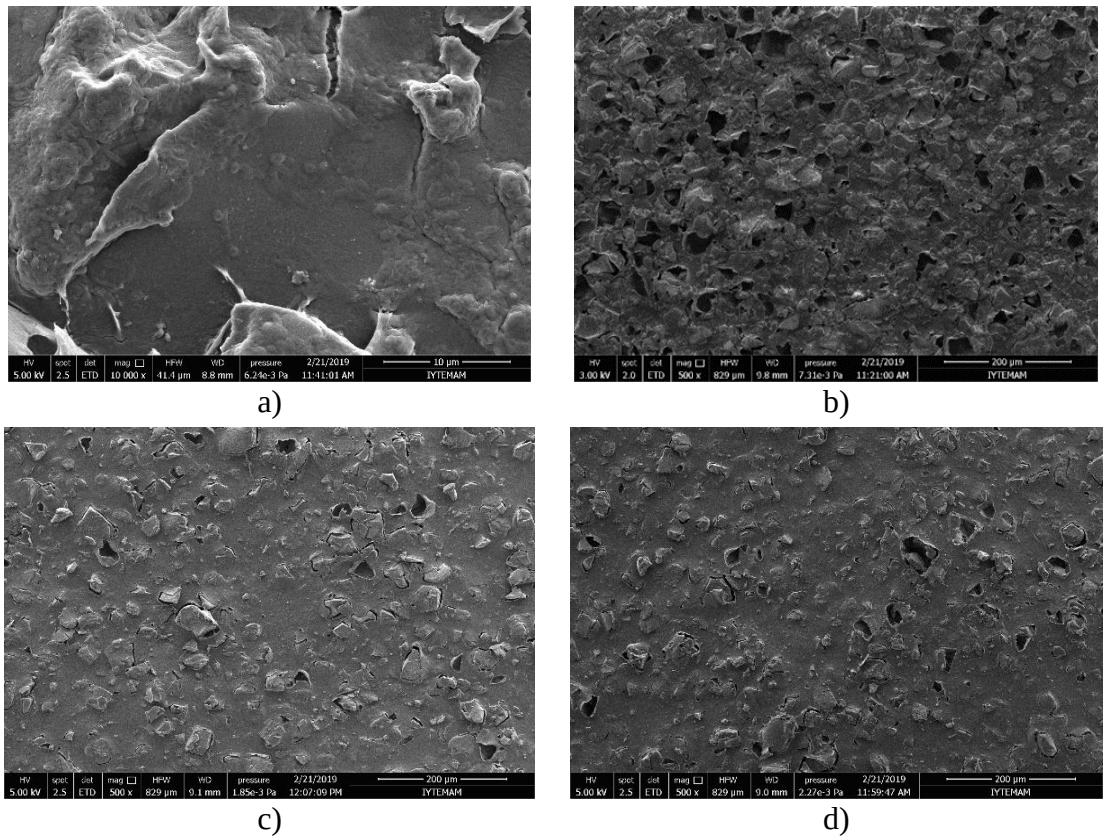

Figure 3.6. SEM images of membranes after operation. AEM surface in anolyte solution a), AEM surface in desalination solution b), CEM surface in catholyte solution c), and CEM surface in solution d).

Furthermore, the EDX results identified salt content on the membrane surfaces (Table 3.1). The EDX results showed a considerable accumulation of chloride and boron on the AEM surfaces facing both desalination and anode chambers. Boron accumulation on the AEM surfaces were found to be 26.91% and 30.31% for surfaces facing the anode

and desalination chambers, respectively. Boron and chloride accumulations on both sides of the AEM were mainly due to the transfer of anions from the desalination to anode chamber. On the other hand, carbon and sulfate contents of the AEM-anode side were not only measured lower than those of the unused AEM but they were also lower than those of the AEM-desalination side. This could be due to consumption of carbon and sulfate by microorganisms, which colonized and formed biofilm on membrane surface.

Table 3. 1. EDX results of the membranes before and after the experiment.

Material (Wt, %)	C	O	S	Na	F	Cl	B
AEM-Fresh	60.15	-	1.15	0.55	38.16	-	-
AEM (anode solution side)	50.50	2.75	0.15	-	10.67	0.25	30.31
AEM (desalination solution side)	56.01	3.12	0.38	-	13.20	0.38	26.91
CEM-Fresh	51.12	-	3.48	-	44.85	-	-
CEM (cathode solution side)	41.02	6.08	3.51	2.53	36.81	-	-
CEM (desalination solution side)	50.96	4.38	2.97	3.99	36.75	-	-

Oxygen deposition on CEM-cathode side was most probably due to the aerated catholyte solution, while the sodium deposition over the CEM-desalination side was due to desalination solution's pH being adjusted using NaOH solution. Other contents including, carbon, sulfate, and fluoride observed in the EDX results were ascribed to the inherent composition of the CEM polymer. Results showed that the membrane fouling mechanisms due to formation of biofilm and salt accumulation were important problems that prevented long-term stability of the system and needed to be further investigated. 36 day-long experiments with the 2D-MDC setup (S:WW ratio of 1:1, electrode surface area of 36 cm^2, catholyte solution of PBS buffer, and air flow rate of 2 L/min) revealed that boron removal rates have significantly decreased in consecutive cycles of 12 days for initial boron concentrations of 5, 10 and 20 mg/L (Goren and Okten, 2021a).

Coating of AEM with nanomaterials may considerably prevent biofilm formation and improve its structural integrity and stability, which may in turn extend its service time and reusability, and enhance efficiency of the MDC process (Guang et al., 2020). Moreover, the AEM fouling problem can be solved with developing effective polymers that may perform steadily with a wide range of temperature and pH values. For instance, the AEM crossed linked with wood-lignin may be a promising option since lignin has a number of desirable features, one of which is its stability (Tawalbeh et al., 2020). Scaling with accumulation of anions and cations on AEM surface is another severe problem when real wastewater and seawater are treated. Several studies have been conducted to prevent

or eliminate membrane fouling (Salehmin et al., 2021). Researchers focused on synthesis of membrane materials integrated with antifouling features to prevent membrane fouling (Vaselbehagh et al., 2014). However, synthesis of antifouling membranes may be impractical to eliminate various types of fouling at once. Therefore, more investigation is needed to enhance the efficiency of existing modified AEMs and elucidate the main mechanism of fouling through understanding characteristics of fouling types.

3.3.6. Control Experiment

In a previous study, a negative control experiment using the 2D-MDC set up was done using 5 mg/L initial boron concentration in the absence of microbial activity. All other operating parameters were kept the same. As a result, only 26.2% of boron was removed from the desalination chamber, pointing to a significant impairment in diffusion rate due to lack of electrochemical gradient (Goren and Okten, 2021a). Moreover, another control experiment was done under optimum operating conditions (initial boron concentration of 5 mg/L, S:WW ratio of 1:1, electrode surface area of 36 cm^2, catholyte solution of PBS buffer, and air flow rate of 2 L/min) at open circuit for both 2D-MDC and 3D-MDC. The removed boron content was found to be 2.52 and 2.80 mg/L for 2D-MDC and 3D MDC at open circuit mode, respectively. The amount of removed boron was lower than that achieved with the closed circuit mode for both 2D-MDC (3.07 mg/L) and 3D-MDC (3.244 mg/L). These results showed that the boron diffusion increased with the increase in the electrochemical gradient, improving the removal efficiency.

3.4. Conclusion

Desalination of geothermal wastewater is crucial for its reuse in agricultural irrigation in water scarce regions. Simultaneous boron and organic matter removal with energy production were effectively achieved using novel MDC with 3D cubic electrodes. It was found that the anolyte solution temperature, S:WW ratio, and electrode type significantly affected performance of MDC. According to results, novel MDC achieved the maximum boron and organic matter removal efficiencies of 64.9% and 90.7%, respectively, with the highest power density of 9.55 mW/m^3 for 5 mg/L of boron containing synthetic solution. The highest boron and organic matter removal efficiencies

were 55.5% and 91.5% with the maximum power density of 9.04 mW/m^3 for real geothermal water. Achieved results were comparable with conventional MDC runs, however it should be noted that if the designed electrode cell was filled with 3D cubic electrodes the removal efficiencies and energy production performance were expected to improve. SEM and EDX results presented significant biofilm formation on AEM facing the anode chamber and salt deposition on the both AEM and CEM at the end of the operation and showed that biofilm formation and salt deposition may adversely affect the performance of MDC, particularly in the operation with higher activates sludge: wastewater ratio. Therefore, there is need for further investigation on membrane scaling by biofilm formation and salt decomposition to enhance the performance of MDC process. Consequently, our results showed that the novel MDC was a promising process for boron and organic matter removal with energy production during industrial wastewater and geothermal water treatment.

CHAPTER 4

PHYTOREMEDIATION OF BORON USING LEMNA MINOR FROM SYNTHETIC AQUEOUS SOLUTIONS AND REAL GEOTHERMAL WATER

4.1. Introduction

Water scarcity problem, which from a strict economical perspective explains in higher cost for clean water and wastewater treatment, poses a significant problem for developing and developed countries alike. World Health Organization (WHO) reported that 748 million people lack access to clean and adequate water resources, while at least 2 billion people use water sources that are contaminated. While roughly 50.0% of the World's inhabitants facing with water scarcity, one third of it have limited excess to energy services (Malley et al., 2009; Supply and Programme, 2014). Therefore, availability and accessibility to safe and secure water resources are the key technological and scientific problems of global significance.

Utilization of geothermal waters for various domestic purposes dates back to ancient times as evidence shows Native Americans using it for cooking approximately 10.000 years ago. However, realization of geothermal resources' economic potential has occurred much recently, starting with the implementation of the first geothermal electric power plant in Larderello, Italy in 1904 and leading to global power generation of 92 TWh as of 2019. China, USA, Sweden, Turkey, and Japan have a largest geothermal energy use with a 55.0% of world use. Turkey has a significant amount of geothermal capacity with 31,500 MWh and almost 77.9% of this capacity is found in west Anatolia (Aydın-Germencik, Denizli-Kızıldere, Çanakkale-Tuzla and others) (Melikoglu, 2017).

This chapter has been published as: A.Y. Goren, H.E. Okten, Phytoremediation of boron using Lemna minor from synthetic aqueous solutions and real geothermal water, Süleyman Demirel University Journal of Natural and Applied Sciences 25 (2021) 217-228.

Apart from utilization for energy, geothermal water resources also serve as drinking, agricultural, industrial, and domestic water supplies, especially in arid regions (Gallup, 2007). Geothermal waters are characterized by diverse physicochemical parameters depending on their hydro geothermal properties, characteristics of the rocks involved, the depth at which resources occur, and the source of water supply. Geothermal waters contain considerable amounts of anions, cations, and neutral species (Baba and Sözbilir, 2012). Evaluating the composition of geothermal waters, boron content stands out as it is higher in comparison to boron concentrations generally found in sea water and brackish water. The main sources of boron are either natural such as leaching from boron containing rocks, borates and borosilicates containing soils, and volcanic activities or industrial such as manufacturing of detergents, cleaning products, semiconductor, borosilicate glass, cosmetics, fertilizers, flame retardants and dyestuff (Kartikaningsih et al., 2016). Boron is commonly found as boric acid (H_3BO_3) and tetrahydroxoborate ions ($B(OH)_4^-$) in geothermal waters and thermal springs. The pKa value of 9.25 marks the transition pH between H_3BO_3 and $B(OH)_4^-$ species. Below pH 9.25, the dominant species in water is H_3BO_3 and above pH 9.25, $B(OH)_4^-$ becomes the dominant species (Barth, 2000; Yilmaz et al., 2008).

Due to high mineral content of geothermal waters, they shall be treated prior to any type of intended use apart from energy utilization. Boron content of these sources may pose significant risks to groundwater, surface water, aquatic life and vegetation (Gude, 2016) in the case of untreated discharges. Even though boron is an important nutrient for plants, it may be toxic at high concentrations for nearly all plants despite their wide range of tolerance. For instance, recommendation level to prevent boron related plant toxicity in irrigation water is lower than 0.5 mg/L for blackberry and lemon orchards; 1 mg/L for walnut, plum, pear, and apple; 2 mg/L for sunflower, potato, cotton, and tomato; 4 mg/L for asparagus, palm, bean, and onion (Gemici and Tarcan, 2002; Hilal et al., 2011; Yilmaz et al., 2008). Moreover, long term exposure to boron through ingestion may cause nausea, lethargy, diarrhea, vomiting, dermatitis, as well as intellectual and physical problems at children and risk of miscarriage in pregnancies (Bryjak et al., 2008; Nielsen, 2002). Therefore, WHO recommended 2.4 and 1 mg/L as the limit values for boron in drinking water and irrigation water, respectively (Organization, 2017).

There are several treatment technologies for boron removal from aqueous solutions including coagulation, sedimentation, filtration, adsorption, ion-exchange, electrocoagulation; membrane processes; bio-electrochemical systems (Banasiak and Schäfer, 2009b; Kabay et al., 2013a; Ozbey-Unal et al., 2018; Yilmaz et al., 2008). Despite achieving above 95% boron removal rates, membrane based desalination processes are need significant energy (Kabay et al., 2013a; Nagaraj et al., 2016; Yavuz et al., 2013). Reverse osmosis (RO) desalination is a widely-used process for bulk water production, consuming around 4 kWh/m^3 energy corresponding to 0.35-0.50 $\$/m^3$ in treatment costs (AlMarzooqi et al., 2014).

Recently, interest in environmental friendly, cheap, and effective treatment technologies have been increasing. The phytoremediation is one of these treatment technologies. Phytoremediation processes are a developing concept used to remove, reduce, and immobilize contaminants from the aqueous solutions to enhance water quality as an environmental friendly treatment method. Phytoremediation based on the application of plant species to accumulate contaminants in aquatic environment. Several aquatic macrophytes, invasive plants, and floating plants have been studied for the removal of various contaminants in water and wastewater sources. Lemna gibba, Lemna minor, Chlorella sp., and S. polyrhiza species were used for the bioremediation and assessment of boron toxicity on plants (Böcük et al., 2013; Taştan et al., 2012; Tatar and Öbek, 2014; Türker et al., 2017). Among these aquatic plants Lemna minor for phytoremediation process is advantageous due to its small size, simple structure, easy adaptation to diverse aquatic conditions, rapid grow rate, and high ability to accumulate contaminants from water sources (Ekperusi et al., 2019; Movafeghi et al., 2013; Yaseen and Scholz, 2016). However, the studies on boron removal of the aquatic plants have been commonly carried out considering the boron accumulation and boron toxicity in plants while the studies about the effect of operational variations on boron accumulation, toxicity, and removal efficiency using these plants are inadequate; therefore, this study aims to fill these gaps.

The goal of this paper was to investigate the effect of operating parameters (initial pH, initial boron concentration, initial natural organic matter concentration, effect of water height in cell) on boron removal efficiency of L. minor from aqueous solutions. Moreover, the boron removal from real geothermal brine was studied at optimized operating parameters. According to our researches this is the first study about boron removal by Lemna minor with proposed targets.

4.2. Materials and Methods

4.2.1. Solutions

Boric acid (H_3BO_3, Sigma Aldrich) solutions were prepared with 5, 10, 20, and 30 mg/L of final B concentrations. Boron concentrations were selected to represent the range that is generally found in geothermal water compositions (Baba and Sözbilir, 2012; Ozbey-Unal et al., 2018). The pH of prepared solutions was adjusted using 0.1 M NaOH and 0.1 M HCl solutions. Hoagland solution, a synthetic nutrient solution for Lemna minor, was prepared by dissolving 118 mg of $Ca(NO_3)_2.4H_2O$, 0.008 mg $CuSO_4$, 0.004 mg of $CoCl_2.2H_2O$, 0.3 mg of $FeSO_4$. $7H_2O$, 0.3 mg of H_3BO_3, 5 mg of KNO_3, 0.68 mg of KH_2PO_4, 0.35 mg of K_2SO_4, 5 mg of $MgSO_4.7H_2O$, 0.15 mg of $MnSO_4.7H_2O$, 0.00128 mg of $(NH_4)6Mo_7O_{24}.4H_2O$, 0.005 mg of $NiSO_4.7H_2O$, and 0.022 mg of $ZnSO_4$ in a liter of DI water (Hoagland, 1948). Humic acid (HA, 50–60%, Acros Organics) was used for simulation of natural organic matter.

4.2.2. Characterization of Real Geothermal Brine

Geothermal brine was obtained from Balçova Geothermal Power Plant in İzmir, Turkey. The pH and electrical conductivity of geothermal water were 8.04 and 1770 µS/cm, respectively. Ionic content of geothermal brine was summarized in Table 4.1.

Table 4. 1. Characterization of geothermal brine.

Parameters	Concentration (mg/L)
K^+	26.49 ± 0.28
NH_4^+	1.66 ± 0.01
Na^+	364.16 ± 1.25
Ca^{2+}	25.73 ± 0.51
Mg^{2+}	9.82 ± 0.47
NO_3^-	1.49 ± 0.68
Cl^-	171.16 ± 2.93
F^-	7.41 ± 1.24
SO_4^{2-}	154.93 ± 1.61
Li	1.17 ± 0.15
As	0.17 ± 0.02
B	10.48 ± 1.63

4.2.3. Lemna minor

Aquatic plant of Lemna minor was purchased from an aquarium shop in İzmir, Turkey. Plants were washed with 2% hypochlorite (ClO^-) to remove any undesired organisms and algae (Frederic et al., 2006). Plants were acclimatized in a 10 L plastic container with specified amount of synthetic nutrient solution under sunlight for one week prior to experiments.

4.2.4. Lemna minor

Batch experiments that lasted 7 days were conducted to investigate boron removal by L. minor. Experimental runs were conducted in glass cells with surface area of 12 cm^2 (Figure 4.1). 5 g of plant was transferred to cell which contained 50 mL of synthetically prepared boron solution. All experiments were conducted at 25 ºC, with a 16 h of light and 8 h of darkness. All experimental runs were carried out with three replicates and averaged data were used. Furthermore, control experiments for all experimental runs were conducted.

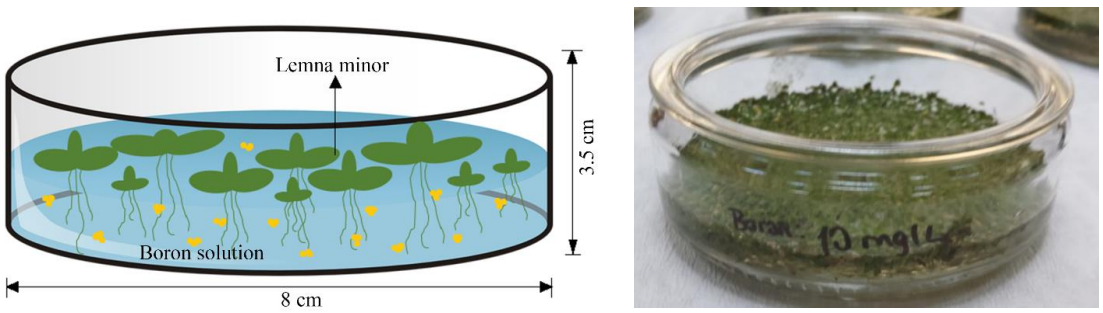

Figure 4.1. Experimental set-up of the Lemna minor containing glass cell.

4.2.5. Analytical Methods and Calculations

The pH was measured in boron containing solutions using a multimeter (Mettler Toledo, SevenCompactTM). Water samples were filtered and analyzed for boron content using inductively coupled plasma optical emission spectrometer (ICP-OES, AGILENT 5110). Plant samples were also processed for boron content. Initially, boron exposed plant samples were dried at 60 ºC for 24 h in an oven. Then, 0.2 g of powdered biomass was

mixed with 10 mL HNO_3, and 1 mL H_2O_2 and was microwave-digested (MARS 6) at 200 ºC for 30 min. Then, digested samples were filtered and afterwards they were analyzed for boron content by ICP-OES. Anions and cations in real geothermal water were analyzed by ion chromatography (IC, Dionex ICS-5000). Humic acid was measured by Shimadzu UV-2600 spectrophotometer at λmax of 254 nm. Standard deviations (SD) of all analyses were presented in supplementary material. Possible changes in surface morphology of dried L. minor before and after boron treatment experiments were investigated using Scanning Electron Microscopy (SEM, Quanta 250FEG). Energy dispersive X-ray spectrometry (EDX) was also performed for analyzing main elements present on raw and boron-exposed plant surfaces. Fourier Transform Infrared (FTIR) spectroscopy analyses were also performed (Shimadzu FTIR 8400S) to compare functional groups before and after boron removal experiments. Boron removal efficiency (Re, %) was calculated by following equation:

$$R_e(\%) = \frac{\left(C_{i,B} - C_{f,B}\right)}{C_{i,B}} \times 100 \quad (4.1)$$

$C_{i,B}$ and $C_{f,B}$ (mg/L) were initial and final boron concentration in aqueous solution, respectively. Bioconcentration factor (BCF) of boron was calculated using following equation (Marín and Oron, 2007; Zayed et al., 1998).

$$BCF = \frac{C_{B,plant}}{C_{i,B}} \quad (4.2)$$

$C_{B,plant}$ was boron concentration (mg/kg) in Lemna minor tissues. Mass balance of boron in treatment system was also calculated by the following equations:

$$B_{total} = B_{soluble} + B_{accumulated} + B_{insoluble} \quad (4.3)$$

where, B_{total}: total boron in the treatment system (mg), $B_{soluble}$: water soluble boron (mg), $B_{accumulated}$: accumulated boron by plant (mg), $B_{insoluble}$: insoluble forms of boron (mg).

$$B_{total} = C_{i,B} \times Q_i \quad (4.4)$$

$$B_{soluble} = C_{f,B} \times Q_f \quad (4.5)$$

$$B_{accumulated} = C_{B,plant} \times W_d \quad (4.6)$$

$$B_{insoluble} = B_{total} - B_{soluble} - B_{accumulated} \quad (4.7)$$

where, Q_i: initial water volume in L. minor containing cell (L), Qf: final water volume in cell (L), W_d: dry weight of L. minor (g).

4.3. Results and Discussion

4.3.1. Boron Removal from Synthetic Solution

Effects of initial pH, boron concentration, natural organic matter, and water height in cell on boron removal efficiency were investigated to elucidate the optimum operating parameters. Furthermore, B removal from real geothermal brine was investigated under optimum operating conditions.

4.3.1.1. Effect of Initial pH

The pH of the aqueous solutions has a significant impact on removal of boron in aqueous solutions and treatment performance of L. minor (Kabay et al., 2013a; Yaseen and Scholz, 2016). To examine the effect of pH (6, 8 and 10), experimental runs were conducted using 20 mg/L of B solution, with 5 g of L. minor and operating time of 7 days. Specified pH values were selected to address the minimum and maximum pH values L. minor species can tolerate and to investigate boron speciation's effect on boron removal efficiency (McLay, 1976). Boron removal efficiencies under different initial pH values were given in Figure 4.2.

Boron removal efficiencies were found to be 49.8%, 53.2%, and 50.5% for pH values of 6, 8, and 10 at the end of the operating time of 7 days, respectively (Figure 4.2). The maximum B contents were 1785, 1815, and 1838 mg/kg at initial pH values of 6, 8, and 10, respectively. L. minor removed B with the highest removal efficiency of 53.2% and maximum B uptake was 1815 mg/kg at pH 8. Further increase in pH to 10 caused a

small decrease in removal efficiency (50.5%) and maximum uptake capacity (1838 mg/kg). Bioconcentration factors (BCF) were calculated to be 89.25, 90.75, and 91.9 for initial pH values of 6, 8, and 10, respectively. There was no noticeable difference at specified pH values.

Researchers studied boron removal from contaminated waters using L. gibba and they found that the boron content in plant tissues were 900 and 1900 mg/kg for initial boron concentrations of 0.2 and 10 mg/L, respectively at operating time of 12 days (Marín and Oron, 2007). In a separate study, (Böcük et al., 2013) investigated boron removal from mine effluent water using L. gibba. Boron content of plant was 2500 mg/kg at operating time of 7 days. These studies showed that our results were in good agreement with literature findings about boron accumulation in plant tissues.

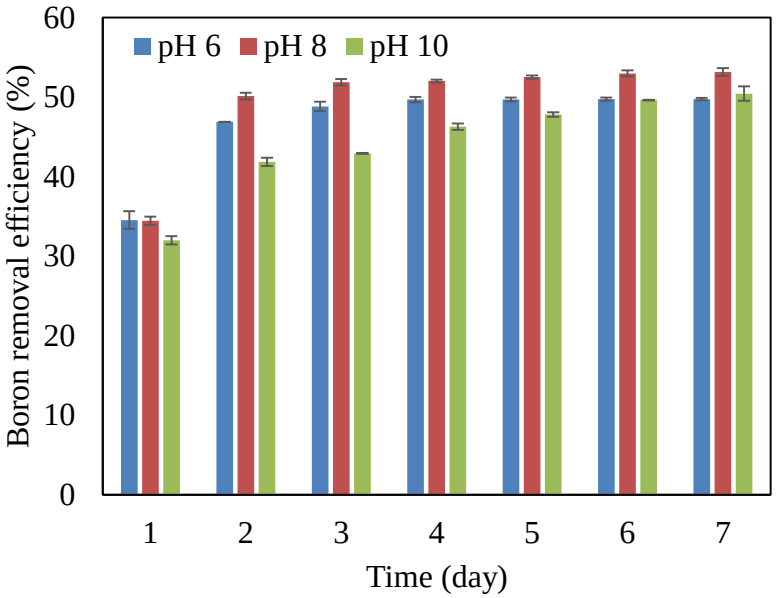

Figure 4.2. Boron removal efficiencies at different initial pH values.

Boron bioaccumulation in plant tissues may occur by diffusion and active transport of boron through plasmalemma, which is the permeability barrier of cell (Pitman, 1963; Wildes and Neales, 1971). When L. minor is exposed to boron containing solution, the boron concentration in tissues is lower than that of solution. Therefore, the uptake of boron from solution to tissues occur as a result of rapid diffusion of $B(OH)_3$ and slower active transport of $B(OH)_4^-$. The diffusion of $B(OH)_3$ will subsequently decrease until the boron concentration in L. minor tissues and boron containing solution equalize. After this stage, the boron uptake occurs only with the active transport of $B(OH)_4^-$. Therefore, boron was probably taken up as boric acid by L. minor with diffusion

mechanism during the operating time of 2 days. At the end of 2 days, the main uptake mechanism was active transport of $B(OH)_4^-$. Accordingly, a significant increase in boron removal efficiencies was observed for 2 days due to rapid diffusion of $B(OH)_3$ while the removal efficiencies were lower at the end of that period. Furthermore, the decrease of removal efficiency with the increase of initial pH from 8 to 10 can be explained with the B species in solution. Boron is found in $B(OH)_3$ and $B(OH)_4^-$ forms at pH 8 and at pH 10, respectively (Barth, 2000). Therefore, boron uptake was relatively higher at pH 8 than pH 10 due to the uptake of boron as $B(OH)_3$ by rapid diffusion mechanism (Blevins and Lukaszewski, 1998). (Taştan et al., 2012) studied boron removal by a Chlorella sp. and they found that the maximum B removal was observed at pH 8.

Results showed that there was no significant effect of initial pH of the solution on boron removal efficiency by L. minor. Since the maximum removal efficiency was observed at pH 8 for boron removal using L. minor, experiments were conducted at pH 8.

4.3.1.2. Effect of Boron Concentration

We studied effect of B concentrations of 5, 10, 20 and 30 mg/L at operating time of 7 days (Figure 4.3). A rapid uptake of boron was observed for the 5 mg/L initial concentration in the first 4 days of operation. Later in the experiment uptake rate has slowed down, with an approximation to 100% removal efficiency. Experimental run with 10 mg/L showed a relatively rapid uptake of boron in the first 3 days. We also observed a delayed increase in uptake on the 7th day of the experiment, which we assumed was due to an error in analysis. The removal efficiency was above 60% at the end of the experiment. Doubling the concentration from 10 to 20 mg/L resulted in a decrease in removal efficiency from 61.2% to 53.2%. Boron uptake rate was higher in the first 2 days for the run with 20 mg/L. The time needed to reach a plateau on boron removal efficiency graph has narrowed with increasing initial concentrations. However, boron removal efficiency kept increasing in the first 5 days of operation at 30 mg B/L. The maximum removal efficiency decreased significantly (36.6%).

The decreases observed in boron uptake rates at different times for 5, 10, and 20 mg/L runs were most probably related to the sorption capacity of L. minor. The plant reached its limit much faster as the concentration was increased. On the other hand, the initial boron concentration of 30 mg/L was toxic for L. minor since we observed leaves

turning yellow and rotting by the end of the experiment, which explained the poor removal efficiency. Despite being an essential nutrient for plant growth, boron overdose may cause toxicity (Davis et al., 2002; Hilal et al., 2011; Yilmaz et al., 2008). Furthermore, ESEM results confirmed that the high concentration (30 mg/L) of B-exposed Lemna minor showed some toxic symptoms such as structural disorders in leaves and decrease in stomata. The steady increase in B uptake in the first 5 days of the experiment was probably due to adsorption rather than diffusion.

Our results were in good agreement with previous results observed by other researchers who studied boron toxicity on L. minor. Researchers reported that the aquatic macrophytes may suffer from necrosis, chlorosis, and may die when exposed to boron concentrations above 22 mg/L. It was reported that high amounts of boron caused teratogenic effect and toxicity (Grieve et al., 2010; Naghii and Samman, 1997; Reid, 2010). For instance, (Frick, 1985) reported that the initial boron concentration reaching up to 20 mg/L was toxic for L. minor at 6 days. In a separate study, (Böcük et al., 2013) studied L. gibba and they found that higher than 25 mg/L initial concentrations caused boron toxicity symptoms in 7 days. Boron content of L. minor samples increased gradually from 1271 mg/kg to 1904 mg/kg with the increase in initial boron concentration from 5 to 30 mg/L, respectively. Our results were in agreement with the literature. For instance, (Türker et al., 2017) found that the boron content in L. gibba was 1296 mg/kg for initial boron concentration of 5.58 mg/L.

The BCFs were determined to evaluate the boron accumulation ability of the plant at different initial boron concentrations. As expected, the BCF values decreased with increasing initial boron concentrations and the maximum and minimum BCF values in Lemna minor were found as 254.12 and 63.48 at B concentrations of 5 and 30 mg L-1, respectively. A similar result was observed by [30], they suggested that the decrease of BCF value at high boron concentrations was probably related to growth inhibition.

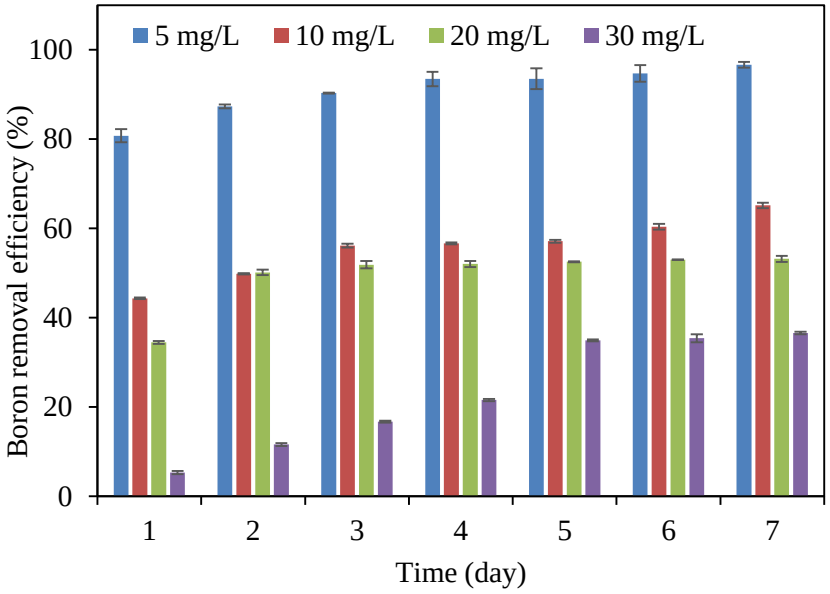

Figure 4.3. Removal efficiencies at different initial boron concentrations.

4.3.1.3. Effect of Humic Acid

Natural organic matter is a chemically active and critical component of water sources that occurs mainly by biological decay of plant and animal residues (Leenheer, 2009). These compounds may interact with heavy metals, through which solubility and toxicity of heavy metals may be adversely affected (Tipping, 2002). Figure 4.4 shows boron removal efficiencies at different humic acid (HA) concentrations (0, 1, 2, and 3 mg/L) at operating time of 7 days and 20 mg-B/ L.

The maximum B removal efficiencies were observed as 33.1%, 38.1%, and 30.9% for humic acid concentrations of 1, 2, and 3 mg/L, respectively, at operating time of 1 day. Boron removal efficiencies decreased steadily in time with all investigated humic acid concentrations, which was probably due to the toxic effect caused by the interaction between boron and humic acid (Goli et al., 2019). Boron and humic acid interaction may form complex/toxic compounds and these compounds cause decomposition of the plant structure. B concentration in solution was 22 mg/L at the end of all experimental runs, while the initial B concentration was 20 mg/L. Raw L. minor's B content was measured as 410 mg/kg. Since all experiments were conducted using 5 g of L. minor and total boron content was calculated to be approximately 2.05 mg. These results revealed that the plant decomposed due to the toxic effect of humic acid/boron complexation and some portion of the boron inherently present in plant structure was released to the solution.

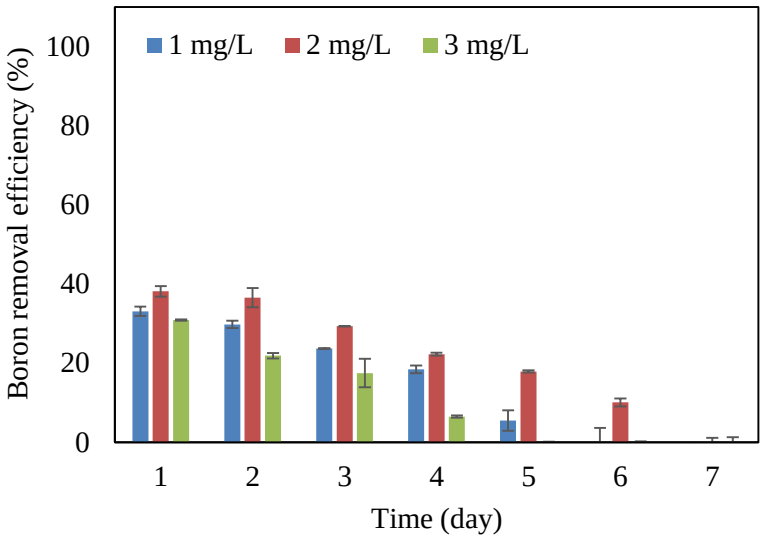

Figure 4.4. Boron removal efficiencies at different HA concentrations.

4.3.1.4. Effect of Water Height in Cell

As seen in Figure 4.5, B removal decreased with the increase in water height in cell. Boron removal efficiencies were found as 53.1%, 35.9%, and 32.7% at water heights of 1.5, 3, and 5 cm, respectively. Boron removal efficiencies remained constant at the end of the operating time of 3 days for all water heights. In nature, L. minor can survive a pond depth of 0.5 m (Hasan et al., 2009). However, boron removal efficiency was negatively affected by increase in water height in cell. This can be explained by mixing rate of solution. Removal experiments were conducted without mixing, while in nature there is always a natural mixing of water in pond systems. We observed that in 1.5 cm depth, roots of L. minor could reach the bottom of the cell and therefore boron content in solution was fully accessible by the roots. However, in depths of 3 cm and 5 cm, the roots were not able to reach the bottom of the cell, deeming some of the boron content inaccessible to the plants. Therefore, we concluded that boron removal efficiency of L. minor decreased due to insufficient mixing of solution.

Boron contents and bioconcentration factors of L. minor at the end of the runs were 1815 mg/L and 90.75 for 1.5 cm depth; 1619 mg/L and 80.95 for 3 cm depth; 1132 mg/L and 56.60 for 5 cm depth. As expected, boron content and BCF values decreased with the increasing water height in cell.

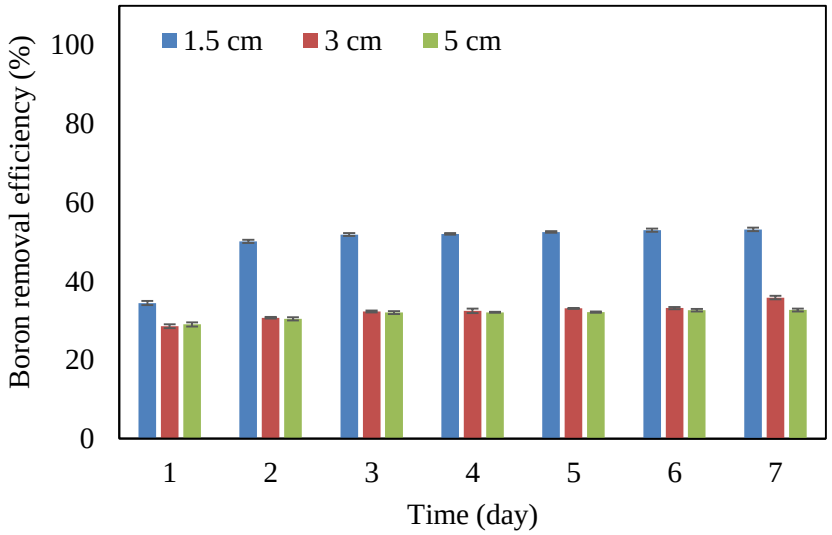

Figure 4.5. Boron removal efficiencies at different water heights in cell.

4.3.2. SEM and FTIR Analysis

Surface morphologies of raw and B-exposed L. minor were examined using SEM (Figure D.1). Results showed that the raw plant exhibited a heterogeneous structure with some cavities. In addition, the small fractures and deteriorations were observed probably resulting from grinding process. On the other hand, relatively small heterogeneous structure was observed on the surface of B-exposed L. minor probably due to agglomeration of boron on the leaf and roots of plant or inclusion of boron into the structure. Furthermore, elemental mapping using SEM revealed that the B-exposed plant consisted of relatively high amounts of B when compared with the raw one. EDX results confirmed elemental mapping results, showing a change in ion content on raw and B-exposed plant surfaces (Figure D.2.). Carbon content of raw plant decreased from the initial value of 53.9% to 48.6% at the end of the experiment (Table D.1). Decreasing carbon content was estimated to be on account of organic matter depletion. On the other hand, there was no considerable change in oxygen content as both raw and B-exposed samples were examined under natural ventilation. Furthermore, Na, Mg, K, and Ca elements were found on both surfaces. B content, which was not determined for raw sample, was found to be 1.97% on B-exposed plant surfaces. Accumulation of B, most probably due to biosorption mechanism for L. minor, was observed (Böcük et al., 2013).

In the FTIR spectra of B-exposed samples, the band at 711 cm^{-1} was attributed to the vibration (doublet) of the B-N group that has medium intensity between 700 and 680

cm^{-1} (Figure D.3) Bands related to the B-H stretching observed at 2515 cm^{-1} which was in the suggested range of 2640-2350 cm^{-1}. A strong "B···H···B" bridge at 1535 cm^{-1} was also observed as given in the range of 1610-1525 cm^{-1}. The methyl deformation vibrations of B-CH_3 were observed at 1421 and 1315 cm^{-1}. According to literature, the vibrations of B-CH_3 observe at 1460-1405 cm^{-1} and 1330-1280 cm^{-1}, respectively (Socrates, 2004). The common peak at 3402.54 cm^{-1} corresponded to N–H stretching related to the amino acids in plant structure while the peaks 2922.25 and 2850.88 cm^{-1} are for C–H stretching due to the high load of lipids. The peaks of L. minor at 1319.35 cm^{-1} for C–O stretching and 1658.84 cm^{-1} for C = O stretching corresponds to amide.

4.3.3. Mass Balance of Boron in Treatment System

Boron removal using L. minor may occur through adsorption of boron on leaves and roots or through absorption. To establish the dominant form of B in the experiments, we conducted the mass balance analyses (Table 4.2).

At the first stage of the treatment process, soluble boron was the main fraction in the system. At the end of the operating time of 7 days, L. minor accumulated boron became the dominant form in the system. It could be observed that 31.7% to 93.6% of B was accumulated by plant, indicating that a considerable portion of boron was removed by biosorption. The maximum boron accumulation was found to be 93.6% at 5 mg-B/L, pH of 8, and water height of 1.5 cm. With the increase in initial pH from 8 to 10, accumulated, water soluble, and insoluble boron concentrations were not significantly changed. Similar results were observed for the water height in cell. However, B content increased from 5 to 30 mg-B/L, accumulated boron concentration decreased dramatically, while the water soluble and insoluble water concentrations were increased by increased initial boron concentration. Under high boron concentrations, plant roots and leaves decomposed due to the toxic effect of boron. These results indicated that with increase in initial boron concentration, more soluble boron was converted to insoluble boron forms that were difficult to remove. Overall, accumulated boron was found to be major form of boron. The mass balance analyses of boron indicated that the main B removal mechanism of L. minor was firstly biosorption and then accumulation in plant tissues.

Table 4. 2. Mass balance of boron at different operating conditions.

Operating parameter		Total boron (mg)	Plant accumulated boron (mg)	Water soluble boron (mg)	Insoluble boron (mg)
pH[a]	6	1 (100%)	0.446 ± 0.016 (44.6%)	0.261 ± 0.054 (26.1%)	0.293 ± 0.047(29.3%)
	8	1 (100%)	0.454 ± 0.021(45.4%)	0.234 ± 0.013 (23.4%)	0.312 ± 0.012(31.2%)
	10	1 (100%)	0.459 ± 0.019 (45.9%)	0.248 ± 0.028 (24.8%)	0.293 ± 0.011 (29.3%)
Boron[b] (mg/L)	5	0.25 (100%)	0.234 ± 0.056 (93.6%)	0.004 ± 0.014 (1.6%)	0.012 ± 0.082 (4.8%)
	10	0.5 (100%)	0.318 ± 0.012 (63.6%)	0.087 ± 0.026 (17.4%)	0.095 ± 0.016 (19.0%)
	20	1 (100%)	0.454 ± 0.021(45.4%)	0.234 ± 0.013 (23.4%)	0.312 ± 0.012 (31.2%)
	30	1.5 (100%)	0.476 ± 0.038 (31.7%)	0.476 ± 0.095 (31.7%)	0.548 ± 0.043 (36.5%)
Height[c] (cm)	1.5	1 (100%)	0.454 ± 0.125 (45.5%)	0.234 ± 0.018 (23.4%)	0.312 ± 0.024 (31.2%)
	3	1 (100%)	0.405 ± 0.056 (40.5%)	0.321 ± 0.127 (32.1%)	0.274 ± 0.138 (27.4%)
	5	1 (100%)	0.283 ± 0.269 (28.3%)	0.337 ± 0.036 (33.7%)	0.380 ± 0.002 (38.0%)

a: initial boron concentration:5 mg/L, water height in cell: 1.5 cm, and humic acid concentration: 0 mg/L, b: initial pH: 8, water height in cell: 1.5 cm, and humic acid concentration: 0 mg/L, c: initial boron concentration:5 mg/L, initial pH: 8, and humic acid concentration: 0 mg/L.

4.3.4. Boron Removal from Geothermal Water

Experiments with real geothermal water were conducted using the previously found optimum operating conditions (initial pH: 8, water height: 1.5 cm, and HA concentration: 0 mg/L). Boron concentration followed a steady decreasing pattern from 10.48 to 4.24 mg/L through 7 days. When the B removal efficiencies were compared, there was a slight decrease from 65.2% (10 mg/L B containing synthetic solution) to 59.5% (real geothermal water). The B content and bioconcentration factor were 1500 mg/kg and 143.13 in geothermal water, respectively, as opposed to 1558 mg/kg and 155.8 in 10 mg/L boron containing synthetic solution. The slight decrease in removal efficiency and consequent decreases in B content and BCF were expected since real geothermal water was rich in ionic content. Moreover, a toxic response was not observed with the real geothermal water, which confirmed previous studies in the literature regarding salt tolerance of L. minor. (Liu et al., 2018) studied boron accumulation using L. minor under salt stress and they found that the growth rate and B absorption capacity were inhibited considerably at a NaCl concentration as high as 100 mM. It is known that the B biosorption is a passive transport process by mass flow across the plasmalemma of L. minor into the cell (Smith et al., 2010). The high salt concentrations (45 mM) decrease the osmotic potential of aqueous solution, preventing transpiration and as a result,

bisorption of B by plants is reduced (Yermiyahu et al., 2008). Furthermore, the growth rate inhibition of the high salt concentrations on several species including, Spirodela polyrhiza, Lemna minor and Lemna gibba have been reported (Sree et al., 2015).

4.4. Conclusion

This study aims at investigating the phytoremediation of boron rich waters using L. minor, a common duckweed. The results revealed that boron was absorbed in the first 2 days of experimental runs. However, at the end of the operating time of 2 days, the boron absorption capacity was constant due to the saturation level of plant. The results showed that the B removal was significantly affected by the B concentration, water height in cell, and initial HA concentration. Optimum pH value of aqueous solution was determined to be pH 8, although no significant effect of pH change on boron removal was observed. However, the B content in synthetic solution increased with the increasing HA concentration due to the decomposition of L. minor.

The maximum boron removal efficiency for 5 mg-B/L was 96.7% (pH 8, water height of 1.5 cm, without HA content). The boron removal efficiency decreased from 96.7% for 5 mg-B/L to 36.6% for 30 mg-B/L due to the toxic effect of high boron content on Lemna minor. Visual assessments and ESEM analyses also showed B toxicity at high concentrations. Furthermore, the removal efficiency and B content of L. minor under optimum operating conditions was found to be 59.5% and 1500 mg/kg for real geothermal water.

Our results presented in this paper indicated that Lemna minor can be efficiently used for B removal from waters with low B concentrations. Hoagland solution is easy to access due to a plethora of suppliers in the agriculture sector. Its ready-to-mix powders that can prepare at least 200 liters of solution are sold for around 150 Turkish Liras (21 USD). Once used up, the L. minor can be screened out of the treatment ponds, dried at ambient temperature and then used for soil amendment at B-deficient areas if the water did not contain any toxic and potentially hazardous ions/compounds. Use of L. minor as fish feed at aquaculture facilities is another option. Therefore, L. minor can be used as an environmentally friendly and low-cost pre-treatment or post-treatment process for the treatment of aqueous solutions containing high boron concentrations.

CHAPTER 5

3D ELECTRODE USE IN MDC FOR ENHANCED REMOVAL OF BORON FROM GEOTHERMAL WATER

5.1. Introduction

Industrialization and population are continually growing and resulting in severe environmental and energy problems due to conventional fossil fuels and chemical agents (Aghbashlo et al., 2019; Tabatabaei et al., 2020). Almost 2.1 million people are without clean water and 4.5 million people do not have access to adequately managed sanitation, as worldwide water use has climbed by 1% a year since 1980 (WHO, 2017; WWAP-UNESCO, 2019). As a result, boosting the availability of clean water with adequate management and effective treatment of contaminated water resources for recycling, particularly for industrial wastewaters, may solve the growing fresh water deficit.

Recently geothermal water resources are being exploited significantly as viable renewable energy sources in Turkey and worldwide (Melikoglu, 2017). Aquacultural pond heating, agricultural drying, balneology, cooling, greenhouse, power production, and industrial activities utilize geothermal water and hot steam (Gude, 2016; Tomaszewska et al., 2018). These applications generate large amounts of wastewater, often disposed of in agricultural fields, subsequently percolating into groundwater. Diverse and concentrated ionic content of geothermal water results in detrimental effects on the agricultural crops. In particular, boron (B) complexation with Cd, Cu, Ni, and Pb metals, which have more toxicity than those metals individually, is intrinsic in geothermal water resources. The high B concentrations could be toxic to plants causing chlorosis and necrosis of shoots, root growth inhabitation, presence of burns, reduction of photosynthesis (Hua et al., 2021).

This chapter has been published as:
A.Y. Goren, H.E. Okten, 3D Electrode Use in MDC for Enhanced Removal of Boron from Geothermal Water, Desalination 530 (2022) 115668.

Moreover, long-term exposure to high B contaminated water and consumption of B-containing vegetables can cause diarrhea, dermatitis, lethargy, nausea, vomiting, and etc., (Bryjak et al., 2008; Nielsen, 2002). Therefore, B removal from geothermal brines becomes crucial, and geothermal brines could also be considered valuable sources that can be used in agricultural and industrial applications and for domestic and drinking water purposes (Ozbey-Unal et al., 2018). Various treatment processes have been performed for B removal from waters, such as adsorption, coagulation, ion exchange, electrocoagulation, membrane processes, and hybrid technologies (Bhagyaraj et al., 2021; Çermikli et al., 2020; Chen et al., 2020; Lin et al., 2021). However, most of these treatment systems have cost-related and environmental challenges, such as resin regeneration, high sludge production, sludge management, high operating costs, and membrane fouling. Therefore, there is a crucial need for further research to develop treatment technologies that are cost-effective and environmentally friendly while effective in removing B from geothermal brines.

Recently, due to the water desalination with simultaneous power production, waste, and wastewater treatment functions, microbial desalination cells (MDCs) gained significant attention as a potential technology (Goren and Okten, 2021a; Saeed et al., 2015; Wang et al., 2020). MDCs are basically three-compartment (anode/desalination/cathode) bio-electrochemical systems (BES) that are modified from microbial fuel cells (MFCs). Separation between anode/desalination chambers and desalination/cathode chambers are done by an anion exchange membrane (AEM) and a cation exchange membrane (CEM), respectively. Organic matter is microbially degraded in the anaerobic anode chamber and in the absence of an electron acceptor such as O_2, generated electrons are transferred to the cathode chamber via a circuit that connects anode and cathode. Through the ion exchange membranes, anions and cations in the middle desalination chamber eventually migrate to anode and cathode chambers, respectively, resulting in desalination of water, for which the driving mechanisms are identified as electrochemical gradient and concentration gradient (Rahman et al., 2021b; Tawalbeh et al., 2020). Simultaneously, the concentration gradient facilitates Fick's diffusion and electrical fields drive the movement of charged ions in the desalination chamber across the AEM into the anode chamber. Following the MDC working principle, desalination can also be applied to boron-rich water streams as long as the transformation of boric acid (H_3BO_3) to borate ions ($B(OH)_4^-$) is achieved. Therefore, a pH adjustment above 9.5 is needed in order to convert boric acid into borate form. Namely, in the borate

form (pH>pKa), the core boron species is fully hydrated in the solution that results in a larger radius and a charge enhancement. Therefore, the ionized borate species readily diffuse through the AEM owing to their negative charge, successfully reducing the B concentration in desalination chamber.

Some crucial drawbacks of MDCs can be listed as high cost and low energy production, which are closely related to electrode material and potential losses during the transfer of electrons (Huggins et al., 2014; Wang et al., 2017). Furthermore, the typically utilized two-dimensional (2D) carbon (felt and paper) and graphite electrode materials have limitations such as low surface area for microbial colonization, low electron and substrate transport, all limiting power generation significantly (Zhang et al., 2019). On the other hand, three-dimensional (3D) carbon-based electrodes not only eliminate the limitations of 2D electrodes but they also provide a macro-porous structure and superior electron storing capacities (Do et al., 2018; Li et al., 2017; You and Kamarudin, 2017). Modifying the electrodes using 3D porous materials such as N-doped carbon cloth, biochar, and graphene/polyaniline nano complex modified carbon improved the microbial fuel cells (MFCs) (Hou et al., 2013; Liu et al., 2011; Sun et al., 2017; Wang et al., 2017; Yuan et al., 2019). The only study on 3D porous sponge electrode-MDC investigated the use of carbon nanotubes-chitosan (Ma and Hou, 2019). Amorphous carbon, carbon nanotubes, graphene, and graphite are commonly used for carbon-based electrodes, however they are complicated to synthesize, have high costs, and there is need for advanced infrastructure (Ahirrao et al., 2019; Do et al., 2018; Zhang et al., 2019). Therefore, activated carbon-based materials are promising options due to their availability and accessibility for producing and modifying electrodes (Li et al., 2020).

In this paper, we investigated the effectiveness of novel 3D activated carbon-chitosan (AC-CS) composite sponge anode electrode in generating energy while treating yeast wastewater with concurrent B removal from synthetic solutions and geothermal brine in an MDC setup. Anode surface area, activated sludge volume, anolyte solution, and B concentration were studied with synthetic B solutions. Then, B removal performance from natural geothermal brine was studied at identified optimal conditions. To our knowledge, this is the first research paper on producing 3D AC-CS composite sponge electrode to enhance the treatment performance and energy production while decreasing the cost of the electrode.

5.2. Materials and Methods

5.2.1. Characterization of Waters

The geothermal brine was obtained from a geothermal district heating facility and yeast wastewater was obtained from a yeast production factory, both located in İzmir, Turkey. Geothermal brine had a pH of 8.14 and an electrical conductivity of 1689 µS/cm. The measured pH and COD values for yeast wastewater were 7.87 and 9254 mg/L, respectively. Physicochemical characterization of water samples is given in Table 1. Samples were kept in polyethylene containers at a temperature of 4°C prior to experiments and they were filtered in order to eliminate particulate matter before characterization and each experimental run. Stock B solution was daily prepared with boric acid (H_3BO_3, Sigma-Aldrich). Acidified water (0.1 M HCl, pH 2.5), potassium phosphate buffer (0.1 M PBS, pH 6.5), and tap water (pH 7.1) were prepared as catholyte solutions.

Table 5. 1.Physicochemical properties of geothermal water and yeast wastewater.

Water type							
Geothermal water				Yeast wastewater			
Parameter	mg/L	Parameter	mg/L	Parameter	mg/L	Parameter	mg/L
K^+	30.1±1.2	F^-	8.21±0.15	K^+	868±12.82	F^-	0.20±0
NH_4^+	1.85±0.13	Si	24±0.1	NH_4^+	452±9.78	Si	66.0±4.59
Na^+	452±2.12	Br	0.38±0.03	Na^+	1608±173	Br	N.D.
Ca^{2+}	24.8±1.18	Al	0.017±0.01	Ca^{2+}	299±1.29	Al	0.075±0.01
Mg^{2+}	7.44±0.21	As	0.173±0.02	Mg^{2+}	77.5±5.13	As	0.007±0
Mn^{2+}	0.027±0	B	10.48±1.62	Mn^{2+}	0.183±0	B	0.142±0.11
NO_3^-	0.25±0.02	Cu	0.002±0	NO_3^-	25.6±1.65	Cu	0.003±0
NO_2^-	N.D.	Cr	0.331±0.23	NO_2^-	N.D.	Cr	0.325±0.18
SO_4^{2-}	178±2.98	Fe	0.055±0	SO_4^{2-}	1117±273	Fe	0.571±0.25
PO_4^{3-}	N.D.	Li	1.41±0.45	PO_4^{3-}	7.68±1.94	Li	N.D.
Cl^-	205±1.34	Ni	N.D.	Cl^-	1573±249	Ni	0.014±0.01

N.D.: Not Detected

5.2.2. Preparation of the 3D AC-CS Sponge Electrode

The AC (Merck, Germany) was washed and dried 24 h in the oven at a temperature of 105 °C to purify the AC. To produce an AC-CS composite, the AC powder was mixed with CS (medium molecular weight, Sigma-Aldrich, USA) with a weight fraction of 4:1. Then, the AC-CS mix was dissolved in distilled water with 2% (wt) of acetic acid and was continuously stirred for 24 h at 350 rpm. Cubic sponges of three different sizes (3 cm, 4 cm and 5 cm side lengths) were dipped in the AC-CS composite mixture and put in an ultrasonic bath for 20 min. Consequently, the AC-CS composite coated sponges were removed from the solution and dried in an oven at a temperature of 60 °C for 2 h. The interaction of amine groups on the CS surface with carboxyl and carbonyl groups on the AC surface increases hardness of AC-CS composite. This particular reaction is known as the Schiff base reaction, and it creates the ideal conditions for the polymer network to stabilize on the AC surface, which facilitates development of a cross-linked binary network covering the surface of the AC. The coating layer protects AC against corrosion. Overall, the Schiff base reaction immobilizes the composite coating layer on the AC surface effectively. Detailed synthesis procedure and reaction between AC and CS functional groups to form AC-CS composite were given in Figure E.1 and Figure E.2, respectively.

5.2.3. Characterization of the 3D AC-CS Sponge Electrode

Scanning electron microscopy (SEM, Quanta 250FEG, USA) investigated the AC-CS composite coated sponge electrode surface morphology. Energy-dispersive X-ray spectrometry (EDX) was also performed for analyzing the main elements present on the electrode surface. Fourier Transform Infrared Spectroscopy (FTIR) analyses were performed using Shimadzu FTIR 8400S to classify functional groups. Brunauer–Emmett–Teller (BET, Micromeritics Gemini V) determined raw and AC-CS composite sponge electrode surface areas. The thermal stabilities were determined by a thermogravimetric analyzer (PerkinElmer Diamond TG/DTA) at a heating rate of 10 °C/min from 22.5 to 950 °C in a nitrogen environment. The contact angle was also measured to determine the wettability of an electrode by a liquid.

5.2.4. MDC Set up and Operation

The setup of a MDC reactor with a 3D AC-CS electrode (Figure 5.1) is described in detail in our previous paper (Goren and Okten, 2021a). For batch mode operation, the 3D AC-CS composite sponge electrode was put into the anode chamber with varying surface areas (54, 96, and 150 cm^2) as an anode, and the carbon plate electrode (Goodfellow, England) was placed into the cathode chamber. In addition, an air pump was used to aerate the cathode chamber, and the connection between electrodes was provided with titanium wire. The external resistance was fixed at 100 Ω to attain a maximum current production under the closed circuit mode.

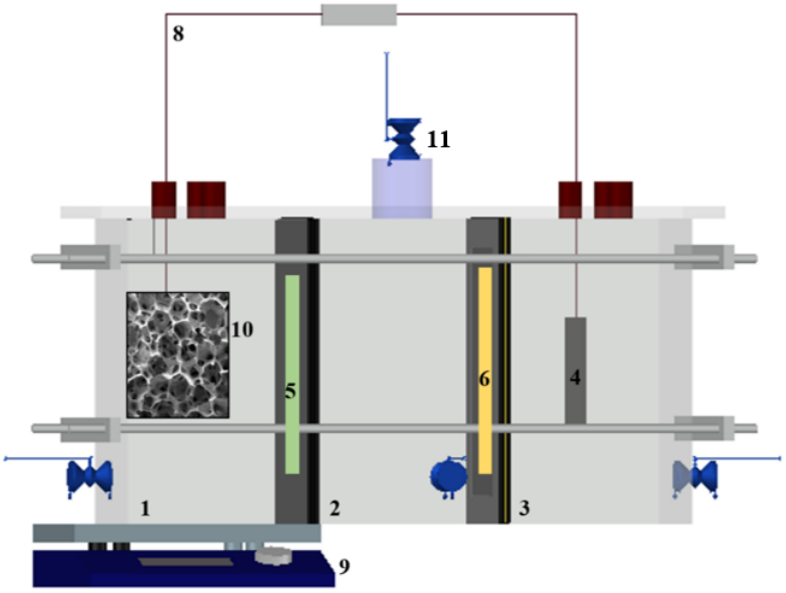

Figure 5. 1. The schematic diagram of MDC reactor: (1) Anode chamber, (2) Desalination chamber, (3) Cathode chamber, (4) Carbon plate electrode, (5) AEM, (6) CEM, (7) External resistor, (8) Copper wire, (9) Mechanic stirrer, (10) 3D sponge electrode, and (11) Inlet port.

Yeast wastewater as a carbon source and anaerobic activate sludge mixture was filled into the anode chamber with specified volumetric ratios (AS: YWW = 1:1, 1:2, and 1:5). The solution was continuously stirred at 185 rpm to provide a homogenous mixture and prevent settling. The cathode chamber was fed with varying catholyte solutions (phosphate buffer, acidified water, and tap water) and aerated continuously at an airflow rate of 2 L/min. The desalination chamber was fed with geothermal water and a specified amount of boron-containing synthetic solution (10, 20, and 30 mg/L). According to our

preliminary experiments, the MDC system was operated for 12 d due to the depletion of COD necessary for the survival of microorganisms.

A negative control experiment, without the use of microorganisms was performed in our previous study (Goren and Okten, 2021a). Anode, cathode and desalination chambers were filled with distilled water, phosphate buffer solution and synthetic solution with 5 mg/L B concentration, respectively. Control experiment results showed only a slight decrease in B concentration in the desalination solution, yet B concentration was not observed in anolyte. Therefore, we concluded that some small amount of B might get adsorbed on the AEM surface and the rate of diffusion was considerably impaired due to the lack of electrochemical gradient.

5.2.5. Analytical Methods and Calculations

The cell voltage (V) through external resistance (Rex=100 Ω) was recorded with a data aquation device (UNI-T, UT71C, China) connected to the computer at 5 min intervals. The current (i, mA) was calculated with $I = V / R_{ex}$. Power density (P_{An}, mW/m^2) normalized by surface area will be calculated with the cross-sectional area of the anode (A_{An}, m^2) due to the microbial reactions occur into an anode chamber as follows (Logan et al., 2006):

$$P_{An} = \frac{V^2}{R_{ex} \times A_{An}} \tag{5.1}$$

The ratio of transferred electric charge to its maximum value obtainable (coulombic efficiency - CE, %), was calculated by equation 5.2:

$$\mathrm{CE}(\%) = \frac{\mathrm{MW}_{O2} \int_0^t \mathrm{Idt}}{\mathrm{nFV_a}\left(\mathrm{C_{COD,i}}\text{-}\mathrm{C_{COD,e}}\right)} \times 100 \tag{5.2}$$

where MWO_2 is molecular mass of oxygen (32 g/mol), n is number of the e- produced from degradation of organic substrate (n: 4 mol e^-/mol), F is Faraday's constant (96485 C/mol), $C_{COD,i}$ and $C_{COD,e}$ is initial and effluent COD concentrations (mg/L), and V_a is anode chamber volume (0.54 L).

Moreover, daily pH changes in each chamber were measured using a pH meter (Mettler Toledo, SevenCompactTM, USA). COD was measured according to standard methods (APHA, 2017). B concentrations were analyzed using an ICP-OES (ICP-OES, AGILENT 5110, USA). In yeast and geothermal wastewater, cations and anions concentrations were analyzed by ion chromatography (IC, Dionex ICS-5000, USA).

5.3. Results and Discussion

5.3.1. Boron Concentration

The initial B concentration is an essential operating parameter as the concentration gradient force is the critical removal mechanism in the MDC system. Therefore, the MDC system was conducted using different B concentrations of 10, 20, and 30 mg/L at constant operating parameters (airflow rate - 2 L/min, anode surface area - 96 cm^2, anolyte solution - phosphate buffer, and YWW:AS ratio 1:1). Effect of B concentration on removal efficiencies and energy production were presented in Figure 5.2.

The highest B removal efficiencies were calculated as 75.9% ($C_{f,B}$: 2.405 mg/L), 45.2% ($C_{f,B}$: 10.968 mg/L) and 32.9% ($C_{f,B}$: 20.128 mg/L) for B concentrations of 10, 20, and 30 mg/L, respectively. However, the removal performance order reverses when the nominal concentration values are checked. At the end of 12 day experiments, 9.87 mg/L B, 9.03 mg/L B and 7.6 mg/L B were removed from the desalination chamber for the initial B concentrations of 10, 20 and 30 mg/L, respectively. The highest boron removal being achieved for the 30 mg/L B run proves the effect of concentration gradient difference between the anode and desalination chambers (Figure 5.2a). The concentration gradient force was suggested as the main mechanism for ion removal in MDC processes, which accelerated removal efficiency at high ion concentrations. On the other hand, at high salt concentrations, the back-diffusion of ions from the anode to the desalination chamber was also reported, which might lead to low desalination efficiency (Meng et al., 2019). Moreover, the fouling on the membrane surface at high salt concentrations might also cause low removal efficiency. At low salt concentrations, electrical gradient forces have been suggested as fundamental desalination mechanisms. These phenomena were in good agreement with our results. Similarly, (Ping et al., 2015) treated B from synthetic solution using MDC-Donnan dialysis hybrid process. They stated that the removal decreased with increased B content, removal efficiencies being calculated 60% and 52%

for 5 mg/L and 20 mg/L B content, respectively. Effluent B concentrations for all experimental runs were above the irrigation water limit value (1 mg/L). In comparison, the limit value of drinking water (2.4 mg/L) was exceeded for B concentrations of 20 and 30 mg/L (Edition, 2011). On the other hand, the effluent B concentration met the recommended WHO value of 2.4 mg/L for the 10 mg/L initial B concentration.

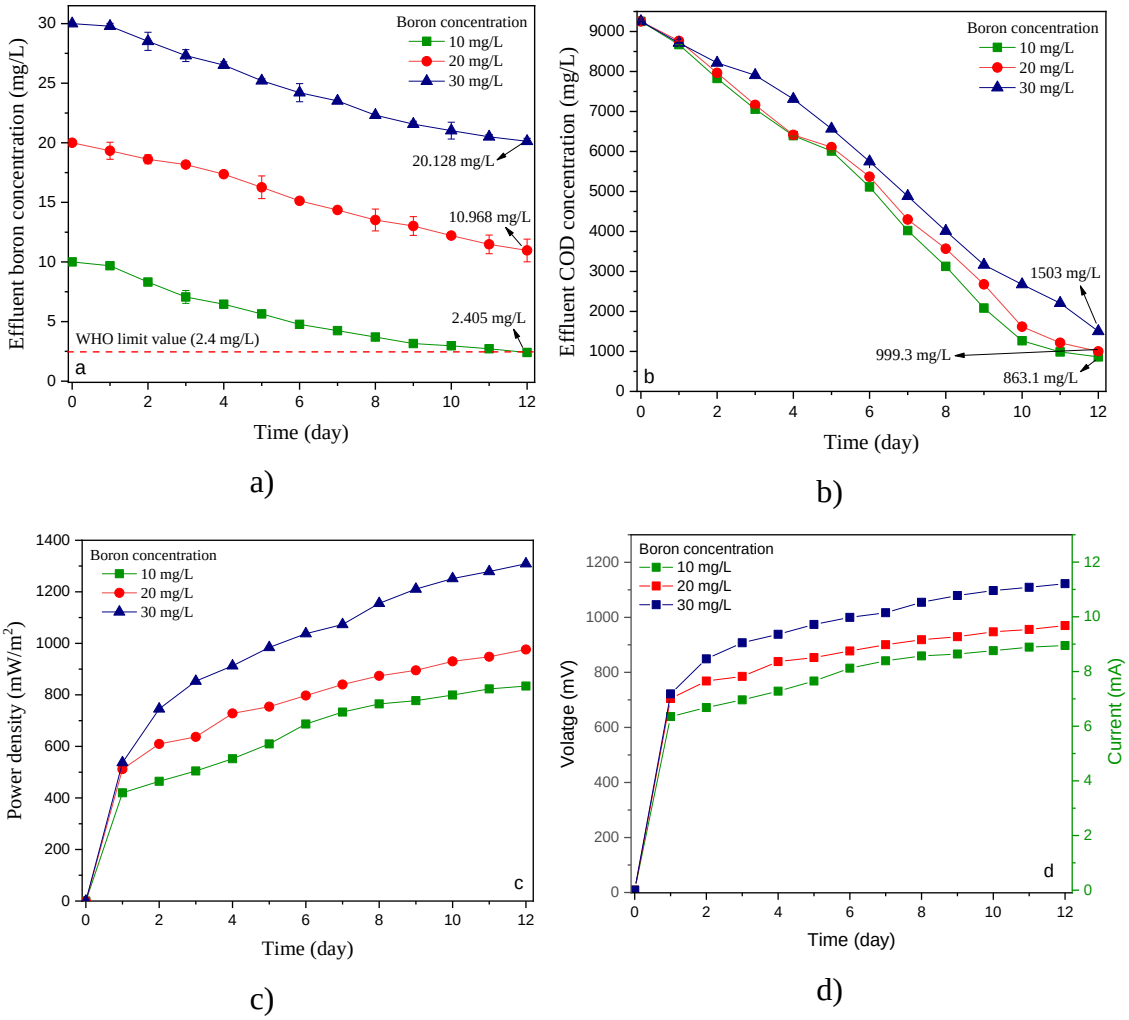

Figure 5.2. Effluent boron concentration a), effluent COD concentration b), power density c), and voltage and current in MDC d) at varying boron concentrations. (Air-flow rate: 2 L/min, electrode surface area: 96 cm2, anolyte solution: PBS, and AS:YWW volume: 1:1).

Organic matter removal from yeast wastewater was measured through COD removal efficiency (Figure 5.2b). The maximum COD removal efficiencies were 90.7% (C_{COD}: 863.1 mg/L), 89.2% (C_{COD}: 999.3 mg/L), and 83.8% (C_{COD}: 1503 mg/L) for initial B concentrations of 10, 20, and 30 mg/L, respectively. The COD removal performance of MDC has shown that borate ions transferred to anode chamber did not have a

substantial impact on microbial degradation processes. When the 30 mg/L B curve in Figure 5.2b is closely observed, it can be seen that despite transfer of approximately 10 mg/L of B to anode chamber, the COD decrease due to microbial activity has been steady throughout the run. Moreover, when 10 mg/L B and 20 mg/L B curves were examined, an increase in COD removal rate from the 5th day of experiment onwards was observed. There was a slight decrease in overall COD removal efficiency at 30 mg/L B, when compared to 10 mg/L B and 20 mg/L B runs, which yielded practically the same results. However, that cannot be explained by the added amounts of NaOH for pH adjustment for different runs since the amounts were basically the same due to the fact boric acid being a weak acid. Two additional reasons came up, one being the aging of microbial consortium and the other being analysis uncertainty, both of which shall be investigated in the future. Nevertheless, COD removal efficiencies were higher than those obtained by (Luo et al., 2012b) using the MDC process. The maximum COD removal efficiency was reported as 53.8% at an operational time of 1200 h. (Ebrahimi et al., 2018a) also investigated the COD removal efficiency of quadripartite MDC systems from municipal wastewater with an initial COD concentration of 4911 mg/L, and the highest COD removal efficiency was 58.4%.

Calculated CE values for all boron concentrations gradually increased through the end of operation. CE values were 16.9-18.7% across a range of B concentrations from 10 mg/L to 20 mg/L. The highest CE value of 23% was achieved at B concentration of 30 mg/L at an operating time of 12 d. Low B concentrations yielded lower CE values and vice versa. The relatively lower CE values for the 10 and 20 mg/L B concentrations were most probably due to the decreased current generation resulting from organic matter consumption and inadequate mass transfer in chambers (Dong et al., 2017).

Energy production performance of MDC was assessed under different boron concentrations. The highest voltage values produced in MDC, for B concentrations of 10, 20, and 30 mg/L, were 895, 968, 1121 mV, respectively. Based on the 3D anode electrode surface area of 96 cm^2, the maximum power density values were 834.4 mW/m^2 (10 mg/L), 976.1 mW/m^2 (20 mg/L), and 1309 mW/m^2 (30 mg/L). Energy production increased with increasing B concentration which translated into increased ionic strength of the solution and ended up enhancing the driving force through AEM (Figure 5.2c-5.2d). Power density values were higher than those obtained by The highest power density value (1309 mW/m^2) observed in this study was almost forty times the value (Liaquat et al., 2021) obtained (32 mW/m^2), proving that anode modification enhanced electricity production

in MDC. The power density of 527 mW/m^2 was reported in another recent study on simultaneous treatment of natural wetland saline water and sewage with MDC (Salman and Ismail, 2020). Overall, the key reason for higher power when compared to the literature was probably the dense microbial formation on the anode, effective electrochemically active area, and low internal resistance owing to the high surface area of 3D sponge anode. Moreover, yeast industry wastewater provided ample e- donors in the form of easily biodegradable substrate for microorganisms in the anode chamber. In order to facilitate easy comparison, different MDC configurations were summarized in Table 5.2 in terms of COD removal efficiencies, desalination efficiencies, and power production.

5.3.2. Anode Surface Area

Anode surface area is a critical parameter since it is directly related to microorganism colonization, biofilm layer development and subsequent organic matter degradation. Optimization of electrode surface area is a significant operating variable to enhance MDC efficiency. Therefore, we studied the effect of 3D sponge anode surface areas of 54, 96, and 150 cm^2 on B and COD removal with energy production. The B removal is enhanced with increasing anode surface area (Figure 5.3a). At operational time of 12 d, the B removal efficiencies were 64.4% ($C_{f,B}$: 3.556 mg/L), 75.9% ($C_{f,B}$: 2.405 mg/L), 76% ($C_{f,B}$: 2.397 mg/L) for surface areas of 54, 96, and 150 cm^2, respectively. The lowest B removal efficiency was achieved at a surface area of 54 cm^2 compared with other runs, most probably due to the small electrochemical active area, relatively high internal resistance, and low biofilm layer production on electrode surface related to its low surface area. The electrical gradient force, which is one of the important mechanisms responsible for B removal, cannot be provided sufficiently for the decrease in electron generation. The highest B removal efficiencies were practically the same for the surface areas of 96 and 150 cm^2. The perfectly aligned B removal trends for surface areas of 96 and 150 cm^2 proved that the B transfer mechanisms, namely chemical gradient and in this case more importantly electrical gradient, have reached their upper limit for the given parameters.

COD removal was considerably stable through the experiments, and the highest removal efficiencies were measured to be 91.1% (C_{COD}: 821.9 mg/L), 90.7% (C_{COD}: 863.1 mg/L), and 73.4% (C_{COD}: 2458 mg/L) for surface areas of 150, 96, and 54 cm2,

respectively (Figure 5.3b). The higher electrode surface area enhanced the organic matter oxidation by microorganisms with most probably due to enhanced biofilm layer formation. The same removal trends for 96 and 150 cm^2 electrodes could be explained by stating that with the given AS:YWW ratio, the system has reached its COD removal limit regardless the electrode area.

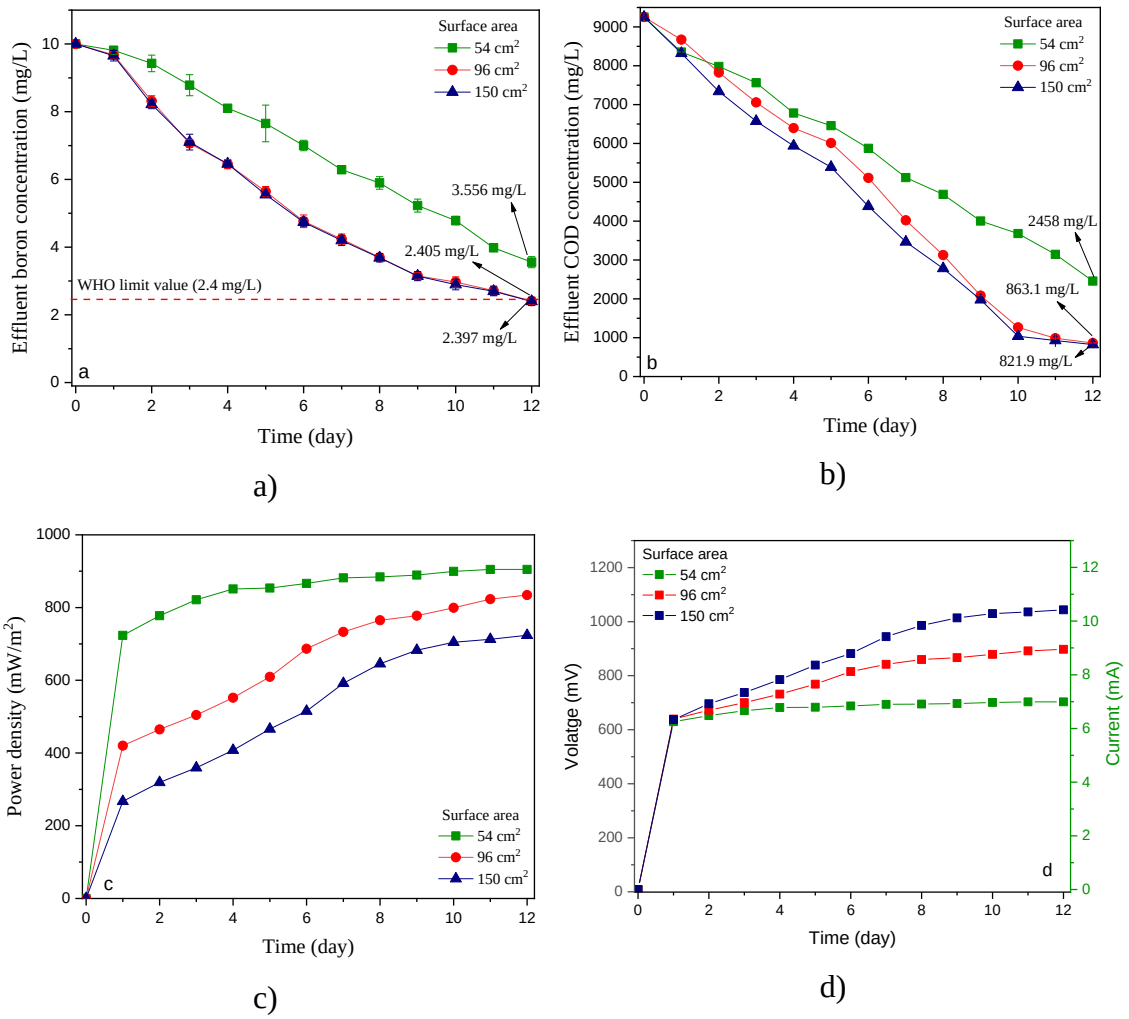

Figure 5.3. Boron concentration a), effluent COD concentration b), power density c), and voltage and current in MDC d) at varying electrode surface areas. (Air-flow rate: 2 L/min, initial boron concentration: 10 mg/L, anolyte solution: phosphate buffer, and AS:YWW volume: 1:1).

Similarly, the MDC process using an anode surface area of 150 cm^2 recovered greater coulombs from yeast wastewater, presenting a CE value of 19.7% compared to the CE value of 16.4% achieved using an anode surface area of 54 cm^2. This was because the decreased internal resistance with the enhanced biofilm formation resulted in high e-generation by microorganisms at higher electrode surface areas. Besides, the highest

voltage was achieved using an anode surface area of 150 cm^2 with increasing electron production (Figure 5.3d). At resistance of 100 Ω, the highest voltage values were 699, 895, and 1042 mV for surface areas of 54, 96, and 150 cm^2, respectively. However, the opposite trend was observed in power density values with 904.8, 834.4, and 723.8 mW/m^2 for surface areas of 54, 96, and 150 cm^2, respectively (Figure 5.3c). The power density decreased with increasing electrode surface area. Even though we observed an increase in the electrical potential with growing electrode surface area, it was not sufficient to cause a simultaneous rise in the power density values – power density was calculated by dividing the square of electrical potential with the product of external resistance and anode area, the former being constant for every case. Overall, results revealed that the anode surface capacity could be an essential operational variable for the MDC process.

5.3.3. Activated Sludge Volume

Electricity generation mechanism of BESs is mainly dependent on the degradation of organic substrates from diverse types of sludge and/or wastewater by microorganisms. The desalination efficiency can also be influenced by organic substrate and microbial community availability and internal resistance of the MDC system (Al-Mamun et al., 2018). Therefore, wastewater characteristics, potential of microbial growth, organic substrate content, activated sludge source, and microorganism types could be important to enhance the MDC system (Tamta et al., 2020; Tawalbeh et al., 2020).

The effect of AS:YWW volumetric ratio (1:1, 1:2, and 1:5) on B removal, COD removal, and energy production was studied in this paper. The maximum boron removal efficiency was found to be almost 76% for all AS: YWW volumetric ratios (Figure 5.4a). While varying AS:YWW have no considerable impact on B removal, increment in activated sludge volume from 1:5 to 1:1 was improved COD removal efficiency from 69.2% (C_{COD}: 2846 mg/L) to 90.7% (C_{COD}: 863.1 mg/L) (Figure 5.4b). The noticeably low COD removal efficiencies at AS: YWW volumetric ratios of 1:5 and 1:2 were possibly related to the low microbial community and hence slight activity to degrade organic substrate. Similarly, the MDC process using AS:YWW volumetric ratio of 1:5 was presented a low CE value of 17% compared to the CE value of 21.1% achieved using AS: YWW volumetric ratio of 1:1. This was because the increase in internal resistance with the insufficient biofilm formation resulted in low e- generation by microorganisms.

Moreover, the low CE value for AS:YWW volumetric ratio of 1:5 occurred with high organic substrate content in solution, which was more than the microorganisms could handle. In addition, the reduction of the current generation in the direction of flow resulting from organic matter degradation and limited e- transfer from anode to cathode chamber could cause low CE values (Dong et al., 2017). Under external resistance of 100 Ω and surface area of 96 cm^2, the power density and voltage of the MDC system was found to be 834.4 mW/m^2 and 895 mV, 786.6 mW/m^2 and 869mV, and 749.1 mW/m^2 and 848 mV for AS:YWW volumetric ratio of 1:1, 1:2, and 1:5, respectively (Figure 5.4c-5.4d).

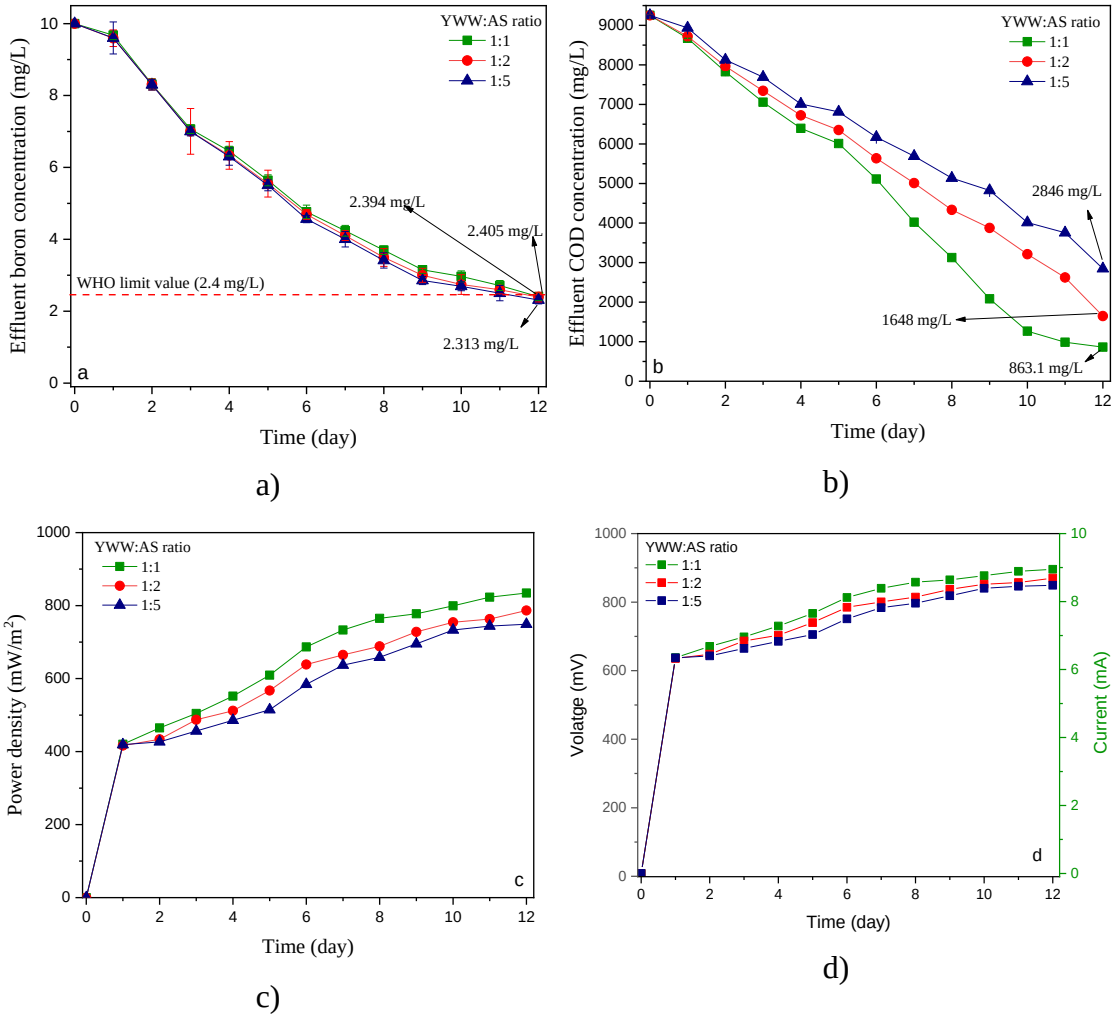

Figure 5.4. Boron concentration a), effluent COD concentration b), power density c), and voltage and current in MDC d) at varying activated sludge volumes. (Air-flow rate: 2 L/min, initial boron concentration: 10 mg/L, anolyte solution: phosphate buffer, and electrode surface area: 96 cm^2).

Table 5.2. The COD removal efficiency, desalination performance, and power production of the different MDC configurations.

Configuration	Anode material	Cathode material	Operating conditions	CE-CR values (%)	COD removal (%)	Desalination efficiency (%)	Power density	REF
MDC	Carbon graphite	Carbon graphite	External resistance: 100 Ω; HRT: 12 d; Anoyte solution: industrial wastewater; Catholyte solution: 0.1 M of phosphate buffer; Desalination solution: 5m g/L boron solution; Air flow rate: 2 L/min; Chamber volume: 540 mL	12.9	61.3	90.3	8.93 mW /m^3	(Goren and Okten, 2021a)
QMDC	Graphite	Graphite	External resistance: 100 Ω; HRT: 120 d; Anoyte solution: septage wastewater; Catholyte solution: treated septage wastewater; Desalination solution: 30 mg/L of salt solution; Anode chamber volume: 410 mL; Cathode and desalination chamber volume: 100 mL	21.4-14.3	91.1	72.8	8.16 W/m^3	(Luo et al., 2012b)
MDC	Graphite brush	Carbon cloth	External resistance: 1000 Ω; HRT: 1200 h; Anoyte solution: municipal wastewater; Catholyte solution: 50 mM of phosphate buffer; Desalination solution: 100 mM NaCl; Anode and cathode chamber volume: 140 mL; Desalination chamber volume: 60 mL	131	52	66	8.01 W/m^3	(Ebrahimi et al., 2018a)
MDC	Graphite rods	Stainless steel grid	Anoyte solution: dairy wastewater; Catholyte acidic water; Desalination solution: 35 g/L NaCl solution; Anode and cathode chamber volume: 300 mL; Desalination chamber volume: 200 mL	-	57	31	-	(Liaquat et al., 2021)
MDC	Carbon brush	Activated carbon and PTFE electrode	External resistance: 10 Ω; HRT: 24 h; Anoyte solution: domestic wastewater; Catholyte solution: 50 mM of phosphate buffer; Desalination solution: 35 g/L NaCl solution	19.4	92.2	76.5	737 mW/m^2	(Dong et al., 2017)

(cont. on next page)

Table 5.2. (cont.)

Configuration	Anode material	Cathode material	Operating conditions	CE-CR values (%)	COD removal (%)	Desalination efficiency (%)	Power density	REF
MDC	Carbon felt	Carbon felt	External resistance: 0.1 Ω; Recirculation flow rate: 95 mL/min; Anoyte solution: 20 mM of acetate; Catholyte solution: 0.06 M of ferric ciyanide; Desalination solution: 6.8 g/L of NaCl solution; Anode and cathode chamber volume: 2510 mL, Desalination chamber volume: 770 mL	81.2	14[a]	93	0.24 kWh/m^3	(Ramírez-Moreno et al., 2021)
PMDC	Graphite plate	Graphite plate	External resistance: 100 Ω; HRT: 24 h; Anoyte solution: dairy wastewater; Catholyte solution: algae (*Oscillatoria sp*.) cultured in BG11 medium; Desalination solution: 20 g/L salt solution	-	78.2	65.8	44.1 mW/m^2	(Bejjanki et al., 2021)
APMDC	Carbon fiber brush	Carbon cloth coated with 0.5 gm Pt/cm^2	External resistance: 1 Ω; Anoyte solution: synthetic wastewater; Catholyte solution: 100 mM of phosphate buffer; Desalination solution: 35 g/L of NaCl solution; Anode and cathode chamber volume: 48 mL, Desalination chamber volume: 32 mL	1.79	83.6	30	880 mW/m^2	(Rahman et al., 2021a)
MDC	AC-CS composite sponge	Carbon graphite	External resistance: 100 Ω; HRT: 12 d; Anoyte solution: domestic wastewater; Catholyte solution: 0.1 M of phosphate buffer; Desalination solution: geothermal brine; Air flow rate: 2 L/min; Anode, desalination, and cathode chamber volumes: 540 mL each	11	81.4	65.5 (B removal)	867 mW/m^2	This study

5.3.4. Catholyte Solution

Acidified water, microalgae-containing solutions, phosphate buffer, ferricyanide, non-buffer saline solution, and sodium chloride solutions were previously utilized as the catholyte (Ebrahimi et al., 2018b; Zhang and He, 2013). For future commercialization and scale-up of MDCs, there is significant need for a cheap, ecologically friendly, and effective catholytes. The effectiveness of the MDC on B and COD removal and on energy generation was investigated using PBS, tap, and acidic water as catholyte (Figure 5.5).

The B removal efficiencies were 75.9% ($C_{f,B}$: 2.405 mg/L) , 46.3% ($C_{f,B}$: 5.375 mg/L), and 42.9% ($C_{f,B}$: 5.713 mg/L) for phosphate buffer, acidified, and tap water, respectively (Figure 5.5a). MDC using phosphate buffer achieved the highest B removal efficiency of 75.9%, showing that the combination of low pH variation due to buffer capacity, high conductivity, and minimum internal resistance had the greatest benefit in B removal. The borate ion transfer in PBS solution was more effective than in acidified water and tap water solution, resulting in a great performance of non-buffer saline catholyte despite pH imbalance. The ionic content of the desalination chamber might become greater than that of the cathode chamber when a low phosphate buffer concentration was utilized. As a result of the salt gradient, water would migrate from the cathode to the desalination cell, resulting in a greater desalination rate in the MDC.

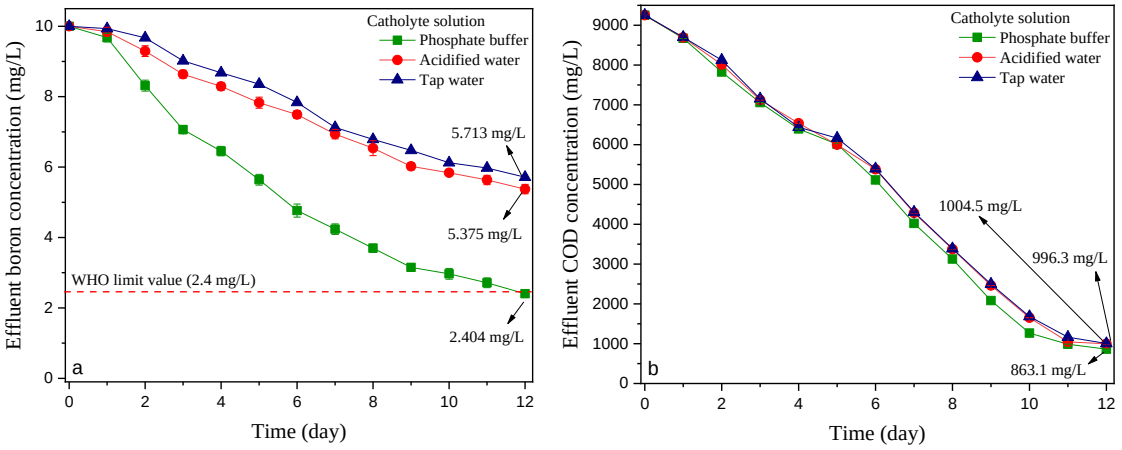

a) b)

Figure 5.5. Boron concentration a), effluent COD concentration b), power density c), and voltage and current in MDC d) at varying catholyte solutions. (Air-flow rate: 2 L/min, initial boron concentration: 10 mg/L, activated sludge volume: 1:1, and electrode surface area: 96 cm^2).

(cont. on next page)

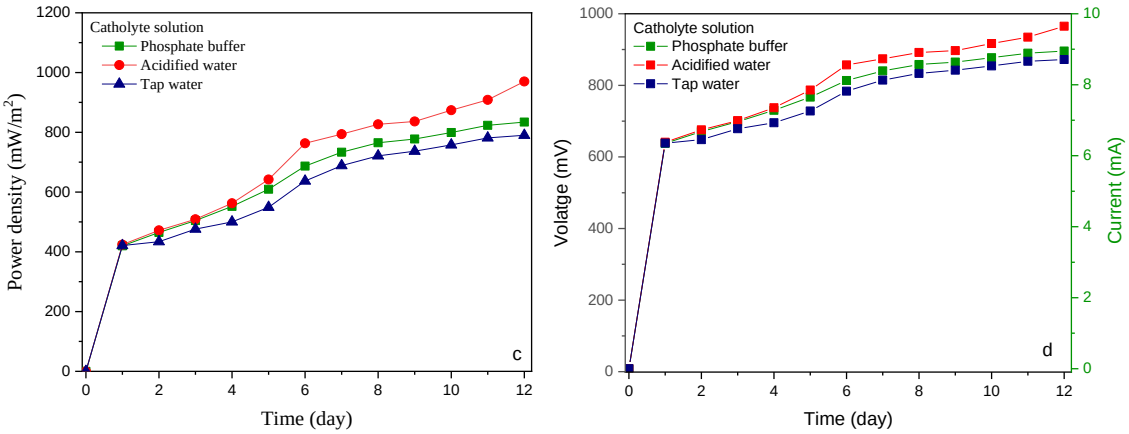

c) d)

Figure 5.5. (cont.)

To understand practical reasons for boron and COD removal and energy generation changes, pH variations in chambers were also examined during the experimental runs. In this study, the highest average pH variation was observed using acidified water, decreasing from 9.5 to 6.48 during the first day of operation. The fundamental reason acidified water decreased B removal might be explained by the desalination solution becoming acidic with the transfer of H^+ ions from cathode chamber to the desalination chamber, hindering hydroxylation of boric acid. On the other hand, the run with phosphate buffer demonstrated minor pH fluctuation at the desalination solution. Due to the large buffer capacity of PBS buffer, the pH in the desalination chamber decreased from 10.5 to 9.01 during the first 24 hours of operation.

Moreover, COD removal efficiencies were 90.7% (C_{COD}: 863.1 mg/L), 89.2% (C_{COD}: 996.3 mg/L), and 89.1% (C_{COD}: 1004.5 mg/L) for PBS, acidified, and tap water, respectively (Figure 5.5b). There was no change in COD content since no inhibitory effect was observed on microbial activity. Similar trends were observed for the CE values, which were 16.8, 17, and 18.6% for tap water, PBS buffer, and acidified water, respectively.

Power density and voltage values in closed-circuit mode were presented in Figure 5.5c-5.5d. The maximum power densities were 790.3, 834.4, and 970 mW/m^2 for tap water, PBS buffer, and acidified water, respectively. These results revealed that as the electron acceptor (oxygen) was the same at all catholyte solutions, there was no significant change in power density and voltage values. Namely, the e- depletion rate in the cathode chamber and transport rate of electrons from anode to cathode chamber were almost identical. Furthermore, the results showed that acidified water enhanced MDC

voltage (965 mV) and power density due to a more significant cell potential due to the solution's lower pH. On the other hand, tap water produced the lowest power density and voltage (871 mV) because of the low cell potential of the solution's neutral pH. Although acidified water had a larger energy production capacity, it was ineffective due to causing considerable pH changes in the MDC system, resulting in excessive chemical use due to the pH adjustment requirement.

5.3.5. Geothermal Brine Treatment

Boron removal from geothermal brine was investigated under optimized operational parameters such as air flow rate of 2 L/min, electrode area of 96 cm^2, YWW:AS ratio of 1:1 and phosphate buffer as catholyte. The B removal efficiency was 65.5% ($C_{f,B}$: 3.128 mg/L), which was 1.2 times lower than that for 10 mg/L B-containing synthetic solutions (75.9%) under the same operational variables. This was most likely due to high ionic content in geothermal brine. Competition between the borate ions and other anions in geothermal brine might decrease the transfer rate of boric acid. The highest COD removal was 81.4% ($C_{f,COD}$: 1724 mg/L) using geothermal brine. The relatively slight decrease in COD removal in geothermal brine was observed most probably due to the inhibitory effects of other ions and heavy metals on microbial activity. Measured power density, voltage, and current were presented in Figure 5.6. The power density increased from 834.4 to 866.9 mW/m^2 for geothermal brine compared with the similar synthetic solution. In addition, the CE value was calculated to be 11%, while the CE value of 10 mg/L boron-containing synthetic solution was 16.9%. This slight increase in CE value may occurs due to the adverse impact of salinity on microbial activity resulting in low organic matter degradation and e- production by microorganisms. Overall, results revealed that the MDC with 3D sponge electrode provided higher B removal, COD removal from yeast wastewater, and electricity generation for treating geothermal brine.

In addition, some anion, cation, and heavy metal removal efficiencies were investigated. At the end of the operating time of 12 days, the highest removal efficiencies were 68.8% (C_f: 0.054 mg/L) for As, 77.3% (C_f: 0.32 mg/L) for Li, 81.8% (C_f: 0.011 mg/L) for Fe, and 100% (C_f: 0.009 mg/L) for Al. Removal efficiencies of major cations were 50.7% (C_f: 223 mg/L) for Na, 66.6% (C_f: 10.05 mg/L) for K, 67.2% (C_f: 93.2 mg/L) for Ca, and 70.3% (C_f: 2.21 mg/L) for Mg. Also, removal efficiencies of chloride and sulfate anions were 85.9% (C_f: 28.75 mg/L) and 45.5% (C_f: 97 mg/L), respectively.

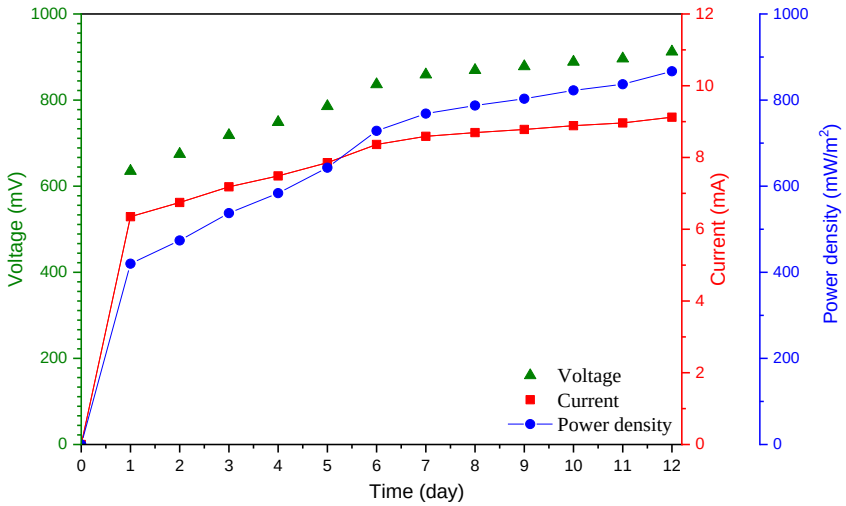

Figure 5.6. Voltage, current, and power density values in MDC for geothermal brine. (Air-flow rate: 2 L/min, initial boron concentration: 10.48 mg/L, activated sludge volume: 1:1, catholyte solution: phosphate buffer, and electrode surface area: 96 cm^2).

5.3.6. Characterization of 3D AC-CS Sponge Electrode

The SEM images show the polyurethane sponge material before the coating process with the AC-CS composite (Figure 5.7a). It is seen that the fresh polyurethane sponge material consists of a macroporous network. After coating the AC-CS composite, the polyurethane sponge still consists of a macroporous network, and the sponge is covered by a layer of conductive AC-CS composite (Figure 5.7b). The outer and inner surfaces of the coated sponge provided a larger surface area than an uncoated sponge. Consequently, the AC-CS coated sponge offers a more extensive surface area for the production of biofilm and bacterial diffusion and efficient mass transport pathways for substrates and electrons. Moreover, EDX results revealed a change of ion content on the electrode surface. The carbon content of the AC-CS composite sponge surface increased to 94.1%, while it was only 54.18% for the raw sponge.

Contact angle images of raw and AC-CS composite coated sponge were presented in Figure 5.8. The raw sponge showed a static water contact angle of 99.4%, specifying its surface hydrophobicity. After AC-CS composite coating, the AC-CS sponge presented a contact angle of 37.6%. The enhanced wetting behavior of the anode material facilitated the migration of aqueous solution into the macro-pore structure.

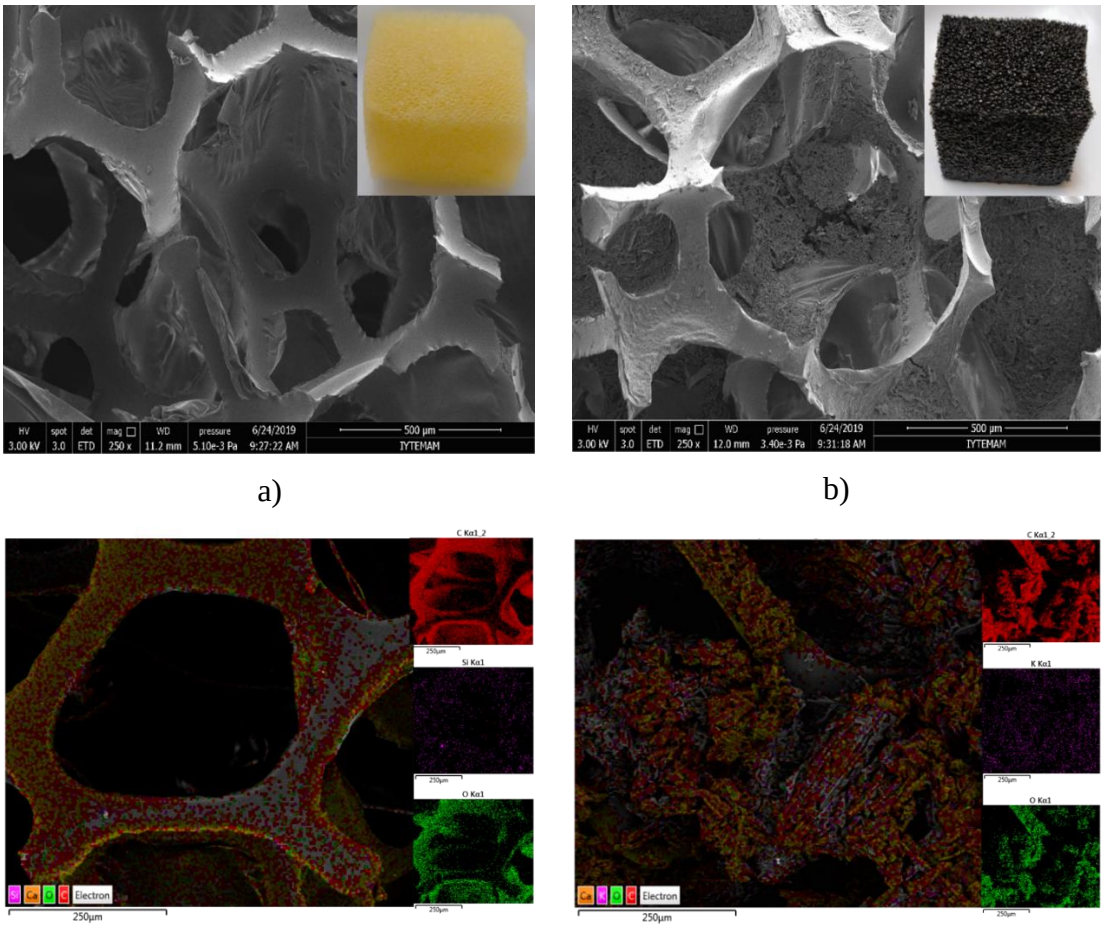

Figure 5.7. SEM images of fresh sponge a) and AC-CS composite coated sponge b) and elemental mapping of raw sponge c) and 3D AC-CS composite coated sponge electrode d).

BET analyses were performed to determine the porous structure and porosity of the 3D AC-CS sponge anode. The BET surface areas were 1.09 and 230 m^2/g for samples of raw and AC-CS composite sponges, respectively. The results proved significantly higher porous texture for AC-CS composite sponge. Pore volume of raw sponge, 0.008 cm^3/g, was lower than that of AC-CS composite sponge (0.202 cm^3/g). Therefore, it was concluded that the AC-CS composite sponge could provide more available sites for microorganism colonization and liquid penetration owing to its larger pore structure and higher surface area (Wang et al., 2013). In comparison to the literature, the BET surface area and pore volume values were higher than the ones (Ma and Hou, 2019) reported using a 3D carbon nanotube-chitosan (CNT-CS) sponge anode in MDC. They noted that the BET specific surface area of the CNT-CS sponge anode was 89.36 m^2/g. Overall, the unique structural features of the novel 3D AC-CS sponge anode presented it as a promising material than reported 2D anodes in the MDC process.

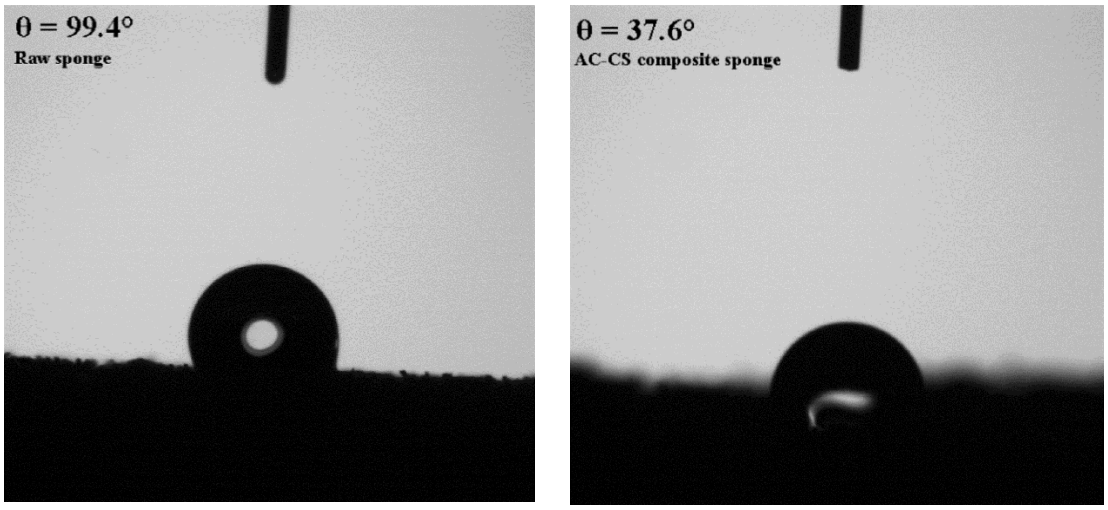

a) b)

Figure 5.8. The contact angle images of raw sponge a) and AC-CS composite coated sponge b).

The FTIR spectra of raw sponge and AC-CS composite coated sponge were given in Figure 5.9. FTIR spectrum of raw sponge showed broad peaks about 3230 cm^{-1} that corresponded to N-H link of urethane group. The peaks between 2968 and 2868 cm^{-1} are represented by symmetric and asymmetric vibrations of the CH_2 group. Moreover, the peak of about 1684 cm^{-1} can correspond to the C-O groups of ester and urethane groups (da Rosa Schio et al., 2019; Mallmann et al., 2014). For the AC-CS composite sponge, the peak at 1598 cm^{-1} most probably occurred through C-N elongation, which was directly in relation to CS (Kumirska et al., 2010). Similarly, the peaks around 2928 cm^{-1} might be corresponded to O-H and N-H stretching, while the peak at 1640 cm^{-1} might represent the C=O bonds (usually amide peak) (Wang et al., 2010; Zhang et al., 2016). The absorption peaks at 1372 cm^{-1} confirmed the N-H deformation vibration in $–NH_2$ while the peaks at 1096-928 cm^{-1} pointed at the existence of skeletal vibration involving C−O stretching, which was common in chitosan saccharide structures. In terms of AC, the peaks at 1640-1659 cm^{-1} in the FTIR spectrum of AC-CS composite sponge showed C=O stretching vibration of C=O, particularly in carboxyl groups, carbonyl, and lactone the C-O stretching in a carboxylic acid (Nifas and Forteza, 2019). Consequently, these results revealed that all the peaks attributed to the CS, raw sponge, and AC were also observed in the spectrum of the AC-CS sponge. In conclusion, following the AC-CS composite sponge coating, the functional groups remained unchanged.

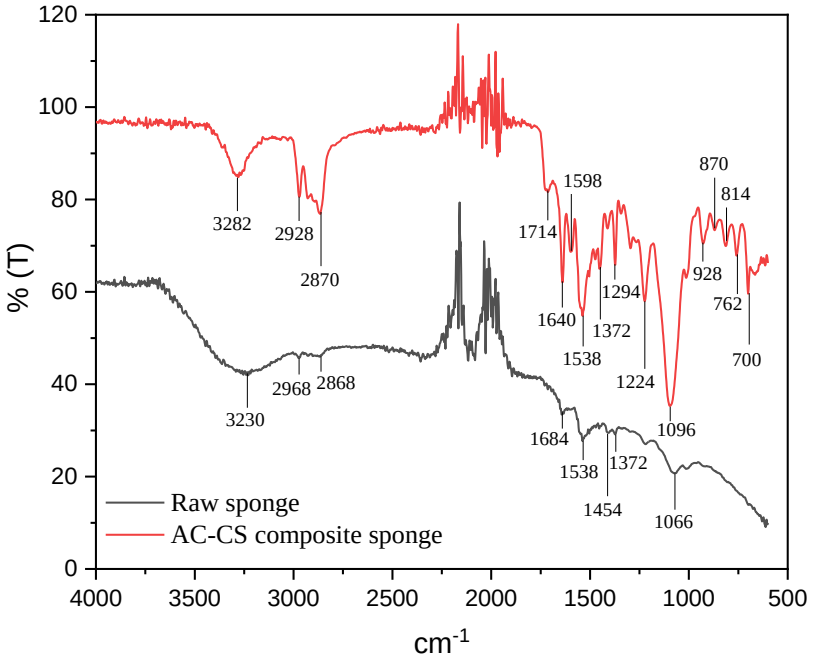

Figure 5. 9. The FTIR results of raw sponge and AC-CS composite coated sponge.

5.3.7. Cost Analysis

Material costs and considerable energy consumption were main factors contributing to the cost of conventional desalination technologies in general. On the other hand, high capital costs and low water production rates of MDCs are major problems holding their real scale application back. For our 3D AC-CS MDC set up the material costs added up to 29.89 USD. As expected, the membrane cost was 73.8% of the total material cost. The cost of 96 cm^2 composite 3D sponge was only 0.52 USD, whereas the commercial 2D carbon graphite electrode material was 2.55 USD for the same area. The MDC in this study showed a similar boron removal performance that was observed with the single pass reverse osmosis process. In terms of operational costs, MDC setup used in this study cannot be compared with an RO system, since the MDC setup was run in batch mode. Once the upscaling issues are solved, a fair comparison can be conducted and MDC may have an advantage for being energy self-sufficient process. However, since MDC is not a pressurized system, the time required to achieve the same treatment performance is much higher for MDC.

The cost analysis of the MDC system was also examined by comparing the innovative 3D AC-CS composite sponge electrode with other conventional materials (carbon paper, carbon felt, carbon brush, and graphite) in terms of desalination

performance and energy production (Table 5.3). The energy production values were in the range of 226-2000 mW/m^2, 101-480 mW/m^2, and 685-860 mW/m^2 using carbon felt, carbon cloth and paper, and carbon brush, respectively. These results showed that the energy production performance was promising for carbon brush anode materials owing to their high surface area. During geothermal brine desalination, the composite sponge anode produced 867 mW/m^2, which is quite promising. Furthermore, comparing the desalination efficiencies of conventional anode materials (26-99.4%) with 3D AC-CS sponge's boron removal performance (65.5%) places the latter in the upper-middle range. However, it should be noted that the MDC studies in the literature were done mostly using synthetic saline solutions with varying NaCl concentrations. Therefore, a true comparison requires the use of geothermal brine as influent. Overall results proved that the use of porous and cost effective AC-CS sponge electrode increased the energy production efficiency while decreasing material costs. Consequently, the MDC system can be used in small scale wastewater treatment plants as an energy efficient and cost effective process profiting from the development of low cost and innovative AC-CS sponge anode material.

Table 5.3. Energy production and desalination efficiency of different anode materials.

MDC configuration	Anode material	Cathode material	Desalination efficiency (%)	Energy production (mW/m^2)	Reference
MDC	Carbon graphite fiber brush	Carbon cloth	97.0	860	(Qu et al., 2013)
MDC	Carbon felt	Carbon felt	90	2000	(Cao et al., 2009)
MDC	Carbon cloth	Carbon cloth	67	480	(Mehanna et al., 2010)
BMDC	Carbon felt	Carbon felt	92	960	(Wen et al., 2012)
SMDC	Graphite fiber brush	Carbon cloth	26	685	(Davis et al., 2013)
IER-MDC	Carbon fiber felt	Carbon fiber felt	98	360	(Zhang et al., 2012)
SMDDC	Carbon paper	Carbon paper	90.5	101	(Zhang and Angelidaki, 2013)

(cont. on next page)

Table 5.3. (cont.)

MDC configuration	Anode material	Cathode material	Desalination efficiency (%)	Energy production (mW/m^2)	Reference
FMDC	Carbon felt	Graphite plate	99.4	226	(An et al., 2014)
MDC	Carbon cloth	Carbon cloth	80.7	348	(Hemalatha et al., 2017)
MDC – 10 mg/L B solution	AC-CS composite sponge	Carbon graphite	75.9	834.4	In this study

MDC: Microbial desalination cell, BMDC: Biocathode microbial desalination cell, SMDC: Stacked microbial desalination cell, IER-MDC: Ion exchange resin- microbial desalination cell, SMDDC: Submerged microbial desalination-denitrification cell, FMDC: Four chamber microbial desalination cell.

5.4. Conclusion

In this study, our aim was to equip the MDC set up with a porous 3D anode electrode that has lower cost than the conventional electrode materials. Material characterization revealed improved surface areas and porosity following the AC-CS application. The novel 3D anode presented high electron transfer efficiency owing to its porous structure. As an overall result, not only the production of 3D sponge anode electrodes with AC-CS composite was achieved but also desalination and power generation results that were comparable with the literature were presented. In order to incorporate MDC technology to real scale water treatment trains, there is need to further study the issues such as decreasing inorganic and organic membrane fouling and reducing internal resistance. Consequently, results revealed that the 3D AC-CS sponge anode presents significant potential for enhancing desalination and energy production in the MDC process.

CHAPTER 6

POLISHING OF REVERSE OSMOSIS CONCENTRATE AND PERMEATE STREAMS USING MICROBIAL DESALINATION CELL

6.1. Introduction

Clean water is on high demand worldwide as global population and industrialization increases in the era of climate change, which means additional burdens on the quantity and quality of water resources. Water contamination is a critical environmental problem, which has significant adverse impacts on socio-economic development and human health. Globally, almost 2.1 million people are experiencing clean water scarcity and 4.5 million people lack safely managed sanitation (WHO and UNICEF, 2017). Therefore, effective treatment of polluted water streams for recycling particularly in water-intensive industries and improving the supply of clean water with proper management may offer the much sought after solution.

When the water demand is evaluated based on sectors, the agriculture sector leads worldwide as the most water consuming sector. The agricultural water withdrawal to total water withdrawal ratios for various countries are as follows: France 10.7%, USA 39.7%, Italy 49.7%, South Africa 57.9%, Spain 65.2%, Türkiye (formerly known as Turkey) 87.1% and Uzbekistan 92.3% (FAO, 2022). In Türkiye, approximately 87% of the total abstracted water is used at the agriculture sector, mostly for irrigation purposes. Although, the high demand is mainly caused by the types of crops cultivated and the vast lands allocated for agriculture, the role of archaic irrigation practices shall also be considered. Also, a paradigm shifts from conventional water resources to unconventional ones such as recycled/upcycled/downcycled wastewater streams is needed.

This chapter has been published as: A.Y. Goren, Y.A. Jarma, N. Kabay, A. Baba, H.E. Okten, Polishing of Reverse Osmosis Concentrate and Permeate Streams using Microbial Desalination Cell, Submitted to Desalination (2022).

Geothermal water is an underexploited renewable energy resource, which is gaining importance currently in Türkiye and globally (Melikoglu, 2017). Energy from geothermal water and hot steams is used in several applications, such as district, greenhouse, and aqua-cultural pond heating, electricity production, agricultural drying, cooling, balneology, and industrial processes (Gude, 2016; Tomaszewska et al., 2018). These applications produce huge amounts of brine, which are generally discharged into nearby fields or water bodies and leach into groundwater through infiltration. Treatment of spent geothermal brine is not only essential for safe disposal but is fast becoming a requirement to tackle water scarcity.

To date, several treatment technologies have been developed for boron removal from water resources, such as adsorption, coagulation-flocculation, electrocoagulation, ion exchange, hybrid processes, and membrane processes (Bhagyaraj et al., 2021; Çermikli et al., 2020; Chen et al., 2020; Lin et al., 2021). However, most of these treatment methods suffer from cost related and environmental issues, such as difficulties in regeneration of resins, formation of high amount of sludge and hardness in sludge management, high capital, operation, and maintenance costs, chemical consumption for pH adjustment, and membrane fouling. Moreover, boron removal using membrane processes (e.g. reverse osmosis (RO), ultrafiltration (UF), nanofiltration (NF), and forward osmosis (FO)) are considerably energy intensive, causing an important challenge for tackling water stress in the areas with limited energy supply. Besides, the individual treatment of industrial wastewater and saline water can cause high capital and maintenance cost. Desalination of water resources using RO process causes significant amount of energy consumption. According to Affordable Desalination Collaboration (ADC), the specific energy requirement is reported to be in the range of 1.8–2.1 kWh/m^3 for RO process with energy recovery devices (MacHarg et al., 2008). Moreover, the energy consumption of RO process ranges from 2.0 to 3.5 kWh/m3 in large scale seawater desalination plants, which is significantly high for cost effective treatment of wastewater and surface or groundwater resources (Lee et al., 2019). Another important drawback of RO process is high amount of concentrated water formation and requirement of further treatment. Usually, the concentrate stream is discharged directly into water or soil without treatment. However, it is estimated that the discharge of concentrated water may cause adverse effects on ecosystem. In addition, the RO process requires accompanying technologies such as sludge treatment, high pressure membrane operations, thermal distillation, and aeration (Al-Mamun et al., 2018). To date, several studies focused on

treatment of RO concentrate as the use of RO processes for water treatment is complicated since the concentrate volume increases. For instance, chemical softening/secondary RO, electrocoagulation/secondary RO, high efficiency RO, seeded slurry precipitation with recycle, intermediate biological reduction/secondary RO, forward osmosis, and membrane distillation processes were used for further treatment of RO concentrate streams (Cob et al., 2012; Gabelich et al., 2010; Ordóñez et al., 2012; Subramani et al., 2012; Subramani and Jacangelo, 2014). Compared the individual treatment processes, the hybrid processes were more sustainable in the case of wastewater treatment with complex composition. However, there are several disadvantages of conventional hybrid treatment technologies such as high capital and operational costs, high waste sludge formation, membrane fouling and scaling, high energy consumption, and relatively low treatment efficiency (Subramani and Jacangelo, 2014). Therefore, there is crucial need for further research to develop novel treatment technologies with integrated wastewater treatment, desalination, and water polishing that are cost-effective and environmentally friendly.

Microbial desalination cells (MDCs) has been developed as a promising technology due to achieving water desalination with simultaneous electricity generation, waste and wastewater treatment (Jafary et al., 2020; Saeed et al., 2015; Wang et al., 2020). MDCs are a modified version of bio-electrochemical systems (BES) that produce electrical energy from the oxidation of organic matters coupled to electron transfer by microorganisms. MDCs are mostly composed of three chambers: an anode chamber, a cathode chamber and a desalination chamber in between. In the anode chamber, anaerobic treatment of organic material is done by microorganisms that leads to production of electron, proton, carbon dioxide, and methane. Electrons, which are generated in the anode chamber, are transferred to the cathode chamber through an external circuit. The unbalanced ionic charge in the cathode chamber due to the exceeding number of electrons cause a propulsive force for dissociation of ionic compounds in the salt water. Eventually, anions and cations migrate to the anode and cathode chambers, respectively, through the ion exchange membranes that finally result in desalination of water (Rahman et al., 2021b; Tawalbeh et al., 2020). Consequently, both wastewater and saline water can be treated with energy production. MDC processes have been utilized to investigate hard water softening, seawater and brackish water desalination, geothermal and groundwater treatment, and chemical and hydrogen production (Goren and Okten, 2022; Sevda et al., 2015; Sophia et al., 2016).

The MDC processes could be significantly promising for integration with the RO technology. This integration could reduce the operational time and energy consumption in the conventional RO treatment while also treating a wastewater stream. Besides, to our best knowledge, water desalination by MDC integration with RO process has only been investigated in two papers (Jacobson et al., 2011b; Shivakumar and Razaviarani, 2021). (Jacobson et al., 2011b) reported that the MDC process could be integrated with RO process as a pretreatment technology in water desalination to reduce energy consumption and number of RO passes. In (Shivakumar and Razaviarani, 2021), the MDC-RO hybrid process was only proposed as an efficient treatment option in UAE, Fujairah RO Desalination Plant. These studies revealed that there was no research on the RO process integration with MDC for further polishing of RO permeate and minimization of RO concentrate with treating in MDC process.

In this paper, we evaluated the feasibility of boron and heavy metals removal from RO permeate and concentrate streams using RO-MDC hybrid process. In RO-MDC hybrid system, geothermal water was first treated in the RO system and then the concentrate and permeate streams were treated using MDC. Moreover, organic matter removal and energy production efficiency of RO-MDC hybrid process from yeast wastewater were investigated. This study is the first and most comprehensive research paper on further polishing of RO permeate and minimization of RO concentrate stream via RO-MDC treatment. Moreover, the applicability of RO-MDC hybrid process for simultaneous boron and heavy metal removal, wastewater treatment, and energy production was investigated.

6.2. Materials and Methods

6.2.1. RO Permeate and Concentrate Sampling

A mini-pilot scale membrane test system (Figure 6.1) installed at Yenikale Geothermal Heating Center located in Izmir, Turkey was employed to run RO tests. The RO membrane, BW30 (Dow FilmTech, 2540), was used in treatment of geothermal water. Due to the fact that, polymeric membranes operate at maximum temperature of 45 ºC, the spent geothermal water at 55 ºC was fed into storage tanks for cooling to ambient temperature. Membrane system consists of low and high pressure pumps, feed and

antiscalant tanks as well as pressure gauge on feed, permeate and concentrate streams. The membrane used had an active area of 2.6 m^2, pH range of 2-11, maximum applied temperature and pressure of 45 ºC and 41 bar, respectively. In order to prevent the precipitation of inorganic scalants like Ca^{2+} and Mg^{2+}, 5 g of Ropur antiscalant per m^3 of spent geothermal water was added to the RO membrane system. At an applied pressure of 15 bar, 60% of water recovery was maintained constant for the collection of the RO permeate as well as the RO concentrate samples. The membrane system was operated for 1 h (for membrane conditioning) prior to sample collection.

Figure 6.1. Front and back view of RO membrane system.

6.2.2. Characterization of Water Samples

The wastewater from primary clarification of a yeast wastewater treatment plant, raw and re-injected geothermal water from Balçova Geothermal Power Plant, and reverse osmosis (RO) permeate and concentrate streams were used in this study. The pH of geothermal water was 8.04. Electrical conductivity of geothermal water was 1770 µS/cm. Yeast wastewater (pH 7.91) had chemical oxygen demand (COD) of 9280 mg/L. The pH, electrical conductivity, and total dissolved solids (TDS) of RO permeate were 8.57, 84.0 µS/cm and 39.8 mg/L, respectively. Those parameters had the values of 8.55, 4320 µS/cm, and 2240 mg/L, respectively for RO concentrate stream. Moreover, the anion, cation, and potentially toxic trace element concentrations of water samples were given in Table 6.1.

Table 6.1. Anion, cation, and potentially toxic trace element concentrations of water samples.

Parameter (mg/L)	Geothermal water	RO permeate	RO concentrate
K^+	30.1	1.14	84.5
NH_4^+	1.85	0.28	0.36
Na^+	452	15.9	1009
Ca^{2+}	24.8	0.62	48.0
Mg^{2+}	7.44	0.06	10.5
Mn^{2+}	0.027	-	0.009
NO_3^-	0.25	1.79	13.9
NO_2^-	-	-	-
SO_4^{2-}	178	2.32	436
PO_4^{3-}	-	-	5.47
Cl^-	205	10.5	455
F^-	8.21	0.18	19.3
Si	24	2.0	26.0
Br	0.38	-	0.88
Al	0.017	0.002	0.024
As	0.173	0.002	0.384
B	11.9	7.46	15.1
Cu	0.002	0.002	0.094
Cr	0.331	0.191	0.377
Fe	0.055	0.004	0.515
Li	1.41	0.06	3.32
Ni	-	-	0.097

6.2.3. MDC Configuration and Operation

The MDC includes three chambers made of plexiglass: anode, desalination, and cathode chambers (15 cm × 6 cm × 6 cm each) (Figure 6.2). Chambers were clamped together to be air tight. An anion exchange membrane (AEM, AMI-7001, Membrane International Inc., USA) separated anode and desalination chambers, while a cation exchange membrane (CEM, CMI-7000, Membrane International Inc., USA) separated desalination and cathode chambers. Flexible carbon graphite plates were used as the anode and cathode electrodes, which were connected using copper wiring.

Anode solution included equal volumes of anaerobic activated sludge and wastewater taken from the primary clarifier unit of yeast wastewater treatment facility. 0.1 M phosphate buffer was used as the cathode solution to enhance current generation and desalination performance of MDC. RO concentrate or permeate were fed to desalination chamber following a pH adjustment to 9.5 using 0.1 M sodium hydroxide (NaOH, Merck-Millipore). Samples were collected from three chambers daily. The experiments were utilized in a fed-batch operation at 40 ºC and operational time of 12

days. As a result of the preliminary studies, operating time was set as 12 days by considering the time 90% of substrate was completely consumed by microorganisms. At the end of 12 days, stirrer was shut down, activated sludge was settled, treated yeast wastewater was drawn (200 mL) and fresh wastewater (200 mL) was fed to the system. Simultaneously, boron and ion removals from RO permeate and RO concentrate samples were studied under optimum operating conditions (V_{sludge}: 270 mL, $V_{wastewater}$: 270 ml, $S_{electrode}$: 36 cm^2, $pH_{catholyte}$: 6.5, $T_{anolyte}$: 40 ºC, operational time: 12 days), according to our previous studies (Goren and Okten, 2021b, 2021a).

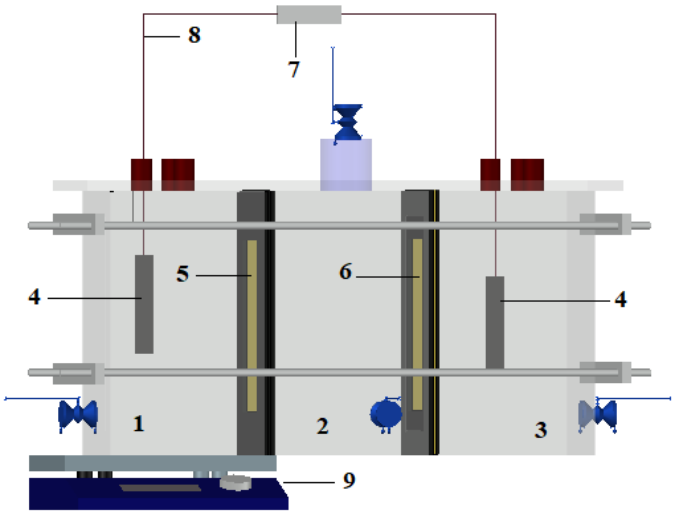

Figure 6.2. The schematic diagram of MDC bioreactor: (1) Anode chamber, (2) Desalination chamber, (3) Cathode chamber, (4) Carbon graphite electrode, (5) AEM, (6) CEM, (7) External resistor, (8) Copper wire, (9) Mechanic stirrer.

6.2.4. Analytical Methods and Calculations

A data logging system (UNI-T, UT71C Digital Multimeter) recorded voltage (V) in the open circuit every 15 min. The pH measurements were done daily by using a pH meter (Mettler Toledo, SevenCompactTM). Boron concentration measurements were performed by an inductively coupled plasma optical emission spectrometer (ICP-OES, AGILENT 5110). Ion chromatography (IC, DionexICS-5000) was used for anions and cations measurements in water samples. COD was measured according to Standard Methods (Federation and Association, 2005). The boron and COD removal efficiencies were calculated as following equations (6.1) and (6.2), respectively:

$$R_B(\%) = \frac{\left(C_{B,i} - C_{B,e}\right)}{C_{B,i}} \times 100 \quad (6.1)$$

$$R_{COD}(\%) = \frac{\left(C_{COD,i} - C_{COD,e}\right)}{C_{COD,i}} \times 100 \quad (6.2)$$

where $C_{B,i}$ and $C_{B,e}$ are the initial and effluent boron concentrations in desalination chamber, respectively. The $C_{COD,i}$ and $C_{COD,e}$ are the initial and effluent COD concentrations in anode chamber, respectively.

The current (i, mA) was calculated with $I = V / R_{ex}$. Power density (P_{An}, mW/m^2) normalized by electrode surface area was calculated based on the cross-sectional area of the anode electrode (A_{An}, m^2) due to the biological reactions take places in the anode chamber as follows (Logan et al., 2006):

$$P_{An} = \frac{V^2}{R_{ex} \times A_{An}} \quad (6.3)$$

Water quality of treated RO permeate and concentrate were also evaluated in terms of their suitability for irrigation purposes. According to Appendix 7 of the Wastewater Treatment Plants Technical Operation Communique (Gazette, 2010), quality of irrigation water was evaluated in three categories: Quality I, Quality II, and Quality III. Water of Quality I indicated that it would not damage crops or soil media (Table 6.2). Water of Quality II had various drawbacks and should be used with caution, whereas Quality III water had substantial adverse effects on the soil media.

The sodium adsorption ratio (SAR) values was calculated following Eq. (6.4) reported by (Yang et al., 2012). SAR values were considered to determine the sodium's effects with relation to magnesium and calcium concentrations on soil penetration. SAR and EC values have a combined effect in determining the infiltration capacity of irrigation water (Table 6.2).

Table 6.2. Evaluation of the chemical parameters for irrigation water.

Parameters	Range	Units	Adverse effects in case of usage		
			None (Quality I)	Minimal to Medium (Quality II)	High (Quality III)
Salinity					
Electrical Conductivity (EC)		dS/m	< 0.7	0.7-3	>3
Total Dissolved Solids		mg/L	< 0.5	0.5-2	>2
Permeability					
SAR	0-3		EC ≥ 0.7	0.7 – 0.2	< 0.2
	3-6		≥ 1.2	1.2 – 0.3	< 0.3
	6-12		≥ 1.9	1.9 – 0.5	< 0.5
	12-20		≥ 2.9	2.9 – 1.3	< 1.3
	20-40		≥ 5.0	5.0 – 2.9	< 2.9
Specific ion toxicity					
Sodium (Na)					
Surface irrigation		mg /L	< 3	3 – 9	> 9
Drip irrigation		mg/L	< 70	> 70	
Chloride (Cl)					
Surface irrigation		mg /L	< 140	140 – 350	> 350
Drip irrigation		mg/L	< 100	> 100	
Boron (B)		mg/L	< 0.7	0.7 – 3	> 3

$$SAR = \frac{[Na^+]}{\sqrt{[Ca^{2+}] + [Mg^{2+}]/2}} \quad (6.4)$$

where $[Na^+]$, $[Ca^{2+}]$, and $[Mg^{2+}]$ are represents the concentrations of sodium, calcium, and magnesium ions in mg/L, respectively.

Moreover, the magnesium adsorption ratio (MAR) was calculated with Eq. (6.6) using the method suggested by (Szabolcs, 1964). When the MAR is below 50% then it is considered as suitable for agricultural irrigation.

$$MAR\ (\%) = \frac{(Mg^{2+})}{(Mg^{2+} + Ca^{2+})} \times 100 \quad (6.5)$$

where magnesium and calcium concentrations of water as represented in meq/L. A further indicator of the suitability of water for irrigation was the permeability index (PI), a measurement of soil's ability to transfer water. The PI value was categorized in three groups: Quality I (PI>75%), Quality II (25% ≤ PI ≤ 75%), and Quality III (PI<25%)

(Jarma et al., 2022). The PI was determined using Eq. (6.6) as reported by Dinka (Dinka, 2016) as follows:

$$PI\ (\%) = \frac{\left(Na^{+} + \sqrt{HCO_3^{-}}\right)}{\left(Na^{+} + Ca^{2+} + Mg^{2+}\right)} \times 100 \qquad (6.6)$$

where concentrations were in mmol/L.

6.3. Results and Discussion

6.3.1. Boron Removal from RO Concentrate

In this study, treatment of RO concentrate from treatment of geothermal was studied. RO concentrate samples were treated under optimum operating conditions using MDC on fed-batch mode. Removal performance of MDC was investigated for heavy metals, anions, cations and COD. Also energy production of the system was measured. Boron removal efficiencies were 66.3% ($C_{f,B}$: 5.095 mg/L), 72.1% ($C_{f,B}$: 4.206 mg/L), and 80.2% ($C_{f,B}$: 2.996 mg/L) at the end of the 1, 2, and 3 cycles respectively (Fig. 6.3). Boron concentration decreased from 15.1 to 2.99 mg/L at the end of the third cycle.

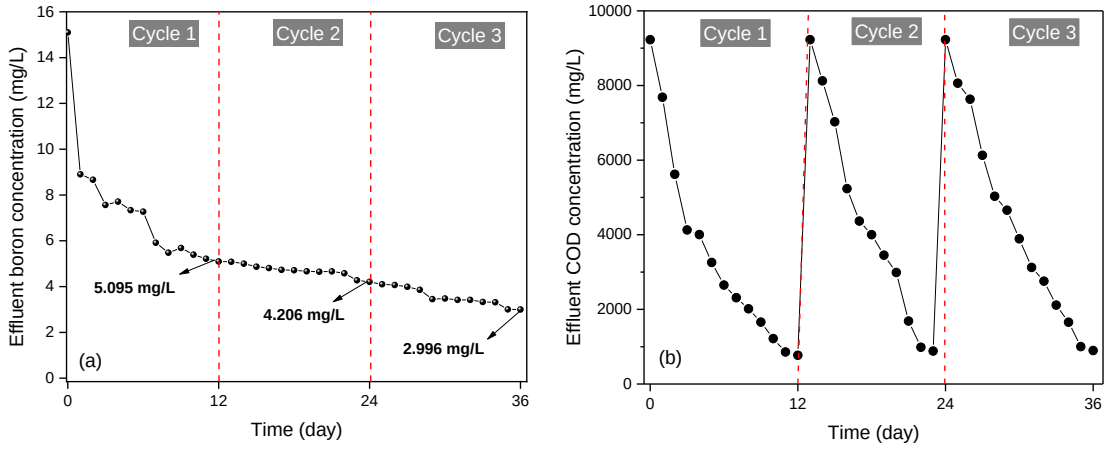

a) b)

Figure 6.3. Effluent boron a) and COD b) concentrations of RO concentrate sample in MDC.

Results showed that the boron removal efficiency significantly increased from the end of the first cycle to the end of the third cycle under fed-batch operating mode. On the other hand, boron removal efficiencies were quite slow at cycles 2 and 3, which was most probably due to the decreasing boron concentration gradient within the system. COD removal efficiencies were 91.7% ($C_{f,COD}$: 769 mg/L), 90.4% ($C_{f,COD}$: 884 mg/L), and 90.3% ($C_{f,COD}$: 896 mg/L) at the end of first, second, and third cycles, respectively. Results showed that the COD concentration did not change at all cycles for various boron concentrations, since fresh organic substrate was being fed at the beginning of each cycle.

Furthermore, arsenic, lithium, chromium, and iron removal efficiencies were investigated (Figure 6.4). Initial arsenic concentration decreased from 0.384 to 0.05 mg/L at operating time of 12 days. The highest arsenic removal efficiency of 100% was archived at cycle of 3. Lithium removal efficiencies were 75.9% ($C_{f,Li}$: 0.799 mg/L), 84.9% ($C_{f,Li}$: 0.502 mg/L), and 92.4% ($C_{f,Li}$: 0.251 mg/L) at the end of the cycles 1, 2, and 3, respectively. At the end of the cycle of 1, iron and chromium removal efficiencies were 93.2% ($C_{f,Fe}$: 0.035 mg/L) and 96.8% ($C_{f,Cr}$: 0.012 mg/L), respectively. The highest iron and chromium removal efficiencies were 98.1% ($C_{f,Fe}$: 0.01 mg/L) and 99.5% ($C_{f,Cr}$: 0.002 mg/L), respectively, at the end of the cycle 3. Moreover, the highest aluminum removal efficiency of 100% was achieved at operating time of 1 day. Consequently, the results revealed that the MDC was an effective system for concentrate treatment owing to its high removal efficiency and energy self-sufficiency.

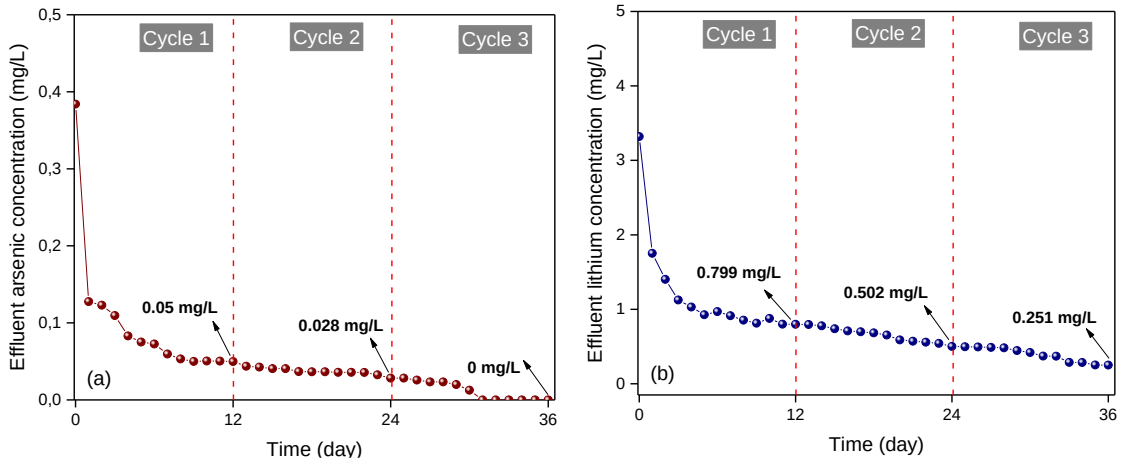

a) b)

Figure 6.4. Effluent arsenic a), lithium b), iron c), and chromium d) concentrations of RO concentrate sample in MDC.

(cont. on next page)

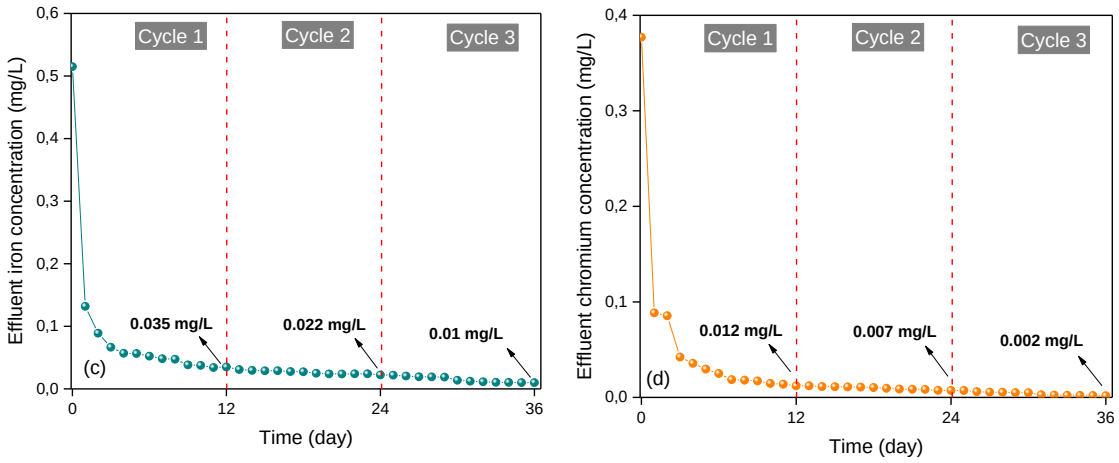

c) d)

Figure 6.4. (cont.)

6.3.2. Boron Removal from RO Permeate

In this study, RO permeate was also treated using MDC in fed-batch operation at optimum operating conditions. Effluent boron and COD concentrations were presented in Figure 6.5. The boron content was continuously decreased under fed-batch operation. Residual boron contents were 4.58, 3.89, and 3.29 mg/L at the end of the cycles 1, 2, and 3, respectively. The highest removal was 55.9% at 3 cycle. COD removal efficiencies were 90.1, 90.0, and 90.2% at the end of each cycle. For instance, (Yuan et al., 2015) studied enhancement of desalination and wastewater treatment using microbial desalination cell with forward osmosis hybrid process. They reported that the highest COD removal efficiency was 93.0% at lowest initial NaCl concentration of 10 mg/L.

The arsenic, aluminum, and iron removal efficiencies were achieved as 100% at the end of the cycle 1. On the other hand, the highest lithium and chromium removal efficiencies were found to be 71.7% ($C_{f,Li}$: 0.017 mg/L) and 97.9% ($C_{f,Cr}$: 0.004 mg/L) at the end of the cycle 3, respectively. Overall, these results confirmed that the MDC process under optimum operating conditions is a promising post treatment technology for RO permeate water treatment.

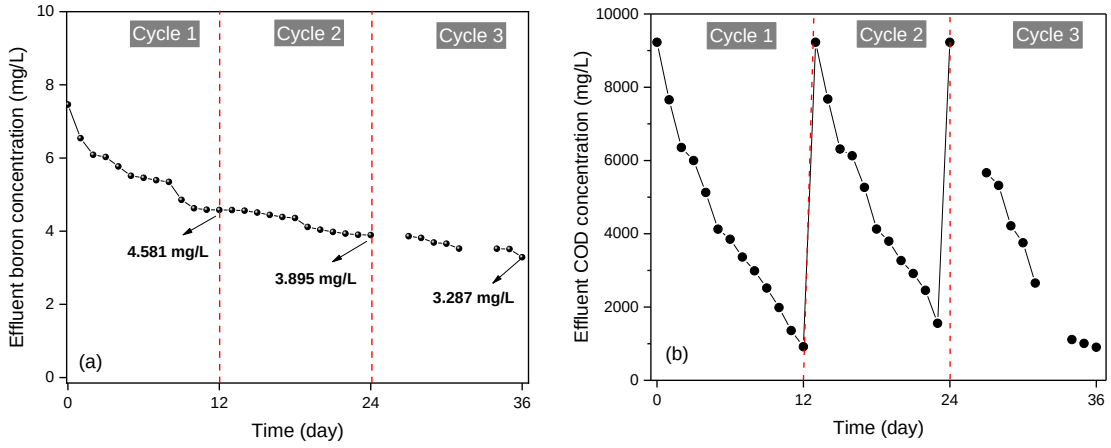

a) b)

Figure 6.5. Effluent boron a) and COD b) concentrations of RO permeate in MDC.

The pre- and post-treatment options for RO process in boron removal from water and wastewaters were summarized in Table 6.3. Namely, although RO water recovery was regarded an essential process for tackling the challenge of meeting high water demand, it had several issues that must be addressed. For instance, fouling causes higher feed stream pressure, higher membrane cleaning regularity, permeate contamination, and limited membrane life in RO membranes.

Table 6.3. Hybrid processes for enhanced boron removal in aqueous solutions.

Hybrid process	**Water type**	**Initial boron concentration (mg/L)**	**Removal efficiency (%)**	**Research highlights**	**References**
ED-RO	Synthetic saline water	10	70	ED pretreatment decreased RO membrane fouling	(Landsman et al., 2020)
ED-RO	Landfill Leachate wastewater	75	>98.7	The RO permeate can be directly discarded to the environment	(Dydo and Turek, 2014)
FO-RO	Synthetic solution	5	80.5	Cost effective and effective process in dilution and pH adjustment properties	(Ban et al., 2019)
RO-S-UF	Synthetic solution	5	>90	Operated system was promising on real scale applications	(Güler et al., 2011)
RO-IE-UF	Geothermal water	11.4	>90	Process achieved permissible boron level for irrigation	(Kabay et al., 2013b)
UF-RO	Synthetic solution	10	97	Boron effectively treated at alkali pH	(Tomaszewska and Bodzek, 2013)
S-MF-RO	Synthetic solution	5	≈100	Sorption and microfiltration effective as a pre-treatment option	(Alharati et al., 2018)

(cont. on next page)

Table 6.3. (cont.)

Hybrid process	Water type	Initial boron concentration (mg/L)	Removal efficiency (%)	Research highlights	References
RO-IE	Seawater	5.1	≈100	Effective hybrid boron treatment process	(Kabay et al., 2008)
RO-IE	Geothermal water	5.4	97	Process achieved permissible boron level for irrigation	(Samatya et al., 2015)
RO-EDI	Geothermal water	10.6	84.9	Process achieved permissible boron level for irrigation and drinking	(Arar et al., 2013)
RO-EDI	Synthetic solution	-	80	Effluent boron yield can be up to the standard	(Hu et al., 2014)
RO-IE	Landfill Leachate wastewater	-	≈70	EI treatment of RO permeate achieved a relatively effective boron recovery	(Ribera-Pi et al., 2021)
SBR-RO	Leachate wastewater	12.7	95	Effective hybrid boron treatment process	(Tałałaj, 2022)
RO-MDC	Geothermal water	11.9	72.5	Self-energetically and high boron and heavy metal removal	In this study
RO-MDC	RO concentrated water	15.1	80.2	Self-energetically and high boron and heavy metal removal	In this study

ED-RO: Electrodialysis-reverse osmosis, BSR: Boron selective resin, UF: Ultrafiltration, NF: Nanofiltration, MF: Microfiltration, IE: Ion exchange, S: Sorption, EDI: Electrodeionization, SBR: Sequencing batch reactor, MDC: Microbial desalination cell

In addition, high material and maintenance costs, energy consumption, and relatively low selectivity for various pollutants were important drawbacks of the RO process. Therefore, integration of various processes with RO had recently emerged as a promising solution to overcome abovementioned drawbacks of RO process. Electrodialysis (ED), forward-osmosis (FO), ultrafiltration (UF), microfiltration (MF), sorption (S), ion exchange (IE), electrodeionization (EDI), and sequencing batch reactor (SBR) processes were utilized as pre- and post-treatment processes in boron removal from water streams of varying ionic strength. Removal efficiencies were reported to be in the range of 70-100% (Table 6.3). Compared with the hybrid processes in literature, RO-MDC hybrid process showed promising results considering high boron removal efficiency and energy production.

6.3.3. Energy Production for RO Concentrate and Permeate Treatment

Under fixed external resistance of 100 Ω, voltage, power density, and current density values were determined for runs with RO permeate and concentrate in MDC (Fig. 6). Voltage values were 700, 692, and 694 mV for RO permeate treatment in MDC at the

end of cycles 1, 2, and 3, respectively. The voltage was constant at voltage of around 690 V for all cycles, which indicated that the microorganisms grew successfully and produced enough electrons at the anode chamber with fresh yeast wastewater being fed in every 12 days. Moreover, the sudden increase in voltage was observed at the end of day 1 for all cycles most probably due to the fresh source of electron donors. Power and current density values of MDC were also calculated.

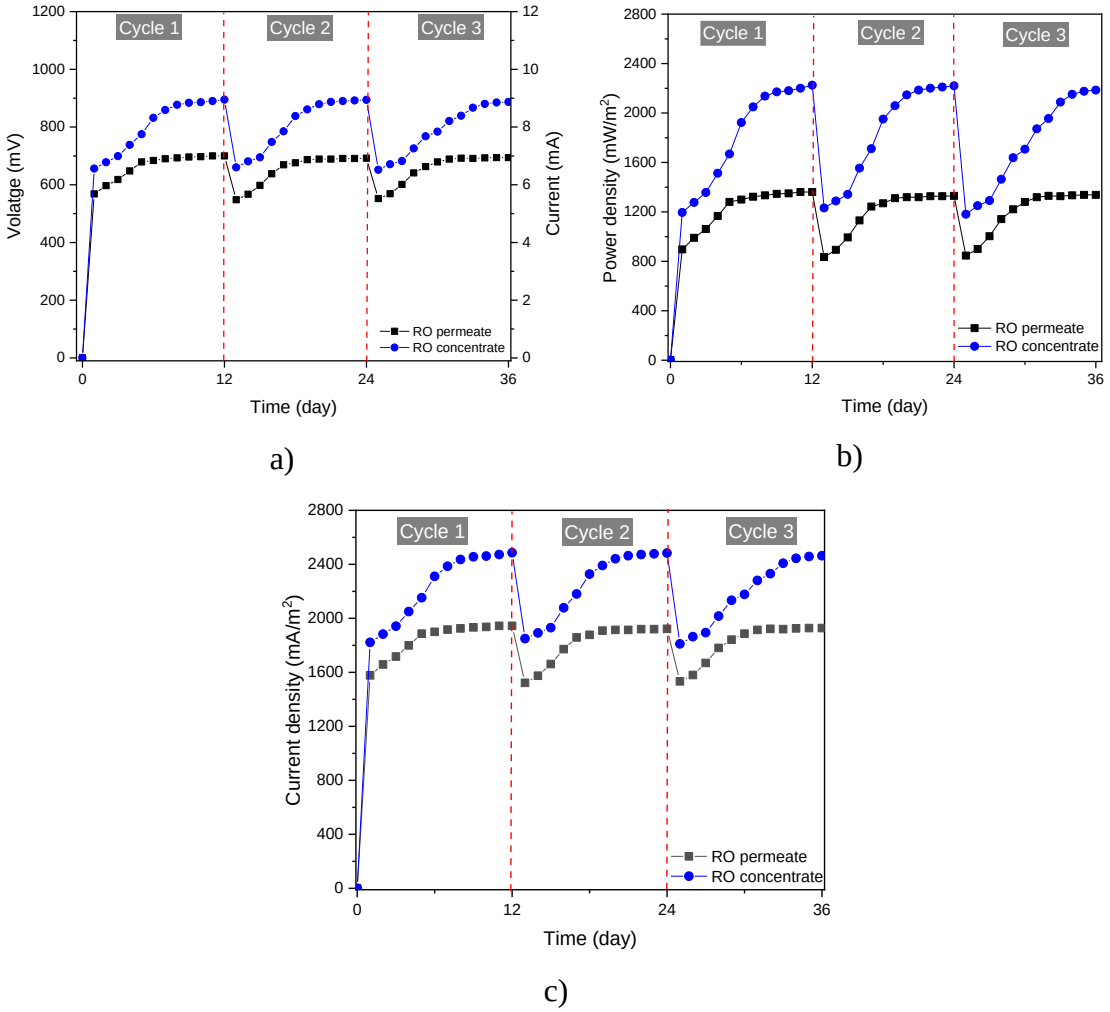

Figure 6.6. Voltage and current a), power density b), and current density c) from treatment of RO permeate and concentrate samples.

The highest power and current density values were calculated to be almost 1330 mW/m^2 and 1920 mA/m^2 at each cycle, respectively. On the other hand, the voltage, power density, and current density values increased when the MDC system was operated using RO concentrate sample. Due to high ion concentration in RO concentrate sample, a stronger driving force was established which in turn significantly improved voltage, power density, and current density values. For instance, at the end of the cycles 1, 2, and

3, the voltage values were measured to be 895, 894, and 887 mV, respectively. We observed that the average voltage value increased from almost 690 mV (permeate) to 890 mV (concentrate). Also, average power and current density values were calculated to be on average 2220 mW/m^2 and 2480 mA/m^2, respectively, at the end of the 12 days for all cycles.

6.3.4. Water Quality for Agricultural Irrigation

In order to calculate the values of parameters such as SAR, MAR and PI that are important to evaluate the produced water's suitability for irrigation, concentrations of Na^+, Ca^{2+}, Mg^{2+} and HCO_3^- were measured (Table 6.4). These measurements were then used to calculate the corresponding parameter values in Table 6.5. Sodium concentrations were decreased by 76.85 % and 66.11% following the MDC treatments for RO permeate and RO concentrate streams, respectively. Also, significant decreases were achieved for calcium and magnesium concentrations.

Table 6.4.Values of some cations and anions in the product water streams.

Parameter (mg/L)	**RO permeate /MDC**	**RO concentrate /MDC**
Na^+	3.68	342
Ca^{2+}	0.16	14.23
Mg^{2+}	0	1.08
HCO_3^-	3.46	634

Evaluation of the produced water streams for irrigation revealed contrasting results for different parameters. When measured EC values were checked against the Wastewater Treatment Plants Technical Operation Communique (Gazette, 2010), RO permeate/MDC effluent has met the criterion set for water of Quality I, whereas the RO concentrate/MDC effluent's value indicated Quality II. Since geothermal water did not contain high concentrations of magnesium to begin with, MAR values verified suitability for irrigation. In calculating the PI values, significantly higher concentrations of sodium and bicarbonate in water samples in comparison to calcium and magnesium concentrations lead to high values (PI>75%), hence indicating Quality I water. However, maybe the mostly used parameter in irrigation water studies, SAR, pointed to Quality III water for all water samples except for RO concentrate. Poor SAR values resulted from

significantly high Na^+ concentrations when compared to Ca^{2+} and Mg^{2+} concentrations. A usual practice to remedy this situation could be to add $CaSO_4$ to irrigation water or to apply directly to soil, as suggested in Wastewater Treatment Plants Technical Operation Communique (Gazette, 2010). As for boron concentrations, only RO concentrate/MDC has barely achieved Quality II water, and rest of the water samples fell in the Quality III range. MDC treated RO concentrate and permeate yielded Quality I water in terms of As concentration (< 0.1 mg/L).

Table 6.5. Evaluation of suitability for irrigation by several parameters.

Parameter	**Geothermal water**	**RO permeate**	**RO concentrate**	**RO permeate /MDC**	**RO concentrate /MDC**
EC (dS/m)	1.7**	0.084*	4.23***	0.012*	2.18**
SAR	20.44***	5.16***	34.37**	2.53***	23.52***
MAR (%)	33.07^{S}	13.75^{S}	26.48^{S}	0^{S}	11.11^{S}
PI (%)	>99*	>99*	>99*	>99*	>99*
pH	8.0*	8.57*	8.55*	8.65*	8.74*
B (mg/L)	11.9***	7.46***	15.1***	3.287***	2.996**
As (mg/L)	0.173^{Us}	0.002^{S}	0.384^{US}	0^{S}	0.005^{S}

*Quality I, **Quality II, ***Quality III, Us: unsuitable, S: Suitable.

6.4. Conclusion

A hybrid RO/MDC system was studied for the first time in desalination of geothermal water. MDC system achieved significant improvements in terms of B concentrations at the first cycles for both RO concentrate (66.3%) and permeate (38.6%). Concentration gradient was observed to play an important role in the transfer of borate ions ($B(OH)_4^-$) to anode chamber. Electrical potential values and related power density values that were produced by microbial degradation of organic compounds were steady throughout the operation of the MDC system. According to the SAR values, while the RO permeate/MDC effluent could be used to irrigate crops with low tolerance such as avocado and citrus fruits, RO concentrate/MDC effluent was only fit for irrigation of medium tolerance crops such as rice, alfalfa and oat. However, application of $CaSO_4$ to either soil or irrigation water was strongly recommended in order to ensure soil permeability.

CHAPTER 7

GEOTHERMAL AND YEAST WASTEWATER TREATMENT AND ENERGY PRODUCTION USING MICROBIAL DESALINATION CELL-DONNAN DIALYSIS HYBRID SYSTEM

7.1. Introduction

Water scarcity is a major problem steadily expanding and affecting most parts of the world in the era of climate change. The problem of water scarcity, which from a strict economical point of view translates into higher cost for clean water and wastewater treatment, is not restricted solely to developing countries but it is of high concern also for developed countries worldwide. Particularly, the Mediterranean region, Middle East, and Asia are known to suffer from high to very high water stress levels (Alsafadi et al., 2022; Ouassanouan et al., 2022; Xanke and Liesch, 2022). As a dire and alarming fact, out of the 26 water basins in Turkey, 25 present water budgets that are in deficit. The natural water cycle cannot keep up with the withdrawal and abstraction rates conducted by humans for various purposes. AQUAREC project (2003-2006) reported that major sectoral water use in Mediterranean countries belonged to agriculture and irrigation followed by public water supply (Wintgens et al., 2002). In Turkey the agriculture sector demands the largest share in water use with 74%. In order to tackle the water scarcity problem in water-stressed areas, there is need to valorize wastewaters in the form of reclamation and reuse. On top of a global environmental crisis such as climate change, we had to adapt to a pandemic that had severe economic and social effects. The COVID-19 pandemic has shown the importance of being self-sufficient in terms of crops production. Recognizing the importance of policy domains on Sustainability and Resilience, climate-resilient water resource management can help advance food security and agricultural sustainability goals SDG 1, 2, 6, 13 (Desa, 2016) while adapting to the effects of climate change and become resilient in line with UNFCCC's Paris Agreement (Nations, 2015). Improved agricultural water use hinge largely on increasing the water

productivity and efficiency of rain-fed and irrigation systems. Given the restrictions of an expanding arid environment, several aspects of the problem should be tackled in order to come up with a sustainable solution. Therefore, not only integration of non-conventional water sources into the water cycle, but also diversifying the supply chain, increasing the implementation of water-efficient irrigation methods, enhancing farming techniques, and switching to water-efficient crops are needed (Plusquellec, 2009). In response to growing water scarcity, there is a need for a paradigm shift towards reuse of unconventional water until it meets the set standards for irrigation, rather than its disposal.

Geothermal brine, which is produced following the energy extraction from high-temperature fluids, is produced locally in large quantities wherever the geothermal energy is exploited. The five countries with the largest annual geothermal energy use are listed as USA, Sweden, China, Turkey and Japan, accounting for 73.4% of the world use (Lund and Toth, 2021). In closed loop systems, the extracted geothermal water is reinjected to wells and does not pose an environmental risk. However, in smaller facilities the uncontrolled discharge of geothermal brine is frequently encountered and due to its diverse physicochemical parameters, it may contain significant amounts of neutral species, cations and anions. The uncontrolled discharge of any wastewater type can be highly problematic, but in this case since the agricultural areas are superimposed with the geothermal areas, the rich ionic content of geothermal brine and in particular boron deteriorates the soil quality and interferes with the crop yield. Therefore, when geothermal brine is used as irrigation water, boron removal becomes an important and difficult process.

To date, several conventional techniques such as coagulation, filtration, adsorption, membrane processes, hybrid processes etc., have been performed for the geothermal water desalination (Jarma et al., 2022; Kim et al., 2022; Zhao et al., 2022). However, several of these treatment processes have cost and environmental challenges, such as resin regeneration difficulties, high sludge production and management difficulty, high capital, operational, and utility costs, chemical utilization for pH control, and membrane fouling (Qasem et al., 2021). Furthermore, boron removal by membrane techniques (e.g. reverse osmosis (RO), ultrafiltration (UF), nanofiltration (NF), and forward osmosis (FO)) is energy demanding, posing a significant obstacle for addressing water issues in locations with limited energy supplies (Cui et al., 2014; De Los Ríos et al., 2013; Nthunya et al., 2022). Furthermore, treating industrial effluent and saline water separately might result in significant operating costs.

Therefore, there is a crucial need for further research to develop novel treatment technologies with integrated wastewater treatment, desalination, and water polishing that are cost-effective and environmentally friendly approaches. The Donnan membrane process (DMP), also known as Donnan Dialysis (DD), is a new green treatment method that combines ion exchange membranes (IEMs) (Prakash and SenGupta, 2003). The stoichiometric counter movement of ions over an IEM is part of the DMP. DMP may be categorized as a 3R-tech since it uses a concentration gradient to recover, separate, and concentrate ions of concern from diluted solutions. The DMP and DD are frequently exchangeable owing to their similar operating principles and application benefits. DMP is used to recover harmful or useful heavy metal ions from waste solutions, whereas DD is used to recover minerals from waste solutions (Luo et al., 2011). The DMP system outperforms the traditional electrodialysis (ED), chemical precipitation, ion exchange process, and pressure driven membrane procedures in terms of functionality. The DMP is an energy-efficient, low-cost construction and operating technique in rural applications (Breytus et al., 2020; Keeley et al., 2016). Overall, the MDC processes could be significantly promising method to integrate such process with the DD technology. This integration could decrease the energy consumption and time requirement spent with simultaneously treating wastewater and producing energy compared with conventional desalination processes.

Microbial desalination cells (MDCs) have been designed as a potential technology in water desalination with simultaneous energy generation and wastewater treatment purposes (Gujjala et al., 2022; Jatoi et al., 2022). MDCs are a specialized version of bio-electrochemical systems (BES), which generate electricity by oxidizing organic materials and transferring electrons by microorganisms. Firstly, microorganisms utilize anaerobic treatment of organic material in the anode chamber, resulting in the generation of electrons, proton, CO_2, and CH_4. Then, electrons produced in the anode chamber are transferred to the cathode via an external circuit. The imbalanced ionic charge in the cathode chamber, caused by an excess of electrons, provides a driving force for ionic compound dissociation in salt water. Consequently, through the IEMs, anions and cations move to the anode and cathode chambers, respectively, following in desalination of water in the desalination chamber (Zahid et al., 2022). Recently, the MDC technology has been performed for geothermal, groundwater, and seawater treatment, water softening, organic matter removal in industrial wastewater, and value-added compound production like energy, H_2O_2, H_2, CH_4, etc. (Al Hinai et al., 2022; Goren and Okten, 2021a; Salehmin et

al., 2021). Besides, to our best knowledge, the water desalination by MDC integration with DD process has only been investigated in only one paper. On the other hand, there was no research on the DD process integration with MDC for further polishing of RO effluent water, minimization of RO concentrated water, and treatment of boron containing real geothermal brine with treating in MDC process.

In this study, we evaluated the feasibility of boron removal from geothermal water and RO concentrated water using MDC-DD hybrid process. Moreover, the organic matter removal and energy production efficiency of MDC-DD hybrid process from yeast wastewater was investigated. This is the first and most extensive investigation on the MDC-DD hybrid process suitability for concurrent boron removal, wastewater treatment, and energy generation.

7.2. Materials and Methods

7.2.1. Experimental Set up of Mini-pilot Scale RO System

The setup of a mini-pilot scale RO reactor using BW30 type membrane (Dow FilmTech, 2540) with antiscalant dosage pump is described in detail in section 6.2.1, Chapter 6. For operation, the geothermal water was cooled to ambient temperature (≈ 25 °C) in poly ethylene containers before being treated using a pilot-scale RO treatment system. Furthermore, the 5 g/m^3 of Ropur (PRI-3000A) type antiscalant was supplied to geothermal water during the treatment process to prevent scaling due to the inorganic scalants (Ca^{2+}, Mg^{2+}, CO_3^-, PO_4^{3-}, etc.). The RO system was equipped with control panel to monitor operational parameters such as pressure at the inlet and the outlet of the membranes, and flow rates of permeate and concentrate streams. The experiments were performed on closed-loop operating mode, with a pressure of 15 bar for 4 h and the water recovery was kept at 60%. The samples from permeate and concentrate streams were gathered during membrane test for additional quality evaluation.

7.2.2. Chemical Properties of Water Samples

Both geothermal brine and yeast wastewater were collected in İzmir, Turkey, from a geothermal heating plant and a yeast manufacturing company, respectively. The pH of geothermal water was 8.04 and the electrical conductivity was 1770 μS/cm. The pH and COD of yeast wastewater were measured to be 7.87 and 9254 mg/L, respectively. Moreover, the pH, electrical conductivity, and total dissolved solids (TDS) of RO permeate and concentrate were 8.57 and 8.55, 84.0 and 4320 μS/cm, 39.8 and 2240 mg/L, respectively. The detailed chemical characterization of water samples is presented in Table 7.1.

Table 7.1. Chemical properties of geothermal, RO permeate, and RO concentrate waters.

Water type											
Geothermal water				RO permeate				RO concentrate			
Ion	mg/L	Ion	mg/L	Ion	mg/L	Ion	mg/L	Ion	mg/L	Ion	mg/L
K^+	30.1±1.2	F^-	8.21±0.15	K^+	1.14±0.16	F^-	0.18±0.02	K^+	84.5±1.45	F^-	19.3±1.32
NH_4^+	1.85±0.13	Si	24±0.1	NH_4^+	0.28±0.01	Si	2.0±0.73	NH_4^+	0.36±0.03	Si	26.0±0.38
Na^+	452±2.12	Br	0.38±0.03	Na^+	15.9±1.34	Br	N.D.	Na^+	1009±1.73	Br	0.88±0.13
Ca^{2+}	24.8±1.18	Al	0.017±0.01	Ca^{2+}	0.62±0.03	Al	0.002±0	Ca^{2+}	48.0±1.36	Al	0.024±0
Mg^{2+}	7.44±0.21	As	0.173±0.02	Mg^{2+}	0.06±0.01	As	0.002±0	Mg^{2+}	10.5±0.53	As	0.384±0.1
Mn^{2+}	0.027±0	B	10.48±1.62	Mn^{2+}	N.D.	B	7.46±1.25	Mn^{2+}	0.009±0	B	15.1±1.27
NO_3^-	0.25±0.02	Cu	0.002±0	NO_3^-	1.79±0.36	Cu	0.002±0.03	NO_3^-	13.9±1.24	Cu	0.094±0
NO_2^-	N.D.	Cr	0.331±0.23	NO_2^-	N.D.	Cr	0.191±0.02	NO_2^-	N.D.	Cr	0.377±0.02
SO_4^{2-}	178±2.98	Fe	0.055±0	SO_4^{2-}	2.32±0.27	Fe	0.004±0.01	SO_4^{2-}	436±1.46	Fe	0.515±0.23
PO_4^{3-}	N.D.	Li	1.41±0.45	PO_4^{3-}	N.D.	Li	0.06±0.01	PO_4^{3-}	5.47±0.67	Li	3.32±1.32

N.D.: Not detected

7.2.3. MDC-DD Hybrid System Set up and Operation

The experimental set up of a specifically designed MDC reactor (Figure 7.2) is explained in detail in our previous paper (Goren and Okten, 2021a). The DD reactor, which was used for pH adjustment purposes, consisted of two chambers with dimensions of 15 cm × 6 cm × 6 cm. Chambers were separated by an AEM and the first chamber was used as a feed tank which was recirculated to desalination chamber, while the second chamber was used as a stripping solution tank, which was recirculated from cathode chamber (Figure 7.1).

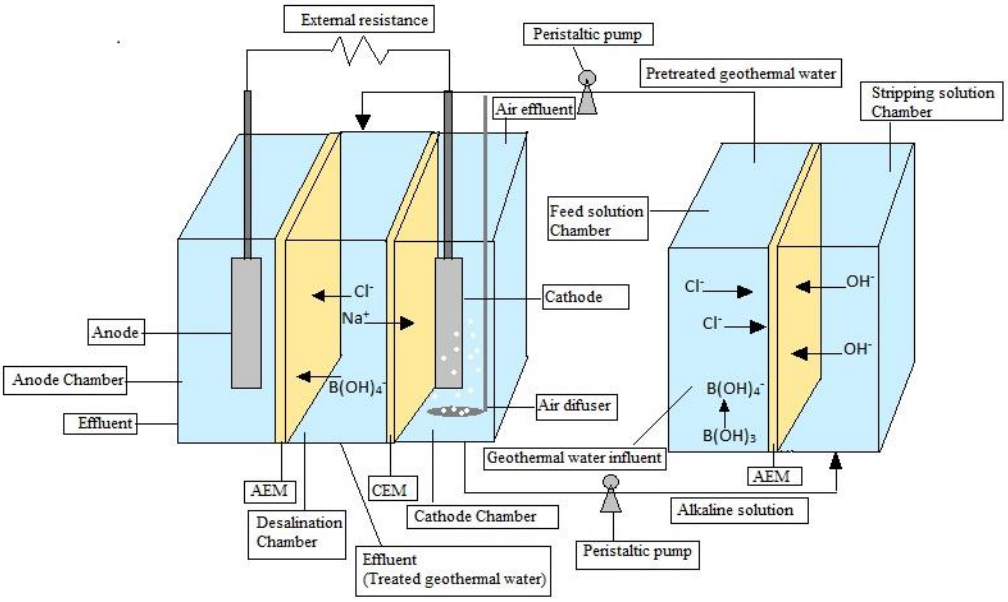

a)

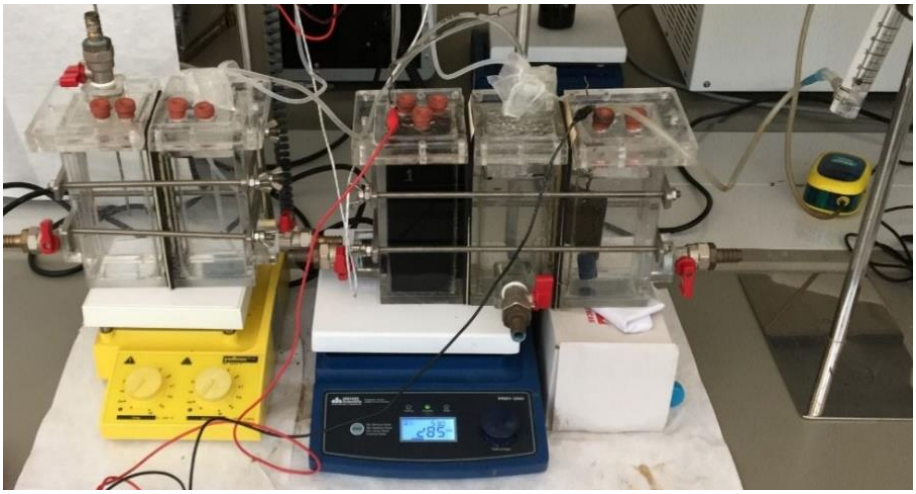

b)

Figure 7.1. Schematic diagram a) and actual view b) of experimental set-up of MDC-DD system.

7.2.4. Analytical Methods and Calculations

A data recording system (UNI-T, UT71C Digital Multimeter) was used to record the voltage (V) in the MDC at open circuit every 15 min. A pH meter (Mettler Toledo, SevenCompactTM) was used to track the daily pH variations. Inductively coupled plasma optical emission spectrometer (ICP-OES, AGILENT 5110) was used to measurement of boron concentration. Ion chromatography was used to quantify anions and cations in water samples (IC, DionexICS-5000). Triplicate measurements were used in all analyses.

The COD was determined using a closed reflux titrimetric technique in accordance with standard methods. (Federation and Association, 2005). The following equations were used to determine the boron and COD removal efficiency:

$$R_B(\%) = \frac{\left(C_{B,i} - C_{B,e}\right)}{C_{B,i}} \times 100 \quad (7.1)$$

$$R_{COD}(\%) = \frac{\left(C_{COD,i} - C_{COD,e}\right)}{C_{COD,i}} \times 100 \quad (7.2)$$

where $C_{B,i}$ and $C_{B,e}$ are the initial and effluent boron concentrations, respectively. The $C_{COD,i}$ and $C_{COD,e}$ are the initial and effluent COD concentrations, respectively.

The current (i, mA) was calculated with $I = V / R_{ex}$. Power density (P_{An}, mW/m^2) normalized by electrode surface area was calculated based on the cross-sectional area of the anode electrode (A_{An}, m^2) due to the biological reactions take places in the anode chamber as follows (Logan et al., 2006):

$$P_{An} = \frac{V^2}{R_{ex} \times A_{An}} \quad (7.3)$$

7.3. Results and Discussion

7.3.1. Boron Removal from Synthetic Solution

The boron removal performance of MDC-DD system was determined using 10 mg/L boron containing synthetic solution in both DD-feed chamber and MDC-desalination chamber. The reason why a DD-alkaline solution was applied instead of the MDC catholyte solution of PBS buffer was to achieve better manipulation of the pH. The effluent boron and COD concentrations in MDC-DD system chambers were presented in Figure 7.2 for synthetic solution.

Boron removal efficiencies were 72.1% ($C_{f,B}$: 2.79 mg/L) and 74.8% ($C_{f,B}$: 2.52 mg/L) in desalination chamber and DD-feed chamber at the end of the operating time 25 days, respectively (Figure 7.2a). Such a high boron removal was most probably occurred by concentration gradient driven Fick's diffusion in MDC, because the high pH of the

synthetic solution allowed the boron to stay in the form of a charged borate ion owing to circulation from alkalinated DD-feed chamber. In DD pre-treatment with the alkaline solution at pH 12, the boron concentration in both DD-feed chamber and desalination chamber considerably decreased. These findings suggest that a DD pre-treatment might help an MDC system remove more boron, and that a greater pH in the alkaline solution might help dissociate boric acid and so increase boron removal. In the DD system, hydroxide ions contributed to boron transport in a two-step process: initially, the transferred hydroxide ions from the alkaline solution elevated the feed solution pH, completely dissociating the boric acid into borate ions; and furthermore, the feed solution's negatively charged borate ions were prompted to exchange with hydroxide ions in the alkaline solution. A higher hydroxide concentration gradient resulted in a larger ion exchange pressure, which increased borate ion transport. Moreover, as we expected, similar trend observed in MDC system owing to circulation between alkaline and dissociated borate ion containing DD-feed solution and MDC-desalination solution. On the other hand, the boron removal efficiency was relatively higher than desalination solution compared with DD-feed solution. These could be explained with that the remaining borate ions in DD-feed solution might be mostly converted to boric acid when it entered the MDC desalination chamber. Moreover, in MDC system the hydroxide ions could migrate faster than borate ions into to the anode chamber with driven by electricity generation. The protons in the anode solution also can diffuse into the desalination chamber neutralizing the desalination solution. In addition, results showed that the boron removal efficiencies were more superior during 12 days, the removal efficiencies were considerably slowed down at the end of the 12 days due to the steady state conditions in both DD-feed and MDC-desalination chambers.

Moreover, the COD removal efficiencies were measured in MDC-DD system (Figure 7.2b). The highest COD removal efficiency of 90.0% ($C_{f,COD}$: 920 mg/L) was obtained at operating time of 25 days. Results also showed that there was no considerable change in COD removal efficiency values after the operating time of 15 days since most of the microorganisms die due to the nutrient deficiency.

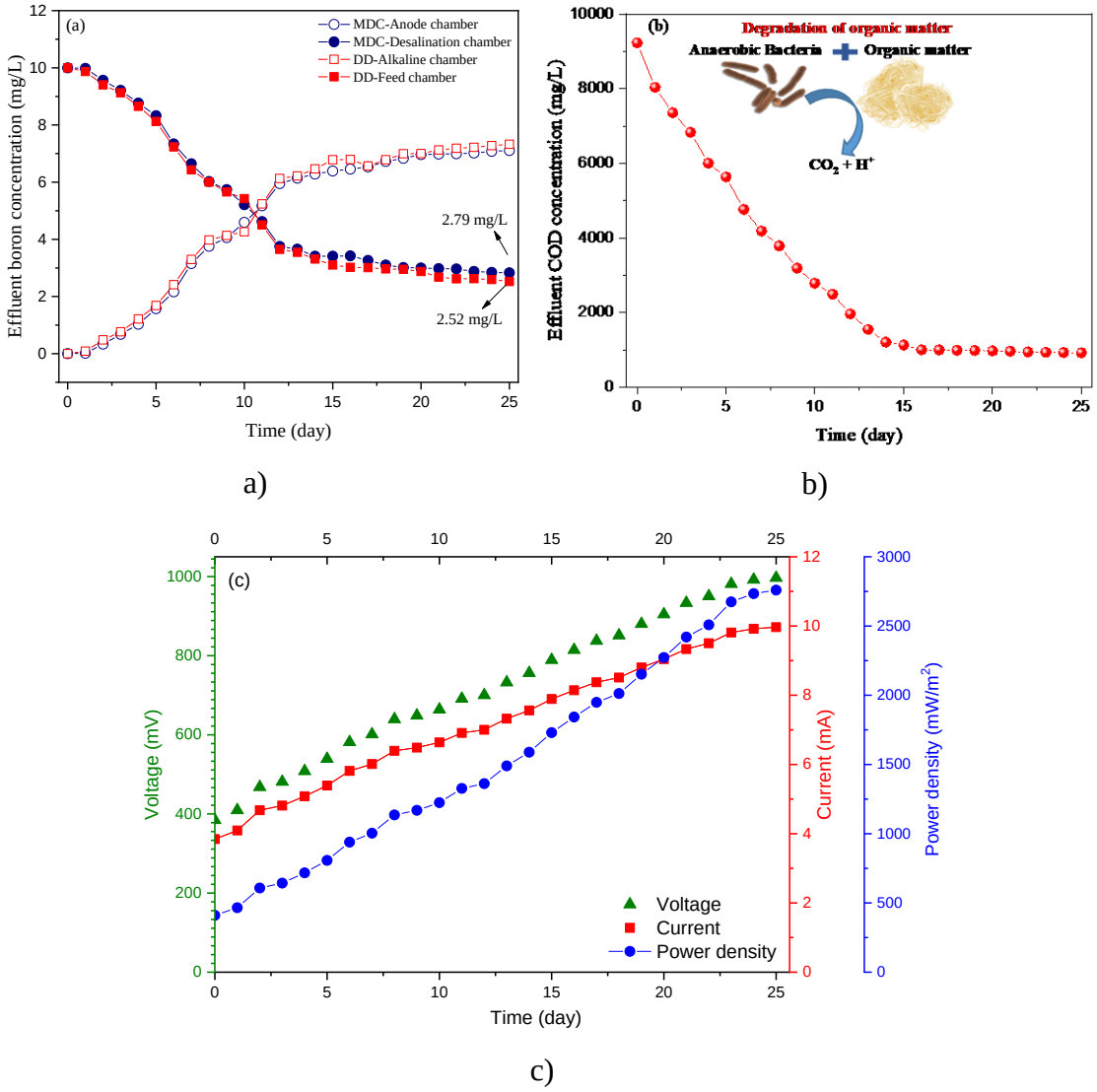

Figure 7.2. Effluent boron concentrations a), effluent COD concentrations b), and voltage, current, and power density c) for MDD-DD hybrid system.

Under fixed external resistance of 100 Ω, the voltage, power density, and current values were determined for boron containing synthetic solution treatment in MDC-DD (Figure 7.2c). The voltage value was 997 mV for synthetic solution treatment at the end of the operating time of 25 days. Results showed that there was no considerable change in voltage values after the operating time of 20 days. The voltage was nearly constant at 920 mV, indicating that the microorganisms had grown well and provided adequate electron for energy generation at the anode chamber. However, after this stage, electron production will not occur due to the lack of nutrient supply required for the survival of microorganisms. Moreover, when the results of COD removal and energy production were compared, it is seen that the organic matter consumption of the microorganisms decreased at the end of 20 days and accordingly, the energy production is expected to

stabilize, but the energy production also increased and stabilized on the 23rd day in this process. The reason for this can be explained by the maintenance of the transfer of electrons that are already produced in the anode solution. The current and power density values of MDC were also determined and same trend of the voltage was observed. The highest current and power density values were almost 9.97 A and 2759 mA/m^2 at the end of the operating time.

To further figure out the boron removal, the pH variations in all chambers were also measured by daily. The pH in DD-feed chamber decreased from 10.5 to 9.7 at the end of the operating time of 25 days most probably due to the abstraction of hydroxide ions from water due to the reaction between boric acid and hydroxide ions resulted with formation of borate ions. As we expected, the alkaline solution pH decreased from 12 to 11 due to the transfer of hydroxide ions from DD-alkaline chamber to DD-feed chamber with hydroxide concentration gradient difference between two chamber. Similar trend observed in desalination chamber. The pH of the desalination solution decreased from 10.5 to 9.6 due to the transfer of hydroxide ions from desalination to anode chamber and also the migration of hydrogen ions from cathode chamber to desalination chamber. As expected, a slight increase (7.68 to 7.8) was observed in the anode chamber due to the hydroxide ions transferred from the desalination chamber. For cathode solution, the pH values were in the range of 6.46-6.57. A slight increase in pH was observed as a result of the water formed with the reaction between hydrogen and oxygen in the cathode chamber.

7.3.2. Boron Removal from RO Concentrate

The boron and COD concentrations in MDC-DD system chambers were presented in Figure 7.3 for RO concentrated water. Boron removal efficiencies were 71.6% ($C_{f,B}$: 4.98 mg/L) and 73.5% ($C_{f,B}$: 4.65 mg/L) in desalination chamber and DD-feed chamber at the end of the operating time 25 days, respectively (Figure 7.3a). The remaining boron in the desalination chamber 17.53 to 4.98 mg/L, and the boron content in anolyte solution increased from 0 to 10.2 mg/L and the remaining boron was detected on the membrane surface and in the activated sludge. Similarly, the boron in DD-feed solution decreased from 17.53 to 4.65 mg/L, while the boron content was 11.4 mg/L at the end of the operating time (remaining boron was detected on the AEM surface). Similar to the results obtained in synthetic water, in the presence of the DD pre-treatment, the boron concentration in both DD-feed chamber and desalination chamber considerably

decreased. The higher pH value in DD-alkaline solution accelerated the dissociation of boric acid in DD-feed solution and then the recirculation of DD-feed solution to desalination chamber also increased the dissociated borate ion amount in desalination chamber, thus improved the boron removal in both chamber. In addition, the boron removal efficiency was relatively higher than desalination solution compared with DD-feed solution. These could be explained with that the remaining borate ions in DD-feed solution might be mostly converted to boric acid when it entered the MDC desalination chamber and the hydroxide ions could migrate faster than borate ions into to the anode chamber with driven by electricity generation. When the boron containing synthetic solution and RO concentrated water treatment performance of MDC-DD system was compared, observed boron removal efficiency for RO concentrated water (71.6% in desalination chamber and 73.5% in DD-feed chamber) was slightly lower than that for 10 mg/L boron containing synthetic solution (72.1% in desalination chamber and 74.8% in DD-feed chamber) under same operational conditions. This was most probably due to the high boron content of RO concentrated water. Besides, RO concentrated water contains other molecules such as anions, cations, and heavy metals causing competition with borate ions.

Moreover, the COD removal efficiencies were measured in MDC-DD system (Figure 7.3b). The highest COD removal efficiency of 89.8% ($C_{f,COD}$: 937 mg/L) was obtained at operating time of 25 days. Results also showed that there was no considerable change in COD removal efficiency values after the operating time of 15 days since most of the microorganisms die due to the nutrient deficiency. Under fixed external resistance of 100 Ω, the voltage, power density, and current values were determined for RO concentrate water treatment in MDC-DD (Figure 7.3c). The voltage value was 1317 mV for RO concentrate treatment at the end of the operating time of 25 days. Results showed that there was no considerable change in voltage values after the operating time of 20 days. The voltage was almost stable at voltage of around 1200 mV which indicated that the microorganisms were successfully grow and produced enough electron for the energy production at the anode chamber. However, after this stage, electron production will not occur due to the lack of nutrient supply required for the survival of microorganisms. Moreover, when the results of COD removal and energy production were compared, it is seen that the organic matter consumption of the microorganisms decreased at the end of 20 days and accordingly, the energy production is expected to stabilize, but the energy production also increased and stabilized on the 23rd day in this process. The reason for

this can be explained by the maintenance of the transfer of electrons that are already produced in the anode solution. The current and power density values of MDC were also determined and same trend of the voltage was observed. The highest current and power density values were calculated to be almost 13.2 A and 4818 mA/m^2, respectively, at the end of the operating time. Compared to the synthetic boron solution treatment, despite low boron removal efficiency was for RO concentrate, the amount of energy produced was higher than synthetic solution. The reason for this was clearly explained by the high ionic strength of RO concentrate. Due to high ionic strength of RO concentrate, transfer of electrons produced in the anode chamber could be rapid and complete.

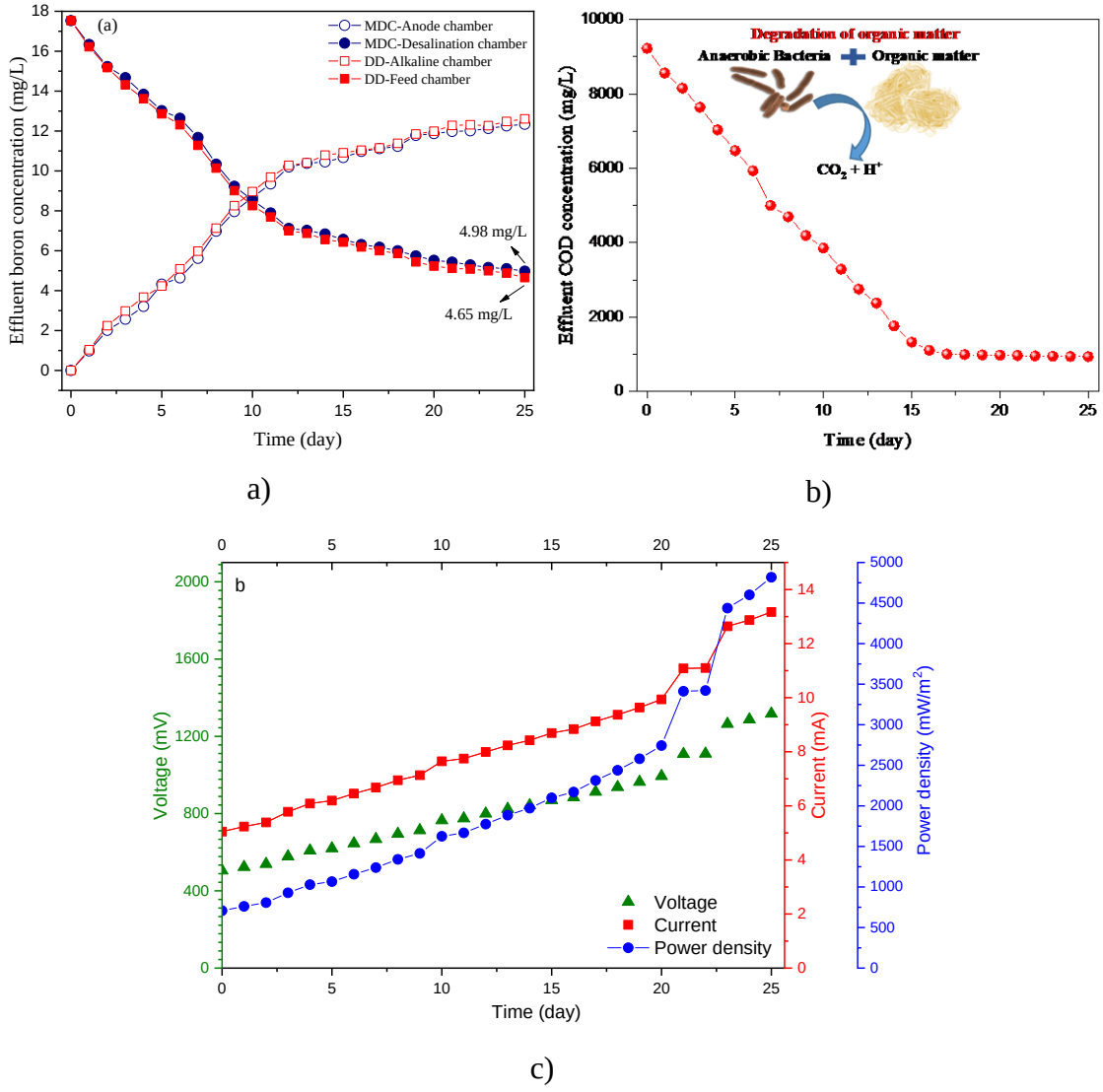

Figure 7.3. Effluent boron concentrations a), effluent COD concentrations b), and voltage, current, and power density c) for MDD-DD hybrid system.

In addition, the pH in desalination chamber decreased from 10.5 to 9.6 at the end of the operating time of 25 days most probably due to the microenvironment (anions, cations, and metal ions) in feed solution, which cause the neutralization of solution. Moreover, the decreasing pH can be explained with the abstraction of hydroxide ions from water due to the reaction between boric acid and hydroxide ions resulted with formation of borate ions. As we expected, the alkaline solution pH decreased from 12 to 10.6 due to the transfer of hydroxide ions from DD-alkaline chamber to DD-feed chamber with hydroxide concentration gradient difference between two chamber. Compared to the synthetic solution, a more pH variation was observed for RO concentrated water, and this can be explained by the tendency of other ions in the RO concentrated solution to react with each other, with hydrogen or hydroxide ions.

7.3.3. Boron Removal from Geothermal Water

Boron and COD content of treated geothermal water using MDC-DD hybrid process were illustrated in Figure 7.4a and 7.4b, respectively. Boron removal efficiencies were 71.9% ($C_{f,B}$: 2.95 mg/L) and 74.0% ($C_{f,B}$: 2.73 mg/L) in desalination and DD-feed chamber for 25 days, respectively. For the similar test conditions, measured boron removal efficiency for geothermal water (71.9%) was substantially lower than the synthetic solution (72.1%) containing 10 mg/L of boron. On the other hand, boron removal for geothermal water (71.9%) was slightly higher than that for RO concentrated (71.6%) for the same experimental conditions in desalination chamber. The boron removal performance of MDC for geothermal water worsened as predicted due to the greater ion concentration as compared to the synthetic solution. On the contrary, lower boron removal was achieved compared to geothermal water, as there are more ions and more competition in the RO concentrate. Furthermore, the COD removal performance was 90.1% in geothermal water, whereas it was 90% in a synthetic solution containing and 89.8% in a RO concentrated water. These findings revealed that COD removal efficiencies for aqueous solutions, geothermal water, and RO concentrate treatment studies did not differ significantly. The slight decrease in COD removal efficiency at RO concentrate water treatment could be explained with the inhibitory effect of high ion and metal content on microorganisms.

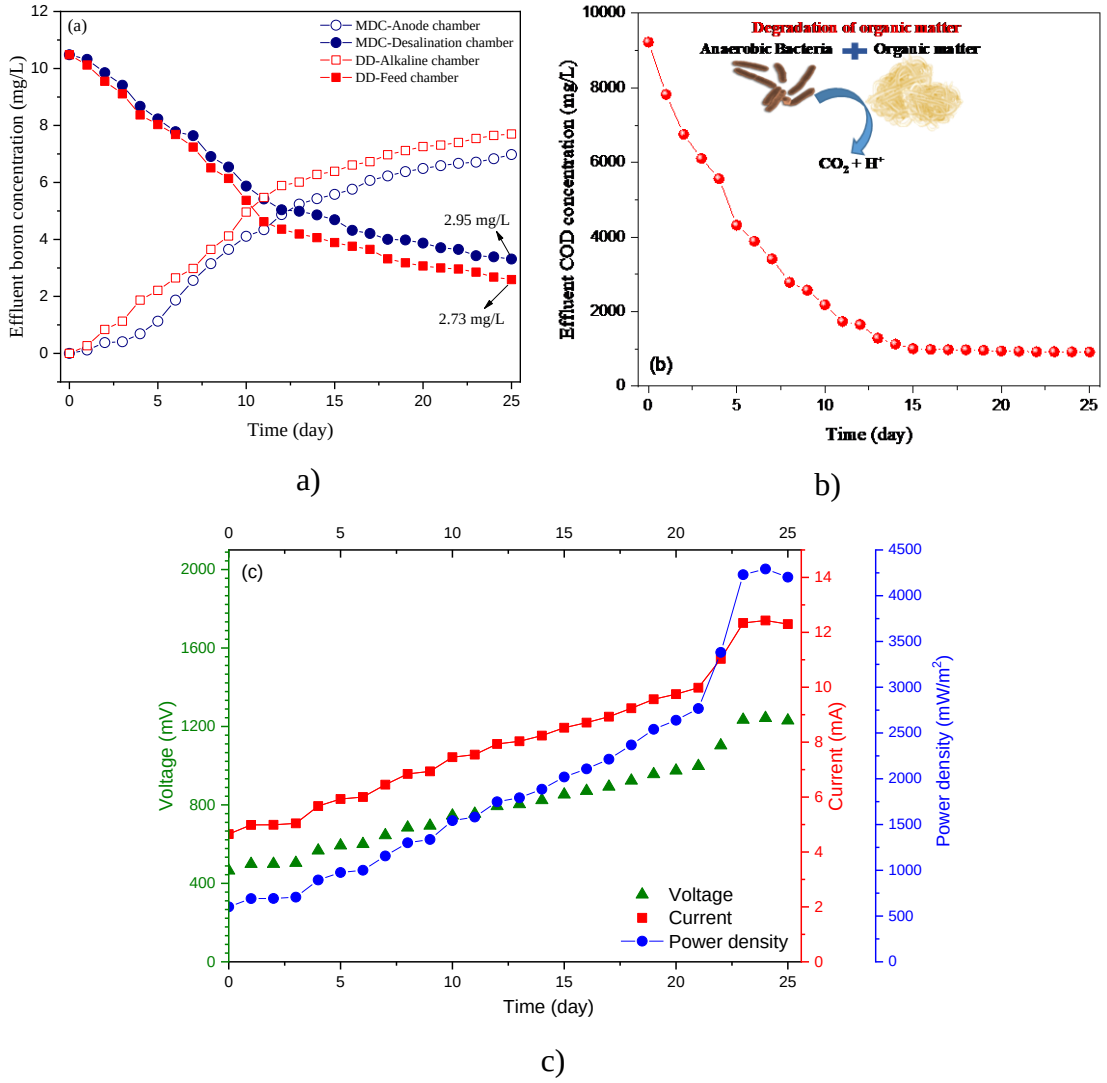

Figure 7.4. Effluent boron concentrations a), effluent COD concentrations b), and voltage, current, and power density c) for MDD-DD hybrid system.

The current and power density values of MDC were also determined and same trend of the voltage was observed (Figure 7.4c). The highest current and power density values were calculated to be almost 12.43 A and 4203 mA/m^2 for 25 days. Compared to the synthetic boron solution treatment, although the boron removal efficiency is low for real geothermal water treatment, the amount of energy produced was found to be higher than synthetic solution. On the other hand, the energy production efficiency of real geothermal water treatment was lower than RO concentrated water treatment. The reason for this is clearly explained by the high ionic strength of RO concentrated water. Moreover, the pH in DD-feed chamber decreased from 10.5 to almost 9.7 for 25 days most probably due to the microenvironment (anions, cations, and metal ions) in feed solution, which cause the neutralization of solution. As expected, the alkaline solution pH

decreased from 12 to 10.8 due to the transfer of hydroxide ions from DD-alkaline chamber to DD-feed chamber with hydroxide concentration gradient difference between two chamber.

7.4. Conclusion

The MDC-DD hybrid system was shown to be an environmentally safe and sustainable method for simultaneous boron removal from geothermal water and RO concentrated water, as well as COD removal and energy production from industrial effluents. MDC-DD hybrid process performance was considerably enhanced boron removal efficiency from synthetic solution, geothermal water, and RO concentrated water. The highest boron removal efficiency was 72.1% in desalination chamber and 74.8% in DD-feed chamber for synthetic solution treatment at optimum operating conditions, while the COD removal efficiency was almost 90% in all experimental runs. On the other hand, the maximum power density was found to be 4818 mW/m^2 with closed circuit voltage of 1317 mV for RO concentrated water treatment. The most important output of this study is that thanks to the better manipulation of the pH by DD system, the pH value of the system did not need to be adjusted continuously in order to convert the uncharged boric acid into the borate ion in the charged form. As a consequence of the findings of this study, the MDC-DD hybrid system has a lot of promise for improving desalination of geothermal water, treatment of RO concentrated water, treatment of yeats wastewater, and energy generation.

CHAPTER 8

CONCLUSION

This thesis study proposed to simultaneous boron removal from geothermal water, wastewater treatment, and energy production using enhanced MDC process with various modifications to produce irrigation quality water. The approaches performed in the enhancement of the MDC and their benefits are summarized as follows:

In Chapter 2, the specifically designed MDC system was performed for concurrent boron removal from geothermal water and organic matter removal from yeast wastewater with energy production under various operational conditions. Based on the results, the MDC system was demonstrated to be an environmentally safe method for removing boron from geothermal water while also removing COD and producing energy from yeast wastewater. The electrode surface area had the greatest impact on boron removal effectiveness among the operational factors studied, followed by air flow rate and catholyte solution. Despite the fact that the WHO's boron content limit in drinking water met the optimal experimental circumstances, none of the experiments provided irrigation-quality water. In this regard, MDC might be utilized as a polishing step on the effluents of other membrane treatment methods. Internal resistance elements including organic and inorganic membrane fouling, as well as inter-membrane distance, might also be attractive targets for further investigations to enhance MDC performance.

In Chapter 3, the anode chamber of a classic MDC cell was modified to integrate 3D cubic electrodes as a novel design to enhance treatment and energy production performance of MDC system. The temperature of the anolyte solution, the activated sludge:wastewater (S:WW) ratio, and the electrode type were found to have a considerable impact on MDC performance. For geothermal water, the maximum boron and organic matter removal efficiency were 55.5% and 91.5%, respectively, with a power density of 9.04 mW/m^3. Results compared with classic MDC, it was observed that the removal efficiencies and energy production performance increase when the designed electrode cell is filled with 3D cubic electrodes. On the other hand, SEM and EDX results revealed significant biofouling on the AEM facing the anode chamber and salt accumulation on both the AEM and CEM at the end of the operation, indicating that biofouling and salt accumulation could compromise MDC performance, especially in

operations with a higher S:WW ratio. Therefore, to improve the performance of the novel MDC configuration and utilized in reality, more research on membrane scaling caused by biofouling and salt accumulation is required.

In Chapter 4, the potential of *Lemna minor* L. to remove boron from synthetic solution and geothermal brine was assessed. Moreover, the obtained results are evaluated in detail to understand whether *Lemna minor* L. can be used as a pre-treatment process to eliminate some of the problems encountered in membrane-based technologies (e.g. MDCs). The results revealed that the boron concentration, water height in the cell, and humic acid concentration all had a considerable impact on boron removal. The highest boron removal efficiency was 96.7% for 5 mg B/L at initial pH 8 and water height of 1.5 cm without humic acid. These results showed that the *Lemna minor* L. might effectively remove boron from waters with low boron contents. In addition, the *Lemna minor* L. can be filtered out of the treatment tanks, dried at room temperature, and then utilized as a natural fertilizer in boron-deficient agricultural areas. Consequently, *Lemna minor* L. can be used as a cost effective and environmentally beneficial pre-treatment method for boron containing aqueous solutions.

In Chapter 5, a novel 3D sponge anode electrode coated with activated carbon-chitosan composite was produced to improve MDC performance with increasing electrode pore size and electrical conductivity. The unique 3D anode electrode was presented a high electron transfer efficiency owing to its macro-porous structure. As a consequence of the findings, the 3D activated carbon-chitosan composite sponge anode had a great promise for improving desalination and energy generation in the MDC process.

In Chapter 6, MDC system was used as a post-treatment process for further polishing of RO permeate water and minimization of RO concentrate. A hybrid RO/MDC system was studied for the first time in desalination of geothermal water. MDC system achieved significant improvements in terms of B concentrations at the first cycles for both RO concentrate (66.3%) and permeate (38.6%). According to the SAR values, while the RO permeate/MDC effluent could be used to irrigate crops with low tolerance such as avocado and citrus fruits, RO concentrate/MDC effluent was only fit for irrigation of medium tolerance crops such as rice, alfalfa and oat. However, application of $CaSO_4$ to either soil or irrigation water was strongly recommended in order to ensure soil permeability.

In Chapter 7, in order to control and counteract the pH fluctuations in the MDC system, a DD reactor was integrated. MDC-DD hybrid process considerably enhanced boron removal efficiency from synthetic solution, geothermal water, and RO concentrate. The highest boron removal efficiency was 72.1% in desalination chamber and 74.8% in DD-feed chamber for synthetic solution treatment at optimum operating conditions, while the COD removal efficiency was almost 90% in all experimental runs. On the other hand, the maximum power density was 4818 mW/m^2 with closed circuit voltage of 1317 mV for RO concentrate. The most important output of this study was due to effective adjustment of the pH by DD system, the previous need of continuous pH monitoring became unnecessary. As a consequence of the findings of this study, the MDC-DD hybrid system had a lot of promise for improving desalination of geothermal water, treatment of RO concentrate and yeast wastewater, and energy generation.

This thesis set out to investigate the Microbial Desalination Cell technology in detail and its application primarily in boron removal from geothermal brine. The operating parameters were studied comprehensively and the most important ones were determined. Moreover, through 4 scientific papers and 3 conference proceedings, the outputs of this Ph.D. thesis were widely disseminated. The limitations of the system were also presented. The most important drawback of the MDC system was its long operation time required for treatment. From this point forward, the scale up of the system should be studied in order to decrease the operation time of the system.

REFERENCES

Aghbashlo, M., Hosseinpour, S., Tabatabaei, M., Soufiyan, M.M., 2019. Multi-objective exergetic and technical optimization of a piezoelectric ultrasonic reactor applied to synthesize biodiesel from waste cooking oil (WCO) using soft computing techniques. Fuel 235, 100–112.

Ahirrao, D.J., Tambat, S., Pandit, A.B., Jha, N., 2019. Sweet-Lime-Peels-Derived Activated-Carbon-Based Electrode for Highly Efficient Supercapacitor and Flow-Through Water Desalination. ChemistrySelect 4, 2610–2625.

Aksoy, N., Şimşek, C., Gunduz, O., 2009. Groundwater contamination mechanism in a geothermal field: a case study of Balcova, Turkey. J. Contam. Hydrol. 103, 13–28.

Al-Bsoul, A., Al-Shannag, M., Tawalbeh, M., Al-Taani, A.A., Lafi, W.K., Al-Othman, A., Alsheyab, M., 2020. Optimal conditions for olive mill wastewater treatment using ultrasound and advanced oxidation processes. Sci. Total Environ. 700, 134576.

Al-Mamun, A., Ahmad, W., Baawain, M.S., Khadem, M., Dhar, B.R., 2018. A review of microbial desalination cell technology: configurations, optimization and applications. J. Clean. Prod. 183, 458–480.

Al-Qodah, Z., Tawalbeh, M., Al-Shannag, M., Al-Anber, Z., Bani-Melhem, K., 2020. Combined electrocoagulation processes as a novel approach for enhanced pollutants removal: A state-of-the-art review. Sci. Total Environ. 744, 140806.

Al Hinai, A., Jafary, T., Alhimali, H., Rahman, S., Al-Mamun, A., 2022. Desalination and acid-base recovery in a novel design of microbial desalination and chemical recovery cell. Desalination 525, 115488.

Alharati, A., Valour, J.-P., Urbaniak, S., Swesi, Y., Fiaty, K., Charcosset, C., 2018. Boron removal from seawater using a hybrid sorption/microfiltration process without continuous addition of resin. Chem. Eng. Process. Intensif. 131, 227–233.

AlMarzooqi, F.A., Al Ghaferi, A.A., Saadat, I., Hilal, N., 2014. Application of capacitive deionisation in water desalination: a review. Desalination 342, 3–15.

Alsafadi, K., Al-Ansari, N., Mokhtar, A., Mohammed, S., Elbeltagi, A., Sammen, S.S., Bi, S., 2022. An evapotranspiration deficit-based drought index to detect variability of terrestrial carbon productivity in the Middle East. Environ. Res. Lett. 17, 14051.

An, Z., Zhang, H., Wen, Q., Chen, Z., Du, M., 2014. Desalination combined with copper (II) removal in a novel microbial desalination cell. Desalination 346, 115–121.

Angelov, A., Bratkova, S., Loukanov, A., 2013. Microbial fuel cell based on electroactive sulfate-reducing biofilm. Energy Convers. Manag. 67, 283–286.

Anusha, G., Noori, M.T., Ghangrekar, M.M., 2018. Application of silver-tin dioxide composite cathode catalyst for enhancing performance of microbial desalination cell. Mater. Sci. Energy Technol. 1, 188–195.

APHA, Standard methods for the examination of water and wastewater, American Public Health Association Manual, New York (twenty-three ed.), 2017.

Arar, Ö., Yüksel, Ü., Kabay, N., Yüksel, M., 2013. Application of electrodeionization (EDI) for removal of boron and silica from reverse osmosis (RO) permeate of geothermal water. Desalination 310, 25–33.

Association, A.P.H., 1926. Standard methods for the examination of water and wastewater. American Public Health Association.

Baba, A., Ármannsson, H., 2006. Environmental impact of the utilization of geothermal areas. Energy Sources, Part B 1, 267–278.

Baba, A., Sözbilir, H., 2012. Source of arsenic based on geological and hydrogeochemical properties of geothermal systems in Western Turkey. Chem. Geol. 334, 364–377.

Ban, S.-H., Im, S.-J., Cho, J., Jang, A., 2019. Comparative performance of FO-RO hybrid and two-pass SWRO desalination processes: Boron removal. Desalination 471, 114114.

Banasiak, L.J., Schäfer, A.I., 2009a. Removal of boron, fluoride and nitrate by

electrodialysis in the presence of organic matter. J. Memb. Sci. 334, 101–109.

Banasiak, L.J., Schäfer, A.I., 2009b. Removal of inorganic trace contaminants by electrodialysis in a remote Australian community. Desalination 248, 48–57.

Bard, A.J., Faulkner, L.R., 2001. Electrochemical methods: fundamentals and applications. 2nd Wiley. New York.

Barth, S.R., 2000. Utilization of boron as a critical parameter in water quality evaluation: implications for thermal and mineral water resources in SW Germany and N Switzerland. Environ. Geol. 40, 73–89.

Bejjanki, D., Muthukumar, K., Radhakrishnan, T.K., Alagarsamy, A., Pugazhendhi, A., Mohamed, S.N., 2021. Simultaneous bioelectricity generation and water desalination using Oscillatoria sp. as biocatalyst in photosynthetic microbial desalination cell. Sci. Total Environ. 754, 142215.

Bergel, A., Féron, D., Mollica, A., 2005. Catalysis of oxygen reduction in PEM fuel cell by seawater biofilm. Electrochem. commun. 7, 900–904.

Bhagyaraj, S., Al-Ghouti, M.A., Kasak, P., Krupa, I., 2021. An updated review on boron removal from water through adsorption processes. Emergent Mater. 4, 1167–1186.

Blevins, D.G., Lukaszewski, K.M., 1998. Boron in plant structure and function. Annu. Rev. Plant Biol. 49, 481–500.

Böcük, H., Yakar, A., Türker, O.C., 2013. Assessment of Lemna gibba L.(duckweed) as a potential ecological indicator for contaminated aquatic ecosystem by boron mine effluent. Ecol. Indic. 29, 538–548.

Borràs, E., Aliaguilla, M., Huidobro, L., Martínez-Crespiera, S., Matencio, S., Molognoni, D., Ortiz, J.M., Ramírez-Moreno, M., Rodenas, P., Faccini, M., 2021. Key elements and materials in microbial desalination cells.

Breytus, A., Hasson, D., Semiat, R., Shemer, H., 2020. Removal of nitrate from groundwater by Donnan dialysis. J. Water Process Eng. 34, 101157.

Bryjak, M., Wolska, J., Kabay, N., 2008. Removal of boron from seawater by adsorption–membrane hybrid process: implementation and challenges. Desalination 223, 57–62.

Cao, X., Huang, X., Liang, P., Xiao, K., Zhou, Y., Zhang, X., Logan, B.E., 2009. A new method for water desalination using microbial desalination cells. Environ. Sci. Technol. 43, 7148–7152.

Çermikli, E., Şen, F., Altıok, E., Wolska, J., Cyganowski, P., Kabay, N., Bryjak, M., Arda, M., Yüksel, M., 2020. Performances of novel chelating ion exchange resins for boron and arsenic removal from saline geothermal water using adsorption-membrane filtration hybrid process. Desalination 491, 114504.

Chen, M., Dollar, O., Shafer-Peltier, K., Randtke, S., Waseem, S., Peltier, E., 2020. Boron removal by electrocoagulation: Removal mechanism, adsorption models and factors influencing removal. Water Res. 170, 115362.

Chen, X., Liang, P., Wei, Z., Zhang, X., Huang, X., 2012. Sustainable water desalination and electricity generation in a separator coupled stacked microbial desalination cell with buffer free electrolyte circulation. Bioresour. Technol. 119, 88–93.

Chen, X., Sun, D., Zhang, X., Liang, P., Huang, X., 2015. Novel self-driven microbial nutrient recovery cell with simultaneous wastewater purification. Sci. Rep. 5, 1–10.

Clauwaert, P., Van der Ha, D., Boon, N., Verbeken, K., Verhaege, M., Rabaey, K., Verstraete, W., 2007. Open air biocathode enables effective electricity generation with microbial fuel cells. Environ. Sci. Technol. 41, 7564–7569.

Cob, S.S., Beaupin, C., Hofs, B., Nederlof, M.M., Harmsen, D.J.H., Cornelissen, E.R., Zwijnenburg, A., Güner, F.E.G., Witkamp, G.-J., 2012. Silica and silicate precipitation as limiting factors in high-recovery reverse osmosis operations. J. Memb. Sci. 423, 1–10.

Cui, Y., Ge, Q., Liu, X.-Y., Chung, T.-S., 2014. Novel forward osmosis process to effectively remove heavy metal ions. J. Memb. Sci. 467, 188–194.

da Rosa Schio, R., da Rosa, B.C., Gonçalves, J.O., Pinto, L.A.A., Mallmann, E.S., Dotto, G.L., 2019. Synthesis of a bio–based polyurethane/chitosan composite foam using ricinoleic acid for the adsorption of Food Red 17 dye. Int. J. Biol. Macromol. 121, 373–380.

Davis, R.J., Kim, Y., Logan, B.E., 2013. Increasing desalination by mitigating anolyte pH imbalance using catholyte effluent addition in a multi-anode bench scale microbial desalination cell. ACS Sustain. Chem. Eng. 1, 1200–1206.

Davis, S.M., Drake, K.D., Maier, K.J., 2002. Toxicity of boron to the duckweed, Spirodella polyrrhiza. Chemosphere 48, 615–620.

De Los Ríos, A.P., Hernández-Fernández, F.J., Lozano, L.J., Sánchez-Segado, S., Ginestá-Anzola, A., Godinez, C., Tomás-Alonso, F., Quesada-Medina, J., 2013. On the selective separation of metal ions from hydrochloride aqueous solution by pertraction through supported ionic liquid membranes. J. Memb. Sci. 444, 469–481.

Desa, U.N., 2016. Transforming our world: The 2030 agenda for sustainable development.

Dinka, M.O., 2016. Quality composition and irrigation suitability of various surface water and groundwater sources at Matahara Plain. Water Resour. 43, 677–689.

Directive, C., 1998. On the quality of water intended for human consumption. Off. J. Eur. Communities 330, 32–54.

Do, M.H., Ngo, H.H., Guo, W.S., Liu, Y., Chang, S.W., Nguyen, D.D., Nghiem, L.D., Ni, B.J., 2018. Challenges in the application of microbial fuel cells to wastewater treatment and energy production: a mini review. Sci. Total Environ. 639, 910–920.

Dominguez-Tagle, C., Romero-Ternero, V.J., Delgado-Torres, A.M., 2011. Boron removal efficiency in small seawater Reverse Osmosis systems. Desalination 265, 43–48.

Dong, Y., Liu, J., Sui, M., Qu, Y., Ambuchi, J.J., Wang, H., Feng, Y., 2017. A

combined microbial desalination cell and electrodialysis system for copper-containing wastewater treatment and high-salinity-water desalination. J. Hazard. Mater. 321, 307–315.

Dydo, P., Turek, M., 2014. The concept for an ED–RO integrated system for boron removal with simultaneous boron recovery in the form of boric acid. Desalination 342, 35–42.

Ebrahimi, A., Kebria, D.Y., Najafpour, G.D., 2018a. Co-treatment of septage and municipal wastewater in a quadripartite microbial desalination cell. Chem. Eng. J. 354, 1092–1099.

Ebrahimi, A., Najafpour, G.D., Kebria, D.Y., 2018b. Performance of microbial desalination cell for salt removal and energy generation using different catholyte solutions. Desalination 432, 1–9.

Edition, F., 2011. Guidelines for drinking-water quality. WHO Chron. 38, 104–108.

Ekperusi, A.O., Sikoki, F.D., Nwachukwu, E.O., 2019. Application of common duckweed (Lemna minor) in phytoremediation of chemicals in the environment: State and future perspective. Chemosphere 223, 285–309.

Federation, W.E., Association, A., 2005. Standard methods for the examination of water and wastewater. Am. Public Heal. Assoc. Washington, DC, USA 21.

Firdous, S., Jin, W., Shahid, N., Bhatti, Z.A., Iqbal, A., Abbasi, U., Mahmood, Q., Ali, A., 2018. The performance of microbial fuel cells treating vegetable oil industrial wastewater. Environ. Technol. Innov. 10, 143–151.

Frederic, M., Samir, L., Louise, M., Abdelkrim, A., 2006. Comprehensive modeling of mat density effect on duckweed (Lemna minor) growth under controlled eutrophication. Water Res. 40, 2901–2910.

Frick, H., 1985. Boron tolerance and accumulation in the duckweed, Lemna minor. J. Plant Nutr. 8, 1123–1129.

Gabelich, C.J., Xu, P., Cohen, Y., 2010. Concentrate treatment for inland desalting. Sustain. Sci. Eng. 2, 295–326.

Gallup, D.L., 2007. Treatment of geothermal waters for production of industrial, agricultural or drinking water. Geothermics 36, 473–483.

García-Sánchez, F., Simón-Grao, S., Martínez-Nicolás, J.J., Alfosea-Simón, M., Liu, C., Chatzissavvidis, C., Pérez-Pérez, J.G., Cámara-Zapata, J.M., 2020. Multiple stresses occurring with boron toxicity and deficiency in plants. J. Hazard. Mater. 397, 122713.

Gazette, T.O., 2010. The law on the foundation of the Presidency for Turks Abroad and Related Communities. Article 5978, 3.

Ge, Z., Dosoretz, C.G., He, Z., 2014. Effects of number of cell pairs on the performance of microbial desalination cells. Desalination 341, 101–106.

Gemici, Ü., Tarcan, G., 2002. Distribution of boron in thermal waters of western Anatolia, Turkey, and examples of their environmental impacts. Environ. Geol. 43, 87–98.

Gholizadeh, A., Ebrahimi, A.A., Salmani, M.H., Ehrampoush, M.H., 2017. Ozone-cathode microbial desalination cell; An innovative option to bioelectricity generation and water desalination. Chemosphere 188, 470–477.

Goli, E., Hiemstra, T., Rahnemaie, R., 2019. Interaction of boron with humic acid and natural organic matter: Experiments and modeling. Chem. Geol. 515, 1–8.

Goren, A.Y., Okten, H.E., 2022. 3D electrode use in MDC for enhanced removal of boron from geothermal water. Desalination 530, 115668.

Goren, A.Y., Okten, H.E., 2021a. Energy production from treatment of industrial wastewater and boron removal in aqueous solutions using microbial desalination cell. Chemosphere 285, 131370.

Goren, A.Y., Okten, H.E., 2021b. Simultaneous energy production, boron and COD removal using a novel microbial desalination cell. Desalination 518, 115267.

Grady Jr, C.P.L., Lim, H.C., 1999. Biological wastewater treatment. Mercel Dekker. Inc. New York.

Grieve, C.M., Poss, J.A., Grattan, S.R., Suarez, D.L., Smith, T.E., 2010. The combined effects of salinity and excess boron on mineral ion relations in broccoli. Sci. Hortic. (Amsterdam). 125, 179–187.

Guang, L., Koomson, D.A., Jingyu, H., Ewusi-Mensah, D., Miwornunyuie, N., 2020. Performance of exoelectrogenic bacteria used in microbial desalination cell technology. Int. J. Environ. Res. Public Health 17, 1121.

Gude, V.G., 2016. Geothermal source potential for water desalination–Current status and future perspective. Renew. Sustain. Energy Rev. 57, 1038–1065.

Gujjala, L.K.S., Dutta, D., Sharma, P., Kundu, D., Vo, D.-V.N., Kumar, S., 2022. A state-of-the-art review on microbial desalination cells. Chemosphere 288, 132386.

Güler, E., Kabay, N., Yüksel, M., Yiğit, N.Ö., Kitiş, M., Bryjak, M., 2011. Integrated solution for boron removal from seawater using RO process and sorption-membrane filtration hybrid method. J. Memb. Sci. 375, 249–257.

Haklıdır, F.S.T., Şengün, R., 2020. Hydrogeochemical similarities and differences between high temperature geothermal systems with similar geologic settings in the Büyük Menderes and Gediz Grabens of Turkey. Geothermics 83, 101717.

Hasan, S.A., Fariduddin, Q., Ali, B., Hayat, S., Ahmad, A., 2009. Cadmium: toxicity and tolerance in plants. J Env. Biol 30, 165–174.

Hemalatha, M., Butti, S.K., Velvizhi, G., Mohan, S.V., 2017. Microbial mediated desalination for ground water softening with simultaneous power generation. Bioresour. Technol. 242, 28–35.

Hilal, N., Kim, G.J., Somerfield, C., 2011. Boron removal from saline water: a comprehensive review. Desalination 273, 23–35.

Hoagland, D.R., 1948. Lectures on the Inorganic Nutrition of Plants, Chronica Botanica Co. Waltham, Mass.

Hoang, A.T., Nižetić, S., Ng, K.H., Papadopoulos, A.M., Le, A.T., Kumar, S., Hadiyanto, H., 2022. Microbial fuel cells for bioelectricity production from waste as sustainable prospect of future energy sector. Chemosphere 287, 132285.

Hou, C.-H., Liu, N.-L., Hsu, H.-L., Den, W., 2014. Development of multi-walled carbon nanotube/poly (vinyl alcohol) composite as electrode for capacitive deionization. Sep. Purif. Technol. 130, 7–14.

Hou, D., Wang, J., Sun, X., Luan, Z., Zhao, C., Ren, X., 2010. Boron removal from aqueous solution by direct contact membrane distillation. J. Hazard. Mater. 177, 613–619.

Hou, J., Liu, Z., Zhang, P., 2013. A new method for fabrication of graphene/polyaniline nanocomplex modified microbial fuel cell anodes. J. Power Sources 224, 139–144.

Hu, Z.J., Hu, Y.L., Ouyang, E.M., Feng, F., 2014. The study on the effect on seawater desalination and boron removal by RO-EDI desalination system, in: Advanced Materials Research. Trans Tech Publ, pp. 3211–3215.

Hua, T., Zhang, R., Sun, H., Liu, C., 2021. Alleviation of boron toxicity in plants: Mechanisms and approaches. Crit. Rev. Environ. Sci. Technol. 51, 2975–3015.

Huang, G., Wang, H., Zhao, H., Wu, P., Yan, Q., 2018. Application of polypyrrole modified cathode in bio-electro-Fenton coupled with microbial desalination cell (MDC) for enhanced degradation of methylene blue. J. Power Sources 400, 350–359.

Huggins, T., Wang, H., Kearns, J., Jenkins, P., Ren, Z.J., 2014. Biochar as a sustainable electrode material for electricity production in microbial fuel cells. Bioresour. Technol. 157, 114–119.

Hussain, A., Sharma, R., Minier-Matar, J., Hirani, Z., Adham, S., 2019. Application of emerging ion exchange resin for boron removal from saline groundwater. J. Water Process Eng. 32, 100906.

Imoro, A.Z., Mensah, M., Buamah, R., 2021. Developments in the microbial desalination cell technology: A review. Water-Energy Nexus 4, 76–87.

Jacobson, K.S., Drew, D.M., He, Z., 2011a. Efficient salt removal in a continuously operated upflow microbial desalination cell with an air cathode. Bioresour.

Technol. 102, 376–380.

Jacobson, K.S., Drew, D.M., He, Z., 2011b. Use of a liter-scale microbial desalination cell as a platform to study bioelectrochemical desalination with salt solution or artificial seawater. Environ. Sci. Technol. 45, 4652–4657.

Jadhav, G.S., Ghangrekar, M.M., 2009. Performance of microbial fuel cell subjected to variation in pH, temperature, external load and substrate concentration. Bioresour. Technol. 100, 717–723.

Jafary, T., Al-Mamun, A., Alhimali, H., Baawain, M.S., Rahman, S., Tarpeh, W.A., Dhar, B.R., Kim, B.H., 2020. Novel two-chamber tubular microbial desalination cell for bioelectricity production, wastewater treatment and desalination with a focus on self-generated pH control. Desalination 481, 114358.

Jarma, Y.A., Karaoğlu, A., Senan, I.R.A., Meriç, M.K., Kukul, Y.S., Özçakal, E., Barlas, N.T., Çakıcı, H., Baba, A., Kabay, N., 2022. Utilization of membrane separation processes for reclamation and reuse of geothermal water in agricultural irrigation of tomato plants-pilot membrane tests and economic analysis. Desalination 528, 115608.

Jatoi, A.S., Hashmi, Z., Mazari, S.A., Mubarak, N.M., Karri, R.R., Ramesh, S., Rezakazemi, M., 2022. A comprehensive review of microbial desalination cells for present and future challenges. Desalination 535, 115808.

Kabay, N., Bryjak, M., Hilal, N., 2015. Boron separation processes. Elsevier.

Kabay, N., Köseoğlu, P., Yapıcı, D., Yüksel, Ü., Yüksel, M., 2013a. Coupling ion exchange with ultrafiltration for boron removal from geothermal water-investigation of process parameters and recycle tests. Desalination 316, 17–22.

Kabay, N., Köseoğlu, P., Yavuz, E., Yüksel, Ü., Yüksel, M., 2013b. An innovative integrated system for boron removal from geothermal water using RO process and ion exchange-ultrafiltration hybrid method. Desalination 316, 1–7.

Kabay, N., Sarp, S., Yuksel, M., Kitis, M., Koseoğlu, H., Arar, Ö., Bryjak, M., Semiat, R., 2008. Removal of boron from SWRO permeate by boron selective ion

exchange resins containing N-methyl glucamine groups. Desalination 223, 49–56.

Kartikaningsih, D., Shih, Y.-J., Huang, Y.-H., 2016. Boron removal from boric acid wastewater by electrocoagulation using aluminum as sacrificial anode. Sustain. Environ. Res. 26, 150–155.

Kayaci, S., Tantekin-Ersolmaz, S.B., Ahunbay, M.G., Krantz, W.B., 2020. Technical and economic feasibility of the concurrent desalination and boron removal (CDBR) process. Desalination 486, 114474.

Keeley, J., Jarvis, P., Smith, A.D., Judd, S.J., 2016. Coagulant recovery and reuse for drinking water treatment. Water Res. 88, 502–509.

Kim, S., Nam, S.-N., Jang, A., Jang, M., Park, C.M., Son, A., Her, N., Heo, J., Yoon, Y., 2022. Review of adsorption–membrane hybrid systems for water and wastewater treatment. Chemosphere 286, 131916.

Kim, Y., Logan, B.E., 2013. Microbial desalination cells for energy production and desalination. Desalination 308, 122–130.

Kim, Y., Logan, B.E., 2011. Series assembly of microbial desalination cells containing stacked electrodialysis cells for partial or complete seawater desalination. Environ. Sci. Technol. 45, 5840–5845.

Kokabian, B., Gude, V.G., 2015. Sustainable photosynthetic biocathode in microbial desalination cells. Chem. Eng. J. 262, 958–965.

Kumirska, J., Czerwicka, M., Kaczyński, Z., Bychowska, A., Brzozowski, K., Thöming, J., Stepnowski, P., 2010. Application of spectroscopic methods for structural analysis of chitin and chitosan. Mar. Drugs 8, 1567–1636.

Landsman, M.R., Lawler, D.F., Katz, L.E., 2020. Application of electrodialysis pretreatment to enhance boron removal and reduce fouling during desalination by nanofiltration/reverse osmosis. Desalination 491, 114563.

Larminie, J., Dicks, A., McDonald, M.S., 2003. Fuel cell systems explained. J. Wiley Chichester, UK.

Larrosa-Guerrero, A., Scott, K., Head, I.M., Mateo, F., Ginesta, A., Godinez, C., 2010. Effect of temperature on the performance of microbial fuel cells. Fuel 89, 3985–3994.

Lee, S., Choi, J., Park, Y.-G., Shon, H., Ahn, C.H., Kim, S.-H., 2019. Hybrid desalination processes for beneficial use of reverse osmosis brine: Current status and future prospects. Desalination 454, 104–111.

Leenheer, J.A., 2009. Systematic approaches to comprehensive analyses of natural organic matter. Ann. Environ. Sci. 3.

Levén, L., Eriksson, A.R.B., Schnürer, A., 2007. Effect of process temperature on bacterial and archaeal communities in two methanogenic bioreactors treating organic household waste. FEMS Microbiol. Ecol. 59, 683–693.

Li, M., Li, Y.-W., Cai, Q.-Y., Zhou, S.-Q., Mo, C.-H., 2020. Spraying carbon powder derived from mango wood biomass as high-performance anode in bio-electrochemical system. Bioresour. Technol. 300, 122623.

Li, S., Cheng, C., Thomas, A., 2017. Carbon-based microbial-fuel-cell electrodes: from conductive supports to active catalysts. Adv. Mater. 29, 1602547.

Liaquat, R., Mehmood, T., Khoja, A.H., Iqbal, N., Ejaz, H., Mumtaz, S., 2021. Investigating the potential of locally sourced wastewater as a feedstock of microbial desalination cell (MDC) for bioenergy production. Bioprocess Biosyst. Eng. 44, 173–184.

Lin, J.-Y., Mahasti, N.N.N., Huang, Y.-H., 2021. Recent advances in adsorption and coagulation for boron removal from wastewater: A comprehensive review. J. Hazard. Mater. 407, 124401.

Liu, C., Gu, W., Dai, Z., Li, J., Jiang, H., Zhang, Q., 2018. Boron accumulation by Lemna minor L. under salt stress. Sci. Rep. 8, 1–6.

Liu, X.-W., Sun, X.-F., Huang, Y.-X., Sheng, G.-P., Wang, S.-G., Yu, H.-Q., 2011. Carbon nanotube/chitosan nanocomposite as a biocompatible biocathode material to enhance the electricity generation of a microbial fuel cell. Energy Environ. Sci.

4, 1422–1427.

Logan, B., Cheng, S., Watson, V., Estadt, G., 2007. Graphite fiber brush anodes for increased power production in air-cathode microbial fuel cells. Environ. Sci. Technol. 41, 3341–3346.

Logan, B.E., Hamelers, B., Rozendal, R., Schröder, U., Keller, J., Freguia, S., Aelterman, P., Verstraete, W., Rabaey, K., 2006. Microbial fuel cells: methodology and technology. Environ. Sci. Technol. 40, 5181–5192.

Lund, J.W., Toth, A.N., 2021. Direct utilization of geothermal energy 2020 worldwide review. Geothermics 90, 101915.

Luo, H., Xu, P., Ren, Z., 2012a. Long-term performance and characterization of microbial desalination cells in treating domestic wastewater. Bioresour. Technol. 120, 187–193.

Luo, H., Xu, P., Roane, T.M., Jenkins, P.E., Ren, Z., 2012b. Microbial desalination cells for improved performance in wastewater treatment, electricity production, and desalination. Bioresour. Technol. 105, 60–66.

Luo, J., Wu, C., Xu, T., Wu, Y., 2011. Diffusion dialysis-concept, principle and applications. J. Memb. Sci. 366, 1–16.

Ma, C.-Y., Hou, C.-H., 2019. Enhancing the water desalination and electricity generation of a microbial desalination cell with a three-dimensional macroporous carbon nanotube-chitosan sponge anode. Sci. Total Environ. 675, 41–50.

MacHarg, J., Seacord, T.F., Sessions, B., 2008. ADC baseline tests reveal trends in membrane performance. Desalin. water reuse 18, 30–39.

Malakootian, M., Mahdizadeh, H., Nasiri, A., Mirzaienia, F., Hajhoseini, M., Amirmahani, N., 2018. Investigation of the efficiency of microbial desalination cell in removal of arsenic from aqueous solutions. Desalination 438, 19–23.

Malakootian, Masha, Mirzaienia, F., Malakootian, Mohammad, 2019. Removal efficiency of Cu2+ and Zn2+ from industrial wastewater by using microbial desalination cell. J. Water Chem. Technol. 41, 334–339.

Malley, Z.J.U., Taeb, M., Matsumoto, T., Takeya, H., 2009. Environmental sustainability and water availability: Analyses of the scarcity and improvement opportunities in the Usangu plain, Tanzania. Phys. Chem. Earth, Parts A/B/C 34, 3–13.

Mallmann, E.S., Barbosa, M.I.R., Maciel Filho, R., 2014. Assessment of biobased polyurethane reaction kinects through DSC and FTIR analysis. IJSRCE 1, 66–73.

Marín, C.M.D.-C., Oron, G., 2007. Boron removal by the duckweed Lemna gibba: a potential method for the remediation of boron-polluted waters. Water Res. 41, 4579–4584.

McLay, C.L., 1976. The effect of pH on the population growth of three species of duckweed: Spirodela oligorrhiza, Lemna minor and Wolffia arrhiza. Freshw. Biol. 6, 125–136.

Mehanna, M., Saito, T., Yan, J., Hickner, M., Cao, X., Huang, X., Logan, B.E., 2010. Using microbial desalination cells to reduce water salinity prior to reverse osmosis. Energy Environ. Sci. 3, 1114–1120. https://doi.org/10.1039/C002307H

Melikoglu, M., 2017. Geothermal energy in Turkey and around the World: A review of the literature and an analysis based on Turkey's Vision 2023 energy targets. Renew. Sustain. Energy Rev. 76, 485–492.

Melnyk, L., Goncharuk, V., Butnyk, I., Tsapiuk, E., 2005. Boron removal from natural and wastewaters using combined sorption/membrane process. Desalination 185, 147–157.

Meng, F., Zhao, Q., Zheng, Z., Wei, L., Wang, K., Jiang, J., Ding, J., Na, X., 2019. Simultaneous sludge degradation, desalination and bioelectricity generation in two-phase microbial desalination cells. Chem. Eng. J. 361, 180–188.

MENS, Ministry of Energy and Natural Resources, https://enerji.gov.tr/homepage, Accesed May 6, 2022.

Mirzaienia, F., Asadipour, A., Jafari, A.J., Malakootian, M., 2017. Removal efficiency of nickel and lead from industrial wastewater using microbial desalination cell.

Appl. Water Sci. 7, 3617–3624.

Mohan, S.V., Srikanth, S., Chiranjeevi, P., Arora, S., Chandra, R., 2014. Algal biocathode for in situ terminal electron acceptor (TEA) production: Synergetic association of bacteria–microalgae metabolism for the functioning of biofuel cell. Bioresour. Technol. 166, 566–574.

Morel, A., Zuo, K., Xia, X., Wei, J., Luo, X., Liang, P., Huang, X., 2012. Microbial desalination cells packed with ion-exchange resin to enhance water desalination rate. Bioresour. Technol. 118, 43–48.

Movafeghi, A., Khataee, A.R., Torbati, S., Zarei, M., Lisar, S.Y.S., 2013. Bioremoval of CI Basic Red 46 as an azo dye from contaminated water by Lemna minor L.: modeling of key factor by neural network. Environ. Prog. Sustain. Energy 32, 1082–1089.

Nagaraj, R., Thirugnanamurthy, D., Rajput, M.M., Panigrahi, B.K., 2016. Techno-economic analysis of hybrid power system sizing applied to small desalination plants for sustainable operation. Int. J. Sustain. Built Environ. 5, 269–276.

Naghii, M.R., Samman, S., 1997. The effect of boron on plasma testosterone and plasma lipids in rats. Nutr. Res. 17, 523–531.

Nations, U., 2015. Paris Agreement to the United Nations Framework Convention on Climate Change.

Nielsen, F.H., 2002. The nutritional importance and pharmacological potential of boron for higher animals and human, in: Boron in Plant and Animal Nutrition. Springer, pp. 37–49.

Nifas, G.N.G., Forteza, R.S., 2019. Synthesis of Activated Carbon/Chitosan Composites and Expanded Graphite for Symmetric Supercapacitor. J Mater. Sci Eng 8, 2.

Noori, P., Najafpour Darzi, G., 2016. Enhanced power generation in annular single-chamber microbial fuel cell via optimization of electrode spacing using chocolate industry wastewater. Biotechnol. Appl. Biochem. 63, 427–434.

Nthunya, L.N., Bopape, M.F., Mahlangu, O.T., Mamba, B.B., Van der Bruggen, B.,

Quist-Jensen, C.A., Richards, H., 2022. Fouling, performance and cost analysis of membrane-based water desalination technologies: A critical review. J. Environ. Manage. 301, 113922.

Official Journal, Regulation on Water Intended for Human Consumption, 28580, 07 March 2013, Ankara (in Turkish).

Ordóñez, R., Moral, A., Hermosilla, D., Blanco, Á., 2012. Combining coagulation, softening and flocculation to dispose reverse osmosis retentates. J. Ind. Eng. Chem. 18, 926–933.

Organization, W.H., 2017. Guidelines for drinking-water quality: first addendum to the fourth edition.

Organization, W.H., 2015. World health statistics 2015. World Health Organization.

Organization, W.H., 1998. Environmental health criteria 204: boron. Geneva, Switz. World Heal. Organ.

Ouassanouan, Y., Fakir, Y., Simonneaux, V., Kharrou, M.H., Bouimouass, H., Najar, I., Benrhanem, M., Sguir, F., Chehbouni, A., 2022. Multi-decadal analysis of water resources and agricultural change in a Mediterranean semiarid irrigated piedmont under water scarcity and human interaction. Sci. Total Environ. 155328.

Ozbey-Unal, B., Imer, D.Y., Keskinler, B., Koyuncu, I., 2018. Boron removal from geothermal water by air gap membrane distillation. Desalination 433, 141–150.

Pandit, S., Sengupta, A., Kale, S., Das, D., 2011. Performance of electron acceptors in catholyte of a two-chambered microbial fuel cell using anion exchange membrane. Bioresour. Technol. 102, 2736–2744.

Pant, D., Van Bogaert, G., Diels, L., Vanbroekhoven, K., 2010. A review of the substrates used in microbial fuel cells (MFCs) for sustainable energy production. Bioresour. Technol. 101, 1533–1543.

Ping, Q., Abu-Reesh, I.M., He, Z., 2016. Mathematical modeling based evaluation and simulation of boron removal in bioelectrochemical systems. Sci. Total Environ. 569, 1380–1389.

Ping, Q., Abu-Reesh, I.M., He, Z., 2015. Boron removal from saline water by a microbial desalination cell integrated with donnan dialysis. Desalination 376, 55–61.

Pitman, M.G., 1963. The determination of the salt relations of the cytoplasmic phase in cells of beetroot tissue. Aust. J. Biol. Sci. 16, 647–668.

Plusquellec, H., 2009. Modernization of large-scale irrigation systems: is it an achievable objective or a lost cause. Irrig. Drain. 58, S104–S120.

Prakash, P., SenGupta, A.K., 2003. Selective coagulant recovery from water treatment plant residuals using Donnan membrane process. Environ. Sci. Technol. 37, 4468–4474.

Qasem, N.A.A., Mohammed, R.H., Lawal, D.U., 2021. Removal of heavy metal ions from wastewater: A comprehensive and critical review. Npj Clean Water 4, 1–15.

Qu, Y., Feng, Y., Liu, J., He, W., Shi, X., Yang, Q., Lv, J., Logan, B.E., 2013. Salt removal using multiple microbial desalination cells under continuous flow conditions. Desalination 317, 17–22.

Qu, Y., Feng, Y., Wang, X., Liu, J., Lv, J., He, W., Logan, B.E., 2012. Simultaneous water desalination and electricity generation in a microbial desalination cell with electrolyte recirculation for pH control. Bioresour. Technol. 106, 89–94.

Ragab, M., Elawwad, A., Abdel-Halim, H., 2019a. Evaluating the performance of microbial desalination cells subjected to different operating temperatures. Desalination 462, 56–66.

Ragab, M., Elawwad, A., Abdel-Halim, H., 2019b. Simultaneous power generation and pollutant removals using microbial desalination cell at variable operation modes. Renew. Energy 143, 939–949.

Rahman, S., Al-Mamun, A., Jafary, T., Alhimali, H., Baawain, M.S., 2021a. Effect of internal and external resistances on desalination in microbial desalination cell. Water Sci. Technol. 83, 2389–2403.

Rahman, S., Jafary, T., Al-Mamun, A., Baawain, M.S., Choudhury, M.R., Alhaimali,

H., Siddiqi, S.A., Dhar, B.R., Sana, A., Lam, S.S., 2021b. Towards upscaling microbial desalination cell technology: A comprehensive review on current challenges and future prospects. J. Clean. Prod. 288, 125597.

Ramírez-Moreno, M., Esteve-Núñez, A., Ortiz, J.M., 2021. Desalination of brackish water using a microbial desalination cell: Analysis of the electrochemical behaviour. Electrochim. Acta 388, 138570.

Ramya, M., Kumar, P.S., 2022. A review on recent advancements in bioenergy production using microbial fuel cells. Chemosphere 288, 132512.

Recepoğlu, Y.K., Kabay, N., Ipek, I.Y., Arda, M., Yüksel, M., Yoshizuka, K., Nishihama, S., 2018. Packed bed column dynamic study for boron removal from geothermal brine by a chelating fiber and breakthrough curve analysis by using mathematical models. Desalination 437. https://doi.org/10.1016/j.desal.2018.02.022

Reid, R., 2010. Can we really increase yields by making crop plants tolerant to boron toxicity? Plant Sci. 178, 9–11.

Ren, L., Ahn, Y., Hou, H., Zhang, F., Logan, B.E., 2014. Electrochemical study of multi-electrode microbial fuel cells under fed-batch and continuous flow conditions. J. Power Sources 257, 454–460.

Ribera-Pi, J., Badia-Fabregat, M., Espí, J., Clarens, F., Jubany, I., Martínez-Lladó, X., 2021. Decreasing environmental impact of landfill leachate treatment by MBR, RO and EDR hybrid treatment. Environ. Technol. 42, 3508–3522.

Rodrigo, M.A., Canizares, P., Lobato, J., Paz, R., Sáez, C., Linares, J.J., 2007. Production of electricity from the treatment of urban waste water using a microbial fuel cell. J. Power Sources 169, 198–204.

Saeed, H.M., Husseini, G.A., Yousef, S., Saif, J., Al-Asheh, S., Abu Fara, A., Azzam, S., Khawaga, R., Aidan, A., 2015. Microbial desalination cell technology: A review and a case study. Desalination 359, 1–13.

Salehmin, M.N.I., Lim, S.S., Satar, I., Daud, W.R.W., 2021. Pushing microbial

desalination cells towards field application: Prevailing challenges, potential mitigation strategies, and future prospects. Sci. Total Environ. 759, 143485.

Salman, H.H., Ismail, Z.Z., 2020. Desalination of actual wetland saline water associated with biotreatment of real sewage and bioenergy production in microbial desalination cell. Sep. Purif. Technol. 250, 117110.

Samatya, S., Tuncel, S.A., Kabay, N., 2015. Boron removal from RO permeate of geothermal water by monodisperse poly (vinylbenzyl chloride-co-divinylbenzene) beads containing N-methyl-D-glucamine. Desalination 364, 75–81.

Sanchez, E., Borja, R., Weiland, P., Travieso, L., Martin, A., 2000. Effect of temperature and pH on the kinetics of methane production, organic nitrogen and phosphorus removal in the batch anaerobic digestion process of cattle manure. Bioprocess Eng. 22, 247–252.

Sevda, S., Abu-Reesh, I.M., Yuan, H., He, Z., 2017. Bioelectricity generation from treatment of petroleum refinery wastewater with simultaneous seawater desalination in microbial desalination cells. Energy Convers. Manag. 141, 101–107.

Sevda, S., Yuan, H., He, Z., Abu-Reesh, I.M., 2015. Microbial desalination cells as a versatile technology: functions, optimization and prospective. Desalination 371, 9–17.

Shivakumar, T., Razaviarani, V., 2021. An integrated approach to enhance the desalination process: coupling reverse osmosis process with microbial desalination cells in the UAE. Water Supply 21, 1127–1143.

Skoczko, I., 2020. Boron removal from the water with chemical precipitation methods. Desalin. Water Treat. 186.

Smith, T.E., Grattan, S.R., Grieve, C.M., Poss, J.A., Suarez, D.L., 2010. Salinity's influence on boron toxicity in broccoli: II. Impacts on boron uptake, uptake mechanisms and tissue ion relations. Agric. Water Manag. 97, 783–791.

Socrates, G., 2004. Infrared and Raman characteristic group frequencies: tables and

charts. John Wiley & Sons.

Song, Y., An, J., Chae, K., 2017. Effect of temperature variation on the performance of microbial fuel cells. Energy Technol. 5, 2163–2167.

Sophia, A.C., Bhalambaal, V.M., Lima, E.C., Thirunavoukkarasu, M., 2016. Microbial desalination cell technology: contribution to sustainable waste water treatment process, current status and future applications. J. Environ. Chem. Eng. 4, 3468–3478.

Sree, K.S., Adelmann, K., Garcia, C., Lam, E., Appenroth, K.-J., 2015. Natural variance in salt tolerance and induction of starch accumulation in duckweeds. Planta 241, 1395–1404.

Subramani, A., Cryer, E., Liu, L., Lehman, S., Ning, R.Y., Jacangelo, J.G., 2012. Impact of intermediate concentrate softening on feed water recovery of reverse osmosis process during treatment of mining contaminated groundwater. Sep. Purif. Technol. 88, 138–145.

Subramani, A., Jacangelo, J.G., 2014. Treatment technologies for reverse osmosis concentrate volume minimization: A review. Sep. Purif. Technol. 122, 472–489.

Sun, D.-Z., Yu, Y.-Y., Xie, R.-R., Zhang, C.-L., Yang, Y., Zhai, D.-D., Yang, G., Liu, L., Yong, Y.-C., 2017. In-situ growth of graphene/polyaniline for synergistic improvement of extracellular electron transfer in bioelectrochemical systems. Biosens. Bioelectron. 87, 195–202.

Supply, W.J.W., Programme, S.M., 2014. Progress on drinking water and sanitation: 2014 update. World Health Organization.

Szabolcs, I., 1964. The influence of irrigation water of high sodium carbonate content on soils. Agrokémia és Talajt. 13, 237–246.

Tabatabaei, M., Aghbashlo, M., Valijanian, E., Panahi, H.K.S., Nizami, A.-S., Ghanavati, H., Sulaiman, A., Mirmohamadsadeghi, S., Karimi, K., 2020. A comprehensive review on recent biological innovations to improve biogas production, part 1: upstream strategies. Renew. Energy 146, 1204–1220.

Tałałaj, I.A., 2022. Performance of integrated sequencing batch reactor (SBR) and reverse osmosis (RO) process for leachate treatment: effect of pH. J. Environ. Heal. Sci. Eng. 1–11.

Tamta, P., Rani, N., Yadav, A.K., 2020. Enhanced wastewater treatment and electricity generation using stacked constructed wetland–microbial fuel cells. Environ. Chem. Lett. 18, 871–879.

Taştan, B.E., Duygu, E., Dönmez, G., 2012. Boron bioremoval by a newly isolated Chlorella sp. and its stimulation by growth stimulators. water Res. 46, 167–175.

Tatar, Ş.Y., Öbek, E., 2014. Potential of Lemna gibba L. and Lemna minor L. for accumulation of Boron from secondary effluents. Ecol. Eng. 70, 332–336.

Tawalbeh, M., Al-Othman, A., Singh, K., Douba, I., Kabakebji, D., Alkasrawi, M., 2020. Microbial desalination cells for water purification and power generation: A critical review. Energy 209, 118493.

Tawalbeh, M., Rajangam, A.S., Salameh, T., Al-Othman, A., Alkasrawi, M., 2021. Characterization of paper mill sludge as a renewable feedstock for sustainable hydrogen and biofuels production. Int. J. Hydrogen Energy 46, 4761–4775.

Tipping, E., 2002. Cation Binding by Humic Substances; Cambridge University Press. Cambridge OpenURL.

Tkach, O., Sangeetha, T., Maria, S., Wang, A., 2017. Performance of low temperature Microbial Fuel Cells (MFCs) catalyzed by mixed bacterial consortia. J. Environ. Sci. 52, 284–292.

Tomaszewska, B., Bodzek, M., 2013. Desalination of geothermal waters using a hybrid UF-RO process. Part I: Boron removal in pilot-scale tests. Desalination 319, 99–106.

Tomaszewska, B., Pająk, L., Bundschuh, J., Bujakowski, W., 2018. Low-enthalpy geothermal energy as a source of energy and integrated freshwater production in inland areas: Technological and economic feasibility. Desalination 435, 35–44.

Türker, O.C., Yakar, A., Gür, N., 2017. Bioaccumulation and toxicity assessment of

irrigation water contaminated with boron (B) using duckweed (Lemna gibba L.) in a batch reactor system. J. Hazard. Mater. 324, 151–159.

TSI, Turkish Statistics Institute Reporte, https://cip.tuik.gov.tr/. Accessed May 6, 2022.

Utami, T.S., Arbianti, R., Manaf, B.N., 2015. Sea water desalination using Debaryomyces hansenii with microbial desalination cell technology. Int. J. Technol 6, 1094–1100.

Vaselbehagh, M., Karkhanechi, H., Mulyati, S., Takagi, R., Matsuyama, H., 2014. Improved antifouling of anion-exchange membrane by polydopamine coating in electrodialysis process. Desalination 332, 126–133.

Villalba, E., Tanjal, C., Borzi, G., Páez, G., Carol, E., 2020. Geogenic arsenic contamination of wet-meadows associated with a geothermal system in an arid region and its relevance for drinking water. Sci. Total Environ. 720, 137571.

Wang, B., Wang, Z., Jiang, Y., Tan, G., Xu, N., Xu, Y., 2017. Enhanced power generation and wastewater treatment in sustainable biochar electrodes based bioelectrochemical system. Bioresour. Technol. 241, 841–848.

Wang, H., Wang, G., Ling, Y., Qian, F., Song, Y., Lu, X., Chen, S., Tong, Y., Li, Y., 2013. High power density microbial fuel cell with flexible 3D graphene–nickel foam as anode. Nanoscale 5, 10283–10290.

Wang, H., Zhao, P., Liang, X., Gong, X., Song, T., Niu, R., Chang, J., 2010. Folate-PEG coated cationic modified chitosan–cholesterol liposomes for tumor-targeted drug delivery. Biomaterials 31, 4129–4138.

Wang, Y., Xu, A., Cui, T., Zhang, J., Yu, H., Han, W., Shen, J., Li, J., Sun, X., Wang, L., 2020. Construction and application of a 1-liter upflow-stacked microbial desalination cell. Chemosphere 248, 126028.

Wei, L., Han, H., Shen, J., 2013. Effects of temperature and ferrous sulfate concentrations on the performance of microbial fuel cell. Int. J. Hydrogen Energy 38, 11110–11116.

Wen, Q., Zhang, H., Chen, Z., Li, Y., Nan, J., Feng, Y., 2012. Using bacterial catalyst in

the cathode of microbial desalination cell to improve wastewater treatment and desalination. Bioresour. Technol. 125, 108–113.

Wen, Q., Zhang, H., Yang, H., Chen, Z., Nan, J., Feng, Y., 2014. Improving desalination by coupling membrane capacitive deionization with microbial desalination cell. Desalination 354, 23–29.

Wildes, R.A., Neales, T.F., 1971. The absorption of boron by disks of plant storage tissues. Aust. J. Biol. Sci. 24, 873–884.

Wintgens, T., Bixio, D., Thoeye, C., Jeffrey, P., Hochstrat, R., Meli, T., 2002. Reclamation and reuse of municipal wastewater in Europe–current status and future perspectives analysed by the AQUAREC research project. AQUAREC.

Wuana, R.A., Okieimen, F.E., 2011. Heavy metals in contaminated soils: a review of sources, chemistry, risks and best available strategies for remediation. Int. Sch. Res. Not. 2011.

WRI, World Resource Institute, https://www.wri.org/, Accessed May 6, 2022.

WHO (World Health Organization), UNICEF (United Nations Childeren's Found) Progress on Drinking Water, Sanitation and Hygiene: 2017 Update and SGD Baselines, 2017.

WWAP-UNESCO (UNESCO World Water Assessment Programme)The United Nations World Water Development Report 2019: Leaving No One behind UNESCO, Paris, 2019.

Xanke, J., Liesch, T., 2022. Quantification and possible causes of declining groundwater resources in the Euro-Mediterranean region from 2003 to 2020. Hydrogeol. J. 1–22.

Yang, E., Choi, M.-J., Kim, K.-Y., Chae, K.-J., Kim, I.S., 2015. Effect of initial salt concentrations on cell performance and distribution of internal resistance in microbial desalination cells. Environ. Technol. 36, 852–860.

Yang, L., Song, X., Zhang, Y., Yuan, R., Ma, Y., Han, D., Bu, H., 2012. A hydrochemical framework and water quality assessment of river water in the

upper reaches of the Huai River Basin, China. Environ. Earth Sci. 67, 2141–2153.

Yaseen, D.A., Scholz, M., 2016. Shallow pond systems planted with Lemna minor treating azo dyes. Ecol. Eng. 94, 295–305.

Yavuz, E., Arar, Ö., Yüksel, M., Yüksel, Ü., Kabay, N., 2013. Removal of boron from geothermal water by RO system-II-effect of pH. Desalination 310, 135–139.

Yermiyahu, U., Ben-Gal, A., Keren, R., Reid, R.J., 2008. Combined effect of salinity and excess boron on plant growth and yield. Plant Soil 304, 73–87.

Yilmaz, A.E., Boncukcuoğlu, R., Kocakerim, M.M., 2007. A quantitative comparison between electrocoagulation and chemical coagulation for boron removal from boron-containing solution. J. Hazard. Mater. 149, 475–481.

Yilmaz, A.E., Boncukcuoğlu, R., Kocakerim, M.M., Yilmaz, M.T., Paluluoğlu, C., 2008. Boron removal from geothermal waters by electrocoagulation. J. Hazard. Mater. 153, 146–151.

You, P.Y., Kamarudin, S.K., 2017. Recent progress of carbonaceous materials in fuel cell applications: An overview. Chem. Eng. J. 309, 489–502.

Yuan, H.-R., Deng, L.-F., Qian, X., Wang, L.-F., Li, D.-N., Chen, Y., Yuan, Y., 2019. Significant enhancement of electron transfer from Shewanella oneidensis using a porous N-doped carbon cloth in a bioelectrochemical system. Sci. Total Environ. 665, 882–889.

Yuan, H., Abu-Reesh, I.M., He, Z., 2015. Enhancing desalination and wastewater treatment by coupling microbial desalination cells with forward osmosis. Chem. Eng. J. 270, 437–443.

Yuan, H., Dong, G., Li, D., Deng, L., Cheng, P., Chen, Y., 2018. Steamed cake-derived 3D carbon foam with surface anchored carbon nanoparticles as freestanding anodes for high-performance microbial fuel cells. Sci. Total Environ. 636, 1081–1088.

Zábranská, J., Štěpová, J., Wachtl, R., Jeníček, P., Dohányos, M., 2000. The activity of anaerobic biomass in thermophilic and mesophilic digesters at different loading

rates. Water Sci. Technol. 42, 49–56.

Zahid, M., Savla, N., Pandit, S., Thakur, V.K., Jung, S.P., Gupta, P.K., Prasad, R., Marsili, E., 2022. Microbial desalination cell: Desalination through conserving energy. Desalination 521, 115381.

Zayed, A., Gowthaman, S., Terry, N., 1998. Phytoaccumulation of trace elements by wetland plants: I. Duckweed. Wiley Online Library.

Zhang, B., He, Z., 2013. Improving water desalination by hydraulically coupling an osmotic microbial fuel cell with a microbial desalination cell. J. Memb. Sci. 441, 18–24.

Zhang, F., Chen, M., Zhang, Y., Zeng, R.J., 2012. Microbial desalination cells with ion exchange resin packed to enhance desalination at low salt concentration. J. Memb. Sci. 417, 28–33.

Zhang, L., Liu, Q., Hu, P., Huang, R., 2016. Adsorptive removal of methyl orange using enhanced cross-linked chitosan/bentonite composite. Desalin. Water Treat. 57, 17011–17022.

Zhang, X., Li, X., Zhao, X., Li, Y., 2019. Factors affecting the efficiency of a bioelectrochemical system: a review. RSC Adv. 9, 19748–19761.

Zhang, Y., Angelidaki, I., 2013. A new method for in situ nitrate removal from groundwater using submerged microbial desalination–denitrification cell (SMDDC). Water Res. 47, 1827–1836.

Zhao, K., Tong, B., Yu, X., Guo, Y., Xie, Y., Deng, T., 2022. Synthesis of porous fiber-supported lithium ion-sieve adsorbent for lithium recovery from geothermal water. Chem. Eng. J. 430, 131423.

Zhu, K., Wang, S., Liu, H., Liu, S., Zhang, J., Yuan, J., Fu, W., Dang, W., Xu, Y., Yang, X., 2022. Heteroatom-doped porous carbon nanoparticle-decorated carbon cloth (HPCN/CC) as efficient anode electrode for microbial fuel cells (MFCs). J. Clean. Prod. 130374.

Zhu, X., Yates, M.D., Hatzell, M.C., Ananda Rao, H., Saikaly, P.E., Logan, B.E., 2014.

Microbial community composition is unaffected by anode potential. Environ. Sci. Technol. 48, 1352–1358.

Zuo, K., Chen, M., Liu, F., Xiao, K., Zuo, J., Cao, X., Zhang, X., Liang, P., Huang, X., 2018. Coupling microfiltration membrane with biocathode microbial desalination cell enhances advanced purification and long-term stability for treatment of domestic wastewater. J. Memb. Sci. 547, 34–42.

Zuo, K., Luo, S., Huang, X., 2022. Membrane-based electrochemical technologies: II. Microbial desalination cell. Electrochem. Membr. Technol. Water Wastewater Treat. 361–401.

APPENDIX A

PERMISSIONS TO REPRODUCE FIGURES AND TEXTS

All permissions have been taken to reproduce the full text presented in Chapters 2, 3, and 5 through the Copyright Clearance Center. All documentation of the approvals is listed on the following pages.

Chapter 2

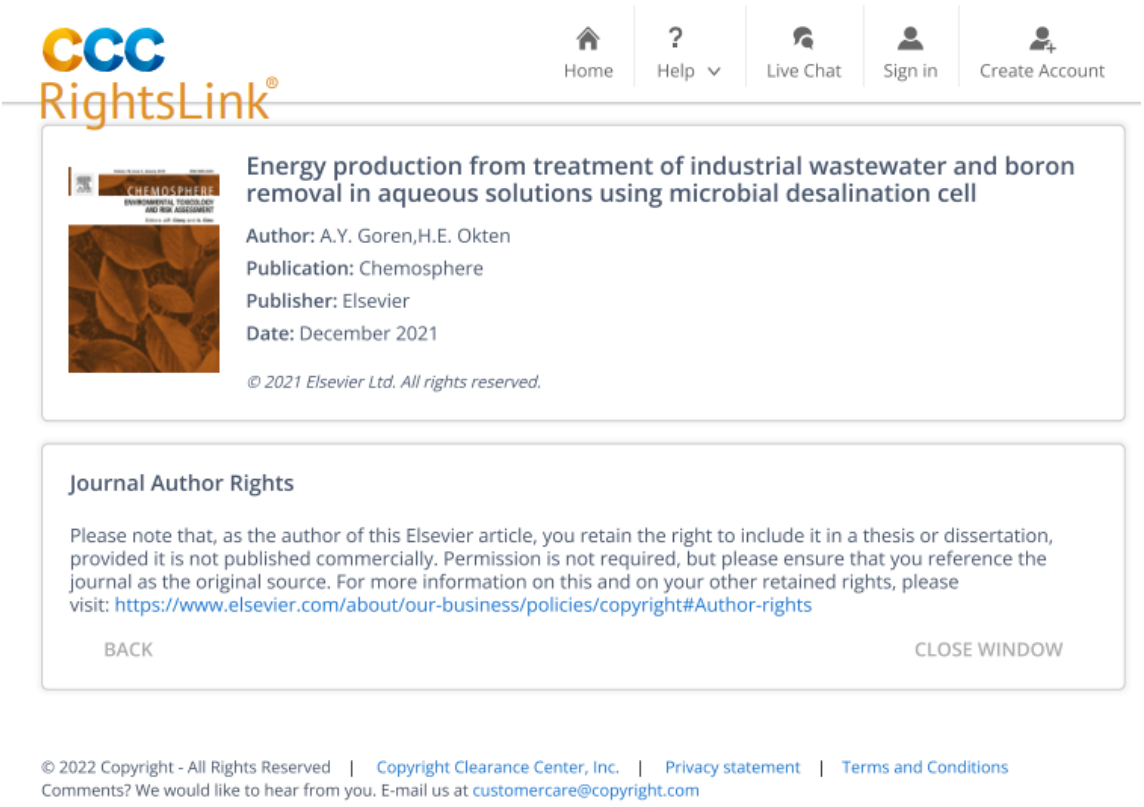

Chapter 3

Chapter 5

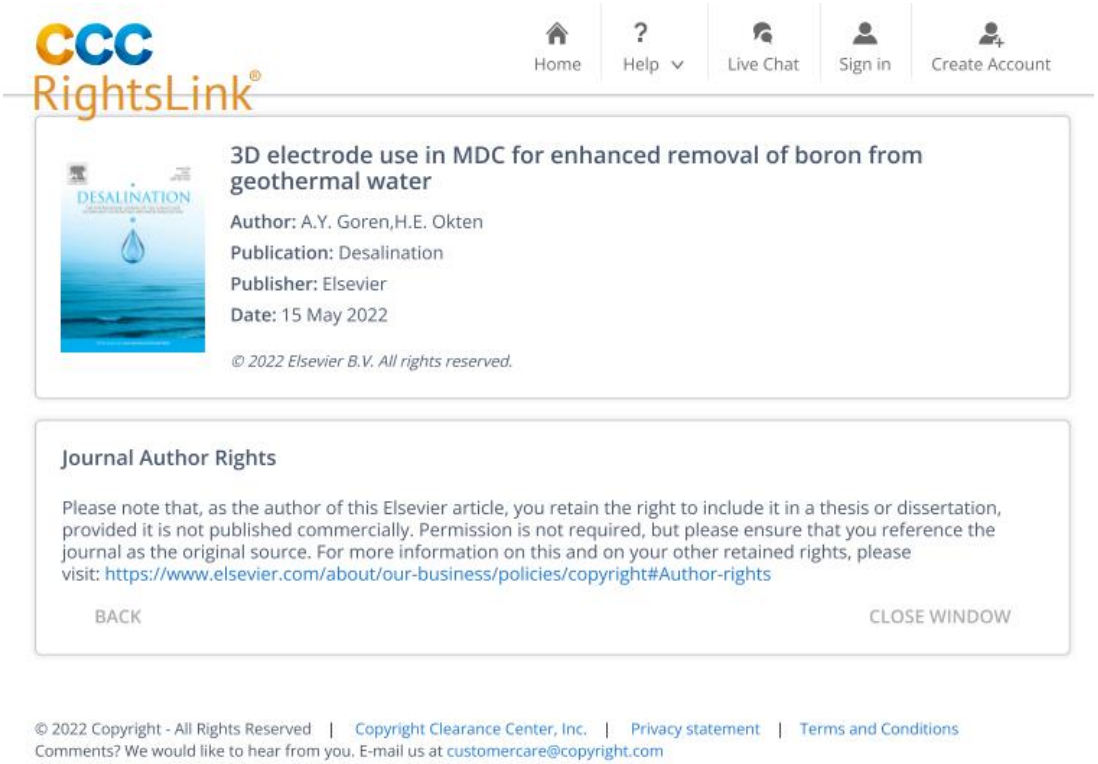
CCC
RightsLink
Home
Help
Live Chat
Sign in
Create Account
3D electrode use in MDC for enhanced removal of boron from geothermal water
Author: A.Y. Goren,H.E. Okten
Publication: Desalination
Publisher: Elsevier
Date: 15 May 2022
© 2022 Elsevier B.V. All rights reserved.
Journal Author Rights
Please note that, as the author of this Elsevier article, you retain the right to include it in a thesis or dissertation, provided it is not published commercially. Permission is not required, but please ensure that you reference the journal as the original source. For more information on this and on your other retained rights, please visit: https://www.elsevier.com/about/our-business/policies/copyright#Author-rights
BACK
CLOSE WINDOW
© 2022 Copyright - All Rights Reserved | Copyright Clearance Center, Inc. | Privacy statement | Terms and Conditions
Comments? We would like to hear from you. E-mail us at customercare@copyright.com

APPENDIX B

SUPPLEMENTARY INFORMATION FOR CHAPTER 2

Table B.1. Physicochemical properties of geothermal water from Balçova Geothermal Power Plant and industrial wastewater.

Parameters (mg/L)	**Water type**	
	Industrial wastewater	**Geothermal water**
K^+	868	30.1
NH_4^+	452	1.85
Na^+	1608	452
Ca^{2+}	299	24.8
Mg^{2+}	77.5	7.44
Mn^{2+}	0.183	0.027
NO_3^-	25.6	0.25
NO_2^-	-	-
SO_4^{2-}	1117	178
PO_4^{3-}	7.68	-
Cl^-	1573	205
F^-	0.20	8.21
Si	66.0	24
Br	-	0.38
Al	0.075	0.017
As	0.007	0.173
B	0.142	10.48
Cu	0.003	0.002
Cr	0.325	0.331
Fe	0.571	0.055
Li	-	1.41
Ni	0.014	-

Table B.2. EDX results in the membranes before and after the experiments.

Material (Wt, %)	C	O	S	Na	F	Cl	B
AEM-Fresh	59.84	-	1.03	0.67	38.47	-	-
AEM (anode solution side)	49.38	3.87	0.28	-	10.54	0.31	30.25
AEM (desalination solution side)	51.89	3.01	0.37	-	16.32	0.46	28.21
CEM-Fresh	50.38	-	-	-	46.29	-	-
CEM (cathode solution side)	49.59	5.49	2.78	1.51	39.59	0.02	-
CEM (desalination solution side)	49.20	4.47	3.83	1.43	38.97	0.06	-

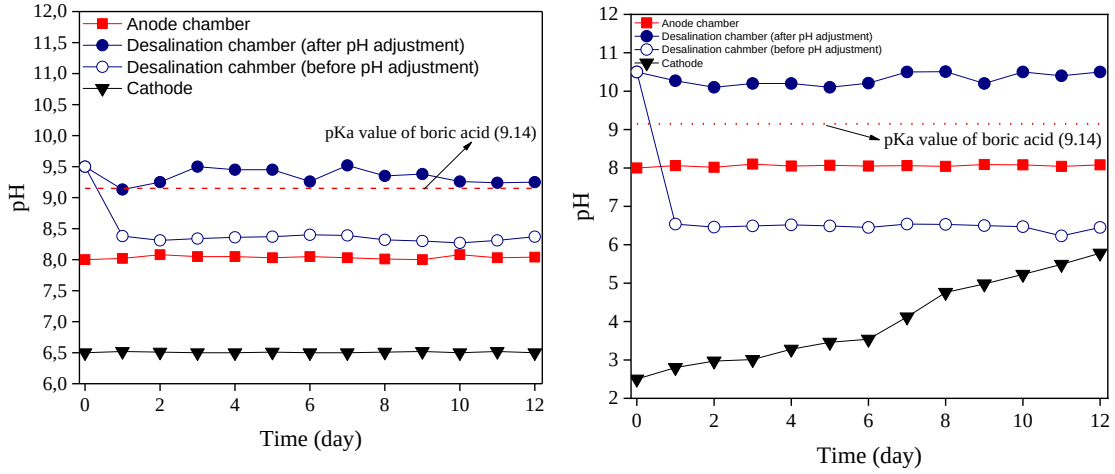

Figure B.1. Solution pH trend using PBS buffer a) and acidified water b) in the cathode, desalination, and anode chambers of MDC during 12 d test.

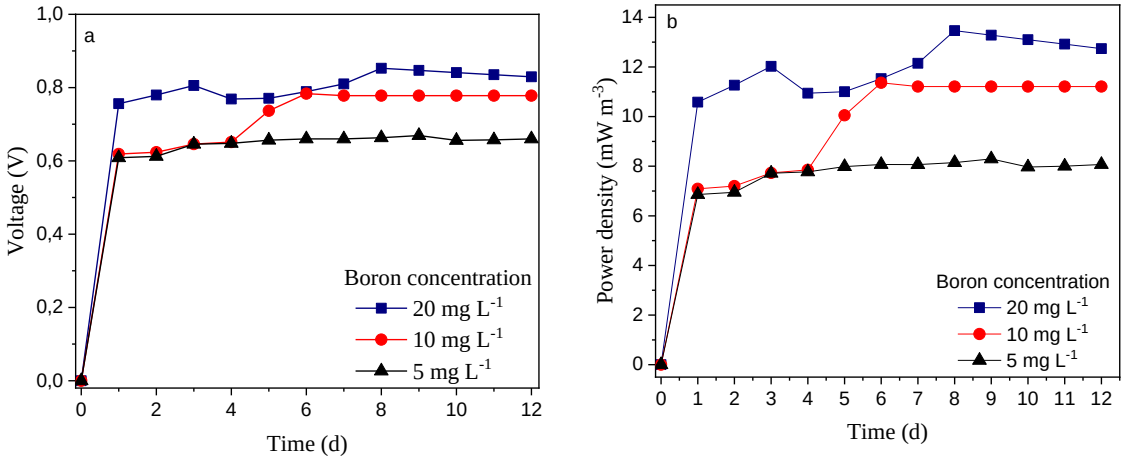

Figure B.2. Cell voltage a) and power density b) of MDC at different initial boron concentrations.

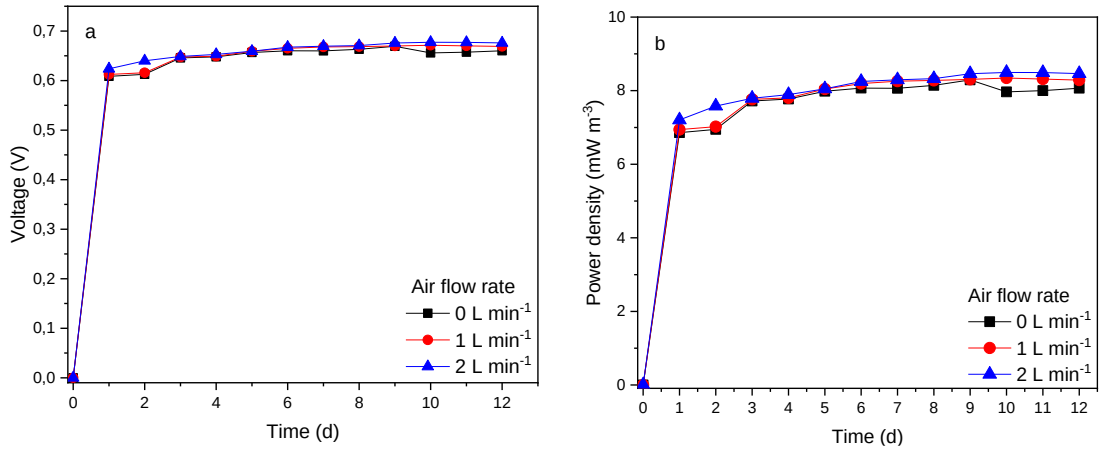

a) b)

Figure B.3. Cell voltage a) and power density b) of MDC at different air flow rates.

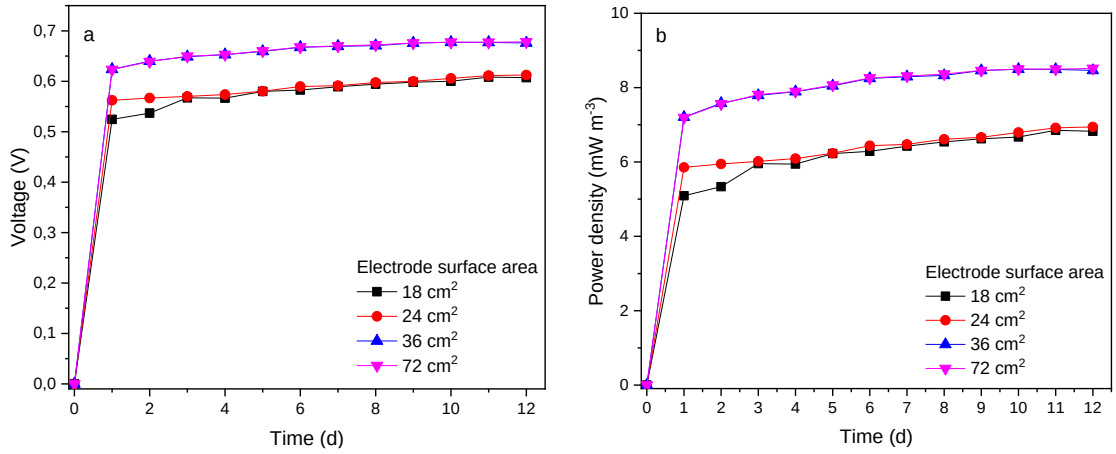

a) b)

Figure B.4. Cell voltage a) and power density b) of MDC at different electrode surface areas.

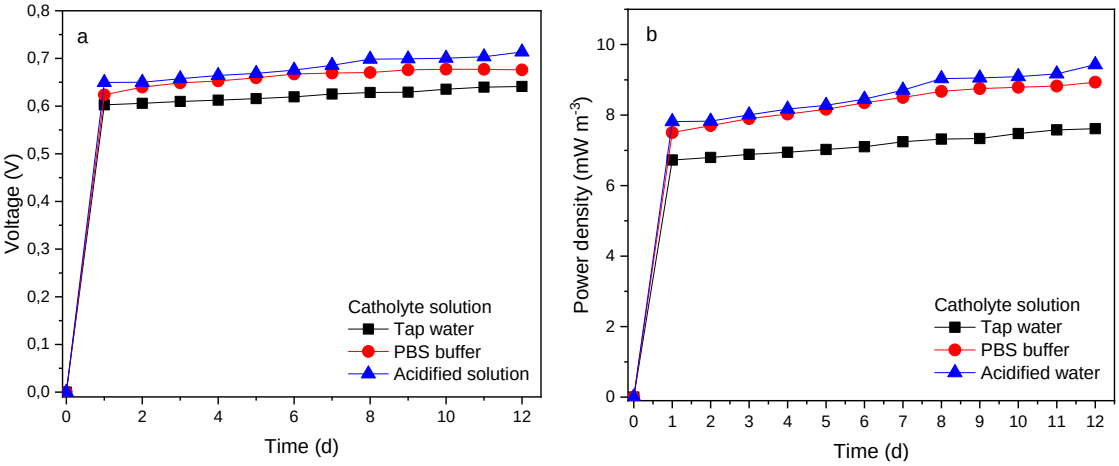

a) b)

Figure B.5. Cell voltage a) and power density b) of MDC at different catholyte solutions.

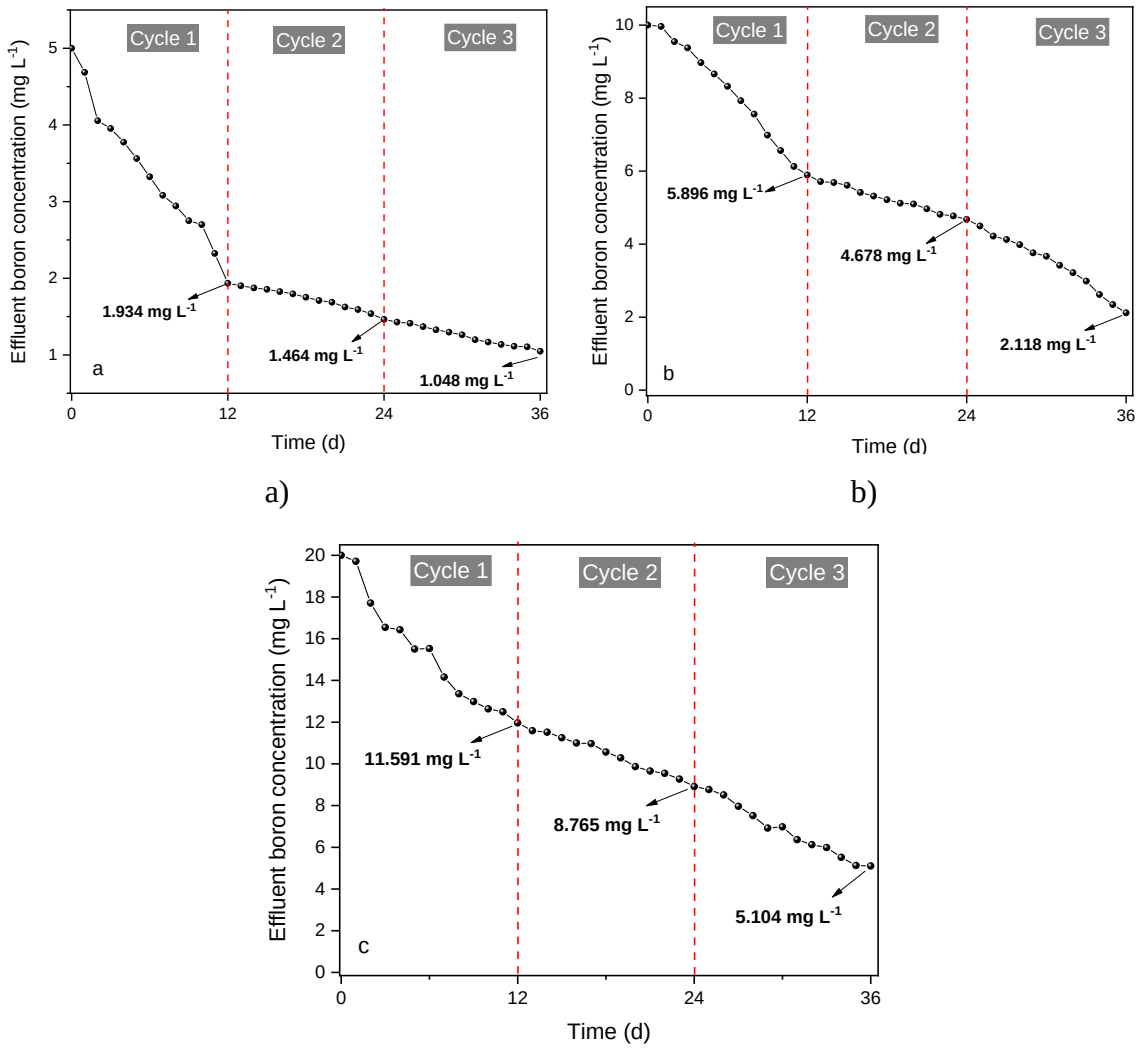

a) b)

c)

Figure B.6. Effluent boron concentration at initial boron concentration of 5 mg/L a), 10 mg/L b), and 20 mg/L c) in fed-batch mode.

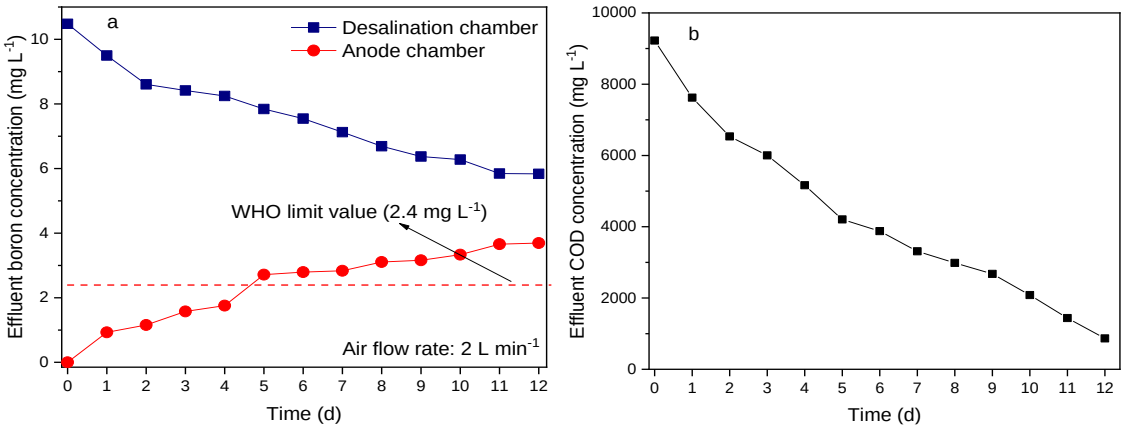

a) b)

Figure B.7. Effluent boron a) and COD b) concentration of treated geothermal brine.

APPENDIX C

SUPPLEMENTARY INFORMATION FOR CHAPTER 3

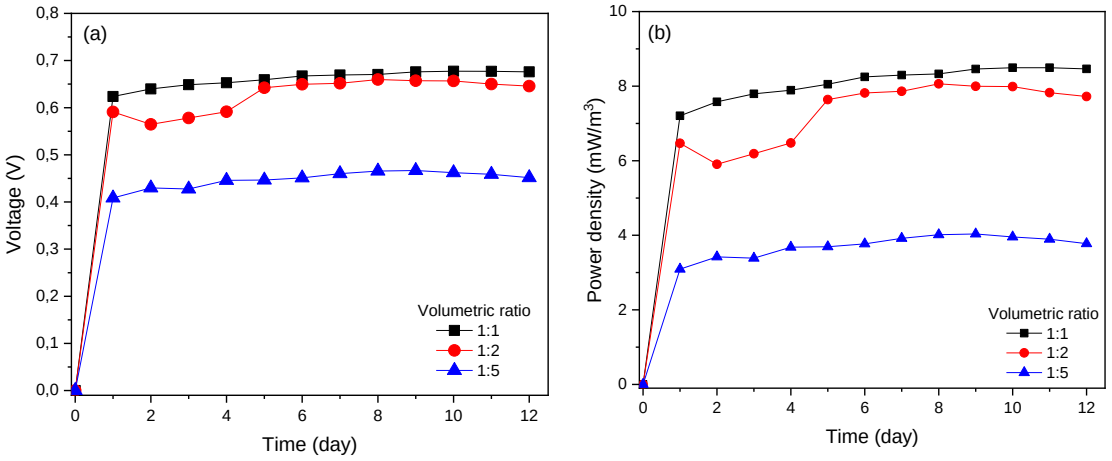

a) b)

Figure C.1. Cell voltage a) and power density b) of MDC at different volumetric ratios.

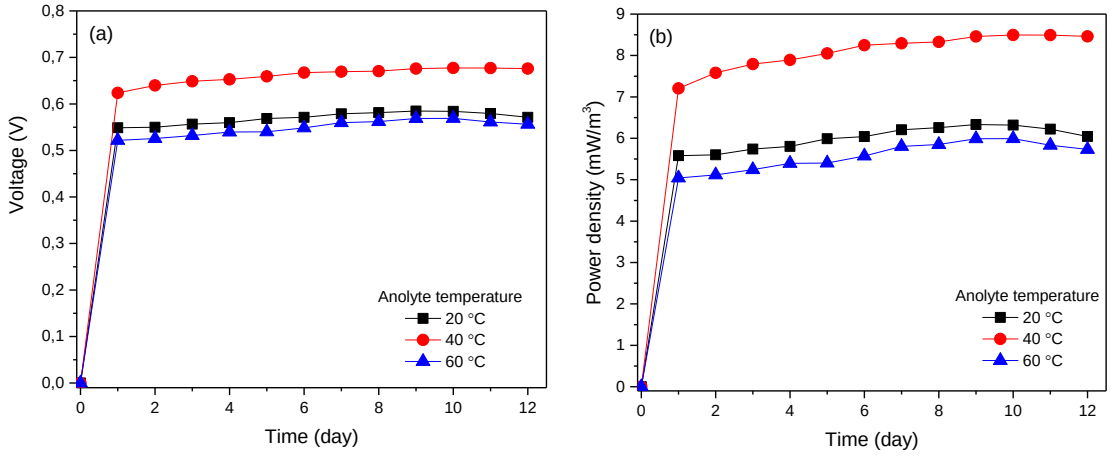

a) b)

Figure C.2. Cell voltage a) and power density b) of MDC at different anolyte temperatures.

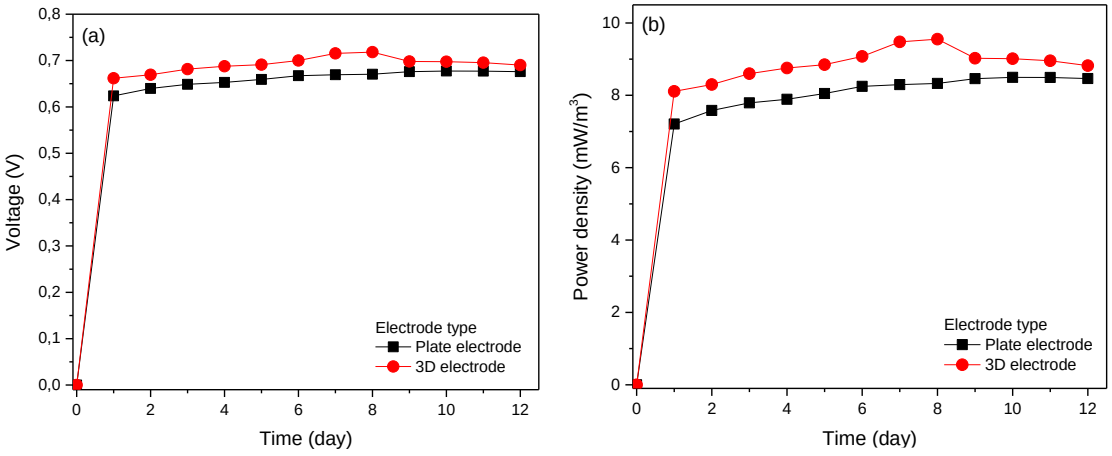

a) b)

Figure C.3. Cell voltage a) and power density b) of MDC at different electrode types.

APPENDIX D

SUPPLEMENTARY INFORMATION FOR CHAPTER 4

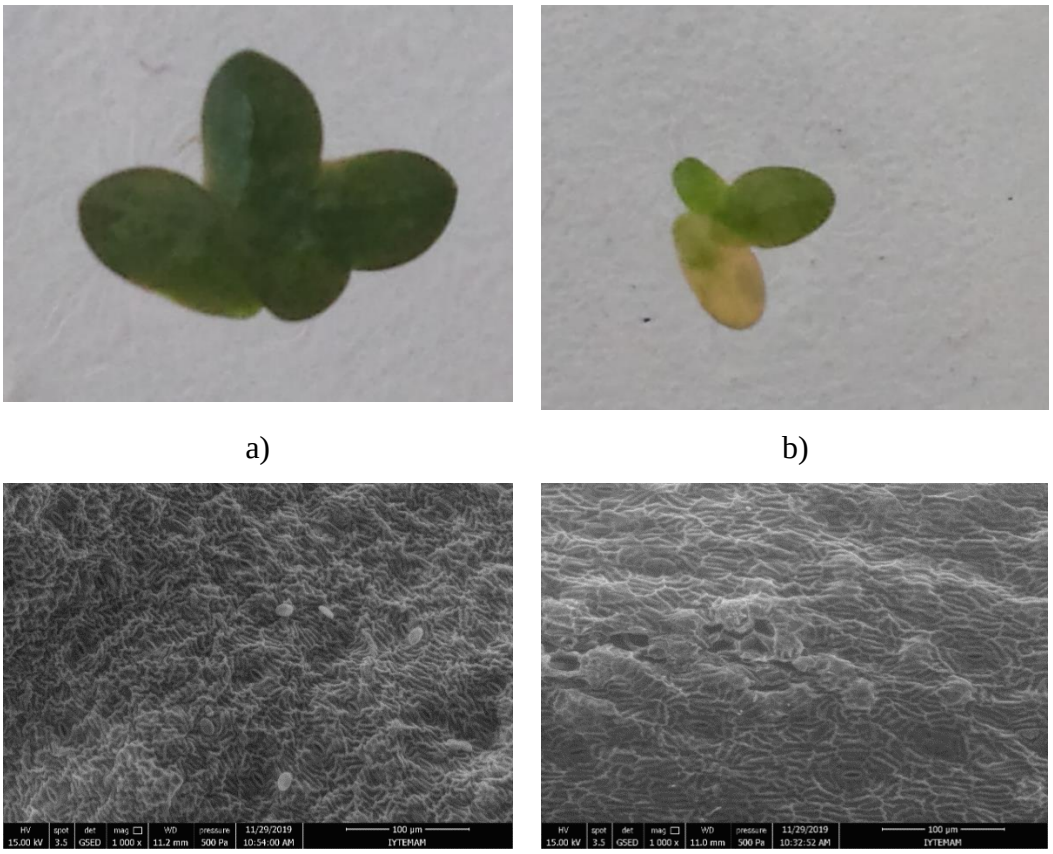

Figure D.1. The toxic effect of boron on Lemna minor: (a) raw L. minor, (b) 30 mg/L of B-exposed L. minor, (c) ESEM images of raw L. minor, (d) ESEM images of 30 mg/L of B-exposed L. minor.

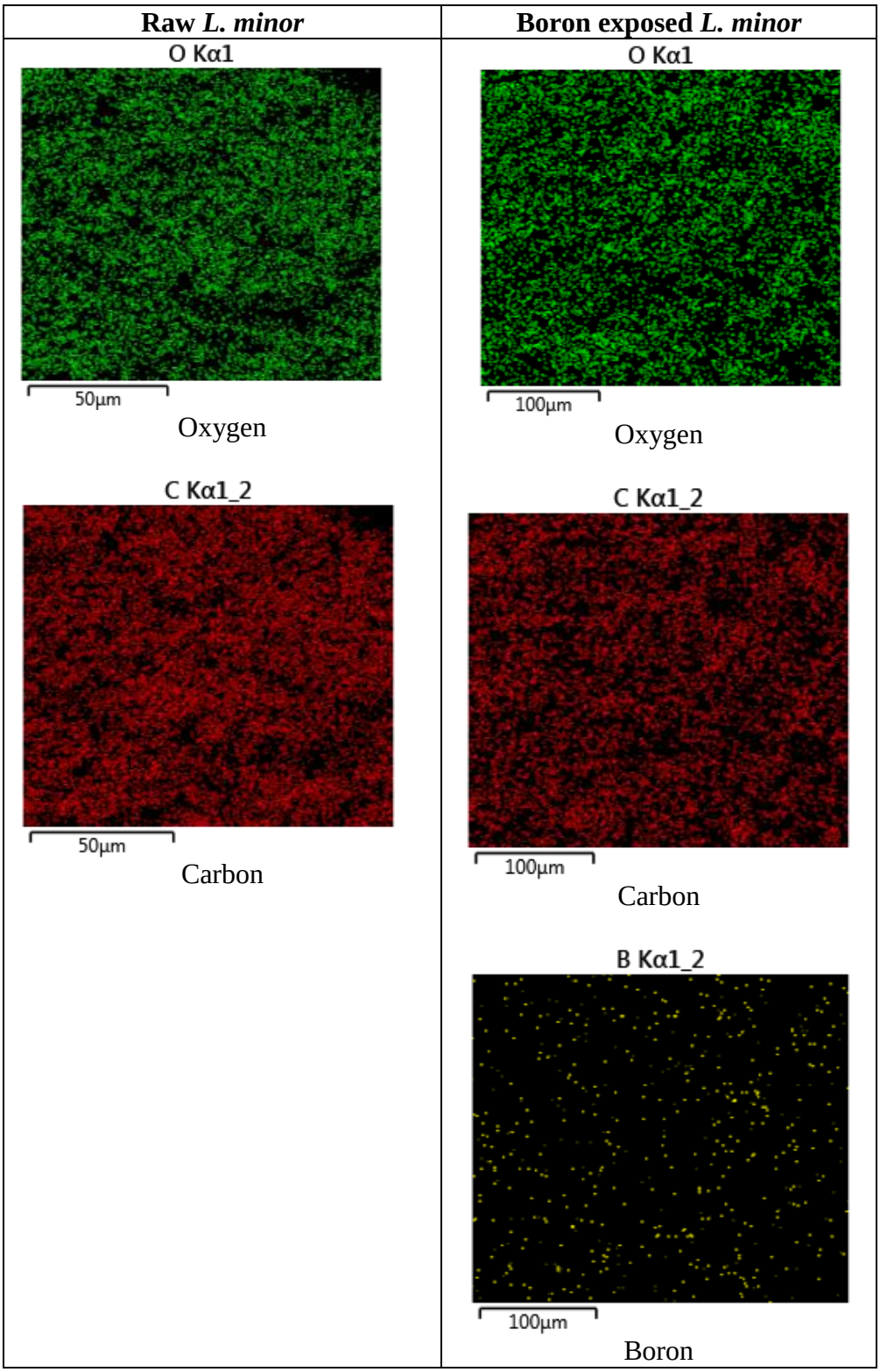

Figure D.2. Elemental mapping results of raw and B-exposed L. minor samples (20 mg/L initial boron concentration, pH 8, 1.5 cm water depth, 0 mg/L HA).

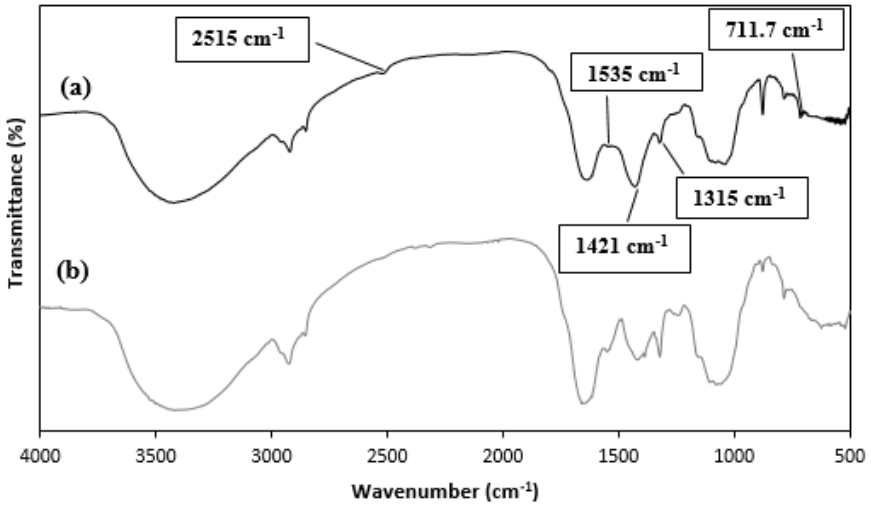

Figure D.3. FTIR results of (a) B-exposed L. minor and (b) raw L. minor.

Table D.1. Elemental composition of raw and B-exposed L. minor samples.

Element	Raw *L. minor*	B-exposed *L. minor*
C (wt.%)	53.89	48.62
O (wt.%)	42.51	41.62
B (wt.%)	N.D	1.97
Na (wt.%)	0.33	0.73
Mg (wt.%)	0.42	0.72
K (wt.%)	0.70	2.30
Ca (wt.%)	2.15	4.04

ND: Not detected

APPENDIX E

SUPPLEMENTARY INFORMATION FOR CHAPTER 5

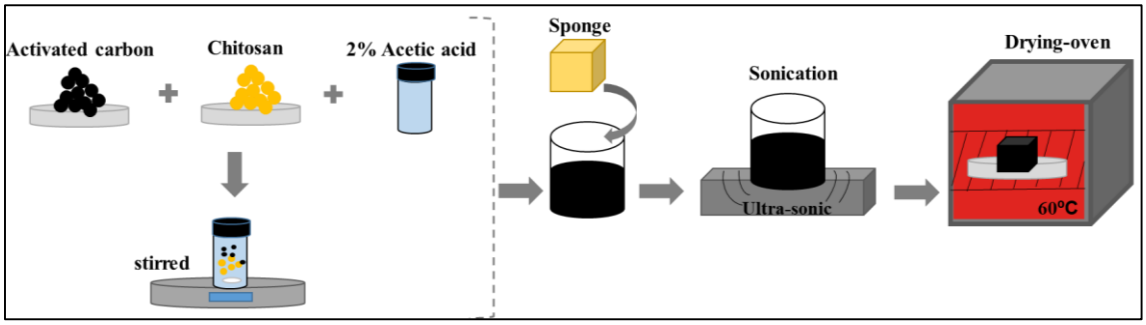

Figure E.1. Preparation of 3D AC-CS composite coated sponge electrode.

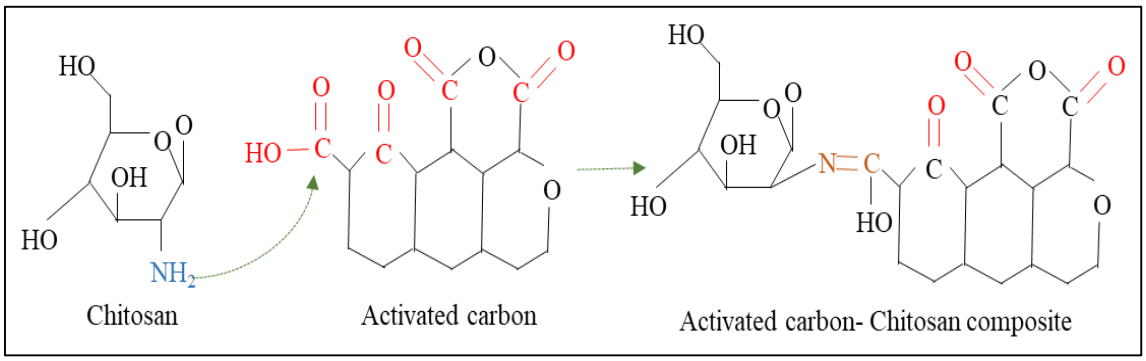

Figure E.2. Reactions between AC and CS functional groups to form AC-CS composite.

VITA

Education

Ph.D.	Environmental Engineering, *İzmir Institute of Technology*, İzmir, Turkey *Thesis*: "Investigation of bioelectrochemical Treatment Efficiency for Removal of Boron from Geothermal Waters" *Advisor*: Assoc. Prof. Dr. Hatice Eser ÖKTEN - *Co-Advisor*: Prof. Dr. Alper BABA(Vice Rector)	2022
M.Sc.	Environmental Engineering, *Gebze Technical University*, Gebze, Turkey *Thesis*: "Modelling and Optimizing of As (III) and As (V) Removal from groundwater by Electrocoagulation Reactor using Aluminum Ball" *Advisor*: Prof. Dr. Mehmet KOBYA	2015
B.S.	Environmental Engineering, *Çanakkale Onsekiz Mart University*, Çanakkale, Turkey *Senior thesis*: "The Sustainable Urban Development and Case Study in Çanakkale" *Advisor*: Prof. Dr. Arzu BAŞARAN UYSAL	2012

Academic Experience

Research Assistant	Environmental Engineering, *İzmir Institute of Technology*, İzmir, Turkey	2015-2022 (7 years)
Project Assistant	Environmental Engineering, *İzmir Institute of Technology*, İzmir, Turkey *Research Subject*: "Treatment of Domestic Wastewater and Energy Production with Photosynthetic Microbial Fuel Cell (PMFC)" *Advisor*: Assist. Prof. Dr. Hatice Eser ÖKTEN	2020-2021 (1 years)
Project Assistant	Environmental Engineering, *İzmir Institute of Technology*, İzmir, Turkey *Research Subject*: "Investigation of Boron Removal Efficiency in Microbial Desalination Cell-Donnan Dialysis System" *Advisor*: Assist. Prof. Dr. Hatice Eser ÖKTEN	2018-2019 (1 years)
Project Assistant	Environmental Engineering, *Gebze Technical University*, Gebze, Turkey *Research Subject*: "Water Recovery and Concentrate Management with Integrated Advanced Oxidation Membrane Filtration System in Industries" *Advisor*: Prof. Dr. Coşkun AYDINER	2014-2015 (1 year)
Project Assistant	Environmental Engineering, *Gebze Technical University*, Gebze, Turkey *Research Subject*: "Arsenic removal from water resources using electrocoagulation process - Process optimization and enhancement" *Advisor*: Prof. Dr. Mehmet KOBYA	2012-2014 (1 years)

Honors and Awards

- PhD research award, Simultaneous Energy Production from Yeast Wastewater and Boron Removal from Geothermal Brine using Novel Microbial Desalination Cell. PhD Med School Online courses held by The university of Naples Federico II, Napoli, 11-16 October 2021.

Publications

- Recepoglu, Y.K., **Goren, A.Y**., Vatanpour, V., Khataee, A., Yoon, Y., "Boron carbon nitride nanosheets in water and wastewater treatment: A critical review", *Desalination*, 2022, 533, 115782.

- **Goren, A.Y**., Okten, H.E., "3D electrode uses in MDC for enhanced removal of boron from geothermal water", *Desalination*, 2022, 530, 115668.

- **Goren, A.Y**., Recepoglu, Y.K., Karagunduz, A., Khataee, A., Yeojoon, Y., "A review of boron removal from aqueous solution using carbon-based materials: An assessment of health risks", *Chemosphere*, 2022, 293, 133587.

- **Goren A.Y**., Kobya M., Khataee, A., "How does arsenic speciation (arsenite and arsenate) in groundwater affect the performance of an aerated electrocoagulation reactor and human health risk?", *Science of the Total Environment*, 2022, 808, 152135.

- Recepoglu, Y.K., **Goren, A.Y**., Orooji, Y., Khataee, A., "Carbonaceous materials for removal and recovery of phosphate species: Limitations, successes and future improvement", *Chemosphere*, 2022, 287, 132177.

- **Goren A.Y**., Yücel, A., Sofuoglu, S.C., Sofuoglu, A., "Phytoremediation of olive mill wastewater with Vetiveria zizanioides (L.) and Cyperus alternifolius L.", *Environmental technology and Innovation*, 2021, 24, 102071.

- **Goren A.Y**., Genisoglu, M., Okten H.E., Sofuoglu, S.C., "Effect of COVID-19 pandemic on ambient air quality and excess risk of particulate matter in Turkey", *Environmental Challenges*, 2021, 5, 100239.

- **Goren A.Y**., Okten H.E., "Simultaneous energy production, boron and COD removal using a novel microbial desalination cell", *Desalination*, 2022, 518, 115267.

- **Goren A.Y**., Okten H.E., "Energy production from treatment of industrial wastewater and boron removal in aqueous solutions using microbial desalination cell", *Chemosphere*, 2021, 285, 131370.

- Can-Terzi, B., **Goren, A.Y**., Okten, H.E., Sofuoglu, S.C., "Biosorption of methylene blue from water by live Lemna minor", *Environmental Technology & Innovation*, 2021, 22, 101432.

- **Goren A.Y**., Topçu, G., Demir, M.M., Baba, A., "Effect of high salinity and temperature on water-acidic volcanic rock interaction", *Environmental Earth Sciences*, 2021, 80, 24.

- **Goren A.Y**., Kobya, M., "Arsenic removal from groundwater using an aerated electrocoagulation reactor with 3D Al electrodes in the presence of anions", *Chemosphere*, 2021, 263, 128253.

- Okten H.E., **Goren A.Y**., "Phytoremediation of Boron Containing Synthetic Aqueous Solutions and Real Geothermal Water using Lemna minor", *Süleyman Demirel University Journal of Natural and Applied Sciences*, 2021, 25, 217-228.

- **Goren A.Y**., Kobya, M., Oncel., M.S., "Arsenite removal from groundwater by aerated electrocoagulation reactor with Al ball electrodes: Human health risk assessment", *Chemosphere*, 2020, 251, 126363.

- **Goren A.Y**., Kobya, M., Şık, E., Demirbas, E., Oncel, M.S., "Combined influence of some cations on arsenic removal by an air-injection EC reactor using aluminum ball electrodes", *Desalination and Wastewater Treatment*, 2020, 178, 240-253.

- **Goren, A.Y**., Oncel, M.S., Kobya., M., "Arsenate removal from groundwater by air-injected EC with al ball anodes: effects of operational parameters", *Pamukkale University Journal of Engineering Sciences*, 2020, 26, 462-467.

- **Goren A.Y**., Genisoglu, M., Okten, H.E., "Use of nano zero-valent iron coated coffee grounds for removal of Zn (II) and Ni (II) from aqueous solutions", *Desalination and Wastewater Treatment*, 2019, 172, 177-183.

- Aydiner C., Kiril Mert B., Can Dogan E., Yatmaz H.C., Dagli S., Aksu S., Tilki Y.M., **Goren A.Y**., Balci E., "Novel hybrid treatments of textile wastewater by membrane oxidation reactor: Performance investigations, optimizations and efficiency comparisons", *Science of the Total Environment*, 2019, 683, 411–426.

- Demirbas E., Kobya M., Oncel M.S., Şık E., **Goren A.Y**., "Arsenite removal from groundwater in a batch electrocoagulation process: Optimization through response surface methodology", *Separation Science and Technology*, 2019, 53, 775-785.

- Genişoğlu M., **Goren A.Y**., Balcı E., Recepoğlu Y.K., Okten H.E., "Methylene Blue Removal of Fixed-Bed Column Reactor with Pumice and nZVI-Pumice: Experimental and Modeling Study", *Süleyman Demirel University Journal of Natural and Applied Sciences*, 2019, 23, 574-581.

- **Goren A.Y**., Oncel M.S., Demirbas E., Şık E., Kobya M., "Removal of arsenate by EC reactor using Al ball anode electrodes", *Water Practice and Technology*, 2018, 13, 753-763.

- Kobya M., Sık E., Demirbas E., **Goren A.Y**., Oncel M.S., "Optimization of some cations for removal of arsenic from groundwater by electrocoagulation process", *Environmental Engineering & Management Journal*, 2018, 17, 1079-1093.

- Kırıl Mert B., Can Dogan E., Balcı E., Tilki Y.M., Aksu Ş., **Goren A.Y**., Aydıner C., "Water recovery with combined membrane system in textile industry, treatment and management of concentrates by hybrid advanced oxidation/membrane filtration", *Pamukkale University Journal of Engineering Sciences*, 2018, 24, 468-475.

- Şık E., Demirbaş E., **Goren A.Y**., Öncel M.S., Kobya M., "Arsenite and arsenate removals from groundwater by electrocoagulation using iron ball anodes: Influence of operating parameters", *Journal of Water Process Engineering*, 2017, 18, 83-91.

- Aydıner C., Kırıl Mert B., Can Dogan E., Balcı E. Tilki Y.M., Aksu Ş., **Goren A.Y**., "Investigation of influence of membrane type on water recovery by pressurized membrane processes from textile washing", *Uludağ University Journal of the Faculty of Engineering*, 2016, 21, 319-330.

- Sık E., Kobya M., Demirbas E., Oncel M.S., **Goren A.Y**., "Removal of As (V) from groundwater by a new electrocoagulation reactor using Fe ball anodes: optimization of operating parameters", *Desalination and Water Treatment*, 2014, 56, 1177–1190.

- Kobya M., Sık E., Oncel M.S., Demirbas E., **Goren A.Y**., Yildirim Y., "Removal of low concentration of As (V) from groundwater using an air injected electrocoagulation reactor with iron ball anodes: RSM modeling and optimization", *Journal of Selçuk University Natural and Applied Science*, 2014, 37-47, ISSN: 2147-3781.

- Kobya M., Demirbas E., Oncel M.S., Yıldırım Y., Şık E., **Goren A.Y**., Akyol A., "Modeling and optimization of arsenite removal from groundwater using Al ball anodes by electrocoagulation process", *Journal of Selçuk University Natural and Applied Science*, 2014, 803-811, ISSN: 2147-3781.

Selected Conferences

- **Goren, A.Y**., Okten, H.E., Baba, A., Kabay, N., "Boron Removal from Geothermal Water using a Hybrid Microbial Desalination Cell-Reverse Osmosis Process with Energy Production", *The 7th International conference Ecological & Environmental Chemistry*, 3-4 March 2022, Moldova. (Oral Presentation)

- **Goren, A.Y**., Okten, H.E., "Energy Production from Wastewater and Boron Removal in Geothermal Water using Novel Microbial Desalination Cell with 3D Sponge Electrode", The 1st

International Conference on Geography and Environmental Sciences (GES22)", 21-31 May 2022, İstanbul. (Oral Presentation)

- **Goren, A.Y**., Recepoglu, Y.K., Edebali, Ö., Sahin, C., Genisoglu, M., Okten, H.E., "Techno-Economic Assessment of Electrochemical Process for Sustainable Removal of Methylene Blue", *The 7th International conference Ecological & Environmental Chemistry*, 3-4 March 2022, Moldova. (Oral Presentation)

- **Goren, A.Y**., Uzelli, T., Okten, H.E., Baba, A., "Geothermal energy: Current status in boron recovery", *World Energy Strategies Congress and Exhibition*, 26-28 August 2019, İstanbul, Turkey. (Oral Presentation)

- **Goren, A.Y**., Okten, H.E., "Boron Removal and Energy Production Using Microbial Desalination Cell", *International Symposium on Boron*, 17-19 April 2019, Nevşehir, Turkey. (Oral Presentation)

- Kazancı, Y., **Goren, A.Y**., Terzi, B., Baba, A., "Effect of gas stations on groundwater resources: Case study, Izmir", *72nd Geological Congress of Turkey*, 28 January - 1 February 2019, Ankara, Turkey. (Oral Presentation)

- **Goren, A.Y**., Genisoglu, M., Sofuoglu, A., Okten, H.E., "Use of Nano Zero-Valent Iron Coated Coffee Grounds Composite for Removal of Zinc and Nickel from Model Electroplating Waste Water", *4th International Conference on Recycling and Reuse*, 24-26 October 2018, İstanbul, Turkey. (Oral Presentation)

- Balcı, E., Genisoglu, M., **Goren, A.Y**., Okten, H.E., "nZVI Enhanced Decolorization of Commercial Textile Dye", *4th International Symposium on Composite Materials*, 6-8 September 2018, İzmir, Turkey. (Oral Presentation)

- **Goren A.Y**., Genisoglu M., Balcı E., Okten H.E., Baba A., "Groundwater Pollution by Nitrate from Agricultural Fertilizers: The case of Menemen Basin (Aegean Region, Turkey)", *4th International Water Congress*, 2-4 November 2017, İzmir, Turkey. (Oral Presentation)

- **Goren A.Y**., Genisoglu, M., Balcı, E., Okten, H.E., "Capability of Nanoscale Zero Valent Iron (nZVI)-Pumice for Methylene Blue Removal by Lab-Scale Mixed-Bed Column Reactor", *3rd International Porous and Powder Materials Symposium and Exhibition*, 12-15 September 2017, Kuşadası, Turkey. (Oral Presentation)

- **Goren A.Y**., Kobya M., Demirbaş E., Şık E., Oncel M.S., "Arsenite Removal from Groundwater by Novel Electrocoagulation Process: Statistical Modeling", *3rd International Porous and Powder Materials Symposium and Exhibition*, 12-15 September 2017, Kuşadası-Turkey. (Oral Presentation)

- **Goren A.Y**., Kobya M., Demirbas E., Sık E., Oncel M.S., "Removal of Arsenate from Groundwater by Electrocoagulation Process Using Al Ball Anodes: Box-Behnken Desıgn for Modelıng and Optımızatıon", *2nd International IWA-PPFW Regional Symposium on Water, Wastewater and Environment*, 22-24 March 2017, İzmir, Turkey. (Oral Presentation)

- Aydiner C., Mert B.K., Dogan E.C., Yatmaz H.C., Aksu S., Tilki Y.M., **Goren, A.Y**. and Balci, E., "A novel hybrid process for industrial wastewater treatment: Fenton and Photo-Fenton enhanced ultrafiltration", *2nd International Conference on Desalination and Environment*, 23-26 January, Doha, Qatar. (Oral Presentation)

- Kobya M., Demirbas E., Oncel M.S., Yıldırım Y., Sık E., **Goren A.Y**., Akyol A., "Modeling and optimization of arsenite removal from groundwater using Al ball anodes by electrocoagulation process", *2nd International Conference on Environmental Science and Technology, 14-17 May 2014*, Antalya-Side, Turkey. (Oral Presentation)